ABSTRACT

SAVADATTI, SIDDHARTH. Accurate and Well-Posed Absorbing Boundary Conditions for Anisotropic Media. (Under the direction of Dr. Murthy N. Guddati).

This dissertation provides (a) an accurate and well-posed local absorbing boundary condition (ABC) for time-dependent modeling of propagating waves in tilted anisotropic acoustic media, (b) an accurate local ABC for time-harmonic modeling of both propagating and evanescent anti-plane and in-plane waves in tilted elliptic anisotropic elastic media, and (c) an accurate local ABC for time-harmonic modeling of in-plane propagating waves in untilted non-elliptic anisotropic elastic media. Such media support wavemodes with opposing signs of phase (c_{px}) and group (c_{gx}) velocities that have long posed a significant challenge to the design of accurate, well-posed and stable local ABCs. By specifically considering the recently developed local ABC, the perfectly matched discrete layer (PMDL), we show that a careful choice of parameters can result in an effective local ABC for anisotropic media.

We first consider a PMDL with real-valued parameters designed to absorb the propagating wavemodes of tilted anisotropic acoustics. Starting with the derivation of the reflection coefficient, we show that the PMDL absorption is based on group (*not* phase) velocities. The group velocity form of the reflection coefficient is used to derive a sufficient condition for PMDL to accurately absorb all outgoing wavemodes (even those with opposing signs of phase and group velocities, i.e. $c_{px}c_{gx} < 0$) and this condition turns out to be a simple bound on the PMDL parameters. By deriving the necessary and sufficient condition for the well-posedness of the initial boundary value problem (IBVP) obtained by coupling an interior with PMDL, we show that the accuracy condition also ensures well-posedness.

We consider next a PMDL with complex-valued parameters designed to absorb both the propagating *and* evanescent wavemodes of tilted elliptic anisotropic elasticity. By first considering the simpler case of scalar anti-plane shear waves, we show that it is possible to overcome the challenges posed by $c_{px}c_{gx} < 0$, in fact by taking advantage of what are considered unwanted and inevitable reflections occurring at the truncation boundaries. This understanding helps us explain the ability of PMDL to accurately model media with

$c_{px}c_{gx} < 0$ *without* the need of intervening space-time transformations; while space-time transformations have been traditionally used to treat wavemodes with $c_{px}c_{gx} < 0$, their extension to heterogeneous (layered) media is unclear. The approximation properties of PMDL quantified through its reflection matrix is used to derive simple bounds on the PMDL parameters necessary for the accurate absorption of all outgoing anti-plane and in-plane wavemodes.

We finally consider a PMDL with real-valued parameters designed to absorb the propagating wavemodes of untilted non-elliptic anisotropic elasticity. While simple space-time transformations are available to treat the wavemodes with $c_{px}c_{gx} < 0$ present in elliptic anisotropic media, no such transformations are known to exist for the non-elliptic case; by using the concept of layer grouping along with a stretching of the finite element mesh, we present an unconventional spatial transformation that guarantees accuracy. The approximation properties of PMDL revealed through its reflection matrix allow us to (a) show that it is impossible to design an accurate PMDL with wavenumber-independent parameters, (b) demonstrate theoretically, the ability of wavenumber-dependent parameters to ensure accuracy, and finally (c) design a practical though unconventional stretching of the finite element PMDL mesh that facilitates the implementation of wavenumber-dependent parameters.

Existing knowledge points to the fact that effective local ABCs can be designed for elliptic anisotropic media only through appropriate space-time transformations and no such transformations are available for non-elliptic anisotropic media. This dissertation proves that: (a) it is possible to design an effective local ABC for elliptic anisotropic media *without* the use of space-time transformations, and (b) there exists a space-time transformation for non-elliptic anisotropic media - at least in the untilted case.

Accurate and Well-posed Absorbing Boundary Conditions for Anisotropic Media

by
Siddharth Savadatti

A dissertation submitted to the Graduate Faculty of
North Carolina State University
in partial fulfillment of the
requirements for the Degree of
Doctor of Philosophy

Civil Engineering

Raleigh, North Carolina

2011

APPROVED BY:

Dr. Murthy N. Guddati Chair of Advisory Committee	Dr. M. Shamimur Rahman
Dr. Kazufumi Ito	Dr. Jie Yu

DEDICATION

To my family and friends, teachers and students.

BIOGRAPHY

Siddharth Savadatti was born in Dharwad, a small town in southern India where he spent the first eighteen years of his life. Moving to Chennai, India, he obtained a Dual Degree (B.Tech + M.Tech) in Infrastructural Civil Engineering from the Indian Institute of Technology Madras in 2003. After a brief stint as a structural design engineer, he taught middle school science and high school mathematics at Rishi Valley School, India. He obtained his doctoral degree in Computational Mechanics from North Carolina State University, Raleigh, USA in 2011.

ACKNOWLEDGMENTS

First and foremost I wish to thank my family. I may not express my gratitude openly or frequently enough, but they are the reason I can even dream of being what I want to be; Appaji, Avvaji and Amma have always been my sources of unconditional love and support, Uncle and Mummy have been my second set of parents, Sannu and Sanghu are sisters every brother should have and Nischu was a brother I would die to have back. Nagu and Ravi, in their own way, complete my family. I love them all.

My teachers have been a constant source of inspiration. I would like to thank Dr. Murthy Guddati for being the kind of doctoral advisor he is. Beyond his technical guidance, I treasure his willingness to listen and to be there whenever I have needed him the most. He has believed in me when I have doubted myself and I hope I have been a decent student to him. I am thankful to Dr. James Nau for giving me the opportunity to teach and for becoming my teaching mentor at North Carolina State University. To Dr. Devdas Menon, Dr. V. Kalyanaraman, Dr P.K. Aravindan and Dr. B.S. Murty of the Indian Institute of Technology Madras, I owe my overall outlook to life; I have, at some point or another, wanted to be just like them. I cannot forget my true teachers through middle and high school, Mr. and Mrs. Sydney Gandhi, who first exposed me to the real joy of understanding. I am indebted to them all.

My graduate school friends should be credited both with preserving my sanity and exposing my insanities. For their generosity and simplicity, Ravi Jenkal and Mithun Acharya unwittingly became people I started looking up to. For their honesty and lack of pretense, Vijay Subramanian and Senganal Thirunavukkarasu became my sounding boards. For easy rapport I had Ankit Ghasi, Abhijit Dawle and Punith Naik at home and Arash Benadaki, Mehran Eslaminia and Jun Zhang at the office. My first roommate here, Yathiraj Udupi made me welcome the minute I set foot in Raleigh. They have made my stay here truly enjoyable.

TABLE OF CONTENTS

LIST OF FIGURES ..... **ix**

CHAPTER 1 INTRODUCTION **1**

1.1 Background 1
1.2 Model Problem 1
1.3 Requirements 4
1.3.1 Well-posedness 6
1.3.2 Accuracy 6
1.3.3 Efficiency 6
1.4 Objective 7
1.5 Challenges 7
1.6 Summary 10
1.7 Outline 11

CHAPTER 2 ACCURATE ABSORBING BOUNDARY CONDITION FOR TILTED ANISOTROPIC ACOUSTICS **14**

2.1 Abstract 14
2.2 Introduction 14
2.3 Preliminaries 18
2.3.1 Model problem 18
2.3.2 Scalar Anisotropic Media 19
2.3.3 Exact ABC 22
2.3.4 Approximate ABCs: need and challenges 24
2.3.5 Approximate ABCs: choices 26
2.3.6 PMDL formulation 27
2.3.7 Objective 32
2.4 PMDL: Approximation properties 32
2.4.1 General approximation properties 32
2.4.2 Reflection Coefficient 34
2.4.3 Points of interpolation 38
2.5 Accuracy 41
2.5.1 Accuracy Criterion 41
2.5.2 Sufficient condition for accuracy 41
2.5.3 Relation between Stiffness and Group velocity 45
2.5.4 Corners 47
2.6 Numerical Examples 47
2.7 Summary and Conclusions 55
2.8 References 56

CHAPTER 3 ACCURATE AND WELL-POSED ABSORBING BOUNDARY CONDITION FOR TILTED ANISOTROPIC ACOUSTICS 61

3.1 Abstract 61
3.2 Introduction 61
3.3 Preliminaries 67
3.3.1 Model problem 67
3.3.2 Scalar Anisotropic Media 67
3.3.3 ABCs: Exact and Approximate 70
3.3.4 PMDL: formulation 72
3.3.5 PMDL: approximation properties 75
3.4 Accuracy 76
3.5 Well-posedness 78
3.5.1 Well-posedness of an ABC 78
3.5.2 Well-posedness criterion 79
3.5.3 Reformulation of the well-posedness criterion 83
3.5.4 Necessary and Sufficient conditions 86
3.5.5 Relation between Tilted and Untilted Anisotropy 90
3.6 Numerical Stability 92
3.6.1 Continuous Time Stability 93
3.6.2 Discretized Time Stability 94
3.6.3 Finite Precision Issues 95
3.7 Numerical Examples 95
3.8 Summary and Conclusions 103
3.9 References 104

CHAPTER 4 ACCURATE ABSORBING BOUNDARY CONDITION FOR TILTED ELLIPTIC ANISOTROPIC ELASTICITY 110

4.1 Abstract 110
4.2 Introduction 111
4.3 Preliminaries 115
4.3.1 Model Problem 115
4.3.2 Anisotropic Elastic Media 116
4.3.3 Outgoing and Incoming Wavemodes 119
4.3.4 Half-space and Finite Layer Wavemodes 122
4.4 Local ABCs: PML and PMDL 124
4.4.1 Construction and Analogies 125
4.4.2 Proof of concept using PML 129
4.4.3 PMDL Properties 131
4.5 Accuracy Requirements 138
4.5.1 Accuracy Criterion 138
4.5.2 Sufficient Conditions for Accuracy 139
4.6 Accurate PMDL 140

4.6.1 Anti-plane shear waves 140
4.6.2 In-plane waves 145
4.7 Numerical Experiments 153
4.8 Summary and Conclusions 157
4.9 References 158

CHAPTER 5 ACCURATE ABSORBING BOUNDARY CONDITION FOR UNTILTED NON-ELLIPTIC ANISOTROPIC ELASTICITY 164

5.1 Abstract 164
5.2 Introduction 164
5.3 Preliminaries 168
5.3.1 Model Problem and Anisotropic Elasticity 169
5.3.2 Reflection Matrix 172
5.3.3 PMDL Properties 173
5.4 Accuracy 177
5.4.1 Accuracy Criterion 177
5.4.2 Accuracy Criterion for Layer Groups 178
5.4.3 Sufficient Conditions for Accuracy 179
5.4.4 Necessary Conditions for Accuracy 181
5.5 Design and Implementation of an Accurate PMDL 181
5.5.1 Inadequacy of Wavenumber-Independent Parameters 182
5.5.2 Wavenumber-Dependent Parameters: Requirements 183
5.5.3 Wavenumber-Dependent Parameters: Implementation 190
5.6 Numerical Experiments 196
5.7 Summary and Conclusions 199
5.8 Appendix: Perfect matching of coordinate transformations 200
5.9 References 201

CHAPTER 6 SUMMARY, CONCLUSIONS AND FUTURE WORK 206

6.1 Summary 206
6.2 Conclusions 206
6.2.1 Accurate ABC for Tilted Anisotropic Acoustics 206
6.2.2 Accurate and Well-posed ABC for Tilted Anisotropic Acoustics 207
6.2.3 Accurate ABC for Tilted Elliptic Anisotropic Elasticity 207
6.2.4 Accurate ABC for Untilted Non-elliptic Anisotropic Elasticity 208
6.3 Future Work 208
6.3.1 Remaining Work on Absorbing Boundary Conditions for Anisotropic Media 208
6.3.1.1 Accuracy and Well-posedness 208
6.3.1.2 Stability 210
6.3.1.3 Heterogeneous Media 210
6.3.1.4 Far-field Response 210
6.3.1.5 Comparative Studies 211
6.3.2 Absorbing Boundary Conditions for Other Complex Cases 211

6.3.2.1 Other Wave Equations 211
6.3.2.2 Geometrical Complexities 211
6.3.2.3 Discrete Systems 211
6.3.3 One-Way Wave Equations in the Context of Subsurface Imaging 211

LIST OF FIGURES

Figure 1.1 A typical unbounded domain foundation problem with the interior and exterior shown 2

Figure 1.2. Idealized physical problem consisting of a full space and its computational model 2

Figure 1.3. Slowness diagrams for propagating wavemodes of tilted elliptic anisotropic acoustics (*left*) and untilted non-elliptic anisotropic elasticity (*right*) 9

Figure 1.4. Slowness diagrams for propagating wavemodes in acoustic media 9

Figure 1.5. Slowness diagrams for in-plane propagating wavemodes in elastic media 10

Figure 2.1. *Left:* The model problem consists of replacing a full space by a left half-space and an efficient ABC that is accurate for a scalar anisotropic medium. *Right:* Global coordinate and material axes along with a typical slowness diagram for $(\sigma_x, \sigma_y) \in \mathbb{R}$. Note that the principal material axes (x_M, y_M) are shown on the ellipse just for reference. 19

Figure 2.2. Representative slowness diagrams for the three kinds of media governed by a scalar wave equation. Only slowness diagram for propagating waves is shown i.e. $(\sigma_x, \sigma_y) \in \mathbb{R}$. Note that the principal material axes (x_M, y_M) are shown on the ellipse just for reference. 22

Figure 2.3. A typical slowness diagram for tilted anisotropic media with the regions of positive group and phase velocities clearly demarcated. 24

Figure 2.4 *Left:* Wavefront in a tilted anisotropic acoustic medium of a source at the center of a domain. *Right:* Wavefronts of the same source in a truncated domain (dotted square) with ABCs designed to absorb positive *phase* velocities. The only difference in the two figures on the right is the choice of their ABC parameters. 26

Figure 2.5. Steps 1 and 2 of PMDL derivation: Replacing a half-space by a linear finite element and another half-space. The use of mid-point integration in the *x* direction eliminates the discretization error. 29

Figure 2.6. Steps 3 and 4 of PMDL derivation: Replacing the half-space by an infinite number of mid-point integrated linear finite elements produces the exact stiffness at *x=0*. Truncating the number of layers to *n* with a Dirichlet boundary at the end results in an implementable but approximate ABC; this is the *n* – layer PMDL. 29

Figure 2.7. *Left:* The four points of at which a 1 – layer PMDL dispersion relation (approximate) matches the exact dispersion relation are the four modes for which the 1 – layer PMDL is exact. *Right:* The two parameters σ_{xj} that result in a particular reference group velocity of c_j (or $\overline{c}_j$) for a 1 – layer PMDL..... 40

Figure 2.8. ***Left:*** Geometric interpretation of the sufficient condition for accuracy. The parameters of PMDL should be chosen above the horizontal line that defines the 'cusp' of the ellipse**.** *Right:* Corner PMDL with parameters (layer lengths) consistent with the two edge PMDLs. 45

Figure 2.9. Interior solution for a 2 – layer PMDL exterior with various PMDL parameters. The first three have parameters under the cusp and thus violate the accuracy criterion. 48

Figure 2.10. Relative error in norm for a 2 layer PMDL with various parameters. The lines demarcating the cusp of the slowness ellipse and its peak are shown..... 49

Figure 2.11. Slowness diagrams for 2 layer PMDL approximation with parameters chosen below the cusp, between the cusp and peak and above the peak. 50

Figure 2.12. Relative error in PMDL approximation with increasing number of PMDL layers for various PMDL parameters that satisfy the accuracy criterion. 51

Figure 2.13. Slowness diagrams for large number of PMDL layers (6 and 10) with different PMDL parameters 51

Figure 2.14. Interior solution for large number of PMDL layers (*n* = 6, 10) with PMDL parameters chosen above and near the cusp ($\sigma_{xj} = 1.0$) and above and far away from the cusp ($\sigma_{xj} = 4.0$). 52

Figure 2.15. Performance of PMDL when used along with padding layers. 53

Figure 2.16. Real part of the slowness approximation for 6 layer PMDL with $\sigma_{xj} = 1.2$ and with padding layers and complex PMDL layers 54

Figure 2.17. Imaginary part of the slowness approximation for 6 layer PMDL with $\sigma_{xj} = 1.2$ and with padding layers and complex PMDL layers. 54

Figure 2.18. Interior solution for 6 layer PMDL with $\sigma_{xj} = 1.2$ and with padding layers and complex PMDL layers 54

Figure 3.1. *Left:* The model problem consists of replacing a full space by a left half-space and an efficient ABC that is both accurate and well-posed for a scalar anisotropic medium. Right: Global coordinate and material axes along with a typical slowness diagram for $(\sigma_x, \sigma_y) \in \mathbb{R}$. Note that the principal material axes (x_M, y_M) are shown on the ellipse just for reference. 67

Figure 3.2. Representative slowness diagrams for the three kinds of media governed by a scalar wave equation. Only slowness diagram for propagating waves is shown i.e. $(\sigma_x, \sigma_y) \in \mathbb{R}$. Note that the principal material axes (x_M, y_M) are shown on the ellipse just for reference. 69

Figure 3.3. A typical slowness diagram for tilted anisotropic media with the regions of positive group and phase velocities clearly demarcated. 71

Figure 3.4. *Left:* Geometric interpretation of the sufficient condition for accuracy. The parameters of PMDL should be chosen above the horizontal line that defines the 'cusp' of the ellipse. *Right:* Corner PMDL with parameters (layer lengths) consistent with the two edge PMDLs. 77

Figure 3.5. Reference solution in a large (500x500) domain at various times. For numerical experiments, the interior chosen is denoted by the square and PMDL is applied at the edges of this square. 96

Figure 3.6. Interior solution for a 2 – layer PMDL exterior with various PMDL parameters. Only the last three simulations have parameters above the cusp and thus satisfy the well-posedness and accuracy criterion. 97

Figure 3.7. Relative error in norm for a 2 layer PMDL with various parameters at different times. The lines demarcating the cusp of the slowness ellipse and its peak are shown. 98

Figure 3.8. Slowness diagrams for 2 layer PMDL approximation with parameters chosen below the cusp, between the cusp and peak and above the peak. The first figure has interpolation points with negative group velocity while the second one has interpolation points with positive group velocity. The last two do not have any interpolation points on the ellipse though they do approximate only the positive group velocity branch. 98

Figure 3.9. Relative error in norm for a 6 layer PMDL with various parameters. The lines demarcating the cusp of the slowness ellipse and its peak are shown..... 99

Figure 3.10. Long time behavior of the interior solution with a 6 layer PMDL approximating the exterior with various parameters..... 100

Figure 3.11. Interior solution for the case where the PMDL parameter is above the cusp but still close to it..... 101

Figure 3.12. Long time behavior of the interior solution with a 6 layer PMDL approximating the exterior with parameters chosen near the cusp. The rogue behavior seen with $\sigma_{xj} = 0.8$ in Figure 3.10 is no longer present. Six padding layers with ad hoc parameters were used. 102

Figure 3.13. Comparison of accuracy achieved with and without padding layers. The gain in accuracy can be attributed to the handling of the evanescent spectrum and the smoothening of the PMDL approximation near zero group velocity modes. 102

Figure 4.2. *Left:* The model problem consists of replacing a full space by a left half-space and an efficient ABC that is accurate for a scalar anisotropic medium. *Right:* Global coordinate and material axes. 116

Figure 4.3. Slowness diagrams for scalar anti-plane waves in elasticity. Only slownesses pertaining to propagating modes are shown $\left(\sigma_x \in \mathbb{R}\right)$ 120

Figure 4.4. Slowness diagrams for coupled in-plane pressure and shear waves in elasticity. Only slownesses pertaining to propagating modes are shown $\left(\sigma_x \in \mathbb{R}\right)$. This paper deals with tilted elliptic anisotropy. 121

Figure 4.5. The three steps in the design of a PML based local ABC; complex coordinate stretching, truncation and discretization with truncation occurring before and after discretization. 128

Figure 4.6. The two steps in the design of PMDL; replacing the exterior by an infinite number of mid-point integrated linear finite elements followed by truncation. 128

Figure 4.7. Steps 1 and 2 of PMDL derivation: Replacing a half-space by a linear finite element and another half-space. The use of mid-point integration in the *x* direction eliminates the discretization error. 135

Figure 4.8. Steps 3 and 4 of PMDL derivation: Replacing the half-space by an infinite number of mid-point integrated linear finite elements produces the exact stiffness at *x=0*. Truncating the number of layers to *n* with a Dirichlet boundary at the end results in an implementable but approximate ABC; this is the *n* – layer PMDL 135

Figure 4.9. Notation for representing outgoing and incoming horizontal slownesses. For anti-plane waves σ_{x1} and $\widetilde{\sigma_{x1}}$ represent respectively the horizontal slownesses of outgoing and incoming wavemodes. For in-plane waves $\sigma_{x1}\left(\sigma_{x2}\right)$ and $\widetilde{\sigma_{x1}}\left(\widetilde{\sigma_{x2}}\right)$ represent respectively the horizontal slownesses for outgoing and incoming pressure (shear) wavemodes..... 138

Figure 4.10. Partitioning of the vertical slowness to facilitate the derivation of accuracy bounds for anti-plane waves. 144

Figure 4.12. Real and Imaginary parts of the horizontal slowness with the outgoing branch in thick lines. An accurate ABC should capture all of the outgoing branch and none of the incoming branch. The first column contains complete slowness diagrams with dotted rectangles being blown up and shown in the second and third columns. 154

Figure 4.13. Real and Imaginary parts of the horizontal slowness obtained by a 200-layer PMDL (thick lines) with reference wavenumbers $\sigma_{xj}^{ref} = 0.576 + 0.252i$. As in Figure 4.12, the first column contains complete slowness diagrams with dotted rectangles being blown up and shown in the second and third columns. 155

Figure 4.14. Real and Imaginary parts of the horizontal slowness obtained by a 200-layer PMDL (thick lines) with reference wavenumbers $\sigma_{xj}^{ref} = 0.650 + 0.250i$ (left) and $\sigma_{xj}^{ref} = 0.650 + 0.150i$ (right). As in Figure 4.12, the dotted rectangles are blown up and shown in the figures that follow. 156

Figure 4.15. Real and Imaginary parts of the horizontal slowness obtained by a 200-layer PMDL (thick lines) with reference wavenumbers $\sigma_{xj}^{ref} = 0.250 + 0.250i$ (left) and $\sigma_{xj}^{ref} = 0.50 + 0.150i$ (right). As in Figure 4.12, the dotted rectangles are blown up and shown in the figures that follow. 157

Figure 5.1. *Left:* Space-time transformations are only available for elliptic anisotropies in homogeneous media. *Right*: No such transformations exist for heterogeneous (layered) and non-elliptic anisotropic media 167

Figure 5.2. *Left:* The model problem consists of replacing a full space of untilted non-elliptic anisotropic elastic media by a left half-space and an efficient ABC that accurately mimics the behavior of the right half-space. *Right:* Global coordinate and material axes. 171

Figure 5.3. Slowness diagrams for in-plane propagating $\left(\sigma_x \in \mathbb{R}\right)$ wavemodes in elasticity. This paper concentrates on accuracy aspects of untilted non-elliptic anisotropy. 171

Figure 5.4. (a) Demarcation of outgoing and incoming propagating slownesses with various intervals of vertical slowness σ_y. (b) Notation for representing outgoing and incoming propagating horizontal slownesses $\left(\sigma_x \in \mathbb{R}\right)$. σ_{x1}, σ_{x2} represent the horizontal slownesses for outgoing wavemodes and $\widetilde{\sigma}_{x1}, \widetilde{\sigma}_{x2}$ represent the horizontal slownesses for incoming wavemodes. (c) Both outgoing and incoming wavemodes with the same horizontal slowness σ_o. (d) Various horizontal slownesses for a fixed vertical slowness $\sigma_y \in \left(-\sigma_{y2}, -\sigma_{y1}\right)$. 176

Figure 5.5. Regions with $\left|r_2\left(\sigma_x, \sigma_{x1}^{ref}, \sigma_{x2}^{ref}\right)\right| < 1$ for a 2-layer grouping of PMDL for a fixed $\sigma_y = \sigma_y^*$. 187

Figure 5.6. (a), (b) Valid choices that ensure *only* the outgoing wavemodes (thick lines) fall in the shaded region and consequently the incoming wavemodes (thin lines) fall outside the shaded region. (c) The two PMDL parameters that are linearly dependent on vertical slownesses σ_y for a 2-layer grouping. (d) Shaded regions with $\left|r_2\left(\sigma_x,\cdot\right)\right|<1$ for the parameters that are linearly dependent on σ_y. Note that all the outgoing wavemodes (thick lines) fall in the shaded region while all the incoming wavemodes (thin lines) fall outside the shaded region. 188

Figure 5.7. Untransformed (a) and transformed (b) exterior with corresponding *n*-layer PMDL mesh. 194

Figure 5.8. The unconventional stretching of the finite element PMDL mesh. The two layers in each 2-layer group have the same length with the stretch angles being equal in magnitude but opposite in sign. 194

Figure 5.9. The unconventional stretching of the PMDL mesh for the two orthogonal edges leads to a an unconventional corner implementation. 195

Figure 5.10. Exact slowness diagram followed by 200-layer PMDL slowness diagrams resulting from three different choices of parameters that all satisfy the accuracy criteria for treating propagating wavemodes $\left(\sigma_x\in\mathbb{R}\right)$ derived in this paper. 197

Figure 5.11. 200-layer PMDL slowness diagrams resulting from four different choices of parameters that all violate at least one of the accuracy criterion specified in this paper. 198

Figure 5.12. Detail of 200-layer PMDL slowness diagrams resulting from three different choices of parameters of which the third and fourth violate at least one of the accuracy criterion specified in this paper. 199

Chapter 1 Introduction

1.1 Background

Many wave propagation problems require the solution to wave equations defined on physically unbounded domains. The propagation of vibrations through the earth or waves through the ocean are some examples. While the actual domain is unbounded, the solution to the problem is usually required only in a small finite region called the interior. The rest of the unbounded domain is termed the exterior. Since we are interested only in the interior solution, the computational expense of solving such a problem can be greatly reduced by replacing the given domain (consisting of a finite interior and an unbounded exterior) by an equivalent model consisting of the same finite interior with appropriate boundary conditions specified at the computational boundary (boundary between interior and exterior). Such boundary conditions should mimic the wave absorption characteristics of the unbounded exterior and are hence known as absorbing boundary conditions (ABCs).

1.2 Model Problem

Consider a simple foundation on unbounded earth as shown in Figure 1.1. The domain of interest here is the vicinity of the foundation (interior). Although we are not interested in the solution in the exterior, its (the exterior's) effect on the interior should be accounted for when solving for the interior. Even though the simplest possible interior is shown in Figure 1.1, it still consists of three computational boundaries along with corners. In order to simplify the issues involved in defining these boundaries, we concentrate on an idealized problem with a single straight boundary shown in Figure 1.2 (left). The idealized computational model in two dimensions is obtained by replacing a full-space (unbounded in both directions) with an interior (left half-space) bounded by a single straight boundary that appropriately mimics the effect of the exterior (right half-space) as shown in Figure 1.2 (right). We thus start with a full-space problem and discuss the issues involved in replacing it by a left half-space and a boundary.

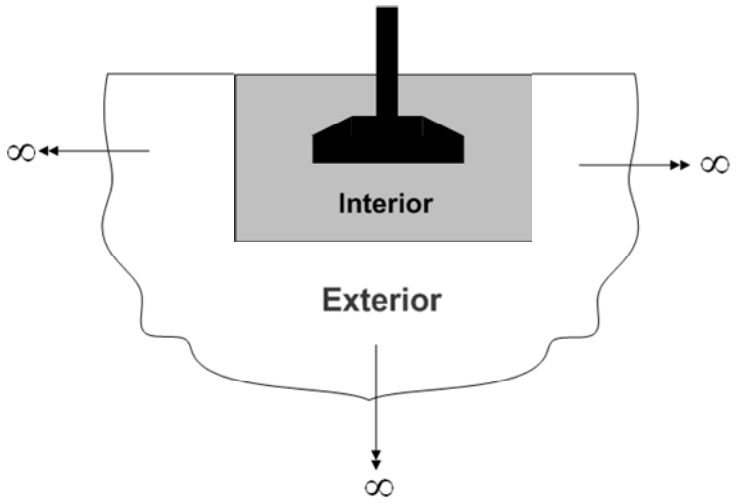

Figure 1.1 A typical unbounded domain foundation problem with the interior and exterior shown

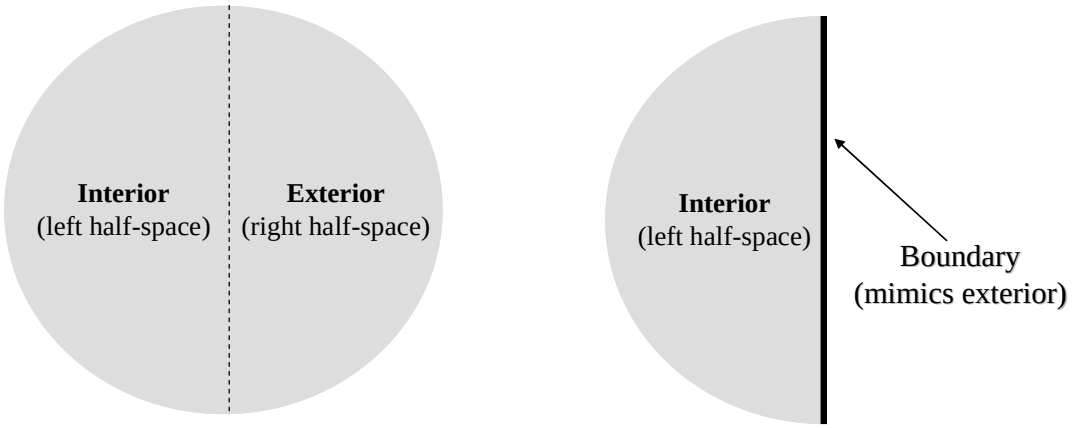

Idealized problem

Computational model of the idealized problem

Full-space divided into a left half-space (interior) and a right half-space (exterior) by a single straight line

Full-space divided into a left half-space (interior) and a single straight boundary that mimics the right half-space (exterior)

Figure 1.2. Idealized physical problem consisting of a full space and its computational model

Consider the simple wave equation defined on the full space in two dimensions,

$$\frac{\partial^2 u}{\partial x^2}+\frac{\partial^2 u}{\partial y^2}=\frac{\partial^2 u}{\partial t^2} \qquad \Big((x,y)\in\mathbb{R}^2, t>0\Big),$$
$$u\Big|_{t=0}=f_1\big(x,y\big), \quad \frac{\partial u}{\partial t}\Big|_{t=0}=f_2\big(x,y\big). \tag{1.1}$$

The equations in (1.1) can, for example, govern the propagation of pressure in an isotropic acoustic medium or anti-plane shear waves in an isotropic elastic medium and form an initial value problem (IVP) defined on an unbounded spatial domain. It is not always possible to derive analytical solutions to (1.1) and more often than not, such problems require numerical solutions (especially in more complicated media). Numerical models need to be finite and hence require the specification of suitable boundaries that limit the extent of the spatial domain. These boundaries are 'artificial' in the sense that the original IVP that we wish to solve has no spatial boundaries. This leads to an initial-boundary value problem (IBVP) that is amenable to numerical solution because of its finite size. For the above problem, we will assume that a single boundary condition $\mathcal{B}u$ is applied at $x=0$ leading to the IBVP,

$$\frac{\partial^2 u}{\partial x^2}+\frac{\partial^2 u}{\partial y^2}=\frac{\partial^2 u}{\partial t^2} \quad \Big(x<0, y\in\mathbb{R}, t>0\Big),$$
$$u\Big|_{t=0}=f_1\big(x,y\big), \quad \frac{\partial u}{\partial t}\Big|_{t=0}=f_2\big(x,y\big), \tag{1.2}$$
$$\mathcal{B}u\Big|_{x=0}=g\big(y,t\big).$$

In reality, at least three more boundaries will need to be prescribed in a two dimensional setting to get a finite spatial domain but we will use the single boundary in (1.2) to illustrate the essential concepts. The boundary at $x=0$ in (1.2) has divided the entire unbounded domain into two parts; the interior and the exterior as shown in Figure 1.2. The interior $\big(-\infty<x\le 0\big)$ is the region where the solution to the differential equation is sought and the

exterior $\left(x > 0\right)$ is the region whose effect on the interior should be properly modeled by applying the boundary condition at $x = 0$.

We are concerned only with homogeneous media for the present. The material properties (like density, elastic moduli etc.) are therefore constants and only act as scaling factors for the governing equations. For simplicity all material properties that are supposed to appear in (1.1), (1.2) are assumed to be 1. Also the above model (1.1), (1.2) is chosen for illustrative purposes because of its simplicity. In general, we will be dealing with wave equations that govern the propagation of disturbances in anisotropic acoustic/elastic media. (1.1) turns out to be a special, simple case of these equations which altogether fall under the category of linear hyperbolic equations.

1.3 Requirements

An exact boundary condition will be such that the solution to (1.2) is identical to the solution to (1.1) in the interior. Exact boundary conditions are not always available for anisotropic and/or heterogeneous media and even when they are, they tend to be computationally expensive due to the presence of operators that are global in space and time. We thus look for approximate local boundary conditions that result in solutions to (1.2) that closely resemble the solution to (1.1). Since the boundary condition should simulate the effect of the unbounded exterior as closely as possible, it should absorb all (or most) of the waves impinging on the boundary at $x = 0$ i.e. it should absorb outgoing waves. At the same time the boundary should *not* admit incoming waves. In the presence of outgoing waves, incoming waves can be looked upon as reflections from an inexact boundary; in the absence of outgoing waves, incoming waves can be interpreted as spurious energy being input from the exterior that is assumed to contain no sources.

In order to be effective, ABCs should satisfy the following criteria:

Well-posedness and **Stability**: The ABC along with the interior governing equation should lead to a well-posed and stable problem. By well-posed, we mean the

existence of a unique solution whose norm in the interior at any time $t > 0$ can be estimated in terms of initial/boundary data.

Accuracy: The ABC coupled with the interior governing equation should produce a solution that closely approximates the solution of the original unbounded problem.

Efficiency: The ABC when used with the interior governing equation should be efficiently solvable. In essence, the additional computational expense of applying the ABC (i.e. obtaining the effect of the unbounded exterior on the interior) should be minimal.

A few points need to be noted:

- The given unbounded problem may have physical boundaries (for example the free surface of the earth). These boundaries are not 'artificial' and do not pose problems. We are only concerned here about the well-posedness/accuracy of solutions to problems into which artificial boundaries in the form of ABCs have been introduced.
- The distinction between 'well-posedness' and 'stability' is not always clear. Some authors make distinctions between these two terms based on whether they refer to the continuous problem or their discrete versions while others make distinctions based on rates of growth (for example exponential vs. polynomial growth of solutions that lead to instabilities). We choose the former distinction with well-posedness referring to existence, uniqueness and boundedness of the solution for the continuous problem and stability referring to the boundedness of the discrete version.
- As mentioned before, our ultimate goal is to obtain numerical solutions where analytical solutions do not exist. This will necessitate discretization of (1.2). Discretization usually introduces further approximations and raises additional concerns of accuracy and stability. Since we expect the discretized model to approach the continuous model in the limit, the criteria of accuracy and well-posedness of the continuous model are necessary conditions for accuracy and stability of the discrete

model. We do not currently concern ourselves with numerical accuracy or stability related to discretization.

1.3.1 Well-posedness

Well-posedness refers in some sense to the boundedness of the energy in a system over time. In the absence of sources in the exterior, there exist only outgoing wavemodes that either propagate energy away from the computational boundary or decay into the exterior. Similarly for well-posedness, the IBVP made up of the interior with the ABC should not allow (a) modes whose amplitude grows unboundedly with time, (b) propagating modes that input energy into the interior, and (c) evanescent modes growing into the exterior. The second and third cases above can be looked upon as equivalent to spurious exterior sources resulting in incoming waves.

1.3.2 Accuracy

Just like the exterior half-space in the model problem, an exact ABC will allow outgoing waves to pass through the computational boundary without any reflections. On the other hand, approximate ABCs will reflect some on the outgoing waves impinging on the boundary and the level of approximation (or accuracy) can be gauged by the reflection coefficient which is the ratio of the amplitudes of the reflected wave to that of the incident wave. Exact absorption implies no reflection and hence a reflection coefficient of zero is desired. Approximate ABCs usually reflect waves travelling in different directions differently and their reflection coefficient seen as a function of the direction of propagation gives us an idea of their accuracy.

1.3.3 Efficiency

For real world problems, the efficiency criterion can only be met by ABCs that are local in space-time. Global ABCs, while being both well-posed and accurate, are computationally very expensive, sometimes prohibitively so.

1.4 Objective

The objective of the present study is to provide accurate and well-posed ABCs for anisotropic acoustic and elastic media.

The requirement of computational efficiency can only be met by ABCs that are local in space-time and hence we confine ourselves to local ABCs in this study. Moreover, we limit ourselves to the design of an accurate and well-posed local ABC for tilted anisotropic acoustics, and the design of accurate local ABCs for tilted elliptic and untilted non-elliptic anisotropic elasticity. We also concentrate our efforts on propagating wavemodes with evanescent wavemodes being considered only in the accuracy studies of tilted anisotropic acoustics and tilted elliptic anisotropic elasticity.

1.5 Challenges

The major challenge to designing well-posed and accurate local ABCs for anisotropic and/or heterogeneous media lies in the presence of propagating wavemodes with opposing signs of phase and group velocity.

A propagating wavemode of (1.2) is a solution of (1.2) of the form $e^{i(k_x x+k_y y-\omega t)}$ with $k_x, k_y, \omega \in \mathbb{R}$. The wave crest of such a mode appears to move in the x direction with a velocity given by $c_{px} = \omega \big/ k_x$ and is termed the phase velocity. The velocity of energy propagating in the x direction however, is given by $c_{gx} = \partial\omega \big/ \partial k_x$ and is termed the group velocity. While the concepts of well-posedness and accuracy are based on group velocities, local ABCs are known to absorb modes based on their phase velocities. This disparity is not of significance for homogeneous isotropic media because such media only support wavemodes with $c_{px} c_{gx} \geq 0$. On the other hand, anisotropic and/or heterogeneous media support wavemodes with $c_{px} c_{gx} < 0$ that pose a significant challenge to the design of well-posed and accurate local ABCs.

The presence of wavemodes with opposing signs of phase and group velocity can be easily represented through slowness diagrams that are plots of variations in horizontal slowness $\sigma_x = k_x / \omega$ with respect to vertical slowness $\sigma_y = k_y / \omega$. Propagating modes are represented by $\sigma_x \in \mathbb{R}$ and evanescent modes have $\sigma_x \notin \mathbb{R}$. It can be shown that for a propagating mode with slownesses $\left(\sigma_x, \sigma_y\right)$, the direction of c_{gx} is given by the direction of the component along σ_x, of the outward normal to the slowness curve at $\left(\sigma_x, \sigma_y\right)$. This is shown in Figure 1.3. Since $c_{px} = 1/\sigma_x$, $c_{px} > 0$ for $\sigma_x > 0$. Figure 1.4 and Figure 1.5 depict the slowness diagrams for homogeneous acoustics and elasticity respectively, and the presence of propagating modes with $c_{px} c_{gx} < 0$ in most anisotropic media is evident.

As far as propagating modes are concerned, a well-posed ABC should *not* capture the non-positive group velocity branch of the slowness diagram and accuracy requires that it capture the non-negative group velocity branch of the slowness diagram in its entirety (see Figure 1.4 and Figure 1.5). The contradiction in terms of zero group velocity modes will be dealt with in detail in later chapters. It can be clearly seen from the above arguments that well-posedness and accuracy are not disjoint. In fact later chapters will show that they are intricately linked.

The objective of this dissertation then, is to design local ABCs that capture only the $c_{gx} > 0$ part of the slowness diagrams (thick lines in Figure 1.4 and Figure 1.5).

For the sake of completion we also mention evanescent wavemodes. We can define outgoing evanescent wavemodes as those with positive imaginary parts i.e. $\Im m\left(\sigma_x\right) > 0$. Hence an ABC that is well-posed for evanescent modes should *not* capture the part of the slowness diagram with $\Im m\left(\sigma_x\right) < 0$ and it needs to capture the branch with $\Im m\left(\sigma_x\right) > 0$ for accuracy.

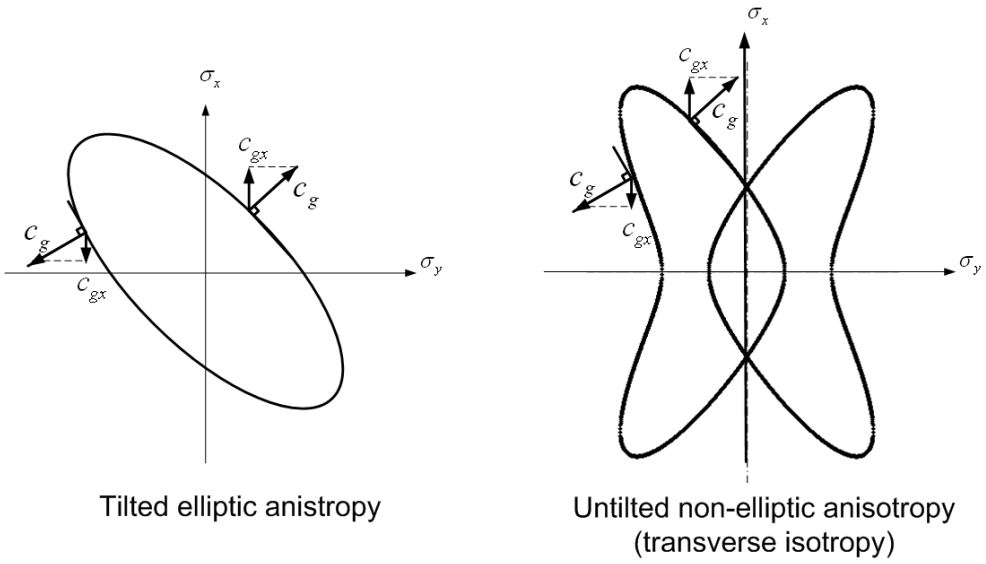

Figure 1.3. Slowness diagrams for propagating wavemodes of tilted elliptic anisotropic acoustics (*left*) and untilted non-elliptic anisotropic elasticity (*right*)

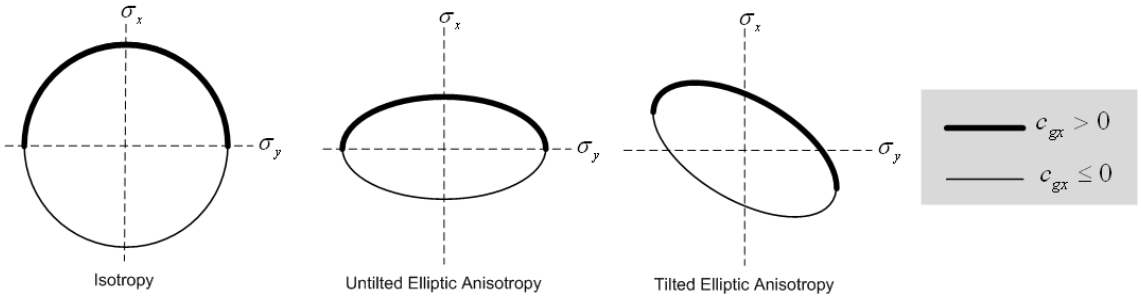

Figure 1.4. Slowness diagrams for propagating wavemodes in acoustic media

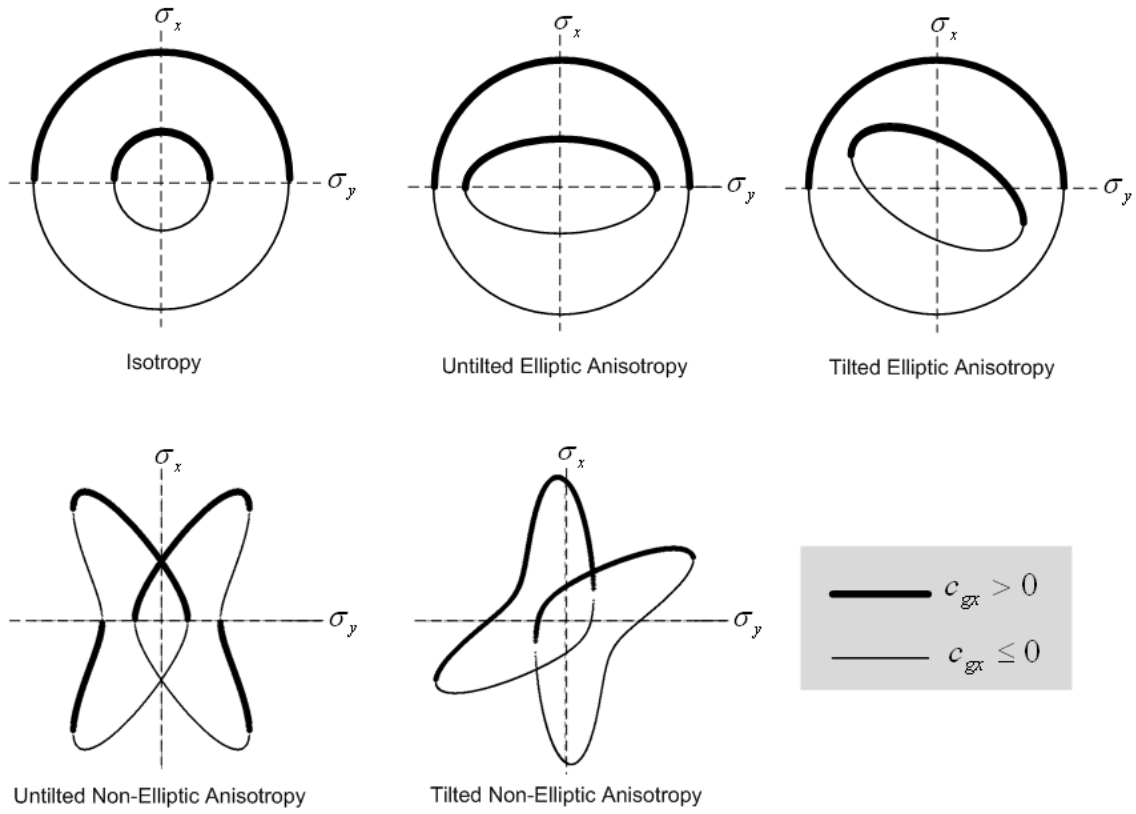

Figure 1.5. Slowness diagrams for in-plane propagating wavemodes in elastic media.

1.6 Summary

Numerical solutions to unbounded domain problems require the specification of artificial boundaries that limit the domain of computation. These boundaries should simulate the effect of the unbounded exterior by absorbing waves impinging on the boundary and are thus termed ABCs. These ABCs, coupled with the interior governing equation, should produce a well-posed problem whose solution accurately simulates the original unbounded problem. For computational efficiency, it is desirable that these ABCs be local.

The objective of this dissertation is to design accurate and well-posed local ABCs that overcome the challenges posed by the existence of wavemodes with $c_{px}c_{gx} < 0$ in

anisotropic media. We limit ourselves to the design of an accurate and well-posed local ABC for tilted anisotropic acoustics and the design of accurate local ABCs for tilted elliptic and untilted non-elliptic anisotropic elasticity. We also concentrate our efforts mainly on propagating wavemodes with evanescent wavemodes considered only in the accuracy studies of tilted anisotropic acoustics and tilted elliptic anisotropic elasticity.

1.7 Outline

The main contributions of this dissertation are organized in the following four chapters. Since each chapter constitutes an individual paper, some repetition between them is inevitable. Chapters 2 and 3 have already been published and Chapters 4 and 5 will be submitted for publication shortly. Hence each chapter is self contained with its own set of references.

In Chapter 2 we investigate the accuracy aspects of local ABCs designed for time-harmonic modeling of scalar waves in tilted anisotropic acoustic media followed by the design of an accurate PMDL for propagating waves. Specifically, in this chapter we (a) derive the PMDL reflection coefficient in terms of group velocities, (b) discuss the PMDL approximation properties, (c) establish an accuracy criterion, and finally (d) derive a sufficient condition that guarantees the accuracy of PMDL for tilted anisotropic acoustics. The reflection coefficient derived in this chapter clearly reveals that the PMDL absorption is based on group velocities, unlike that of other local ABCs that are based on phase velocities. Hence a PMDL can be designed to correctly identify and accurately absorb all outgoing wave modes (even those with opposing signs of phase and group velocities) without the need for space-time transformations.

In Chapter 3 we investigate the well-posedness and accuracy aspects of local ABCs designed for the transient modeling of scalar waves in tilted anisotropic acoustic media followed by the design of a well-posed PMDL that is accurate for propagating waves. Specifically, in this chapter we (a) discuss the well-posedness theory developed by Kreiss for general hyperbolic IBVPs, and the well-posedness conditions for ABCs derived by Trefethen and Halpern for isotropic acoustics, and (b) prove that the sufficient condition for accuracy of PMDL derived in the previous chapter is both necessary and sufficient for well-posedness of

the IBVP obtained by coupling an interior with PMDL. The algebraic criterion derived in this chapter provides a simple bound for the PMDL layer lengths and ensures well-posedness in Kreiss's sense. This bound depends on the anisotropy of the medium, in particular the tilt, and guarantees strong well-posedness of any PMDL satisfying the bound. Unlike other works that study well-posedness from an IVP point of view, this work tackles well-posedness from the more appropriate IBVP viewpoint. The relation between group velocity and half-space stiffness presented here, along with the knowledge that PMDL approximates stiffness instead of wavenumber provides some hints in understanding the ability of PMDL to capture group velocities instead of phase velocities.

In Chapter 4 we design an accurate PMDL for time-harmonic modeling of scalar anti-plane and vector in-plane waves in tilted elliptic anisotropic elastic media. Specifically, in this chapter we (a) establish detailed analogies between PMDL, PML and a half-space that provide an intuitive understanding of the PMDL behavior, (b) present a simple idea that demonstrates the use of truncation reflections in ensuring net spatial decay, and finally (c) derive sufficient conditions that ensure the accurate absorption of scalar anti-plane and coupled vector in-plane waves. Since we show that real-valued PMDL parameters are inadequate in absorbing wavemodes in the presence of mode coupling, the sufficient conditions derived here are bounds on the complex-valued PMDL parameters and are sufficient for the accurate absorption of both propagating and evanescent waves. The effect of truncation reflections on solution decay presented in this chapter clearly explains the ability of acoustic PMDL presented in chapter 2 to handle the challenges posed by opposing phase and group velocity signs without the need of intervening space-time transformations. This understanding also underscores the importance of studying the accuracy and well-posedness issues of ABCs from an IBVP point of view instead of using the easier and more common IVP point of view; IVPs do not support reflections that in this work have proved central to the design of accurate ABCs.

In Chapter 5 we design an accurate PMDL for time-harmonic modeling of vector in-plane waves in untilted non-elliptic anisotropic elastic media. Specifically, in this chapter we (a)

establish a sequence of sufficient conditions and two necessary conditions based on layer groupings, (b) prove that it is impossible to design a standard PMDL with wavenumber-independent parameters to accurately treat propagating waves, (c) derive a sufficient condition on the wavenumber-dependent parameters of PMDL, and finally (d) design an unconventional stretching of the finite element PMDL mesh to implement an ABC with wavenumber-dependent parameters. The work presented in this chapter uses the concept of layer groupings to prove that at least two PMDL layers with parameters that depend linearly on wavenumber are necessary to ensure the accurate absorption of propagating waves. This work presents, to the best of our knowledge, the *only* local ABC developed to date, whose accuracy is rigorously proven for all the propagating modes of untilted non-elliptic anisotropic elasticity.

We conclude in Chapter 6 with a summary and a discussion of further work.

.

Chapter 2 Accurate Absorbing Boundary Condition for Tilted Anisotropic Acoustics

This chapter is a slightly modified version of the following manuscript: S. Savadatti and M. N. Guddati, Absorbing Boundary Conditions for Scalar Waves in Anisotropic Media. Part 1: Time Harmonic Modeling, *Journal of Computational Physics*, Vol. 229, Issue 19, 2010, pp. 6696-6714.

2.1 Abstract

With the ultimate goal of devising effective absorbing boundary conditions (ABCs) for general anisotropic media, we investigate the accuracy aspects of local ABCs designed for the scalar anisotropic wave equation in the frequency domain (time harmonic case). The ABC analyzed in this paper is the perfectly matched discrete layers (PMDL). PMDL is a simple variant of perfectly matched layers (PML) and is equivalent to rational approximation-based local ABCs. Specifically, we derive a sufficient condition for PMDL to accurately absorb wave modes with outgoing group velocities and this condition turns out to be a simple bound on the PMDL parameters. The reflection coefficient derived in this paper clearly reveals that the PMDL absorption is based on group velocities, and *not* phase velocities, and hence a PMDL can be designed to correctly identify and accurately absorb all outgoing wave modes (even those with opposing signs of phase and group velocities). The validity of the sufficient condition is demonstrated through a series of frequency domain simulations. In part 2 of this paper (Chapter 3), the accuracy condition presented here is shown to govern both the well-posedness and accuracy aspects of PMDL designed for *transient* (time-dependent) modeling of scalar waves in anisotropic media.

2.2 Introduction

There exists a class of wave propagation problems defined on physically unbounded domains wherein the actual solution is required only in a small bounded region (the interior) which is separated from the rest of the unbounded domain (the exterior) by a computational boundary.

Since the effect of the exterior is required only at the computational boundary, the computational domain can be restricted to just the interior by specifying *appropriate* absorbing boundary conditions (ABCs) that mimic the exterior by absorbing the outgoing waves at the computational boundary. In time harmonic modeling, appropriateness refers mainly to *accuracy* - the closeness of the computational model (interior + ABC) solution to the exact solution of the physical model (interior + exterior). In addition, computational *efficiency* is often critical for large scale simulations [1,2].

Exact ABCs are accurate by default, but their availability is restricted to simple exteriors with regular computational boundaries. They also tend to be prohibitively expensive for large scale simulations. Approximate ABCs that contain nonlocal spatial and temporal operators (global ABCs) are similarly unsuitable for large scale problems (in-spite of their accuracy) and hence local ABCs are preferred [1,2]. The most popular local ABCs currently available are rational ABCs and perfectly matched layers (PMLs) [3]. Rational ABCs approximate the exact stiffness (or associated dispersion relation) of an exterior with rational functions and were first introduced by Lindman [4]. Initial lower order implementations of Engquist and Majda's sequence of rational ABCs [5,6], Bayliss and Turkel's radiation BCs [7] and Higdon's multidirectional ABCs [8] were followed later by higher order formulations [9,10]. In one way or another, most of these formulations implemented higher order continued fraction expansions through the use of lower order functions of auxiliary variables and can be collectively called the auxiliary variable formulations. The other popular local ABC, the PML, is a 'special' absorbing medium that uses complex coordinate stretching to dampen out (or decay) propagating waves without creating artificial reflections at the computational boundary. The PML formulation was first introduced by Bérenger [11] and the complex coordinate stretching viewpoint was provided by Chew *et al.* [12-14] . Originally presented in a split variable formulation, PMLs are now available in unsplit forms along with variations like the conformal PML [15], complex frequency shifted PML (CFS-PML) [16], convolutional PML (CPML) [17] and multiaxial PML (M-PML) [18].

Currently, both rational ABCs and PMLs are available for a wide variety of governing equations that include, among many others, Maxwell's, linearized Euler's and elastodynamic equations. In comparison, neither ABC is absolutely superior to the other in all respects; the choice between the two is usually determined by specialized requirements of different problems. Rational ABCs tend to be more accurate than PML because the effect of the ABC parameters on solution accuracy is better understood in their case. On the other hand, ABCs based on PML have proven to be more versatile by being easily extendible to complicated exteriors [3]. The term complicated here implies material complications like heterogeneities and/or anisotropy and geometrical complications like corners and conformal boundaries.

In-spite of their many differences rational ABCs and PML have deep underlying links as shown by Asvadurov *et al* [19]. This link can be used to view certain rational ABCs as particular versions of PML e.g. a rational ABC designed purely for propagating waves can be viewed as an efficient form of PML with purely imaginary layer lengths. One such ABC is the perfectly matched *discrete* layer (PMDL), formerly known as continued fraction ABC (CFABC) [20, 21]. PMDL uses mid-point integrated linear finite elements to approximate the stiffness of an unbounded domain *without* discretization error. The parameters of this approximation are the element lengths, which can in general be complex. The details of the PMDL formulation can be found in [22] and are summarized in Section 2.3.6. PMDL is known to possess several advantages over other local ABCs (see Section 2.3.6). Specifically, PMDL combines the accuracy of rational ABCs along with the versatility of PML and is thus used for the present study; moreover, the underlying links make the results of this paper applicable to other rational ABCs and PML in general.

In order to be accurate, ABCs should absorb most of the outgoing wave modes and, in the absence of exterior sources, they should not support incoming modes. While propagating waves are distinguished into incoming and outgoing wave modes depending on their group velocity, rational ABCs and PML have both been traditionally formulated to absorb waves depending on their phase velocities. This dependence on phase velocities (instead of group velocities) does not affect simple media where the phase and group velocities are always of

the same sign (e.g. homogeneous isotropic acoustic medium) and hence accuracy requirements of ABC formulations for simple media have turned out to be relatively easy to satisfy. Recognizing the fact that many anisotropic and/or inhomogeneous media admit wave modes with opposing phase and group velocity directions, much recent research has been focused on developing techniques that result in accurate and stable ABCs for such media e.g. see [23-34] in reference to anisotropic or inhomogeneous (e.g. layered) electromagnetism, advective acoustics and elastodynamics. In particular reference to a medium governed by the linearized Euler equations, the inability of traditional PML to dampen outgoing wave modes in ducted domains in the presence of a mean flow was shown in [22] and attributed to the existence of wave modes with opposite signs of phase and group velocities. Space-time transformations proposed in [23,24] to address instabilities that were not at the time explicitly attributed to such modes, eventually became a remedy to this problem. Similar space-time transformations were developed in subsequent works [26-34] to specifically address the issue of opposing phase/group velocity signs in the case of acoustic, vorticity and entropy waves supported by the linearized Euler equations with parallel and oblique mean flows.

The scalar waves present in an anisotropic acoustic medium whose principal material axis is tilted with respect to the coordinate axis is one of the simple examples of a medium that allows wave modes with differing phase and group velocity signs (see Sections 2.3.3, 2.3.4). This paper provides a sufficient condition for accuracy of PMDL for time harmonic modeling of scalar waves in such an anisotropic medium. In essence, we prove that the parameters of PMDL (its layer lengths) need to satisfy a simple bound to be able to absorb outgoing wave modes without allowing incoming ones; this effectively guarantees accuracy. The criterion derived here, solely from the viewpoint of rational ABCs, bears similarity to the ones derived through coordinate transformations of PML and other ABCs in [26-34], even though the PMDL we use for this purpose *does not* require any coordinate transformation to be enforced. The absence of such transformations makes the PMDL ABC more amenable to extensions involving layered media.

This paper is concerned with the accuracy issues of the frequency domain analysis of the continuous problem with a straight computational boundary. Accuracy considerations here are limited to propagating waves only. As such, interior discretization errors, corners, curved computational boundaries and loss in accuracy due to neglecting the treatment of evanescent waves are outside the scope of this paper. It should be noted that the above restrictions are imposed to make the problem more tractable; they are, with the exception of curved boundaries, not due to any limitations of the PMDL formulation. PMDLs, capable of handling both propagating and evanescent waves for scalar isotropic media have already been implemented on domains with convex polygonal corners in [20]. As such, this paper can be considered as the necessary first step towards a complete PMDL implementation for anisotropic media. An analogous study for the transient case can be found in Part 2 of this paper (Chapter 3).

The outline of the rest of the paper is as follows. Section 2.3 contains preliminaries related to scalar anisotropic wave equation, followed by a discussion of the challenges inherent in designing accurate ABCs for such equations. A brief review of currently available ABCs is also presented in the same section followed by the choice of a particular ABC - the PMDL - that best suits the purposes of this paper. Section 2.4, which is the key to understanding the results of this paper, contains a detailed discussion of the approximation properties of PMDL along with a derivation of the reflection coefficient and a description of its interpolation points. A sufficient condition for accuracy of PMDL is derived in Section 2.5 by utilizing the reflection coefficient. Various numerical experiments are presented in Section 2.6 and finally, Section 2.7 contains a summary and conclusions. References are presented in Section 2.8.

2.3 Preliminaries

2.3.1 Model problem

The ultimate aim of this paper is to provide a practical ABC for the time-harmonic scalar anisotropic wave equation. To this end, we choose the simplest possible boundary in two dimensions: a straight edge without corners. Figure 2.1 (*left*) shows such a boundary ($x = 0$)

and the model problem shown therein consists of replacing the exact full-space by a left half-space (interior) along with an ABC that simulates the effect of the right half-space (exterior). The interior and exterior in (*left*) are given by $x < 0$ and $x > 0$ respectively.

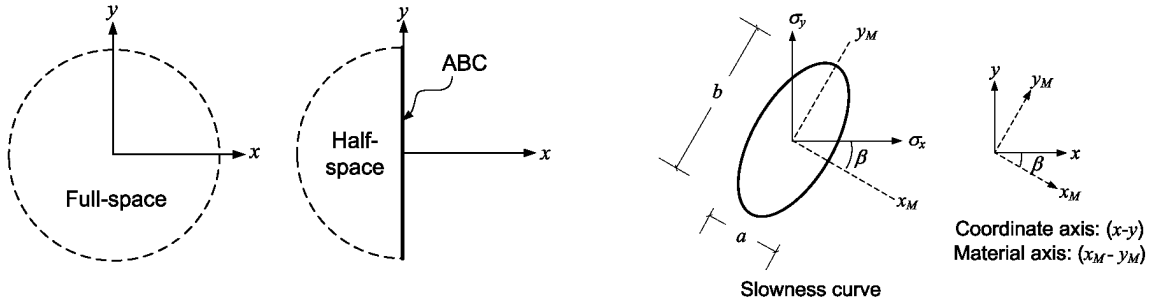

Figure 2.1. *Left:* The model problem consists of replacing a full space by a left half-space and an efficient ABC that is accurate for a scalar anisotropic medium. *Right:* Global coordinate and material axes along with a typical slowness diagram for $(\sigma_x, \sigma_y) \in \mathbb{R}$. Note that the principal material axes (x_M, y_M) are shown on the ellipse just for reference.

2.3.2 Scalar Anisotropic Media

We consider the time-harmonic scalar wave equation in two dimensions $\left(x - y\right)$ given by,

$$A\frac{\partial^2 u}{\partial x^2} + B\frac{\partial^2 u}{\partial y^2} + C\frac{\partial^2 u}{\partial x \partial y} + \omega^2 u = 0\,, \tag{2.1}$$

where the three independent parameters A, B, C define the material properties of the medium and ω is the temporal frequency. Equation (2.1), e.g., arises in the study of anti-plane shear waves in transversely isotropic elastic media where the parameters A, B, C are functions of shear moduli, density and orientation of principal material axes of the medium. Similar scalar equations arise in the study of electromagnetism and advective acoustics.

For the sake of presentation, we Fourier transform (2.1) in y resulting in the reduced equation,

$$A\frac{\partial^2 u}{\partial x^2} - Bk_y^2 u + iCk_y \frac{\partial u}{\partial x} + \omega^2 u = 0\,, \tag{2.2}$$

where the following dualities apply:

$$\frac{\partial}{\partial y} \leftrightarrow ik_y \;\; and \;\; \frac{\partial}{\partial t} \leftrightarrow -i\omega\,. \tag{2.3}$$

For the sake of simplicity, the same notation u is used for both the field variable and its Fourier transform. In terms of individual modes, (2.1) admits solutions of the form $e^{ik_x x + ik_y y - i\omega t}$, where k_x and k_y are the horizontal and vertical wavenumbers respectively. The horizontal wavenumber k_x is the root of the dispersion relation,

$$-Ak_x^2 - Bk_y^2 - Ck_x k_y + \omega^2 = 0\,. \tag{2.4}$$

In terms of horizontal slowness ($\sigma_x = k_x \big/ \omega$) and vertical slowness ($\sigma_y = k_y \big/ \omega$), (2.4) can be written as,

$$-A\sigma_x^2 - B\sigma_y^2 - C\sigma_x\sigma_y + 1 = 0\,. \tag{2.5}$$

For $\left(\sigma_x, \sigma_y\right) \in \mathbb{R}$, (2.5) represents an ellipse in the slowness space that is completely defined by three independent parameters representing its semiminor axis (a), semimajor axis (b) and angle of tilt (β) with respect to the $x - y$ axis as shown in Figure 2.1 (*right*). If we consider an anisotropic medium whose principal material axis (x_M, y_M) is tilted at an angle β with respect to the coordinate axes (x, y) (see Figure 2.1), the wave equation in $x_M - y_M$ can be written as,

$$\frac{1}{a^2}\frac{\partial^2 u}{\partial x_M^2} + \frac{1}{b^2}\frac{\partial^2 u}{\partial y_M^2} + \omega^2 u = 0\,, \tag{2.6}$$

where the parameters a, b represent the material properties along x_M, y_M directions respectively, e.g. if the medium has shear moduli μ_{x_M}, μ_{y_M} and density ρ, we have $1/a = \sqrt{\mu_{x_M}/\rho}$ and $1/b = \sqrt{\mu_{y_M}/\rho}$ (these are the wave velocities in $x_M - y_M$ directions). Equation (2.1) is just the wave equation (2.6) expressed in $(x - y)$; simple coordinate rotations show that:

$$A = \left(\frac{\cos\beta}{a}\right)^2 + \left(\frac{\sin\beta}{b}\right)^2, \quad B = \left(\frac{\cos\beta}{b}\right)^2 + \left(\frac{\sin\beta}{a}\right)^2, \quad C = \sin 2\beta\left(\frac{1}{a^2} - \frac{1}{b^2}\right). \quad (2.7)$$

For later reference, we need the traction on the computational boundary $(x = 0)$. For the medium defined by (2.6), the tractions in $x_M - y_M$ are $\left(a^{-2}\right)\partial/\partial x_M$, $\left(b^{-2}\right)\partial/\partial y_M$. These can be transformed into the tractions in $x - y$ through the usual second order tensor transformations to get,

$$T_x : A\frac{\partial u}{\partial x} + \left(C/2\right)\frac{\partial u}{\partial y}, \qquad T_y : B\frac{\partial u}{\partial y} + \left(C/2\right)\frac{\partial u}{\partial x}, \quad (2.8)$$

where T_x, T_y are the tractions on surfaces perpendicular to x, y axes respectively. Furthermore, without loss of generality, we consider the following with the direction of β being counter clockwise positive:

$$b \geq a > 0, \quad -\frac{\pi}{2} \leq \beta < \frac{\pi}{2}. \quad (2.9)$$

Equations (2.7) and (2.9) together ensure that

$$A > 0, \quad B > 0, \quad 4AB - C^2 > 0. \quad (2.10)$$

Variations of the three material properties A, B, C result in three kinds of slowness diagrams representing isotropic, untilted anisotropic and tilted anisotropic media as shown in Figure 2.2. Since the solutions of (2.1) are of the form $e^{ik_x x + ik_y y - i\omega t}$, a wave mode can be

defined as the solution for fixed k_y, ω, or equivalently, fixed σ_y. The behavior of such a mode in x direction is determined by the value of k_x which is the root of the dispersion relation (2.4).

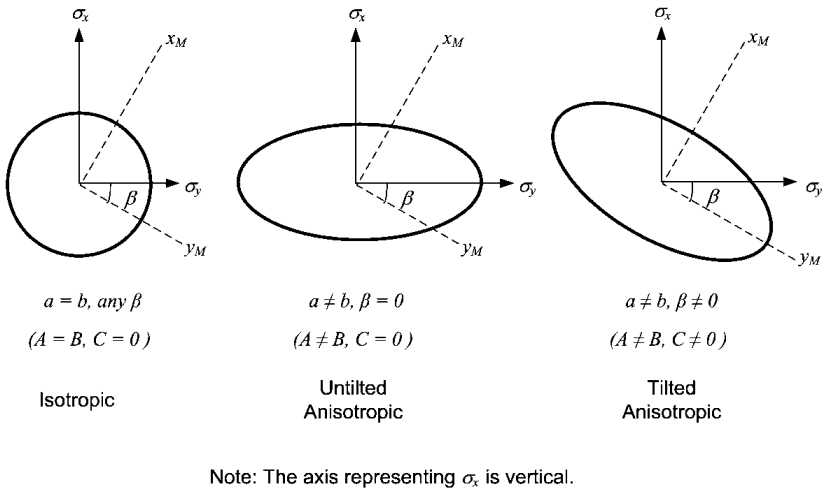

Figure 2.2. Representative slowness diagrams for the three kinds of media governed by a scalar wave equation. Only slowness diagram for propagating waves is shown i.e. $(\sigma_x, \sigma_y) \in \mathbb{R}$. Note that the principal material axes (x_M, y_M) are shown on the ellipse just for reference.

2.3.3 Exact ABC

For a given mode i.e. for a fixed σ_y, (2.5) allows as its solutions, the two σ_x given by,

$$\sigma_x = \frac{-C\sigma_y \pm \sqrt{4A - \left(4AB - C^2\right)\sigma_y^2}}{2A}. \tag{2.11}$$

Equation (2.11) allows both propagating $\left(\sigma_x \in \mathbb{R}\right)$ and evanescent modes $\left(\sigma_x \notin \mathbb{R}\right)$. Each propagating wave mode is associated with a phase velocity (c_{px}) and a group velocity (c_{gx}) in the x-direction defined by:

$$c_{px} = \frac{\omega}{k_x} = \frac{1}{\sigma_x},$$
$$c_{gx} = \frac{\partial \omega}{\partial k_x} = \frac{Ak_x + Ck_y/2}{\omega} = A\sigma_x + \frac{C\sigma_y}{2}. \tag{2.12}$$

It is known that while c_{px} represents the apparent velocity of propagation, c_{gx} represents the true velocity of energy propagation in the x-direction. For the rest of the paper, the terms 'phase velocity' and 'group velocity' will refer to c_{px} and c_{gx} respectively with the understanding that these velocities are always in the x direction. The propagating solutions of (2.11) can be classified in terms of c_{gx} as rightward and leftward propagating waves; their horizontal slownesses are given by,

$$\sigma_x = \frac{-C\sigma_y + \sqrt{4A - \left(4AB - C^2\right)\sigma_y^2}}{2A} \quad : c_{gx} \geq 0 \left(rightward\ propagating\right), \tag{2.13}$$

$$\sigma_x = \frac{-C\sigma_y - \sqrt{4A - \left(4AB - C^2\right)\sigma_y^2}}{2A} \quad : c_{gx} \leq 0 \left(leftward\ propagating\right). \tag{2.14}$$

Graphically, the propagating wave modes of (2.11) are represented by the ellipses in Figure 2.3, where the rightward and leftward propagating waves of (2.13) and (2.14) are denoted by the solid and broken lines respectively of the left ellipse in Figure 2.3.

An exact right half-space, in the absence of any sources within it, admits waves that either propagate to the right $(c_{gx} \geq 0)$ or decay with increasing x $(\mathrm{Im}(\sigma_x) > 0)$. The equation of an ABC that exactly simulates a right half-space is thus given by,

$$\sigma_x = \frac{-C\sigma_y + \sqrt{4A - \left(4AB - C^2\right)\sigma_y^2}}{2A} \quad : Exact\ ABC\ (slowness\ form), \tag{2.15}$$

where the square root is defined by the standard branch cut and $(\sigma_y, \omega) \in \mathbb{R}$. The slowness diagram of an exact ABC for propagating waves $(\sigma_x \in \mathbb{R})$ will thus be the solid portion of the left ellipse in Figure 2.3.

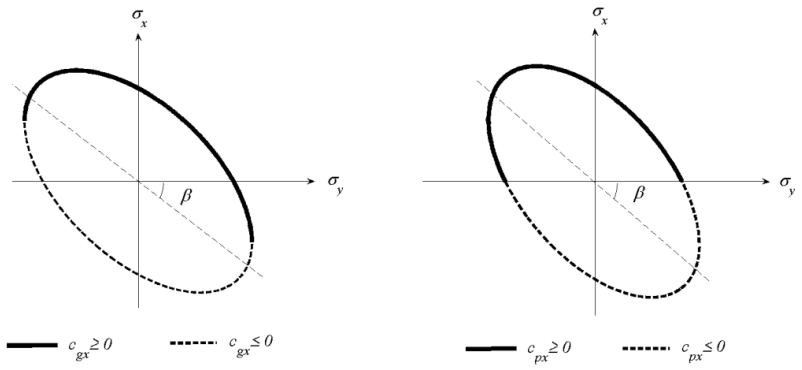

Figure 2.3. A typical slowness diagram for tilted anisotropic media with the regions of positive group and phase velocities clearly demarcated.

2.3.4 Approximate ABCs: need and challenges

It is known that, on inverse Fourier transforming, the square root in (2.15) results in pseudo differential operators that are global in both space and time [5]. An exact ABC is thus computationally expensive and hence ABCs that approximate (2.15), but lead to local operators are preferred.

Since the approximate ABC is supposed to represent the equation of an exact ABC (2.15) in some sense, it should try to capture, as accurately as possible, the solid part of the ellipse in i.e., the non-negative group velocity branch of the ellipse. An obvious sign of inaccuracy is the capturing of the negative group velocity branch. However, none of the approximate ABCs, neither rational ABCs nor PML, were developed with the explicit purpose of capturing positive group velocities. While the rational approximation of the square root operator employed by Engquist and Majda [5,6] ends up capturing the correct group velocities for scalar anisotropic waves, to the best of our knowledge it was never really implemented for the anisotropic case and hence it is not apparent that it would capture the

right group velocities in general. Moreover, Engquist and Majda's ABCs are limited to scalar wave equations and robust extensions to vector systems may not be possible. A straightforward implementation of Higdon's multidirectional ABCs [8], as well as the complex coordinate stretching of PML in the direction of unboundedness can be shown to capture only positive phase velocities (*not* group velocities). This hardly poses a problem for the cases of isotropic or untilted anisotropic media (see Figure 2.2) because every point on these slowness diagrams has phase and group velocities of the same sign. This can easily be inferred from (2.4), (2.7) and (2.12); because $C = 0$ for untilted anisoptropy and hence c_{gx} and c_{px} have the same sign. In fact, approximate ABCs that are well-posed, accurate and efficient for isotropic and untilted anisotropic media have existed for more than two decades, e.g. [5].

Consider however the case of tilted anisotropy. Figure 2.3 clearly shows that there are portions on the slowness diagram which have group and phase velocities of differing signs. This implies that a typical approximate ABC (developed originally for isotropic or untilted anisotropic media and based on phase velocities) will try to capture the positive phase velocity branch (solid portion of the right ellipse in Figure 2.3) instead of the positive group velocity branch (solid portion of the left ellipse in Figure 2.3). Hence, such an approximate ABC is clearly inaccurate for tilted anisotropic media because it will end up capturing portions of the slowness diagram with negative group velocities. To demonstrate, frequency domain simulations transformed back in time are presented in Figure 2.4. The figure on the left shows the wavefront in a tilted anisotropic acoustic medium of a source at the center of the domain. The wavefronts of the same source in domains half the size (dotted square) with ABCs applied at the truncated boundaries are shown in the two figures on the top and bottom right of Figure 2.4. The two cases correspond to the same ABC with two different choices of the ABC parameters, *both* designed to capture positive *phase* velocities. The obvious inaccuracies due to reflections in the figure on the bottom right demonstrate the ineffectiveness of ABCs designed with reference to positive phase velocities.

2.3.5 Approximate ABCs: choices

As mentioned in the introduction, PML and rational ABCs are the most popular local ABCs; though seemingly disparate, recent works have demonstrated underlying links between the two. It was shown in [19] that optimal PML for propagating wave modes can be obtained by purely imaginary stretching and as such PML discretization is algebraically equivalent to rational ABCs obtained by approximating the square root operator. Hence, in the purely imaginary stretching case, rational ABCs can also be viewed as PML. The advantage of this viewpoint is that ABCs can now be developed to inherit the accuracy of rational ABCs while maintaining the versatility of PML. One such local ABC is the arbitrarily wide angle wave equation (AWWE) based CFABC first introduced in [37], with the underlying theory presented in [38] and linked to PML in [20] . These CFABCs can be viewed as particularly efficient discrete versions of PML where the *'perfect matching'* property of continuous PML is preserved even after discretization. This property of CFABCs later prompted the more appropriate term: 'Perfectly Matched *Discrete* Layers' (PMDLs) (see [22]).

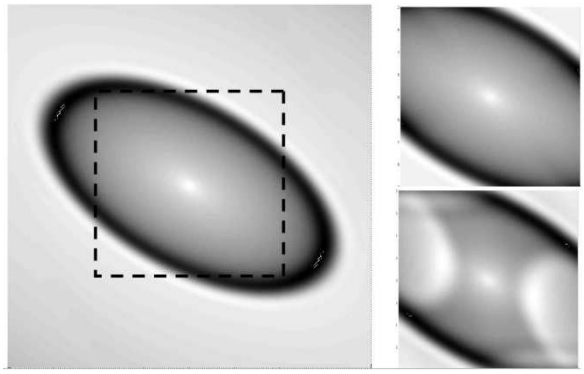

Figure 2.4 *Left:* Wavefront in a tilted anisotropic acoustic medium of a source at the center of a domain. *Right:* Wavefronts of the same source in a truncated domain (dotted square) with ABCs designed to absorb positive *phase* velocities. The only difference in the two figures on the right is the choice of their ABC parameters.

PMDL forms the basis of this study because of their attractive properties (see [22,38]): **(a)** *Generality* - The PMDL formulation is applicable to general second order hyperbolic systems

including (but not limited to) media governed by Maxwell's, linearized Euler's and elastodynamic equations, **(b)** *Completeness* - PMDL is capable of acting as an ABC for both propagating and evanescent waves, **(c)** *Accuracy* - *PMD*L can be implemented to an arbitrarily high degree of accuracy without a substantial loss in efficiency, **(d)** *Efficiency* - The PMDL formulation is local and is computationally efficient, **(e)** *Transparent* – The PMDL lends itself to explicit error calculation (the truncation error, the only kind of error in PMDL, can be calculated *a-priori* for each wave mode), **(f)** *Versatility* - PMDL can be viewed as an optimal PML and hence it inherits the versatility of PML with respect to being extendible to complicated boundary geometries, and **(g)** *Ease of Use* - The PMDL formulation was derived within the finite element framework and can hence be directly incorporated into existing finite element or finite difference codes. Other ABCs that exhibit many of the above properties do exist. For example, although developed through a different, independent viewpoint, the auxiliary variable Hagstrom-Warburton formulation [39] can be shown to be equivalent to PMDL and exhibits most of the above properties. However, the derivation of Hagstrom-Warburton formulation is currently limited to the scalar case and as such it lacks the generality of PMDL.

Notwithstanding the above merits, effectiveness of PMDL is not assured, especially for general anisotropic and heterogeneous exteriors. The subsequent discussion is limited to propagating wave modes only, i.e., we are interested in properties of ABCs that only approximate the real part of (2.15). Even though neglecting evanescent modes $\left(\sigma_x \notin \mathbb{R}\right)$ is expected to affect the long term accuracy of the solution in the interior [40] , and even though PMDL *can* handle evanescent wave modes, we consider this paper to be a preliminary work on rational ABCs for tilted anisotropic media and so restrict ourselves to propagating wave modes.

2.3.6 PMDL formulation

PMDL derivation can best be presented in (x, σ_y, ω) space with the governing equation given by (2.2). Since we wish to replace the right half-space in Figure 2.1 by an ABC, consider just

the right half-space $\left(0 \le x < \infty\right)$ with a stiffness (or Dirichlet to Neumann map) given by K_{exact}. The traction F_0 on the left boundary $\left(x = 0\right)$ and the field variable there (u_0), are related by:

$$F_0 = K_{exact} u_0 \quad : Exact\ ABC\ (stiffness\ form). \tag{2.16}$$

Equation (2.16) can be viewed as the stiffness form of the equation of an exact ABC as compared to the slowness form of (2.15). The traction for a tilted anisotropic medium governed by (2.2) is given by (2.8) and on the left boundary $\left(x = 0\right)$, the traction T_x can be written as,

$$F_0 = -\left(A\frac{\partial}{\partial x} + \frac{C}{2} i\omega\sigma_y\right) u\Big|_{x=0}. \tag{2.17}$$

For a mode $u = e^{i\omega\left(\sigma_x x + \sigma_y y - t\right)}$, (2.16) with (2.17) leads to

$$K_{exact} = -i\omega\left(A\sigma_x + \frac{C}{2}\sigma_y\right). \tag{2.18}$$

In the absence of sources inside the right half-space, the horizontal slowness is given by (2.15). This allows us to write the exact stiffness (2.18) as

$$K_{exact} = \frac{-i\omega\sqrt{4A - \left(4AB - C^2\right)\sigma_y^2}}{2}. \tag{2.19}$$

PMDL approximates the exact stiffness K_{exact} in (2.19) by an approximate stiffness K_n to obtain an approximate ABC for Figure 2.1 that mimics the absorption behavior of the right half-space; the PMDL equation approximating (2.16) takes the form,

$$F_0 = K_n u_0 \quad : Approx\ ABC\ (stiffness\ form) \tag{2.20}$$

where the approximate stiffness K_n is obtained by using n mid-point integrated finite elements to approximate the stiffness of the right half-space at $x = 0$. The rationale behind this approximation can be summarized in the following four steps which are graphically depicted in Figure 2.5 and Figure 2.6.

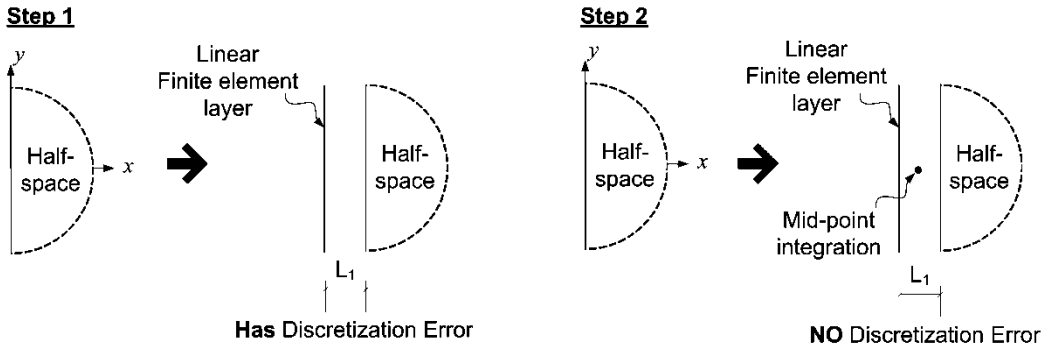

Figure 2.5. Steps 1 and 2 of PMDL derivation: Replacing a half-space by a linear finite element and another half-space. The use of mid-point integration in the *x* direction eliminates the discretization error.

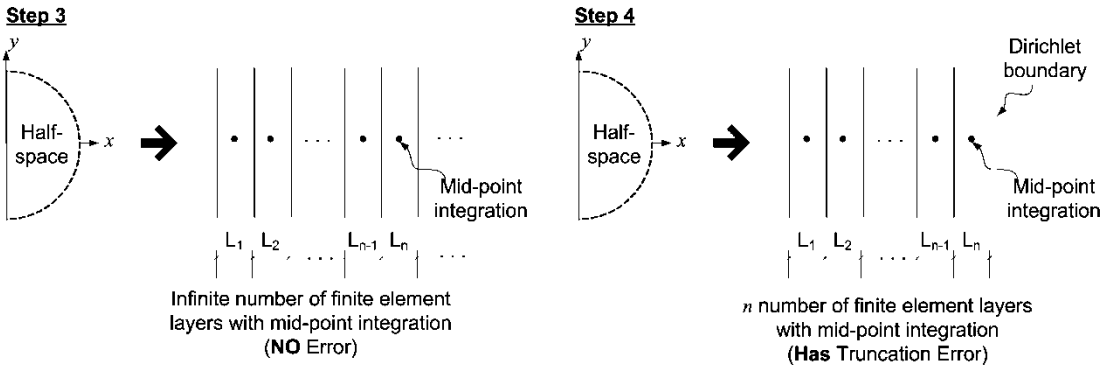

Figure 2.6. Steps 3 and 4 of PMDL derivation: Replacing the half-space by an infinite number of mid-point integrated linear finite elements produces the exact stiffness at *x=0*. Truncating the number of layers to *n* with a Dirichlet boundary at the end results in an implementable but approximate ABC; this is the *n* – layer PMDL.

STEP 1, involves splitting the half-space $[0, \infty)$ into a finite element $[0, L_1]$ and another half-space $[L_1, \infty)$, with the finite element using linear shape functions to represent the

displacement in $[0, L_1]$. As expected, the stiffness of the finite element $[0, L_1]$ plus half space $[L_1, \infty)$ model can only approximate K_{exact} because of the error inherent in the finite element discretization.

STEP 2, *which is the key to PMDL development*, involves the elimination of the finite-element discretization error with respect to the half-space stiffness at $x = 0$. This is achieved by simply using mid-point integration to approximately evaluate the finite element stiffness matrix (see [20,21,38]). The stiffness of this mid-point integrated linear finite element is denoted by $\mathbf{S}_j$ (with $j = 1$) with $\sigma_{x1} = 2i/\omega L_1$:

$$\mathbf{S}_j = \begin{bmatrix} S_j^{11} & S_j^{12} \\ S_j^{21} & S_j^{22} \end{bmatrix} = \frac{-i\omega\sigma_{xj}A}{2}\begin{bmatrix} 1 & -1 \\ -1 & 1 \end{bmatrix} + \frac{iC\omega\sigma_y}{2}\begin{bmatrix} 0 & -1 \\ 1 & 0 \end{bmatrix} + \frac{i\omega\left(B\sigma_y^2 - 1\right)}{2\sigma_{xj}}\begin{bmatrix} 1 & 1 \\ 1 & 1 \end{bmatrix} \quad \text{for } \left(j = 1 \ldots n\right). \tag{2.21}$$

Note that the mid-point integrated linear finite element $[0, L_1]$ plus half space $[L_1, \infty)$ model provides represents the *exact* stiffness of the original half-space $[0, \infty)$ at $x = 0$ *irrespective* of the element length L_j; it can be arbitrarily large and is not even restricted to real numbers.

STEP 3 involves applying the above splitting recursively to discretize the original half-space into an infinite number of finite element layers, $[0, L_1]$, $[L_1, L_1 + L_2]$, … as shown in Figure 2.6. Such splitting does not introduce any further discretization error because the mid-point integration in step 2 eliminates *all* discretization errors in the half-space stiffness. Hence, this discretized half-space containing an infinite number of layers is *exact* as far as the stiffness at $x = 0$ (K_{exact}) is concerned.

STEP 4 involves limiting the number of layers for computational tractability. The number of layers is limited to n with a Dirichlet boundary condition $u_n = 0$ applied at $x = \sum L_j$

as shown in Figure 2.6. This results in a *n*-layer finite element model of the half space whose stiffness K_n can be written in the continued fraction form:

$$K_n = S_1^{11} - \cfrac{S_1^{12} S_1^{21}}{S_1^{22} + S_2^{11} - \cfrac{S_2^{12} S_2^{21}}{S_2^{22} + S_3^{11} - \cfrac{}{\cdots \cfrac{S_{n-1}^{12} S_{n-1}^{21}}{S_{n-1}^{22} + S_n^{11}}}}}. \tag{2.22}$$

The above expression is obtained by assembling the n element matrices $\mathbf{S_j}\,(j = 1 \ldots n)$ in (2.21) and eliminating the auxiliary variables $u_1, \ldots u_{n-1}$. Note that the truncation to n layers introduces errors, which makes K_n an approximation of K_{exact}. Hence (2.20) is the equation of an approximate ABC which will be referred to as the *n*-layer PMDL.

In (2.21), σ_{xj} with $\left(j = 1 \ldots n\right)$ are termed the n parameters of PMDL. The finite element layer lengths L_j are related to these parameters as $L_j = 2i/\omega\,\sigma_{xj}$. This particular choice of frequency dependent imaginary lengths ensures that the boundary condition, when transformed back into the time domain, will have all real-valued coefficients, thus avoiding any complex arithmetic [38]. Comparing (2.20) to (2.16) we see that PMDL approximates the exact stiffness $(K_n \approx K_{exact})$ and the properties of this approximation are dictated solely by the choice of the n arbitrary parameters σ_{xj}. A detailed derivation of the formulation presented in this subsection is given in [38]. For later use, the following identities can be easily derived from (2.19) and (2.21):

$$\begin{aligned} S_j^{11} &= S_j^{22}, \\ K_{exact}^2 &= S_j^{11} S_j^{22} - S_j^{12} S_j^{21}. \end{aligned} \tag{2.23}$$

2.3.7 Objective

To restate, the objective of this paper is to develop an accurate PMDL for scalar wave propagation in tilted anisotropic media. Specifically, we will derive criteria for the parameters σ_{xj} that will make the n-layer PMDL an accurate ABC for the model problem in Figure 2.1.

2.4 PMDL: Approximation properties

In this section, we closely examine the approximation properties of PMDL for tilted anisotropic media. This section is key to understanding the rest of the paper.

2.4.1 General approximation properties

The PMDL presented in the previous section is a special form of rational ABCs. Rational ABCs use rational functions $P_{r,s}$ of the form,

$$P_{r,s}(\sigma_y) = \frac{p_r(\sigma_y)}{q_s(\sigma_y)}, \tag{2.24}$$

to approximate irrational square root operator present in the definition of an exact ABC (2.15). Here p_r and q_s are polynomials of exact degrees $r \geq 0$ and $s \geq 0$ respectively with no common zeros. In the case of isotropic and untilted anisotropic media, for a particular choice of r, s and the $r+s+2$ coefficients of p_r and q_s, the dispersion relation of every rational ABC can be represented as $\sigma_x = P_{r,s}(\sigma_y)$. This dispersion relation can be viewed as an approximation of the dispersion relation of the exact ABC (2.15). Using $C = 0$ in (2.15), we get the exact ABC for isotropic and untilted anisotropic media as $\sigma_x = +\sqrt{A\left(1 - B\sigma_y^2\right)}\Big/A$. Hence, rational ABCs for isotropic and untilted anisotropic media approximate the irrational square root by a rational function i.e. $P_{r,s}(\sigma_y) \approx +\sqrt{A\left(1 - B\sigma_y^2\right)}\Big/A$.

PMDL approximates the exact stiffness K_{exact} in (2.16) by K_n. The continued fraction form of K_n in (2.22) can also be expressed as

$$K_n = -i\omega P_{2n,2n-2}(\sigma_y). \tag{2.25}$$

Using $K_n \approx K_{exact}$, (2.19) and (2.25) we can see that the n-layer PMDL is equivalent to a rational approximation of the positive square root operator,

$$P_{2n,2n-2}(\sigma_y) \approx \frac{+\sqrt{4A - \left(4AB - C^2\right)\sigma_y^2}}{2}. \tag{2.26}$$

The rational approximation of (2.26) can be used in the slowness form of the exact ABC in (2.15) to obtain the slowness form of the n-layer PMDL as

$$\sigma_x = \frac{-C\sigma_y \big/ 2 + P_{2n,2n-2}(\sigma_y)}{A} \quad : Approx\ ABC\ (slowness\ form). \tag{2.27}$$

As far as this paper is concerned, we are interested in modeling propagating waves only. When the parameters of n-layer PMDL σ_{xj} are chosen to be real, $P_{2n,2n-2}$ becomes a real rational function and (2.27) approximates the real part of (2.15) i.e. (2.27) treats propagating waves only. Hence we restrict ourselves to $\sigma_{xj} \in \mathbb{R}$. A few points need to be clarified here. (a) It should be noted that a choice of $\sigma_{xj} \in \mathbb{R}$ is in no way due to a limitation of the PMDL itself. It has already been shown that PMDL models propagating waves for purely real σ_{xj}, evanescent waves for purely imaginary σ_{xj} and both propagating and evanescent waves for complex σ_{xj} [38]. (b) Choosing purely real σ_{xj} also implies choosing purely imaginary finite element layer lengths since we assumed $L_j = 2i \big/ \omega\, \sigma_{xj}$. This should not pose any problem because, as mentioned in Step 2 of Section 2.3.6, the elimination of discretization error due to mid-point integration is independent of L_j. (c) Since L_j can be real, imaginary or

complex, the domain $x \in \left(0, \sum L_j\right)$ of the n-layer PMDL can, in general, be complex; this complex domain in no way represents *or* approximates the physical right half-space that forms the exterior $[0, \infty)$. However, the stiffness of this n-layer PMDL at $x = 0$ is an approximation of the stiffness of the right half-space i.e. $K_n \approx K_{exact}$.

2.4.2 Reflection Coefficient

The reflection coefficient is defined as the ratio of amplitudes of the reflected wave to the incident wave and the approximation properties of an ABC designed for propagating waves can be studied through the magnitude of its reflection coefficient. The reflection coefficient R_n for a n-layer PMDL can be derived by considering individual propagating wave modes with a fixed $(\sigma_y, \omega) \in \mathbb{R}$. Since we are interested in propagating wave modes only, σ_y is chosen so as to yield real σ_x. The dispersion relation (2.5) admits two σ_x for a given σ_y. These two modes (2.13) and (2.14) have group velocities that are negative of each other and can be categorized into rightward and leftward propagating waves. For the left half-space with an approximate ABC at $x = 0$, we can consider the rightward propagating wave as the incident wave on the boundary $x = 0$ and the leftward propagating wave as the reflected wave. Using the definition of reflection coefficient, the total wave field in the left half-space can be represented by $u = e^{i\omega\left(\sigma_x x + \sigma_y y - t\right)} + R_n e^{i\omega\left(\tilde{\sigma}_x x + \sigma_y y - t\right)}$ where σ_x and $\tilde{\sigma}_x$ are the two roots given by (2.13) and (2.14) respectively. Since σ_x is the slowness in the incident wave mode $e^{i\omega\left(\sigma_x x + \sigma_y y - t\right)}$, it is the root with the non-negative group velocity i.e. $c_{gx} = +\sqrt{4A - \left(4AB - C^2\right)\sigma_y^2}\Big/ 2 \geq 0$. The other root can be written as $\tilde{\sigma}_x = -\left(\sigma_x + C\sigma_y \big/ A\right)$ and the reflected wave mode $e^{i\omega\left(\tilde{\sigma}_x x + \sigma_y y - t\right)}$ has non-positive group velocity. The reflection coefficient derivation will not need a precise classification of zero group velocity modes as either incident or reflected modes; hence the obvious overlap

between rightward and leftward propagating modes for $c_{gx} = 0$ can be neglected. Substituting u into the equation defining a n-layer PMDL (2.20) and using (2.17), we get:

$$\omega\left(-iA\left(\sigma_x + R_n\tilde{\sigma}_x\right) - i\frac{C}{2}\left(1+R_n\right)\sigma_y\right)e^{i\omega(\sigma_y y - t)} = K_n u_0 . \tag{2.28}$$

Since the displacement $u_0 = u\big|_{x=0} = \left(1+R_n\right)e^{i\omega(\sigma_y y - t)}$, (2.28) becomes,

$$\left(1+R_n\right)K_n = -i\omega A\left(\sigma_x + R_n\tilde{\sigma}_x\right) - i\omega\frac{C}{2}\left(1+R_n\right)\sigma_y . \tag{2.29}$$

We can solve for the reflection coefficient R_n in (2.29) and write it either in terms of slowness or stiffness. Using $\tilde{\sigma}_x = -\left(\sigma_x + C\sigma_y / A\right)$, (2.13) and (2.25), (2.29) can be written in slowness form as,

$$R_n = \left(\frac{\sqrt{4A - \left(4AB - C^2\right)\sigma_y^2}\Big/ 2 - P_{2n,2n-2}(\sigma_y)}{\sqrt{4A - \left(4AB - C^2\right)\sigma_y^2}\Big/ 2 + P_{2n,2n-2}(\sigma_y)}\right) \quad : \begin{matrix} Reflection\ coefficient \\ (slowness\ form) \end{matrix} \tag{2.30}$$

On the other hand, using $\tilde{\sigma}_x = -\left(\sigma_x + C\sigma_y / A\right)$ and (2.18), (2.29) can be written in stiffness form as,

$$R_n = \left(\frac{K_{exact} - K_n}{K_{exact} + K_n}\right) : Reflection\ coefficient\ (stiffness\ form) . \tag{2.31}$$

Expressions (2.30) and (2.31) are of course equivalent to each other considering (2.19) and (2.25). From (2.22)and (2.23)we have $K_n = K_{exact}^2 / \left(S_n^{11} + K_{n-1}\right)$. This allows us to write (2.31) in the recursive form,

$$R_n = \left(\frac{S_n^{11} - K_{exact}}{S_n^{11} + K_{exact}}\right) R_{n-1} . \tag{2.32}$$

Since the reflection coefficient for the 0-layer PMDL (the Dirichlet boundary in Figure 2.6) is $R_0 = -1$, the magnitude of the reflection coefficient turns out to be (in stiffness form),

$$\left|R_n\right| = \left|\prod_{j=1}^{n}\left(\frac{S_j^{11} - K_{exact}}{S_j^{11} + K_{exact}}\right)\right|. \tag{2.33}$$

By utilizing (2.18), (2.19) and (2.23), the reflection coefficient of (2.33) can be also written in slowness form as:

$$\left|R_n\right| = \left|\prod_{j=1}^{n}\left(\frac{A\sigma_x - A\sigma_{xj}}{A\sigma_x + A\sigma_{xj}}\right)\left(\frac{A\left(\sigma_x - \sigma_{xj}\right) + C\sigma_y}{A\left(\sigma_x + \sigma_{xj}\right) + C\sigma_y}\right)\right|. \tag{2.34}$$

An exact ABC produces no reflections and hence its reflection coefficient is zero for all wave modes ($R \equiv 0$). The *n*-layer PMDL results in $R_n = 0$ for only some (not all) modes and these are termed the reference modes. The horizontal slownesses of the reference modes are termed the reference slownesses. By setting $R_n = 0$ in (2.34), the reference slownesses can be seen to be

$$\sigma_x = \sigma_{xj}, \;\; \sigma_{xj} - \left(C/A\right)\sigma_y . \tag{2.35}$$

The choice of the notation σ_{xj} for the parameters of the PMDL is now apparent because they represent some of the horizontal slownesses for which the PMDL is exact. The form of the reflection coefficient in (2.34) can be specialized for isotropic media by substituting $C = 0$ and compared to the reflection coefficient derived in [21] for isotropic acoustics.

Since we are interested in the ability of PMDL to absorb wave modes with non-negative group velocities, we rearrange (2.34) to get

$$\begin{aligned}\left|R_n\right| &= \left|\prod_{j=1}^{n}\left(\frac{A\sigma_x - A\sigma_{xj}}{A\left(\sigma_x + \sigma_{xj}\right) + C\sigma_y}\right)\left(\frac{A\left(\sigma_x - \sigma_{xj}\right) + C\sigma_y}{A\sigma_x + A\sigma_{xj}}\right)\right| \\ &= \left|\prod_{j=1}^{n}\left(\frac{c_{gx} - \left(A\sigma_{xj} + \left(C/2\right)\sigma_y\right)}{c_{gx} + \left(A\sigma_{xj} + \left(C/2\right)\sigma_y\right)}\right)\left(\frac{c_{gx} - \left(A\sigma_{xj} - \left(C/2\right)\sigma_y\right)}{c_{gx} + \left(A\sigma_{xj} - \left(C/2\right)\sigma_y\right)}\right)\right|.\end{aligned} \tag{2.36}$$

From (2.12), (2.18) and (2.19) we have $c_{gx} = A\sigma_x + \left(C/2\right)\sigma_y = +\sqrt{4A - \left(4AB - C^2\right)\sigma_y^2}\Big/2 \geq 0$. Hence the group velocity in (2.36) is non-negative, i.e., it is the group velocity of the incident wave mode propagating rightward ($c_{gx} \geq 0$).

Equation (2.36) shows that for a given $\sigma_y \in \mathbb{R}$, $R_n = 0$ for all modes with group velocities $c_{gx} = A\sigma_{xj} + \left(C/2\right)\sigma_y$ and $c_{gx} = A\sigma_{xj} - \left(C/2\right)\sigma_y$. Hence these are referred to as the reference group velocities corresponding to the reference slownesses in (2.35). Noting that the PMDL is exact for the reference modes, the reference slownesses (2.35) should satisfy the exact dispersion relation (2.5). Substituting (2.35) separately in (2.5), we get the following reference group velocities:

$$\begin{aligned}A\sigma_{xj} + \left(C/2\right)\sigma_y &= A\sigma_{xj} + \left(C/2\right)\left(\frac{-C\sigma_{xj} \pm \sqrt{4B - \left(4AB - C^2\right)\sigma_{xj}^2}}{2B}\right), \\ A\sigma_{xj} - \left(C/2\right)\sigma_y &= A\sigma_{xj} - \left(C/2\right)\left(\frac{C\sigma_{xj} \pm \sqrt{4B - \left(4AB - C^2\right)\sigma_{xj}^2}}{2B}\right).\end{aligned} \tag{2.37}$$

Note that either the positive or the negative square root should be chosen in both the equations of (2.37) and either choice leads to the same pair of group velocities. By defining,

$$c_j = A\sigma_{xj} + \left(C/2\right)\left(\frac{-C\sigma_{xj} + \sqrt{4B - \left(4AB - C^2\right)\sigma_{xj}^2}}{2B}\right),$$
$$\overline{c}_j = A\sigma_{xj} + \left(C/2\right)\left(\frac{-C\sigma_{xj} - \sqrt{4B - \left(4AB - C^2\right)\sigma_{xj}^2}}{2B}\right), \qquad (2.38)$$

we can rewrite (2.36) using (2.37) and (2.38) as:

$$\left|R_n\right| = \left|\prod_{j=1}^{n}\left(\frac{c_{gx} - c_j}{c_{gx} + c_j}\right)\left(\frac{c_{gx} - \overline{c}_j}{c_{gx} + \overline{c}_j}\right)\right| \quad (c_{gx} \geq 0) \quad : \begin{matrix} Reflection\ coefficient\ . \\ (group\ velocity\ form) \end{matrix} \qquad (2.39)$$

For any given parameter σ_{xj}, the PMDL is exact ($R_n = 0$) for wave modes with two different group velocities c_j, $\overline{c}_j$ given by (2.38) and hence these are the reference group velocities. The requirement $c_{gx} \geq 0$ in (2.39) is just a reminder that the c_{gx} in (2.39) is the group velocity of the incident wave mode that is propagating rightward.

2.4.3 Points of interpolation

Since the n - layer PMDL is exact for the reference modes, the vertical and horizontal slowness pairs of these modes are the points at which (2.27) interpolates (2.11). The reference horizontal slownesses given by (2.35) can be substituted in (2.11) to get the reference vertical slownesses $\sigma_y = \pm\sigma_{yj}, \pm\overline{\sigma}_{yj}$, where,

$$\sigma_{yj} = \frac{-C\sigma_{xj} + \sqrt{4B - \left(4AB - C^2\right)\sigma_{xj}^2}}{2B},$$
$$\overline{\sigma}_{yj} = \frac{-C\sigma_{xj} - \sqrt{4B - \left(4AB - C^2\right)\sigma_{xj}^2}}{2B}. \qquad (2.40)$$

For a given parameter σ_{xj}, there exist two reference group velocities (c_j, $\overline{c}_j$), and for each reference group velocity, there exist two reference wave modes. Hence there are four reference modes for every σ_{xj}; these four modes (with their group velocities) are given by:

$$\left.\begin{array}{l} e^{i\omega\left(\sigma_{xj}x+\sigma_{yj}y-t\right)} \\ e^{i\omega\left(\left(\sigma_{xj}+\left(C/A\right)\sigma_{yj}\right)x-\sigma_{yj}y-t\right)} \end{array}\right\} \quad c_{gx} = c_j, \qquad (2.41)$$

$$\left.\begin{array}{l} e^{i\omega\left(\sigma_{xj}x+\bar{\sigma}_{yj}y-t\right)} \\ e^{i\omega\left(\left(\sigma_{xj}+\left(C/A\right)\bar{\sigma}_{yj}\right)x-\bar{\sigma}_{yj}y-t\right)} \end{array}\right\} \quad c_{gx} = \overline{c}_j.$$

Hence, for every σ_{xj}, the PMDL slowness (2.27) interpolates the exact slowness (2.11) at the four points given by $(\sigma_{yj}, \sigma_{xj})$, $(-\sigma_{yj}, \sigma_{xj} + (C/A)\sigma_{yj})$, $(\overline{\sigma}_{yj}, \sigma_{xj})$ and $(-\overline{\sigma}_{yj}, \sigma_{xj} + \left(C/A\right)\overline{\sigma}_{yj})$. It should be noted that these four points of interpolation need not necessarily be distinct; For $C \neq 0$ (tilted anisotropy of Figure 2.2), there are indeed four distinct points of interpolation when $\sigma_{xj} \neq \pm\sqrt{4B/(4AB - C^2)}$ but only two distinct points of interpolation (each with multiplicity 2) when $\sigma_{xj} = \pm\sqrt{4B/(4AB - C^2)}$. Similarly for $C = 0$ (isotropy and untilted anisotropy of Figure 2.2), there are two distinct points of interpolation (each with multiplicity 2) when $\sigma_{xj} \neq \pm\sqrt{4B/(4AB - C^2)}$ and just one point of interpolation (with a multiplicity of 4) when $\sigma_{xj} = \pm\sqrt{4B/(4AB - C^2)}$. However, for every choice of σ_{xj}, there are four points of interpolation counted *with multiplicity*. Since a n-layer PMDL has n parameters (σ_{xj} with $j = 1 \cdots n$), it has $4n$ points of interpolation in all counted with multiplicity. These $4n$ points for a single layer PMDL $(n = 1)$ are graphically represented on a typical slowness curve in (left).

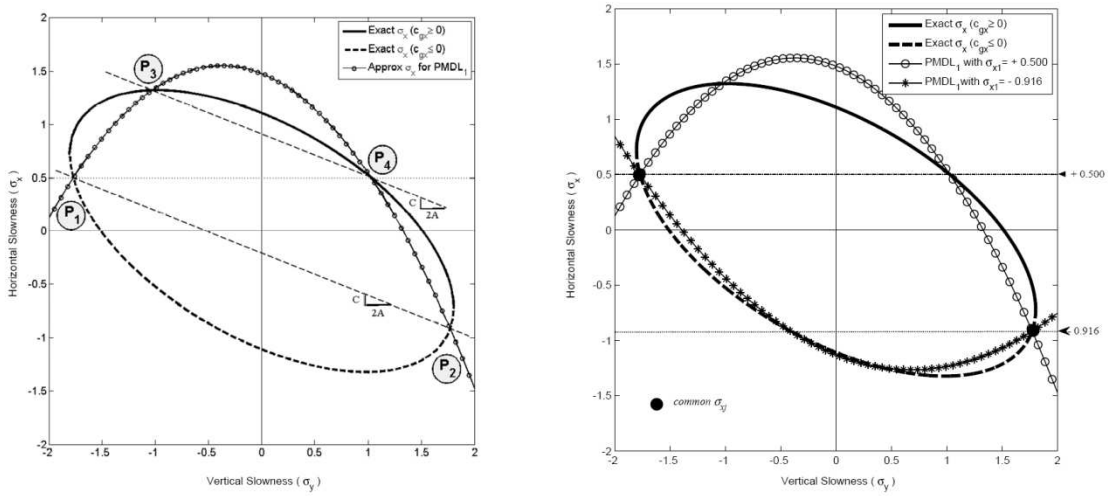

Figure 2.7. *Left:* The four points of at which a 1 – layer PMDL dispersion relation (approximate) matches the exact dispersion relation are the four modes for which the 1 – layer PMDL is exact. *Right:* The two parameters σ_{xj} that result in a particular reference group velocity of c_j (or $\overline{c}_j$) for a 1 – layer PMDL.

A few observations about interpolation points should be kept in mind: (a) A choice of real parameters $\sigma_{xj} \in \mathbb{R}$ may lead to complex σ_{yj} and $\overline{\sigma}_{yj}$. This means that the interpolation points need not be real and hence may not be depicted on a typical slowness diagram which is a plot of $(\sigma_y, \sigma_x) \in \mathbb{R}$. However, (2.27) still interpolates (2.11), albeit now in complex space $(\sigma_y, \sigma_x) \in \mathbb{C}$. (b) We can choose the parameters σ_{xj} arbitrarily but we cannot choose the two related reference group velocities (c_j, $\overline{c}_j$) independent of one another. Of the three - σ_{xj}, c_j, $\overline{c}_j$ - only one can be chosen. A choice of σ_{xj} uniquely determines c_j and $\overline{c}_j$ from (2.38) and this is the only choice that we truly have. For theoretical purposes however, it may appear advantageous to be able to design a PMDL that is exact for a given group velocity. This is equivalent to choosing c_j (or $\overline{c}_j$). A choice of c_j (or $\overline{c}_j$) however can be obtained from two different σ_{xj} in general and this in turn results in two different $\overline{c}_j$ (or c_j) - this is shown in Figure 2.7. Because of this ambiguity, we focus on σ_{xj} as the parameters of the

PMDL. Note that this is true only for tilted anisotropy; in the untilted anisotropic or isotropic case, there is a unique parameter for a given group velocity.

2.5 Accuracy

2.5.1 Accuracy Criterion

The ideal accuracy criterion for a n-layer PMDL is $R_n(c_{gx}) = 0$ for all $c_{gx} \geq 0$. We use $R_n(c_{gx})$ to emphasize the fact that the reflection coefficient is a function of the group velocity of the incident wave mode (see (2.39)). The reflection coefficient of a n-layer PMDL (2.39) is zero for exactly $2n$ group velocities given by the reference group velocities c_j, $\overline{c}_j$ ($j = 1 \ldots n$). Hence, the ideal of $R_n(c_{gx}) = 0$ for all $c_{gx} \geq 0$ can never be realized in practice by a n-layer PMDL with a finite n. This necessitates the formulation of an attainable accuracy criterion.

Accuracy criterion: An n-layer PMDL is considered accurate if, by increasing the number of layers n, the magnitude of its reflection coefficient can be made arbitrarily small for every rightward propagating wave mode, i.e.,

$$\lim_{n\to\infty} \left| R_n(c_{gx}) \right| = 0 \qquad \forall\ c_{gx} \geq 0 : Accuracy\ criterion. \tag{2.42}$$

To be precise (2.42) is a *convergence* criterion that is necessary for a PMDL to act as a meaningful ABC for rightward propagating waves. If the rate of convergence is slow, the number of PMDL layers required for sufficient accuracy might render the ABC inefficient. The usage of the term *accuracy* instead of the term *convergence* is mainly for the sake of compatibility with existing ABC literature.

2.5.2 Sufficient condition for accuracy

In order to facilitate the derivation of conditions under which a PMDL is accurate, we restate the accuracy criterion and reformulate the reflection coefficient. The accuracy criterion (2.42) , written separately for zero and positive group velocities is:

$$\lim_{n\to\infty}\left|R_n(c_{gx})\right| = 0 \qquad for\ c_{gx} = 0\,, \tag{2.43}$$

$$\lim_{n\to\infty}\left|R_n(c_{gx})\right| = 0 \qquad \forall\ c_{gx} > 0\,. \tag{2.44}$$

The reflection coefficient is given by (2.39) and can be expressed as:

$$\left|R_n\right| = \left|\prod_{j=1}^{n} R_{nj}\right| = \left|\prod_{j=1}^{n} r_j \overline{r}_j\right|, \tag{2.45}$$

where,

$$R_{nj} = r_j \overline{r}_j, \quad r_j = \left(\frac{c_{gx} - c_j}{c_{gx} + c_j}\right), \quad \overline{r}_j = \left(\frac{c_{gx} - \overline{c}_j}{c_{gx} + \overline{c}_j}\right) \quad for\ c_{gx} \geq 0,\ j = 1 \ldots n\,. \tag{2.46}$$

The accuracy criteria (2.43) and (2.44) can be satisfied by choosing either zero, negative or positive reference group velocities ($c_j, \overline{c}_j$) in (2.45) and (2.46).

Consider (2.43) with various (zero, negative and positive) reference group velocities. Criterion (2.43) cannot be satisfied if all reference group velocities are non-zero because in this case, $\left|R_n\right| = 1$ and hence $\lim_{n\to\infty}\left|R_n\right| = 1$ for $c_{gx} = 0$. One way to ensure accuracy for $c_{gx} = 0$ is to have at least one zero reference group velocity. This makes the n-layer PMDL exact for zero group velocity modes and hence by definition $\left|R_n\right| = 0$ for $c_{gx} = 0$ (which satisfies (2.43)). In other words, the PMDL will allow wave modes with $c_{gx} = 0$ to exist in the left half-space (interior). While this is perfectly acceptable from the viewpoint of accuracy - an exact right half-space that the PMDL is trying to emulate does allow zero group velocity modes in the interior – we do not allow zero reference group velocity because of the following reasons. Since untilted anisotropy (and isotropy) are special cases of tilted anisotropy, we expect the conclusions presented here to hold for these cases as well i.e. for the case $C = 0$ in Figure 2.2. But from (2.38), it is clear that for $C = 0$, a zero reference group velocity translates to $\sigma_{xj} = 0$ which in turn requires $L_j = \infty$. This is not practically

feasible and we violate (2.43) and consider the PMDL with $\left|R_n\right| = 1$ (and with $\lim_{n\to\infty}\left|R_n\right| = 1$) for $c_{gx} = 0$ to be *'accurate enough'*. An even more potent reason for not allowing zero reference group velocites is that such a choice will lead to ill-posedness of the ABC in *transient* modeling of acoustic waves (see [40]). Moreover, for the case of untilted anisotropy and isotropy, (2.43) cannot be satisfied by any local ABC. This discussion thus eliminates (2.43) and entirely excludes the choice of zero reference group velocities. This leaves us with a choice of positive or negative reference group velocities in trying to satisfy (2.44).

Consider the choice of negative reference group velocities in ensuring (2.44). Without loss of generality let $c_1 < 0$. As $c_{gx} \to -c_1 (> 0)$, we have $\left|r_1\right| \to \infty$. Unless there is another factor r_j or $\overline{r}_j$ in (2.45) that tends to zero as fast or faster than $\left|r_1\right| \to \infty$, the reflection coefficient will grow without bound $\left(\left|R_n\right| \to \infty\right)$ and hence (2.44) cannot be satisfied for c_{gx} in the neighborhood of $-c_1$. It is however possible to prevent the unbounded growth in $\left|R_n\right|$ by a careful choice of other reference group velocities. For example if $c_2 = -c_1$, then $\left|r_2\right| \to 0$ as $c_{gx} \to -c_1$. The reflection coefficient need not necessarily tend to ∞ now because $\left|r_1 r_2\right| = 1$ and this prevents the unbounded growth of $\left|R_n\right|$ due to $\left|r_1\right| \to \infty$. However, such a choice of parameters results in a loss of factors in the expression for R_n; the factor r_2 is 'lost' in canceling out the effect of r_1 and does not contribute to reducing the reflection coefficient. In many cases this reduces the efficiency of a PMDL i.e. we might need a larger n to ensure a sufficiently small R_n. Hence, we will not consider negative reference group velocities unless they are necessary for meeting the accuracy criterion (2.44).

Fortunately, it is possible to satisfy (2.44) with only positive reference group velocities. Noting the product form of (2.45), the accuracy criterion (2.44) is satisfied if each term in the product is less than one. Thus, a sufficient condition for (2.44) is:

$$\left|R_{nj}\right| < 1 \quad \forall\ c_{gx} > 0\,. \tag{2.47}$$

It is obvious from (2.45) that a choice of positive reference group velocities ($c_j > 0$ and $\overline{c}_j > 0$) is sufficient for (2.47) to be satisfied. Hence a choice of $c_j > 0$ and $\overline{c}_j > 0$ is also sufficient for (2.44). Using (2.38), this sufficient condition becomes

$$A\sigma_{xj} + \left(C/2\right)\left(\frac{-C\sigma_{xj} \pm \sqrt{4B - \left(4AB - C^2\right)\sigma_{xj}^2}}{2B}\right) > 0\,. \tag{2.48}$$

Using (2.10), (2.48) can be reduced to,

$$\left(4AB - C^2\right)\sigma_{xj} > \left|C\sqrt{4B - \left(4AB - C^2\right)\sigma_{xj}^2}\right|. \tag{2.49}$$

Noting that $4AB - C^2 > 0$ (see (2.10)), (2.49) can be reduced to,

$$\sigma_{xj} > \frac{\left|C\sqrt{4B - \left(4AB - C^2\right)\sigma_{xj}^2}\right|}{\left(4AB - C^2\right)}, \tag{2.50}$$

which, on squaring and rearranging results in,

$$\sigma_{xj} > \left|\frac{C}{\sqrt{A\left(4AB - C^2\right)}}\right|. \tag{2.51}$$

The condition (2.51) has a simple geometric interpretation that is shown in Figure 2.8 (left).

The above discussion (from (2.48) onward) implicitly assumed that $c_j, \overline{c}_j \in \mathbb{R}$ which is not true when $\sigma_{xj} > 2\sqrt{B}\Big/\left(\sqrt{4AB - C^2}\right)$. However, for $\sigma_{xj} > 2\sqrt{B}\Big/\left(\sqrt{4AB - C^2}\right)$, (2.47) is satisfied if $\mathrm{Re}\left(c_j\right) = \mathrm{Re}\left(\overline{c}_j\right) > 0$, which in turn requires:

$$for\ c_j, \overline{c}_j \notin \mathbb{R}: \qquad \mathrm{Re}\left(c_j\right) = \mathrm{Re}\left(\overline{c}_j\right) = \frac{\left(4AB - C^2\right)}{4B}\sigma_{xj} > 0 \Leftrightarrow \sigma_{xj} > 0\,. \tag{2.52}$$

The condition (2.51) encompasses (2.52), and (2.51) is hence a sufficient condition for satisfying the accuracy criterion (2.47). Note that (2.51) results in $\left|R_n\right| = 1$ for $c_{gx} = 0$; for reasons stated before, we consider this to be acceptable.

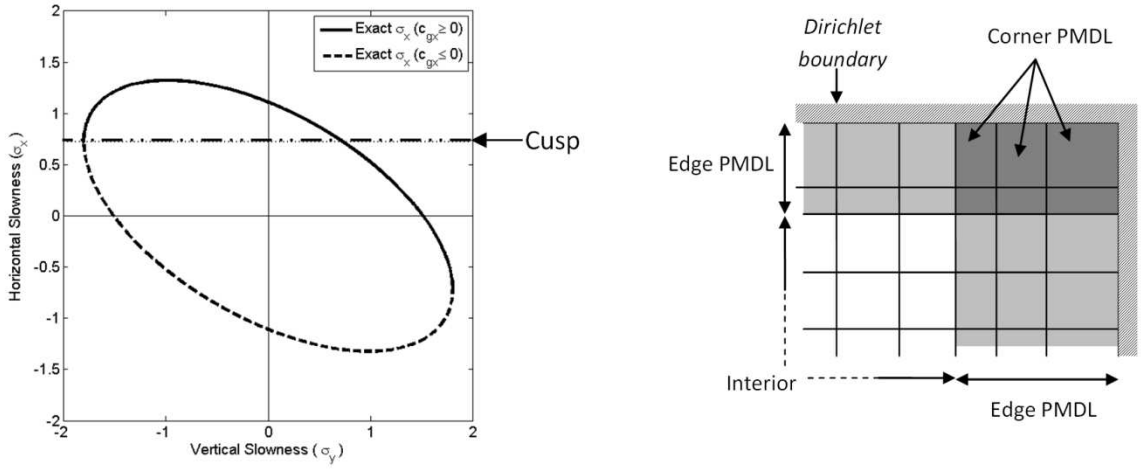

Figure 2.8. ***Left:*** Geometric interpretation of the sufficient condition for accuracy. The parameters of PMDL should be chosen above the horizontal line that defines the 'cusp' of the ellipse**.** *Right:* Corner PMDL with parameters (layer lengths) consistent with the two edge PMDLs.

2.5.3 Relation between Stiffness and Group velocity

It should be noted that being able to express the reflection coefficient in terms of group velocities is key to the derivation of the simple accuracy condition (2.51). Not every ABC produces a reflection coefficient of this kind. A straightforward implementation of Higdon's multidirectional ABCs or an implementation of complex coordinate stretching in the direction of unboundedness (traditional PML) will result in a reflection coefficient of the form,

$$\tilde{R}_n = \prod_{j=1}^{n} \left(\frac{\sigma_x - \sigma_{xj}}{\sigma_x + \sigma_{xj}} \right) = \prod_{j=1}^{n} \left(\frac{c_{pxj} - c_{px}}{c_{pxj} + c_{px}} \right), \tag{2.53}$$

where $c_{pxj} = 1/\sigma_{xj}$ are the reference phase velocities. For isotropic and untilted anisotropic media ($C = 0$), $c_{gx} = A/c_{px}$ from (2.12); approximating phase velocities is the same as approximating group velocities and a choice of $\sigma_{xj} > 0$ (or $c_{pxj} > 0$) is enough to ensure accuracy in this case. An ABC that results in a reflection coefficient of the form (2.53) is however not too useful for the case of tilted anisotropy because, as discussed in Section 2.3.4, there exist modes with positive phase velocities but with negative group velocities (and vice versa). In this case, a choice of positive reference phase velocities $c_{pxj} > 0$ is no guarantee that the ABC will accurately absorb modes with positive group velocities. While Engquist and Majda's rational approximation of the square root operator, when applied to anisotropic media, will lead to the group velocity form of the reflection coefficient (2.39), it is not of much practical interest because of its implementation being restricted to lower orders. Moreover, since their ABC was never developed for cases with phase and group velocities of differing signs, it is not apparent that their rational approximation was developed with the explicit goal of capturing positive group velocities.

The n-layer PMDL approximates the stiffness (2.18) by a rational function instead of approximating the horizontal slowness directly. It can be seen from (2.18) and (2.12) that the stiffness for propagating wave modes is in fact related to their group velocity as $K = -i\omega c_{gx}$. Hence, approximating stiffness is the same as approximating group velocities. It is therefore not surprising that the form of the rational approximation (2.25) with (2.21) and (2.22) leads us to a reflection coefficient that is expressible purely in terms of group velocities (2.39). As noted before, this form of (2.39) is *key* to the derivation of the simple accuracy condition (2.51).

2.5.4 Corners

The PMDL formulation is known to be applicable to convex polygonal corners [20,21]. Analogous to the description of corner PML in [11], a corner PMDL acts as an ABC for each of the edge PMDLs. Since the parameters of the corner PMDL are consistent with those of the edge PMDLs, as shown in Figure 2.8 (right), it will absorb the corresponding 'outgoing' waves provided the parameters of *both* of the edge PMDLs satisfy (2.51).

2.6 Numerical Examples

We consider a 2D model problem with a square or rectangular interior consisting of a tilted anisotropic acoustic medium that is modeled by regular square bilinear finite elements. The exterior is represented by ABCs on all four edges/corners. For a given frequency ω, the characteristic wavenumber is $k = \omega / c$, with $c = \sqrt{1/a^2 + 1/b^2}$ being the velocity (see (2.6)). Using a conservative element size, $h = 0.05 / \omega$, we get the number of elements per characteristic wavelength $N_e = 2\pi c / \omega h \approx 120$. Using the material parameters $a = 1, b = 2, \beta = 30^o$ in (2.7), the accuracy condition (2.51) for PMDL in the *x* direction is $\sigma_{xj} > 0.72$. For PMDL in the *y* direction we have $a = 1, b = 2, \beta = 60^o$ and hence (2.51) becomes $\sigma_{yj} > 0.98$. For simplicity, in all experiments we assume $\sigma_{yj} = 1.5\sigma_{xj}$ and $\sigma_{x1} = \sigma_{x2} = \ldots = \sigma_{xn}$, thus reducing the number the PMDL parameters to just one. The excitation consists of a normalized Gaussian given by $\left(\sigma\sqrt{2\pi}\right)^{-1} e^{-\left(0.5(r/\sigma)^2\right)}$ for $r \le 5\sigma$ and zero elsewhere. Here r is the radial distance from the Gaussian center and $\sigma = 1.5h$. The Gaussian center is positioned at the center of the lower left quarter. For comparison, the exact solution for tilted anisotropic medium is obtained by appropriately transforming in space, the Green's function of an isotropic medium (the Hankel function). The interior is modeled by a mesh of 600×600 finite elements with two PMDL layers forming the exterior on all four edges. The frequency is assumed to be $\omega = 1000$.

The accuracy obtained for different values of the PMDL parameters σ_{xj} can be visually inferred from Figure 2.9 and is numerically quantified in Figure 2.10. The relative error is calculated as $\left\|u_{PMDL} - u_{exact}\right\|_2 \Big/ \left\|u_{exact}\right\|_2$ and expressed as a percentage. The least accurate results are obtained when σ_{xj} is below the cusp i.e. when the parameters violate the accuracy criterion (2.51), which in the present case is $\sigma_{xj} > 0.72$. Note that we have used $\sigma_{yj} = 1.5\sigma_{xj}$ and thus the accuracy criterion is violated in the y direction too. The inaccuracies of violating (2.51) are dramatic in the first two snapshots of Figure 2.9.

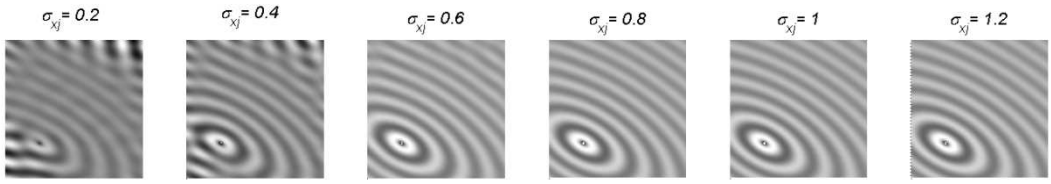

Figure 2.9. Interior solution for a 2 – layer PMDL exterior with various PMDL parameters. The first three have parameters under the cusp and thus violate the accuracy criterion.

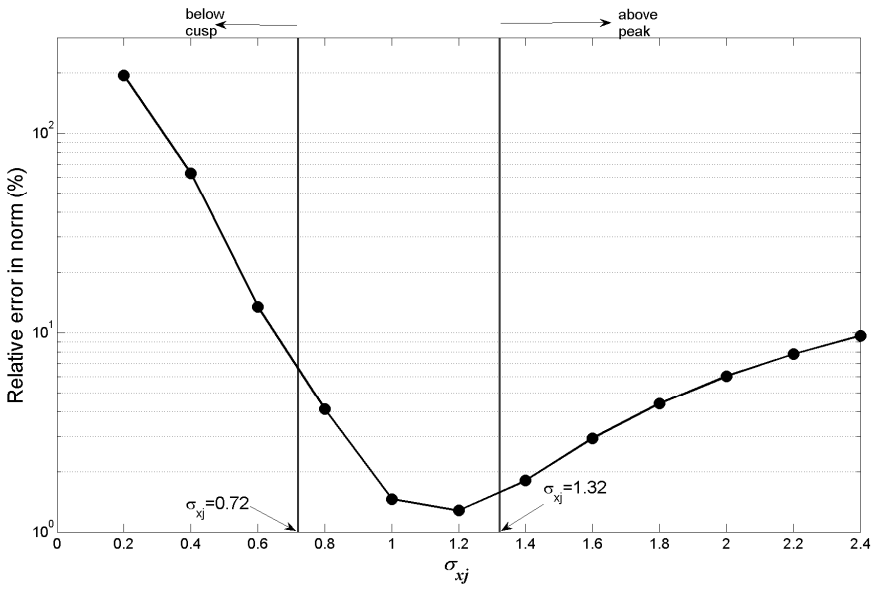

Figure 2.10. Relative error in norm for a 2 layer PMDL with various parameters. The lines demarcating the cusp of the slowness ellipse and its peak are shown.

Figure 2.10 shows that the minimum relative error obtained with a 2-layer PMDL is around 1%. It should be noted that this includes the interior discretization error which can be reduced with a reduction in the interior element size; experiments with finer interior discretizations have confirmed this. Since we wish to compare the relative effect of changing PMDL parameters, our observations are valid as long as the interior discretization remains constant.

The relative error is also seen to increase when the parameters are chosen above the peak of the ellipse. This is because of the fact that for such parameters there will be no interpolation points on the ellipse and since we wish to capture a part of the ellipse (the positive group velocity part) we should expect some loss in accuracy in this case. The slowness diagrams presented in Figure 2.11 clearly demonstrate this. The case of $\sigma_{xj} = 0.4$ violates (2.51) with the parameter being below the cusp and the capturing of the negative group velocity branch is evident. The remaining three cases with $\sigma_{xj} = 1.0, 2.4, 4.0$ all lie

above the cusp and hence approximate the positive group velocity branch only. However $\sigma_{xj} = 1.0$ also lies under the peak and hence interpolates the ellipse at $\sigma_x = 1.0$. The last two cases lie beyond the peak and hence have no points of interpolation with the exact curve.

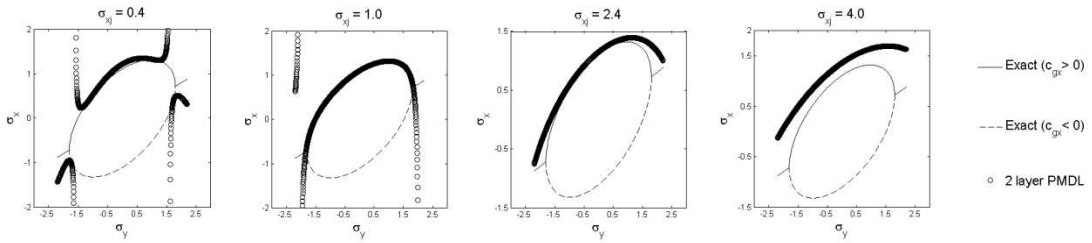

Figure 2.11. Slowness diagrams for 2 layer PMDL approximation with parameters chosen below the cusp, between the cusp and peak and above the peak.

It is expected that increasing the number of PMDL layers should reduce the error in approximation as long as (2.51) is satisfied. The relative error in approximation with increasing number of PMDL layers for various PMDL parameters that satisfy (2.51) is shown in Figure 2.12 and it depicts a clear worsening of the approximation with increasing number of PMDL layers especially for lower PMDL parameters. This counter intuitive behavior can be explained by studying the slowness diagrams shown in Figure 2.13 for a large number of PMDL layers. Since the parameters of PMDL were chosen to be real, they approximate the propagating part of the slowness curve (the tilted ellipse) without capturing the evanescent part (σ_y beyond the ellipse). As the number of layers increase, the PMDL approximates the propagating part of the slowness curve with rational polynomials of increasing degrees. While this results in a better approximation inside the ellipse, just outside the ellipse, however, it invariably leads to the very highly oscillatory behavior typical of high degree rational functions due to the increasing number of alternating poles and zeros. This indicates that there are large errors in the evanescent spectrum, leading to worsening of the solution quantified in Figure 2.12. The interior solution corresponding to the slowness diagrams of

Figure 2.13 are shown in Figure 2.14 and clearly show the desired solution being polluted near the boundary ($\sigma_{xj} = 1.0,\ \ n = 6$) and being completely overshadowed throughout the interior ($\sigma_{xj} = 1.0,\ \ n = 10$).

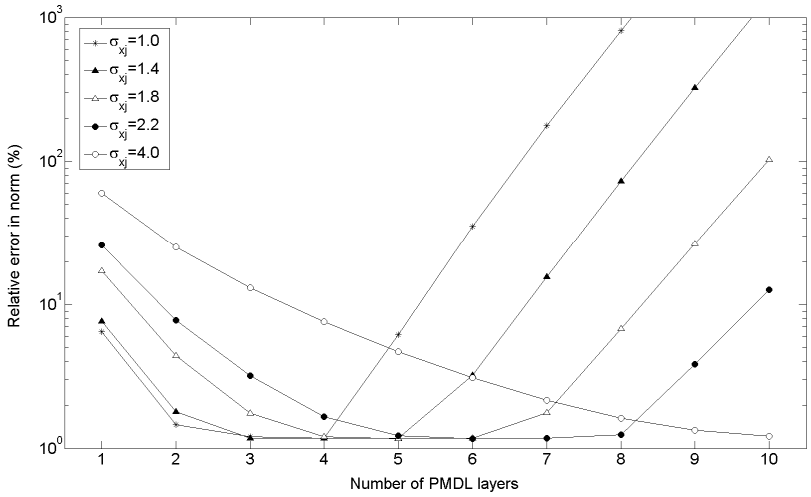

Figure 2.12. Relative error in PMDL approximation with increasing number of PMDL layers for various PMDL parameters that satisfy the accuracy criterion.

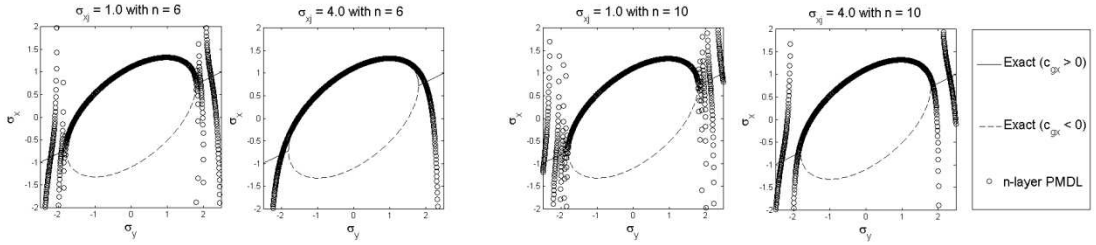

Figure 2.13. Slowness diagrams for large number of PMDL layers (6 and 10) with different PMDL parameters

Notice however, that using parameters far above the cusp, $\sigma_{xj} = 4.0 \gg 0.72$ for instance, will result in a bad approximation for smaller number of layers, but a much better

approximation for larger number of layers according to Figure 2.12. This can be explained by comparing the last diagram in Figure 2.11 ($\sigma_{xj} = 4.0,\ \ n = 2$) with the second and fourth diagrams in Figure 2.13 ($\sigma_{xj} = 4.0,\ \ n = 6, 10$). It is also interesting to note that the error does not reduce beyond 1% (approximately) irrespective of the number of PMDL layers used with any parameter satisfying the accuracy criterion (2.51). With the knowledge that this minimum error reduces with finer interior discretization (not shown here), we can conclude that (a) this 1% error is mainly due to the interior discretization and (b) just 2 to 3 PMDL layers are sufficient to reduce the error to the interior discretization error as long as the parameters of PMDL satisfy the accuracy criterion.

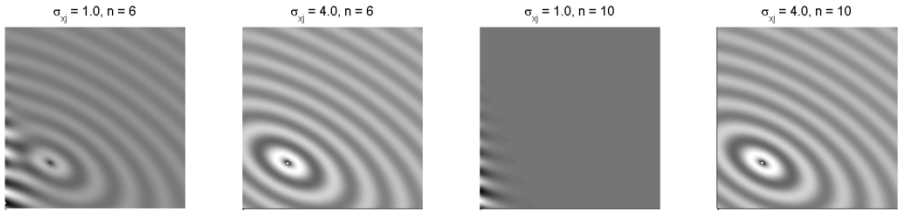

Figure 2.14. Interior solution for large number of PMDL layers (n = 6, 10) with PMDL parameters chosen above and near the cusp ($\sigma_{xj} = 1.0$) and above and far away from the cusp ($\sigma_{xj} = 4.0$).

We conclude this section with two methods for handling the errors due to the presence of clustered zeros and poles for large number of PMDL layers. Just like PMDL layers with real parameters capture propagating waves, PMDL layers with *imaginary* or *complex* parameters have been shown to capture decaying waves (with purely imaginary and complex wavenumbers) [22,38]. These are termed the *padding* layers (purely imaginary parameters) and *complex PMDL* (complex parameters). The performance of PMDL with varying number of padding layers is shown in Figure 2.15. The parameters of the padding layers are chosen as those that smoothen the highly oscillatory part of the slowness curves the most. Similar

results are obtained for PMDL parameters chosen much above the cusp $\sigma_{xj} \gg 0.72$. The slowness diagrams with padding and complex layers and their visual snapshots are shown in Figure 2.16, Figure 2.17 and Figure 2.18. The smoothening of the real part of the slowness approximation is evident in Figure 2.16; this leads to a better approximation of propagating waves. The imaginary part of the approximation is shown in Figure 2.17; the presence of the non-zero imaginary part in the approximation models decaying waves appropriately. The corresponding snapshots can be seen in Figure 2.18.

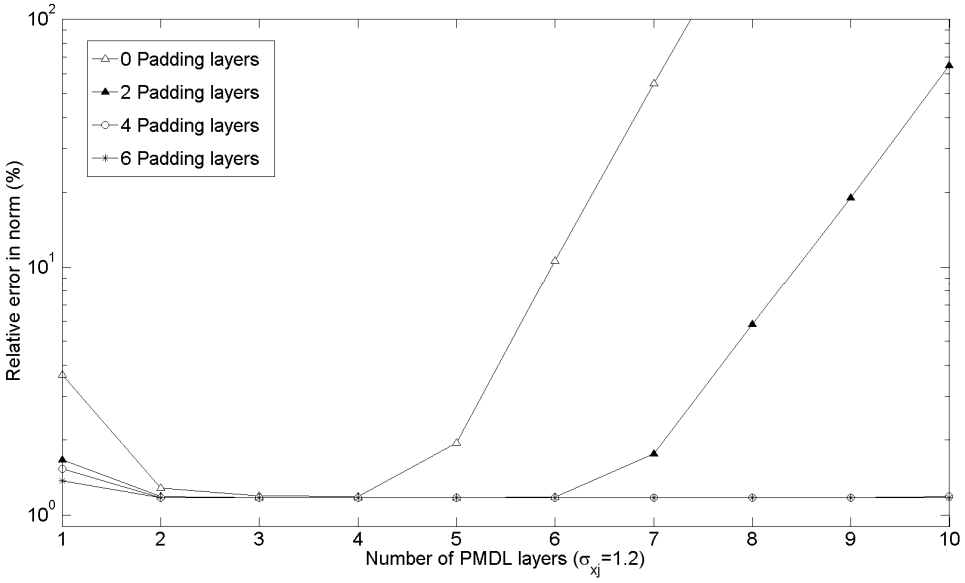

Figure 2.15. Performance of PMDL when used along with padding layers.

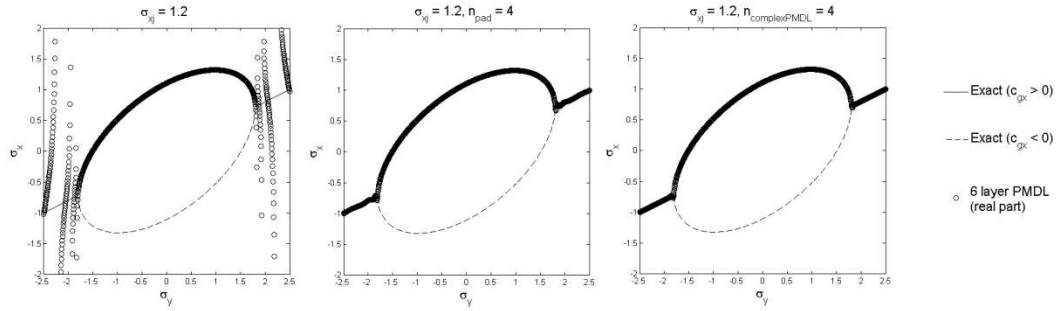

Figure 2.16. Real part of the slowness approximation for 6 layer PMDL with $\sigma_{xj} = 1.2$ and with padding layers and complex PMDL layers

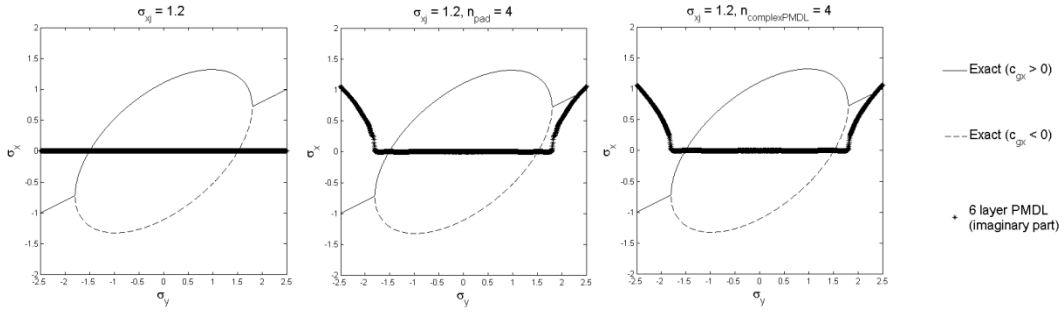

Figure 2.17. Imaginary part of the slowness approximation for 6 layer PMDL with $\sigma_{xj} = 1.2$ and with padding layers and complex PMDL layers.

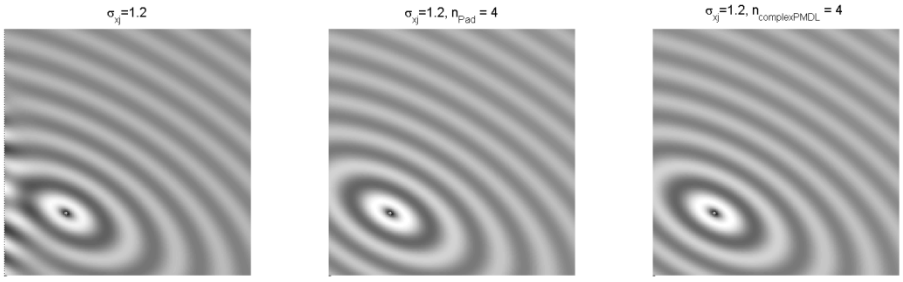

Figure 2.18. Interior solution for 6 layer PMDL with $\sigma_{xj} = 1.2$ and with padding layers and complex PMDL layers

2.7 Summary and Conclusions

A sufficient condition for the accuracy of PMDL ABC for the time harmonic modeling of scalar waves in an anisotropic acoustic medium is presented. In deriving this accuracy criterion, the PMDL formulation is shown to naturally overcome challenges posed by the existence of wave modes with differing phase and group velocity signs *without the need of an explicit coordinate transformation;* the absence of such transformations make the current study more amenable to extensions involving layered media. The distinctive property of PMDL, namely approximation of half-space stiffness instead of the wavenumber, is central to the ability of PMDL to capture the correct group velocities even when the group and phase velocities are not aligned in the same direction. This is because the group velocity and stiffness are related (at least in this case) and PMDL approximates the stiffness. We hypothesize that the link between group velocity and stiffness extends to general vector systems and that this link can be used to ensure accuracy of PMDL in general anisotropic media.

PMDL is known to possess several advantages over other local ABCs and is thus used for the present study. The PMDL derivation is applicable to any second order hyperbolic system and to general anisotropic, heterogeneous exteriors, with heterogeneity confined to directions orthogonal to the direction of unboundedness. PMDL is equally applicable to propagating and evanescent waves and can be implemented to an arbitrarily high degree of accuracy without discretization errors. PMDL is also linked to PML and show promise in inheriting their versatility.

The present study is confined to propagating scalar wave modes in homogeneous (though anisotropic) exteriors. Since none of these restrictions are due to actual limitations of the PMDL formulation, further studies will (hopefully) eliminate all of them. Establishing links between group velocity and stiffness for complicated media and taking evanescent waves into account are of immediate concern. Further developments need to address more complex vector wave equations related to anisotropic electromagnetism and elastodynamics.

2.8 References

[1] D. Givoli, Nonreflecting Boundary-Conditions, J. Comput. Phys. 1 (1991), 1-29.

[2] S.V. Tsynkov, Numerical solution of problems on unbounded domains. A review, Appl. Numer. Math. 4 (1998), 465-532.

[3] T. Hagstrom, New results on absorbing layers and radiation boundary conditions, Topics in Computational Wave Propagation - Direct and Inverse Problems (2003), 1-42.

[4] E.L. Lindman, Free-Space Boundary-Conditions for Time-Dependent Wave-Equation, J. Comput. Phys. 1 (1975), 66-78.

[5] B. Engquist and A. Majda, Absorbing Boundary-Conditions for Numerical-Simulation of Waves, Math. Comput. 139 (1977), 629-651.

[6] B. Engquist and A. Majda, Radiation Boundary-Conditions for Acoustic and Elastic Wave Calculations, Commun. Pure Appl. Math. 3 (1979), 313-357.

[7] A. Bayliss and E. Turkel, Radiation Boundary-Conditions for Wave-Like Equations, Commun. Pure Appl. Math. 6 (1980), 707-725.

[8] R.L. Higdon, Numerical Absorbing Boundary-Conditions for the Wave-Equation, Math. Comput. 179 (1987), 65-90.

[9] D. Givoli, High-order local non-reflecting boundary conditions: a review, Wave Motion 4 (2004), 319-326.

[10] T. Hagstrom, A. Mar-Or and D. Givoli, High-order local absorbing conditions for the wave equation: Extensions and improvements, J. Comput. Phys. 6 (2008), 3322-3357.

[11] J.P. Bérenger, A Perfectly Matched Layer for the Absorption of Electromagnetic-Waves, J. Comput. Phys. 2 (1994), 185-200.

[12] W.C. Chew, J.M. Jin and E. Michielssen, Complex coordinate stretching as a generalized absorbing boundary condition, Microwave Opt Technol Lett 6 (1997), 363-369.

[13] W.C. Chew and W.H. Weedon, A 3d Perfectly Matched Medium from Modified Maxwells Equations with Stretched Coordinates, Microwave Opt Technol Lett 13 (1994), 599-604.

[14] Z.S. Sacks, D.M. Kingsland, R. Lee and J.F. Lee, A perfectly matched anisotropic absorber for use as an absorbing boundary condition, IEEE Trans. Antennas Propag. 12 (1995), 1460-1463.

[15] F. L. Teixeira, W. C. Chew, Analytical Derivation of a Conformal Perfectly Matched Absorber for Electromagnetic Waves, Microwave Opt Technol Lett 17 (1998), 231-236.

[16] Kuzuoglu and Mittra, Frequency dependence of the constitutive parameters of causal perfectly matched anisotropic absorbers, IEEE Microwave Guided Wave Lett. 12 (1996), 447.

[17] Roden and Gedney, Convolution PML (CPML): An efficient FDTD implementation of the CFS-PML for arbitrary media, Microwave Opt Technol Lett 5 (2000), 334.

[18] Meza-Fajardo, Papageorgiou, A nonconvolutional, split-field, perfectly matched layer for wave propagation in isotropic and anisotropic elastic media: Stability analysis. Bulletin of the Seismological Society of America 4 (2008), 1811-1836.

[19] S. Asvadurov, V. Druskin, M.N. Guddati and L. Knizhnerman, On optimal finite-difference approximation of PML, SIAM J. Numer. Anal. 1 (2003), 287-305.

[20] K.W. Lim, Absorbing Boundary Conditions For Corner Regions, Master's Thesis, North Carolina State University, 2003.

[21] M.N. Guddati and K.W. Lim, Continued fraction absorbing boundary conditions for convex polygonal domains, Int J Numer Methods Eng 6 (2006), 949-977.

[22] M.N. Guddati, K.W. Lim and M.A. Zahid, Perfectly Matched Discrete layers for Unbounded Domain Modeling, in: Computational Methods for Acoustics Problem, F. Magoulès, ed., Saxe-Coburg Publications, Scotland, 2008, pp. 69-98.

[23] Tam CKW, Auriault L, Cambuli F. Perfectly matched layer as an absorbing boundary condition for the linearized Euler equations in open and ducted domains. Journal of Computational Physics 144 (1998), 213-34.

[24] Turkel E, Yefet A. Absorbing PML boundary layers for wave-like equations. Applied Numerical Mathematics 27 (1998), 533-57.

[25] S. Abarbanel, D. Gottlieb and J.S. Hesthaven, Well-posed perfectly matched layers for advective acoustics, J. Comput. Phys. 2 (1999), 266-83.

[26] F.Q. Hu, A stable, perfectly matched layer for linearized Euler equations in unsplit physical variables, J. Comput. Phys. 2 (2001), 455-480.

[27] Hagstrom T. A new construction of perfectly matched layers for hyperbolic systems with applications to the linearized Euler equations, in: Mathematical and numerical aspects of wave propagation, Proceedings Waves 2003, Cohen et al, ed., Springer-Verlag, 2003, pp. 125-129.

[28] E. Bécache, S. Fauqueux and P. Joly, Stability of perfectly matched layers, group velocities and anisotropic waves, J. Comput. Phys. 2 (2003), 399-433.

[29] E. Bécache, A.S. Bonnet-Ben Dhia and G. Legendre, Perfectly matched layers for the convected Helmholtz equation, SIAM J. Numer. Anal. 1 (2004), 409-433.

[30] F.Q. Hu, A Perfectly Matched Layer absorbing boundary condition for linearized Euler equations with a non-uniform mean flow, J. Comput. Phys. 208(2005), 469-492.

[31] E. Bécache, A.S.B.B. Dhia and G. Legendre, Perfectly matched layers for time-harmonic acoustics in the presence of a uniform flow, SIAM J. Numer. Anal. 3 (2006), 1191-1217.

[32] J. Diaz and P. Joly, A time domain analysis of PML models in acoustics, Comput. Methods Appl. Mech. Eng. 29-32 (2006), 3820-3853.

[33] Parrish S, Hu F. PML absorbing boundary conditions for the linearized and nonlinear Euler equations in the case of oblique mean flow. Int.J.Numer.Methods Fluids, 60(2009), 565-589.

[34] Becache E, Givoli D, Hagstrom T. High-order Absorbing Boundary Conditions for anisotropic and convective wave equations. J. of Comput. Phys., 229(2010), 1099-1129.

[35] M.A. Zahid, M.N. Guddati, Padded continued fraction absorbing boundary conditions for dispersive waves, Comput. Methods Appl. Mech. Eng. 29-32 (2006), 3797-3819.

[36] S. Savadatti, M.N. Guddati, Absorbing Boundary Conditions for Scalar Waves in Anisotropic Media: Part 2 - Time-dependent Modeling, J. Comput. Phys. 229-18 (2010), 6644-6662.

[37] M.N. Guddati and J.L. Tassoulas, Continued-fraction absorbing boundary conditions for the wave equation, J. Comput. Acoust. 1 (2000), 139-156.

[38] M.N. Guddati, Arbitrarily wide-angle wave equations for complex media, Comput. Methods Appl. Mech. Eng. 1-3 (2006), 65-93.

[39] T. Hagstrom and T. Warburton, A new auxiliary variable formulation of high-order local radiation boundary conditions: corner compatibility conditions and extensions to first-order systems, Wave Motion 4 (2004), 327-338.

[40] T. Hagstrom and T. Warburton, Complete radiation boundary conditions: minimizing the long time error growth of local methods, http://faculty.smu.edu/thagstrom/HWcomplete.pdf (2008).

[41] R.L. Higdon, Initial-Boundary Value-Problems for Linear Hyperbolic Systems, SIAM Rev 2 (1986), 177-217.

Chapter 3 Accurate and Well-posed Absorbing Boundary Condition for Tilted Anisotropic Acoustics

This chapter is a slightly modified version of the following manuscript: S. Savadatti and M. N. Guddati, Absorbing Boundary Conditions for Scalar Waves in Anisotropic Media. Part 2: Time-dependent Modeling, *Journal of Computational Physics*, Vol. 229, Issue 18, 2010, pp. 6644-6662.

3.1 Abstract

With the ultimate goal of devising effective absorbing boundary conditions (ABCs) for general anisotropic media, we investigate the well-posedness and accuracy aspects of local ABCs designed for the transient modeling of the scalar anisotropic wave equation. The ABC analyzed in this paper is the perfectly matched discrete layers (PMDL), a simple variant of perfectly matched layers (PML) that is also equivalent to rational approximation based ABCs. Specifically, we derive the necessary and sufficient condition for the well-posedness of the initial boundary value problem (IBVP) obtained by coupling an interior and a PMDL ABC. The derivation of the reflection coefficient presented in a companion paper (Chapter 2) has shown that PMDL can correctly identify and accurately absorb outgoing waves with opposing signs of group and phase velocities provided the PMDL layer lengths satisfy a certain bound. Utilizing the well-posedness theory developed by Kreiss for general hyperbolic IBVPs, and the well-posedness conditions for ABCs derived by Trefethen and Halpern for isotropic acoustics, we show that this bound on layer lengths also ensures well-posedness. The time discretized form of PMDL is also shown to be theoretically stable and some instability related to finite precision arithmetic is discussed.

3.2 Introduction

Many wave propagation problems defined on physically unbounded domains can be divided into two regions; the interior and the exterior, with the interface between them termed the computational boundary. The interior is a small bounded region where the solution to the

governing equations is sought while the exterior is the rest of the unbounded domain whose effect on the interior is required *only* at the computational boundary. The computational boundary is a boundary introduced solely for computational purposes and should be distinguished from physical boundaries. Since the solution to the governing equations is not required in the exterior, the computational domain can be restricted to just the interior by specifying appropriate absorbing boundary conditions (ABCs) at the computational boundary.

ABCs are thus used to replace a 'physical' model by an equivalent 'computational' model. The physical model consists of the interior and exterior governing equations, along with initial conditions (ICs) and physical boundary conditions (BCs) defined on the physical domain (interior + exterior). The computational model consists of the interior governing equations, ICs, physical BCs and ABCs defined on the computational domain (interior + computational boundary). Both these systems are initial boundary value problems (IBVPs) and will henceforth be referred to as 'physical IBVP' and 'computational IBVP' respectively. ABCs can thus be viewed as additional constraints on the physical IBVP that limit (or expand) the space of existing solutions. If the constraints are too restrictive, all valid solutions of the physical IBVP might be excluded rendering the computational IBVP unsolvable. If they are too lax, spurious, unphysical solutions might be admitted rendering the computational IBVP inaccurate. Hence, it is essential to ensure that the ABCs used are 'appropriate'; appropriateness here being determined through the criteria of *well-posedness* and *accuracy*. Roughly speaking, well-posedness refers to the existence of a unique solution that is bounded in some way by the initial and boundary data of the computational IBVP, while accuracy refers to the close resemblance of this unique solution to the exact solution. In addition to these two, a third criterion, namely that of computational *efficiency*, is many a times required by large scale simulations [1,2].

Exact ABCs are well-posed and accurate by default, but their availability is restricted to simple exteriors with regular computational boundaries. Approximate ABCs provide acceptable accuracy and are available for more complicated problems, but their well-

posedness is not guaranteed. For large scale simulations, however, exact ABCs are prohibitively expensive; this necessitates the use of approximate ABCs. Even amongst approximate ABCs, those containing nonlocal spatial and temporal operators (global ABCs) are unsuitable for large scale problems and hence local ABCs are preferred [1,2]. The most popular local ABCs currently available are rational ABCs and perfectly matched layers (PMLs) [3]. Rational ABCs approximate the exact stiffness of an exterior (or associated dispersion relation) with rational functions of varying orders; Lindman [4], Engquist and Majda [5,6] , Bayliss and Turkel [7] and Higdon [8] were their early developers followed by many others [2]. Initial numerical implementations of rational ABCs were restricted to low orders but later auxiliary variable formulations provided practical high order rational ABCs [9]. The other popular local ABC, the PML, is a 'special' absorbing medium that uses complex coordinate stretching to dampen out (or decay) propagating waves without creating artificial reflections at the computational boundary. First introduced by Bérenger [11] and closely followed by the complex coordinate stretching viewpoint provided by Chew *et al.* [12-14], PMLs are now available in split and unsplit forms with variations like the conformal PML [15], complex frequency shifted PML (CFS-PML) [16], convolutional PML (CPML) [17] and multiaxial PML (M-PML) [18]. Currently, both rational ABCs and PMLs are available for a wide variety of governing equations that include, among many others, Maxwell's, linearized Euler's and elastodynamic equations.

Rational ABCs tend to be more accurate than PML because the effect of the rational ABC parameters on solution accuracy is better understood (and hence more easily handled). On the other hand, ABCs based on PML have proven to be more versatile by being easily extendible to complicated exteriors [3]. The term complicated here implies material complications like heterogeneities and/or anisotropy and geometrical complications like corners and conformal boundaries. While both local ABCs satisfy the criteria of accuracy and efficiency, neither of them is assured to be well-posed *per se*. The development of both these ABCs is fraught with examples of seemingly reasonable formulations that have been found to lack well-posedness in one sense or another e.g., see [19,20]. In fact, proving well-posedness (or stability) of newly formulated ABCs is now *de rigueur* e.g., see [5,6,8,21-33]. Studies focusing solely on

well-posedness issues have been rare with some accessible papers being by Higdon [34], Trefethen *et al* [35] , Bécache *et al* [26] and Appelö *et al* [36]. The references within these papers can be used to get a more comprehensive review of previous works. While the mathematical well-posedness theories are well developed today and most of their physical implications have been understood [34], their application to specific governing equations is not always straightforward; especially for complicated media.

One of the challenges to devising well-posed local ABCs for complicated (anisotropic and/or inhomogeneous) media comes from the well-posedness criterion imposed on propagating waves. Well-posedness requires that an ABC should not admit propagating modes travelling into the interior (incoming modes) in the absence of outgoing modes and sources on the boundary [34]. This makes physical sense in as much as an ABC should not allow spontaneous emission of energy into the interior without interior or boundary excitation [35]. While propagating waves are distinguished into incoming and outgoing waves depending on their group velocity, rational ABCs and PML have both been traditionally formulated to absorb waves depending on their phase velocities. This dependence on phase velocities (instead of group velocities) does not affect simple media where the phase and group velocities are always of the same sign (e.g. homogeneous isotropic media) and hence ABC formulations for simple media have turned out to be well-posed. In fact, it has been shown that a condition necessary for stability of PML (a concept related to well-posedness in the sense of providing bounds for solutions) is the absence of wave modes with phase and group velocities of differing signs [26]. Recognizing the fact that many anisotropic and/or inhomogeneous media admit such wave modes, much recent research has been focused on developing techniques that result in well-posed (or stable) local ABCs for such media. A scalar anisotropic medium whose principal material axis is tilted with respect to the coordinate axis is a simple example of a medium that allows wave modes with differing phase and group velocity signs (see Sections 3.3.2, 3.3.3). A similar challenge, arising from the existence of wave modes with inconsistent phase and group velocity signs, has already been recognized in the cases of anisotropic electromagnetism, advective acoustics and anisotropic elastodynamics, e.g. [24-33]. Most of these studies

approach the well-posedness issues from a PML viewpoint and, for the particular case of advective acoustics, all of them specify linear space-time transformations that nullify the inconsistencies in phase and group velocity signs. Moreover, many of these studies model the problem as an initial value problem (IVP) and deal with the continuous form of the ABC prior to discretization. However, actual implementations of these ABCs are discretized IBVPs and it is not entirely clear how their behavior can be inferred from the continuous IVP results.

In this paper, we consider well-posedness from a rational ABC point of view and hence deal with IBVPs. Moreover, the ABC chosen for this purpose is the perfectly matched *discrete* layer (PMDL) [37-39] that is inherently discrete. We provide a necessary and sufficient criterion for well-posedness of PMDL, when it is used as an ABC for the scalar anisotropic wave equation. In fact, this criterion is also sufficient for accuracy and is the same as the accuracy condition developed for the time harmonic case in [40]. In essence, we prove that the parameters of PMDL (its layer lengths), need to satisfy a simple bound to exclude all ill-posed (and none of the well-posed) IBVPs resulting from the use of PMDL BCs while accurately modeling an unbounded domain governed by the scalar anisotropic wave equation. Also, we deal with strong well-posedness; even though weak well-posedness is generally sufficient for constant coefficient problems, more realistic varying coefficient problems can be well-posed only when their 'frozen' coefficient counterparts are strongly well-posed. It is hence necessary to ensure the strong well-posedness of constant coefficient problems and we do this by utilizing the well-known well-posedness theory of Kreiss [41,42]. The well-posedness criterion derived here, solely from the viewpoint of rational ABCs, bears similarity to the ones derived through coordinate transformations of PML and other ABCs in [21-33] even though the rational ABC we use for this purpose *does not* require any coordinate transformation to be enforced. This similarity is not too surprising because of the link shown to exist between rational ABCs and PML by Asvadurov *et al* [43]. This link can be used to view PMDL as particularly efficient versions of PML where the perfectly matching property is preserved even after discretization making the analysis presented here meaningful to other rational ABCs and PML in general. Moreover, the absence of any

coordinate transformations makes the PMDL ABC more amenable to extensions involving layered media. The details of the PMDL formulation can be found in [44] and are summarized in Section 3.3.4.

In this paper we deal with well-posedness and accuracy issues of a continuous interior (but discretized exterior) with a straight computational boundary. Moreover, accuracy considerations here are limited to propagating waves only. As such, interior discretization errors, corners, curved computational boundaries, loss in accuracy due to neglecting the treatment of evanescent waves and treatment of numerical instabilities related to finite precision arithmetic are outside the scope of this paper. It should be noted that the above restrictions are imposed to make the problem more tractable; they are not, with the exception of curved boundaries, due to any limitations of the PMDL formulation. Numerically stable PMDLs, capable of handling both propagating and evanescent waves for scalar isotropic media have already been implemented on domains with convex polygonal corners in [37-39]. As such, this paper can be considered as the necessary first step towards a complete PMDL implementation for anisotropic media.

The outline of the rest of the paper is as follows. Preliminaries related to scalar anisotropic wave equation are presented in Section 3.3 followed by a discussion of the challenges inherent in designing well-posed and accurate ABCs for such equations. A brief review of the formulation of PMDL is also presented in the same section. Section 3.4, which is *necessary* to understanding the results of this paper, contains a summary of the PMDL approximation properties derived in [40] and states the condition sufficient for accuracy of PMDL. Section 3.5 contains a statement of the well-posedness criterion and the derivation of a condition that is both necessary and sufficient for well-posedness of PMDL. Numerical stability issues are presented in Section 3.6 with numerical experiments presented in Section 3.7. Section 3.8 contains a summary and conclusions. References are presented in Section 3.9.

3.3 Preliminaries

3.3.1 Model problem

The ultimate aim of this paper is to provide a practical ABC for the scalar anisotropic wave equation. To this end, we choose the simplest possible boundary in two dimensions: a straight edge without corners. Figure 3.1 (left) shows such a boundary ($x = 0$) and the model problem shown therein consists of replacing the exact full-space by a left half-space (interior) along with an ABC that simulates the effect of the right half-space (exterior). The interior and exterior in Figure 3.1 (left) are given by $x < 0$ and $x > 0$ respectively.

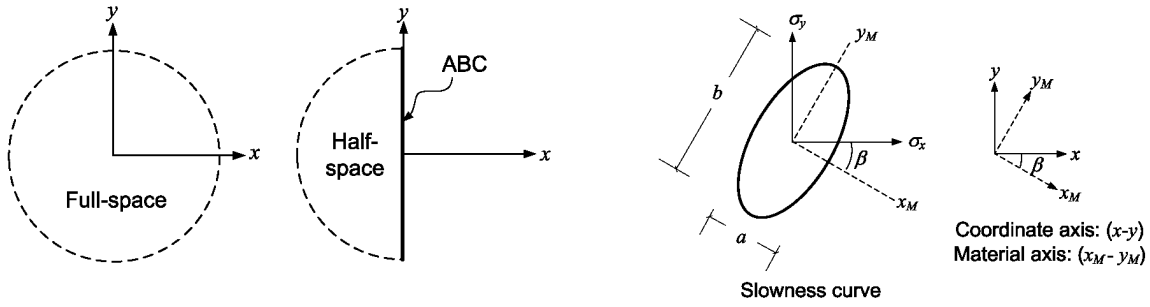

Figure 3.1. *Left:* The model problem consists of replacing a full space by a left half-space and an efficient ABC that is both accurate and well-posed for a scalar anisotropic medium. Right: Global coordinate and material axes along with a typical slowness diagram for $(\sigma_x, \sigma_y) \in \mathbb{R}$. Note that the principal material axes (x_M, y_M) are shown on the ellipse just for reference.

3.3.2 Scalar Anisotropic Media

We consider the scalar wave equation in two dimensions $\left(x - y\right)$ given by,

$$A\frac{\partial^2 u}{\partial x^2} + B\frac{\partial^2 u}{\partial y^2} + C\frac{\partial^2 u}{\partial x \partial y} - \frac{\partial^2 u}{\partial t^2} = 0\,, \tag{3.1}$$

where the three independent parameters A, B, C define the material properties of the medium and can be easily obtained by coordinate stretching and rotation of the isotropic wave equation. Equation (3.1), e.g., arises in the study of anti-plane shear waves in transversely

isotropic elastic media, where the parameters A, B, C are functions of shear moduli, density and orientation of principal material axes of the medium. Similar scalar equations arise in the study of electromagnetism and advective acoustics. Fourier transforming (3.1) in y, t with the dualities $\partial/\partial y \leftrightarrow ik_y$, $\partial/\partial t \leftrightarrow -i\omega$, results in a dispersion relation in terms of horizontal slowness ($\sigma_x = k_x/\omega$) and vertical slowness ($\sigma_y = k_y/\omega$),

$$-A\sigma_x^2 - B\sigma_y^2 - C\sigma_x\sigma_y + 1 = 0\,. \tag{3.2}$$

For $(\sigma_x, \sigma_y) \in \mathbb{R}$, (3.2) represents an ellipse in the slowness space defined by its semiminor axis (a), semimajor axis (b) and angle of tilt (β) with respect to the $x - y$ axis as shown in Figure 3.1 (right). The parameters a, b represent the material properties along $x_M - y_M$; e.g. if the medium has shear moduli μ_{x_M}, μ_{y_M} and density ρ, we have $1/a = \sqrt{\mu_{x_M}/\rho}$ and $1/b = \sqrt{\mu_{y_M}/\rho}$ representing the wave velocities along $x_M - y_M$. Simple coordinate transformations yield:

$$A = \left(\frac{\cos\beta}{a}\right)^2 + \left(\frac{\sin\beta}{b}\right)^2, \quad B = \left(\frac{\cos\beta}{b}\right)^2 + \left(\frac{\sin\beta}{a}\right)^2, \quad C = \sin 2\beta\left(\frac{1}{a^2} - \frac{1}{b^2}\right). \tag{3.3}$$

For later reference, we need the traction on the computational boundary $(x = 0)$. The traction components in $x_M - y_M$ directions are $\left(a^{-2}\right)\partial/\partial x_M$, $\left(b^{-2}\right)\partial/\partial y_M$. These can be transformed through the usual second order tensor transformations to get into the traction components in $x - y$:

$$T_x : A\frac{\partial u}{\partial x} + \left(C/2\right)\frac{\partial u}{\partial y}, \qquad T_y : B\frac{\partial u}{\partial y} + \left(C/2\right)\frac{\partial u}{\partial x}. \tag{3.4}$$

Precisely, T_x, T_y are the traction components on surfaces perpendicular to x, y axis. Without loss of generality, we consider $b \geq a > 0, \beta \in \left[\pi/2, \pi/2\right)$ and this results in,

$$A > 0, \quad B > 0, \quad 4AB - C^2 > 0. \tag{3.5}$$

Variations of the three material properties A, B, C result in three kinds of slowness diagrams representing isotropic, untilted anisotropic and tilted anisotropic media as shown in Figure 3.2. Note that henceforth σ_x will be represented on the vertical axis (as in Figure 3.2).

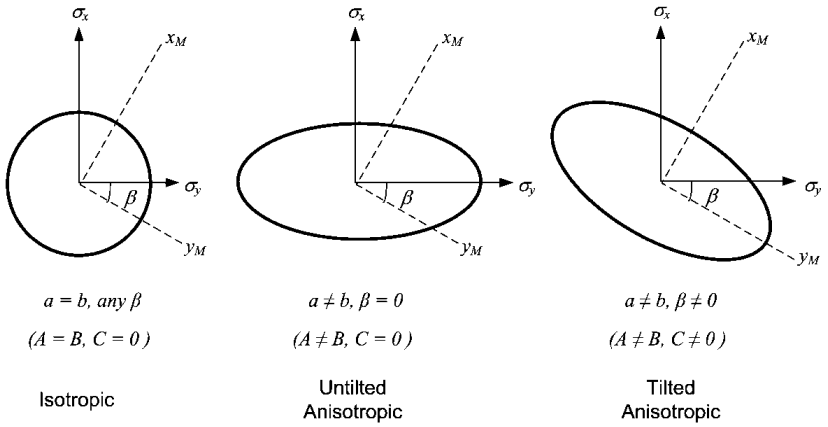

Figure 3.2. Representative slowness diagrams for the three kinds of media governed by a scalar wave equation. Only slowness diagram for propagating waves is shown i.e. $(\sigma_x, \sigma_y) \in \mathbb{R}$. Note that the principal material axes (x_M, y_M) are shown on the ellipse just for reference.

For a given $\sigma_y \in \mathbb{R}$, (3.2) allows both propagating $\left(\sigma_x \in \mathbb{R}\right)$ and evanescent modes $\left(\sigma_x \notin \mathbb{R}\right)$ where each propagating wave mode is associated with a phase velocity (c_{px}) and a group velocity (c_{gx}) in the x-direction defined by:

$$c_{px} = \frac{\omega}{k_x} = \frac{1}{\sigma_x},$$
$$c_{gx} = \frac{\partial \omega}{\partial k_x} = \frac{Ak_x + Ck_y/2}{\omega} = A\sigma_x + \frac{C\sigma_y}{2}. \tag{3.6}$$

It is known that while c_{px} represents the apparent velocity of propagation, c_{gx} represents the true velocity of energy propagation in the x-direction. For the rest of the paper, the terms 'phase velocity' and 'group velocity' will refer to c_{px} and c_{gx} respectively with the understanding that these velocities are always in the x-direction.

3.3.3 ABCs: Exact and Approximate

For a given $\sigma_y \in \mathbb{R}$, the propagating modes $\left(\sigma_x \in \mathbb{R}\right)$ allowed by the quadratic equation (3.2) can be classified in terms of c_{gx} as rightward and leftward propagating waves; their horizontal slownesses are given by,

$$\sigma_x = \frac{-C\sigma_y + \sqrt{4A - \left(4AB - C^2\right)\sigma_y^2}}{2A} \quad : c_{gx} \geq 0 \left(rightward\ propagating\right), \tag{3.7}$$

$$\sigma_x = \frac{-C\sigma_y - \sqrt{4A - \left(4AB - C^2\right)\sigma_y^2}}{2A} \quad : c_{gx} \leq 0 \left(leftward\ propagating\right). \tag{3.8}$$

Graphically, the propagating wave modes of (3.2) are represented by the ellipse in Figure 3.3, where the rightward and leftward propagating waves of (3.7) and (3.8) are denoted by the solid and broken lines respectively of the left ellipse in Figure 3.3 . An exact right half-space, in the absence of any sources within it, admits waves that either propagate to the right $(c_{gx} \geq 0)$ or decay with increasing x $(\mathrm{Im}(\sigma_x) > 0)$. The equation of an ABC that exactly simulates a right half-space is thus given by,

$$\sigma_x = \frac{-C\sigma_y + \sqrt{4A - \left(4AB - C^2\right)\sigma_y^2}}{2A} \quad : Exact\ ABC\ (slowness\ form), \tag{3.9}$$

where the square root is defined by the standard branch cut and $(\sigma_y, \omega) \in \mathbb{R}$. The slowness diagram of an exact ABC for propagating waves $(\sigma_x \in \mathbb{R})$ will thus be the solid portion of the left ellipse in Figure 3.3.

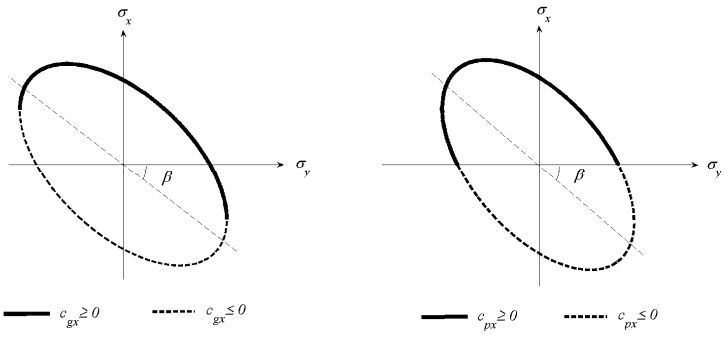

Figure 3.3. A typical slowness diagram for tilted anisotropic media with the regions of positive group and phase velocities clearly demarcated.

Most approximate ABCs like traditional rational ABCs and PML are based on capturing positive phase velocities (and not group velocities) and hence cannot result in accurate ABCs when the signs of both these velocities are different i.e. when $c_{gx} c_{px} < 0$. Since there exist wavemodes with opposing signs of phase and group velocities in the case of scalar waves in tilted anisotropic media (see Figure 3.3), implementations of ABCs with an arbitrary choice of parameters will, in general, allow modes with negative group velocities. Capturing the negative group velocity branch does not just lead to inaccuracies. One of the criteria necessary for the well-posedness of an ABC is that the ABC should not admit leftward propagating wave modes i.e. those with non-positive group velocities [34]. Hence, a typical approximate ABC, in conjunction with a left half-space (as in Figure 3.1) actually results in an ill-posed problem - not just an inaccurate one. Designing well-posed approximate ABCs for interiors allowing modes with phase and group velocities of differing signs is a challenge that has attracted much current research, e.g., [23-30,32,33].

PMDL is a local ABC based on arbitrarily wide angle wave equations (AWWEs) [44] that can be considered to be a particularly efficient discretization of PML that has *no* discretization error [37]. PMDL forms the basis of this study because of its many attractive properties enumerated in [40]. Notwithstanding these merits however, well-posedness of PMDL is not assured, especially for general anisotropic and heterogeneous exteriors. The original PMDL formulation was shown to exhibit characteristics that might lead to ill-posedness and instabilities in complicated media [44]. In fact, this paper is a first step towards tackling the issue of ill-posedness due to anisotropy with the purpose of obtaining a well-posed PMDL for scalar waves in tilted anisotropic media.

3.3.4 PMDL: formulation

The model problem in Figure 3.1 involves replacing the right half-space $\left(0 \le x < \infty\right)$ by an ABC. If the right half-space stiffness (or Dirichlet to Neumann map) is given by K_{exact}, the traction F_0 on the left boundary $\left(x = 0\right)$ and the field variable there (u_0), are related by:

$$F_0 = K_{exact} u_0 \quad : Exact\ ABC\ (stiffness\ form). \tag{3.10}$$

Equation (3.10) can be viewed as the stiffness form of the equation of an exact ABC as compared to the slowness form of (3.9). Substituting a mode $u = e^{i\omega\left(\sigma_x x + \sigma_y y - t\right)}$ in (3.4), comparing it with (3.10), and using (3.9) we get,

$$K_{exact} = -i\omega\left(A\sigma_x + \frac{C}{2}\sigma_y\right) = \frac{-i\omega\sqrt{4A - \left(4AB - C^2\right)\sigma_y^2}}{2}. \tag{3.11}$$

The PMDL model replaces the exterior right half-space with $n\ (< \infty)$ mid-point integrated finite element layers of lengths $L_1 \ldots L_n$ with a Dirichlet boundary at the end (see [40]). Using $\tilde{u}_1, \ldots \tilde{u}_{n-1}, \tilde{u}_n$ to denote the values of the field variable at the right edge of each layer, the Dirichlet condition becomes $\tilde{u}_n = 0$. If $\tilde{u}_0$ is the displacement at the left edge of the n-layer PMDL model, the assembled finite element matrix takes the form,

$$\begin{Bmatrix} F_0 \\ 0 \\ 0 \\ \vdots \\ 0 \\ 0 \end{Bmatrix} = \begin{bmatrix} S_1^{11} & S_1^{12} & & & & \\ S_1^{21} & S_1^{22}+S_2^{11} & S_2^{12} & & & \\ & S_2^{21} & S_2^{22}+S_3^{11} & S_3^{12} & & \\ & & \ddots & \ddots & \ddots & \\ & & & S_{n-2}^{21} & S_{n-2}^{22}+S_{n-1}^{11} & S_{n-1}^{12} \\ & & & & S_{n-1}^{21} & S_{n-1}^{22}+S_n^{11} \end{bmatrix} \begin{Bmatrix} \tilde{u}_0 \\ \tilde{u}_1 \\ \tilde{u}_2 \\ \vdots \\ \tilde{u}_{n-2} \\ \tilde{u}_{n-1} \end{Bmatrix}, \tag{3.12}$$

where the element stiffness matrix for each of the n midpoint integrated layers is,

$$\mathbf{S}_j = \begin{bmatrix} S_j^{11} & S_j^{12} \\ S_j^{21} & S_j^{22} \end{bmatrix} = \frac{A}{L_j}\begin{bmatrix} 1 & -1 \\ -1 & 1 \end{bmatrix} + \frac{iC\omega\sigma_y}{2}\begin{bmatrix} 0 & -1 \\ 1 & 0 \end{bmatrix} + \frac{L_j\omega^2\left(B\sigma_y^2-1\right)}{4}\begin{bmatrix} 1 & 1 \\ 1 & 1 \end{bmatrix} \quad for\ j=\left(1\ldots n\right). \tag{3.13}$$

A choice of frequency dependent purely imaginary layer lengths of $L_j = 2i/\omega\,\sigma_{xj}$ will make the n-layer PMDL exact for a choice of slownesses $\sigma_x = \sigma_{xj}$ and these σ_{xj} are termed the n parameters of PMDL. With this, (3.13) becomes

$$\mathbf{S}_j = \begin{bmatrix} S_j^{11} & S_j^{12} \\ S_j^{21} & S_j^{22} \end{bmatrix} = \frac{-i\omega\sigma_{xj}A}{2}\begin{bmatrix} 1 & -1 \\ -1 & 1 \end{bmatrix} + \frac{iC\omega\sigma_y}{2}\begin{bmatrix} 0 & -1 \\ 1 & 0 \end{bmatrix} + \frac{i\omega\left(B\sigma_y^2-1\right)}{2\sigma_{xj}}\begin{bmatrix} 1 & 1 \\ 1 & 1 \end{bmatrix} \quad for\ j=\left(1\ldots n\right). \tag{3.14}$$

In order to simplify later calculations, (3.14) is written as

$$\mathbf{S}_j = -i\omega\mathbf{C}_j + \mathbf{K}_j + \left(i/\omega\right)\mathbf{R}_j, \tag{3.15}$$

where,

$$\mathbf{C}_j = \frac{\sigma_{xj}A}{2}\begin{bmatrix} 1 & -1 \\ -1 & 1 \end{bmatrix} + \frac{1}{2\sigma_{xj}}\begin{bmatrix} 1 & 1 \\ 1 & 1 \end{bmatrix}, \quad \mathbf{K}_j = \frac{iCk_y}{2}\begin{bmatrix} 0 & -1 \\ 1 & 0 \end{bmatrix}, \quad \mathbf{R}_j = \frac{Bk_y^2}{2\sigma_{xj}}\begin{bmatrix} 1 & 1 \\ 1 & 1 \end{bmatrix}. \tag{3.16}$$

Assembling the finite element matrices $\mathbf{S}_j$ and using (3.16), we can write (3.12) as,

$$\mathbf{F} = \left[-i\omega\mathbf{C} + \mathbf{K} + \left(i/\omega\right)\mathbf{R}\right]\tilde{\mathbf{u}}\,, \tag{3.17}$$

where $\mathbf{C}, \mathbf{K}, \mathbf{R}$ are finite element assemblies of element contributions $\mathbf{C}_j, \mathbf{K}_j, \mathbf{R}_j$ and $\mathbf{u} = \left[\tilde{u}_0 \quad \dots \quad \tilde{u}_{n-1}\right]^T$, $\mathbf{F} = \left[F_0 \quad 0 \quad \dots \quad 0\right]^T$. By eliminating the variables $\tilde{u}_1, \dots \tilde{u}_{n-1}$ from (3.12) we get the form,

$$F_0 = K_n \tilde{u}_0 \quad : Approx\ ABC\ (stiffness\ form). \tag{3.18}$$

In essence, the n-layer PMDL model approximates only the stiffness K_{exact} and hence the displacement u_0 (both at $x = 0$) and *not* the displacement inside the half-space $u\,(x > 0)$. Hence we have $\tilde{u}_0 \approx u_0$ but $\tilde{u}_1, \dots \tilde{u}_{n-1}$ are just 'auxiliary' variables that have no physical interpretation. Comparing (3.18) to (3.10) we see that PMDL approximates the exact stiffness $(K_n \approx K_{exact})$ and the properties of this approximation are dictated solely by the choice of the n arbitrary parameters σ_{xj}. A detailed derivation of the formulation is presented in [44] with a summary in [40]. K_n is obtained by eliminating the auxiliary variables from (3.17) and has a rational function / continued fraction form,

$$K_n = -i\omega P_{2n,2n-2}(\sigma_y) = S_1^{11} - \cfrac{S_1^{12}S_1^{21}}{S_1^{22} + S_2^{11} - \cfrac{S_2^{12}S_2^{21}}{S_2^{22} + S_3^{11} - \ddots \cfrac{S_{n-1}^{12}S_{n-1}^{21}}{S_{n-1}^{22} + S_n^{11}}}}. \tag{3.19}$$

In (3.19), $\sigma_y = k_y/\omega$ and $P_{2n,2n-2}(\sigma_y)$ is a real rational function in σ_y of exact degrees $2n$ and $2n-2$ with $n \geq 1$. Comparing (3.19) to (3.11) and noting that $K_n \approx K_{exact}$, the rational approximation basis of PMDL becomes evident as,

$$P_{2n,2n-2}(\sigma_y) \approx \frac{+\sqrt{4A - \left(4AB - C^2\right)\sigma_y^2}}{2}, \tag{3.20}$$

and by using (3.20) in (3.9), the slowness form of PMDL becomes,

$$\sigma_x = \frac{-C\sigma_y \big/ 2 + P_{2n,2n-2}(\sigma_y)}{A} \quad : Approx\ ABC\ (slowness\ form). \tag{3.21}$$

Equations (3.17) and (3.19) also lead to,

$$K_n = \left| -i\omega \mathbf{C} + \mathbf{K} + \left(i \big/ \omega\right) \mathbf{R} \right|. \tag{3.22}$$

3.3.5 PMDL: approximation properties

This work is limited to propagating wave modes only i.e., we are interested in properties of ABCs that only approximate the real part of (3.9). Even though neglecting evanescent modes $\left(\sigma_x \notin \mathbb{R}\right)$ is expected to affect the long term accuracy of the solution in the interior [10,46], and even though PMDL *can* handle evanescent wave modes [44,45], we consider this paper to be a preliminary work on rational ABCs for tilted anisotropic media and so restrict ourselves to propagating wave modes. The approximation properties of PMDL for propagating modes are best understood through the reflection coefficient that was derived in [40] and shown to have the two forms,

$$R_n = \left(\frac{\sqrt{4A - \left(4AB - C^2\right)\sigma_y^2} \big/ 2 - P_{2n,2n-2}(\sigma_y)}{\sqrt{4A - \left(4AB - C^2\right)\sigma_y^2} \big/ 2 + P_{2n,2n-2}(\sigma_y)} \right) \quad : \begin{matrix} Reflection\ coefficient \\ (slowness\ form) \end{matrix}, \tag{3.23}$$

$$\left|R_n\right| = \left| \prod_{j=1}^{n} \left(\frac{c_{gx} - c_j}{c_{gx} + c_j} \right) \left(\frac{c_{gx} - \overline{c}_j}{c_{gx} + \overline{c}_j} \right) \right| \quad (c_{gx} \geq 0) \quad : \begin{matrix} Reflection\ coefficient \\ (group\ velocity\ form) \end{matrix}, \tag{3.24}$$

where $P_{2n,2n-2}(\sigma_y)$ is the rational function encountered in (3.19), and c_j, $\overline{c}_j$ are the reference group velocities given by,

$$c_j = A\sigma_{xj} + \left(C/2\right)\left(\frac{-C\sigma_{xj} + \sqrt{4B - \left(4AB - C^2\right)\sigma_{xj}^2}}{2B}\right),$$
$$\overline{c}_j = A\sigma_{xj} + \left(C/2\right)\left(\frac{-C\sigma_{xj} - \sqrt{4B - \left(4AB - C^2\right)\sigma_{xj}^2}}{2B}\right). \tag{3.25}$$

c_{gx} in (3.24) is the group velocity of the incident wave mode that is propagating rightward and hence $c_{gx} \geq 0$. Defining the vertical slownesses,

$$\sigma_{yj} = \frac{-C\sigma_{xj} + \sqrt{4B - \left(4AB - C^2\right)\sigma_{xj}^2}}{2B},$$
$$\overline{\sigma}_{yj} = \frac{-C\sigma_{xj} - \sqrt{4B - \left(4AB - C^2\right)\sigma_{xj}^2}}{2B}, \tag{3.26}$$

for every σ_{xj} (i.e. every layer of length $L_j = 2i/\omega\sigma_{xj}$), the PMDL slowness interpolates the exact slowness (3.2) at the four points given by $(\sigma_{yj}, \sigma_{xj}), (-\sigma_{yj}, \sigma_{xj} + (C/A)\sigma_{yj})$, $(\overline{\sigma}_{yj}, \sigma_{xj})$ and $(-\overline{\sigma}_{yj}, \sigma_{xj} + \left(C/A\right)\overline{\sigma}_{yj})$. It should be noted that these four points of interpolation need not necessarily be distinct, but for every choice of σ_{xj}, there are four points of interpolation counted *with multiplicity*. A n-layer PMDL has n parameters (σ_{xj} with $j = 1 \cdots n$) and hence it has $4n$ points of interpolation in all counted with multiplicity. Detailed discussion can be found in [40].

3.4 Accuracy

A n-layer PMDL is considered convergent (or accurate, following the terminology in the ABC literature) if, by increasing the number of layers n, the magnitude of its reflection coefficient can be made arbitrarily small for every strictly rightward propagating wave mode, i.e.,

$$\lim_{n\to\infty}\left|R_n(c_{gx})\right| = 0 \qquad \forall\ c_{gx} > 0 : Accuracy\ criterion\,. \tag{3.27}$$

The reason for the criterion (3.27) to be 'accurate enough' while excluding the zero group velocity mode ($c_{gx} = 0$) is stated in [40] and essentially reduces to the fact that a PMDL ABC that allows $c_{gx} = 0$ to exist in the interior ends up being ill-posed [34].

This incompatibility between being well-posed and being able to represent zero group velocity modes accurately is not unique to PMDL. A similar situation occurs between accuracy and stability of difference approximations in [47]. In fact, for the case of untilted anisotropy, $\lim_{n\to\infty}\left|R_n(0)\right| = 0$ cannot be satisfied by any existing local ABC. The calculations in [40] show that a sufficient condition for (3.27) to be satisfied is,

$$\sigma_{xj} > \left|\frac{C}{\sqrt{A\left(4AB - C^2\right)}}\right|. \tag{3.28}$$

The above condition (3.28) has a simple geometric interpretation that is shown in Figure 3.4.

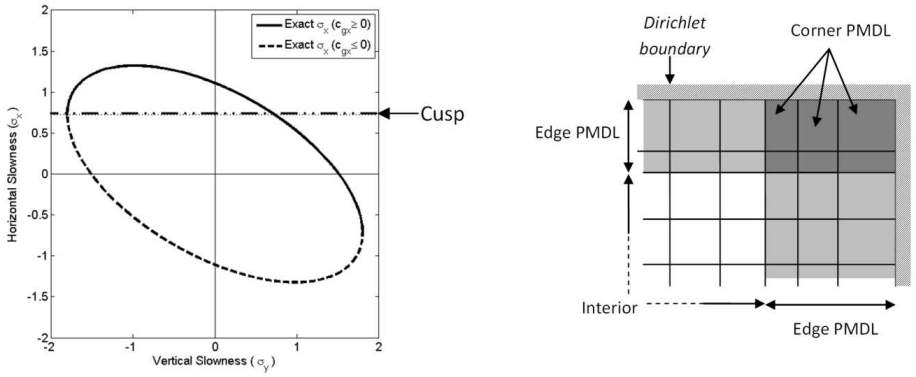

Figure 3.4. *Left:* Geometric interpretation of the sufficient condition for accuracy. The parameters of PMDL should be chosen above the horizontal line that defines the 'cusp' of the ellipse. *Right:* Corner PMDL with parameters (layer lengths) consistent with the two edge PMDLs.

The n-layer PMDL approximates the stiffness (3.11) by a rational function instead of approximating the horizontal slowness directly. It can be seen from (3.11) and (3.6) that the stiffness for propagating wave modes is in fact related to their group velocity as $K = -i\omega c_{gx}$ and hence approximating stiffness is the same as approximating group velocities. This is the reason why the PMDL reflection coefficient (3.24) is expressible purely in terms of group velocities and as noted in [40], the form of (3.24) is *key* to the derivation of the simple accuracy condition (3.28).

3.5 Well-posedness

3.5.1 Well-posedness of an ABC

Kreiss gave necessary and sufficient algebraic conditions for well-posedness of systems of linear hyperbolic initial boundary value problems (IBVPs) defined on a half-space [41] by specifying energy estimates depending on initial and boundary data that need to be satisfied. Well-posedness in Kreiss's sense reduces to avoiding certain ill-posed normal modes of the form $e^{ik_x x + ik_y y - i\omega t}$ where $k_y \in \mathbb{R}$ but where k_x and ω are allowed to be complex. In general, these ill-posed modes are solutions to the computational IBVP that are L_2 integrable in $x \leq 0$ but fail to satisfy the specified energy estimate [34]. Trefethen and Higdon have both provided useful physical interpretation of Kreiss's ill-posed normal modes in the context of ABCs for wave propagation problems [34,48]. In the case of the model problem containing an interior left half-space with an ABC at $x = 0$, ill-posed normal modes are solutions to (3.1) of the form $e^{ik_x x + ik_y y - i\omega t}$ with $k_y \in \mathbb{R}$ and with the (k_x, ω) pair satisfying any one of the following three criteria:

- $\mathrm{Im}\left(\omega\right) > 0, \mathrm{Im}\left(k_x\right) < 0$ (modes growing exponentially in time while decaying into the interior)
- $\mathrm{Im}\left(\omega\right) = 0, \mathrm{Im}\left(k_x\right) = 0, c_{gx} \leq 0$ (leftward propagating modes)

- $\mathrm{Im}\left(\omega\right) = 0,\ \mathrm{Im}\left(k_x\right) < 0$ (evanescent modes decaying into the interior).

The first of these modes is L_2 integrable in $x \leq 0$ but grows exponentially in time. The second mode contains propagating waves that propagate energy into the interior $\left(c_{gx} < 0\right)$ without any interior or boundary excitation. This again leads to unbounded growth in time though at a much slower rate. Physically, it is not immediately apparent why propagating waves moving tangential to the boundary (the case of $c_{gx} = 0$ for the second ill-posed mode) and evanescent modes decaying into the interior (third ill-posed mode) should result in ill-posedness. Mathematically, however, the second and third modes are limiting cases of the first mode that is clearly ill-posed. A more detailed discussion of these ill-posed modes can be found in [34]. If any of the above three modes is allowed by the interior governing equation in conjunction with the ABC, then the model in Figure 3.1 containing a left-half space with an ABC on its boundary is ill-posed. Additionally, the exclusion of these ill-posed modes is known to be sufficient for ensuring well-posedness [34,35].

3.5.2 Well-posedness criterion

Trefethen and Halpern [35] provided well-posedness criterion for rational ABCs for isotropic acoustics ($A = B = 1, C = 0$ in (3.1)). In this sub-section we extend this criterion to tilted anisotropic acoustics, and state it in relation to a n-layer PMDL. In order to facilitate understanding and comparison, we reproduce the order and flow of [35] even if it leads to the restatement of a few equations.

The exact dispersion relation of (3.1) is:

$$-Ak_x^2 - Bk_y^2 - Ck_x k_y + \omega^2 = 0\,. \tag{3.29}$$

Equation (3.29) admits two solutions for k_x given by,

$$k_x = \frac{-Ck_y + \omega\sqrt{4A - \left(4AB - C^2\right)\left(k_y^2 \big/ \omega^2\right)}}{2A}, \tag{3.30}$$

$$k_x = \frac{-Ck_y - \omega\sqrt{4A - \left(4AB - C^2\right)\left(k_y^2 \big/ \omega^2\right)}}{2A}. \tag{3.31}$$

For $\left(k_x, k_y, \omega\right) \in \mathbb{R}$, (3.30) represents rightward propagating waves $\left(c_{gx} \geq 0\right)$ and (3.31) represents leftward propagating waves $\left(c_{gx} \leq 0\right)$. The distinction of tangential waves $\left(c_{gx} = 0\right)$ is ignored for now; it will become necessary only later. The ABC in Figure 3.1 should admit rightward propagating waves ($c_{gx} \geq 0$), and so it approximates (3.30) with a rational function given by (from (3.21)),

$$k_x = \frac{-Ck_y \big/ 2 + \omega P_{2n,2n-2}}{A} \quad : Approx\ ABC\left(n - layer\ PMDL\right), \tag{3.32}$$

where $\sigma_y = k_y \big/ \omega$ and $P_{2n,2n-2} = p_{2n}(\sigma_y) \big/ q_{2n-2}(\sigma_y)$. Here, $p_{2n}(\sigma_y)$ and $q_{2n-2}(\sigma_y)$ are polynomials of exact degrees $2n$ and $2n-2$ respectively with $n \geq 1$ and with no common zeros. Multiplying (3.32) by $A\omega^{2n-1} q_{2n-2}\left(\sigma_y\right)$ and rearranging we get:

$$Q\left(k_x, k_y, \omega\right) = 0, \tag{3.33}$$

where Q is a homogeneous polynomial of degree *2n* in the three variables k_x, k_y, ω and is given by:

$$Q\left(k_x, k_y, \omega\right) = A\omega^{2n-1} k_x q_{2n-2} + C\omega^{2n-1} k_y q_{2n-2} \big/ 2 - \omega^{2n} p_{2n}. \tag{3.34}$$

Equation (3.33) is the dispersion relation of the n-layer PMDL. Since the rational function $P_{2n,2n-2}$ and hence p_{2n}, q_{2n-2} are given by (3.14) and (3.19), their coefficients are determined by the n parameters σ_{xj}. Thus, for real parameters $(\sigma_{xj} \in \mathbb{R})$, (3.34) represents a polynomial with real coefficients.

It should be noted that in the previous sections, we were concerned with modes of the kind $e^{i\left(k_x x+k_y y-\omega t\right)}$ with $\left(k_y,\omega\right)\in\mathbb{R}$. However, since well-posedness is also concerned with modes growing in time, the restriction to real ω is no longer sufficient. This is suggested by the first ill-posed mode. The existence of complex ω is a result of Laplace transforms used in the derivation of these ill-posed modes [34,41]. Hence we have $k_y\in\mathbb{R}$ and $\left(k_x,\omega\right)\in\mathbb{C}$; this requires a clear definition for the square root used in (3.30) and (3.31). To facilitate comparison with [35], we define the square root in (3.31); the square root in (3.30) can be inferred accordingly.

Consider the case of $k_y=0$ first. A natural definition of the square root branch in (3.31) gives $k_x=-\omega\big/\sqrt{A}$. For later use note that $k_x=-\omega\big/\sqrt{A}$ has the following implication: $\mathrm{Im}\left(\omega\right)>0\Rightarrow\mathrm{Im}\left(k_x\right)<0$. For $k_y\neq 0$, we can define the function $k_x=\left(-Ck_y-\sqrt{4A\omega^2-\left(4AB-C^2\right)k_y^2}\right)\Big/2A$ to be an analytic continuation of the function $k_x=-\omega\big/\sqrt{A}$. When $\mathrm{Im}\left(\omega\right)\neq 0$, this continuation preserves the implication $\mathrm{Im}\left(\omega\right)>0\Rightarrow\mathrm{Im}\left(k_x\right)<0$. When $\omega\in\mathbb{R}$, k_x can be defined as the limit obtained through $\mathrm{Im}\left(\omega\right)\to 0^+$. The limiting process involves $\mathrm{Im}\left(\omega\right)>0$ and hence results in $\mathrm{Im}\left(k_x\right)<0$ when $\left|\omega\right|<\left(\sqrt{B-C^2\big/4A}\right)\left|k_y\right|$ in (3.31). Formally this leads to the following definition:

Definition of square root:

For $\mathrm{Im}\left(\omega\right)>0$, the branch (3.31) refers to the analytic function $k_x=\left(-Ck_y-\sqrt{4A\omega^2-\left(4AB-C^2\right)k_y^2}\right)\Big/2A$ of k_y and ω obtained by analytic continuation from the values $k_x=-\omega\big/\sqrt{A}$ for $k_y=0$ with $\mathrm{Im}\left(k_x\right)<0$.

For $\omega \in \mathbb{R}$, k_x in branch (3.31) is defined by limits in the half-plane $\mathrm{Im}\left(\omega\right) > 0$, and satisfies:

$$\mathrm{Im}\left(k_x\right) < 0 \text{ if } \left|\omega\right| < \left(\sqrt{B - C^2/4A}\right)\left|k_y\right| ,$$

$$k_x \in \left(-Ck_y - 2\sqrt{A}\omega\left[0,1\right]\right)/2A \text{ if } \left|\omega\right| \geq \left(\sqrt{B - C^2/4A}\right)\left|k_y\right| .$$

Similarly, for $\mathrm{Im}\left(\omega\right) \geq 0$, branch (3.30) results in $\mathrm{Im}\left(k_x\right) > 0$ or $k_x \in \left(-Ck_y + 2\sqrt{A}\omega\left[0,1\right]\right)/2A$. The same logic can also be followed to define (3.30), (3.31) for $\mathrm{Im}\left(\omega\right) < 0$.

With this definition of the square root, we can immediately see that all the three ill-posed modes belong to branch (3.31). This is obvious for the first and third ill-posed modes because only branch (3.31) results in $\mathrm{Im}\left(k_x\right) < 0$. The second ill-posed mode contains propagating wave modes that have non-positive group velocity. Propagating wave modes i.e. those with $(k_x, k_y, \omega) \in \mathbb{R}$ have group velocity given by $c_{gx} \in \sqrt{A}\left[-1,1\right]$. This can be seen by substituting (3.30) and (3.31) into the group velocity expression (3.31). Since branch (3.31) allows propagating wave modes with $k_x \in \left(-Ck_y - 2\sqrt{A}\omega\left[0,1\right]\right)/2A$, we can see that it allows modes with $c_{gx} \in \sqrt{A}\left[-1,0\right] \leq 0$. Since this includes all non-positive group velocities, the second ill-posed mode also belongs to branch (3.31). Moreover, the branch (3.31) does not admit any well-posed modes. All modes admitted by (3.31) with $\mathrm{Im}\left(\omega\right) \geq 0$ are ill-posed as shown above. For $\mathrm{Im}\left(\omega\right) < 0$, (3.31) results in $\mathrm{Im}\left(k_x\right) > 0$; these modes are *not* L_2 integrable in the domain $\left(x \leq 0\right)$ and hence physically inadmissible in the first place. Thus the IBVP is well-posed if and only if the approximation does not contain the branch (3.31), i.e.,

Well-posedness criterion: The model problem of Figure 3.1 is well posed if and only if (3.34) and (3.29) have no mutual solutions $\left(k_x, k_y, \omega\right) \neq \left(0,0,0\right)$ with $k_y \in \mathbb{R}$, $\mathrm{Im}\left(\omega\right) > 0$, and k_x belonging to the branch (3.31).

This criterion can be rewritten solely in terms of vertical slowness σ_y and the rational approximation provided by the n-layer PMDL. For this we can assume $\omega \neq 0$; for if it is, equation (3.29) gives $k_x = \left(-C \pm i\sqrt{4AB - C^2}\right) k_y \Big/ 2A$ and this with (3.33) implies $k_x = k_y = 0$ which is of no interest. For $k_y \in \mathbb{R}$ and $\mathrm{Im}\left(\omega\right) > 0$, the variable $\sigma_y = k_y \Big/ \omega$ lies in the set $\mathbb{C} \setminus \left((-\infty, 0) \cup (0, \infty)\right)$. Including limits $\mathrm{Im}(\omega) \to 0, \omega \not\to 0$ amounts to letting σ_y range all over $\mathbb{C}$ with points on the two sides of the cuts $(-\infty, 0), (0, \infty)$ viewed as distinct. Hence the well posedness criteria reduces to (3.34) and (3.31) having no mutual solutions for $\sigma_y \in \mathbb{C}$. Since (3.34) is but a form of (3.32), the well-posedness criterion further reduces to:

$$\frac{-C\sigma_y - \sqrt{4A - \left(4AB - C^2\right)\sigma_y^2}}{2A} \neq \frac{-C\sigma_y \Big/ 2 + P_{2n,2n-2}}{A}, \quad (\sigma_y \in \mathbb{C}) \qquad (3.35)$$

$$: Well - posedness\ criterion.$$

Equation (3.35) is the criterion for a n-layer PMDL to act as a well-posed ABC for the model problem in Figure 3.1 with a tilted anisotropic interior. The above arguments from (3.33) till (3.35), except for some explanations and extensions to the case of tilted anisotropy, are straightforward extensions of the arguments presented in [35] for isotropic acoustics.

3.5.3 Reformulation of the well-posedness criterion

As noted before, necessary and sufficient conditions for well-posedness of general rational ABCs have been derived by Trefethen and Halpern [35] for isotropic acoustics ($A = B = 1, C = 0$ in (3.1)). These results are applicable to scalar, *untilted* anisotropic

media without any modification. In this sub-section, we show that the form of the n-layer PMDL (3.21) is such that it will allow us to extend Trefethen and Halpern's isotropic acoustics results to tilted anisotropy. To this end, we reformulate (3.35) in terms of interpolation points before deriving necessary and sufficient conditions for well-posedness of PMDL.

Since $A \neq 0$, (3.35) is equivalent to:

$$\frac{-\sqrt{4A-\left(4AB-C^2\right)\sigma_y^2}}{2} \neq P_{2n,2n-2}, \quad for\ \sigma_y \in \mathbb{C}. \tag{3.36}$$

Using $A>0, 4AB-C^2>0$ from (3.5), we can divide (3.36) by $\sqrt{A}$ to get $-\sqrt{1-\left(B-C^2/4A\right)\sigma_y^2} \neq P_{2n,2n-2}/\sqrt{A}$, which, with the following,

$$\begin{aligned} \tilde{\sigma}_y &= \left(\sqrt{\left(B-C^2/4A\right)}\right)\sigma_y, \\ \tilde{P}_{2n,2n-2} &= P_{2n,2n-2}/\sqrt{A}, \end{aligned} \tag{3.37}$$

results in the form:

$$-\sqrt{1-\tilde{\sigma}_y^2} \neq \tilde{P}_{2n,2n-2}\left(\tilde{\sigma}_y\right), \quad for\ \tilde{\sigma}_y \in \mathbb{C}. \tag{3.38}$$

$\tilde{P}_{2n,2n-2}(\tilde{\sigma}_y)$, like $P_{2n,2n-2}(\sigma_y)$, is a rational function with real coefficients.

Equation (3.38) can further be simplified by noting that, on $\left(-\infty,-1\right)$ and $\left(1,\infty\right)$, the inequality is always true because the left-hand side is imaginary, finite and non-zero while the right-hand side is real or infinite. Hence the well-posedness criterion reduces to,

$$-\sqrt{1-\tilde{\sigma}_y^2} \neq \tilde{P}_{2n,2n-2}\left(\tilde{\sigma}_y\right), \quad for\ \tilde{\sigma}_y \in \mathbb{C}-(-\infty,-1)-(1,\infty). \tag{3.39}$$

It should be remembered that (3.38) is still the well-posedness criterion for *tilted* anisotropic media. Since the rational function $P_{2n,2n-2}\left(\sigma_y\right)$ and hence $\tilde{P}_{2n,2n-2}\left(\tilde{\sigma}_y\right)$ are

defined by (3.19) and (3.14), the well-posedness criterion reduces to finding the parameters σ_{xj} of (3.14), so that (3.39) is satisfied. The form of (3.38), (3.39) is the form that occurs in the well-posedness study of *isotropic* acoustics and as such, those results are directly applicable to our problem. It should be noted that we were able to arrive at the form of (3.38) and (3.39) *only* because of the special form of (3.32) wherein the stiffness of the exact right half-space is approximated by a rational function (3.19) to get $K_n \approx K_{exact}$.

We now use the results derived for isotropic acoustics and reformulate (3.39) in terms of interpolation points. One of these results concerns a real rational function $P_{r,s}$ of exact type (r,s) with $P_{r,s}(0) \neq 0,\infty$. It has been shown in [35] (lemma 2) that the following conditions are equivalent:

(a) $P_{r,s}(\sigma) = -\sqrt{1-\sigma^2}$ has no solutions in $\mathbb{C} - (-\infty,-1) - (1,\infty)$.

(b) $s \le r \le s+2$ and $P_{r,s}(\sigma) = +\sqrt{1-\sigma^2}$ has $r+s+1+\chi_{rs}$ solutions in $\mathbb{C} - \left(-\infty,-1\right] - \left[1,\infty\right)$, counted with multiplicity. Here $\chi_{rs} = 0$ if $r+s$ is odd and $\chi_{rs} = 1$ if $r+s$ is even.

In our case $P_{2n,2n-2}\left(\sigma_y\right)$ and hence $\tilde{P}_{2n,2n-2}\left(\tilde{\sigma}_y\right)$ are real rational functions of exact type $(2n, 2n-2)$ for $\sigma_{xj} \in \mathbb{R}$. If we can show that $\tilde{P}_{2n,2n-2}\left(0\right) \neq 0,\infty$, then (3.39) is precisely the statement (a) above and can hence be replaced by the equivalent statement (b). The rational function $\tilde{P}_{2n,2n-2}\left(\tilde{\sigma}_y\right)$ already satisfies the condition $s \le r \le s+2$, and hence (3.39) becomes: For $\sigma_{xj} \in \mathbb{R}$, $+\sqrt{1-\tilde{\sigma}_y^2} = \tilde{P}_{2n,2n-2}\left(\tilde{\sigma}_y\right)$ has $4n$ solutions in $\mathbb{C} - \left(-\infty,-1\right] - \left[1,\infty\right)$ counted with multiplicity. We can now undo the change instigated in (3.37) to write the above well-posedness criterion as: For $\sigma_{xj} \in \mathbb{R}$,

$+\sqrt{4A-\left(4AB-C^2\right)\sigma_y^2}\Big/2 = P_{2n,2n-2}\left(\sigma_y\right)$ has $4n$ solutions in $\mathbb{C}-\left(-\infty,-d\right]-\left[d,\infty\right)$ counted with multiplicity. Here $d = 2\sqrt{A}\Big/\sqrt{4AB-C^2}$. An equivalent statement in terms of interpolation points is:

A n -layer PMDL is well-posed if and only if $\left(-C\sigma_y/2 + P_{2n,2n-2}\right)\Big/A$ interpolates $\left(-C\sigma_y + \sqrt{4A-\left(4AB-C^2\right)\sigma_y^2}\right)\Big/2A$ at $4n$ points in $\mathbb{C}-\left(-\infty,-d\right]-\left[d,\infty\right)$ counted with multiplicity.

The above well-posedness criterion requires $\tilde{P}_{2n,2n-2}\left(0\right) \neq 0,\infty$. Using (3.5) and (3.37) an equivalent requirement is $P_{2n,2n-2}\left(0\right) \neq 0,\infty$. Instead of proving $P_{2n,2n-2}\left(0\right) \neq 0,\infty$ right now, we assume it to be true and derive conditions under which the last stated well-posedness criterion is satisfied. We then show that these conditions ensure $P_{2n,2n-2}\left(0\right) \neq 0,\infty$.

It has already been stated in Section 3.3.5 that the n -layer PMDL exactly interpolates $4n$ points (counted with multiplicity) on the slowness curve [40]. Comparing this with the last stated well-posedness criterion, we can see that the only thing that remains to be done, is to find conditions under which all these $4n$ points are on $\left(-C\sigma_y + \sqrt{4A-\left(4AB-C^2\right)\sigma_y^2}\right)\Big/2A$ in the required domain $\mathbb{C}-\left(-\infty,-d\right]-\left[d,\infty\right)$ and not on $\left(-C\sigma_y - \sqrt{4A-\left(4AB-C^2\right)\sigma_y^2}\right)\Big/2A$. This is done in the following sub-section.

3.5.4 Necessary and Sufficient conditions

For clarity, we rewrite the positive and negative branches of the horizontal slowness,

$$\sigma_x = \frac{-C\sigma_y + \sqrt{4A-\left(4AB-C^2\right)\sigma_y^2}}{2A}, \tag{3.40}$$

$$\sigma_x = \frac{-C\sigma_y - \sqrt{4A - \left(4AB - C^2\right)\sigma_y^2}}{2A}, \tag{3.41}$$

and restate the well-posedness criterion obtained at the end of the previous sub-section.

Well-posedness criterion: The model problem of Figure 3.1 with a scalar anisotropic medium and with a n-layer PMDL is well-posed if and only if $\left(-C\sigma_y/2 + P_{2n,2n-2}\right)/A$ interpolates (3.40) at $4n$ points in $\mathbb{C} - \left(-\infty, -d\right] - \left[d, \infty\right)$ counted with multiplicity where $d = 2\sqrt{A}/\sqrt{4AB - C^2}$.

In Section 3.4 we stated the sufficient criterion for accuracy (3.28) by first imposing the condition of positive reference group velocities $c_j > 0, \overline{c}_j > 0$ at each of the $4n$ interpolation points. The condition $c_j > 0, \overline{c}_j > 0$, by definition, forces interpolation of the positive group velocity branch (3.40) and hence we expect (3.28) to play some role in assuring well-posedness. In-fact, we now show that (3.28) is *both* necessary and sufficient for satisfying the above well-posedness criterion.

Motivated by the derivation of the sufficient condition for accuracy, we first consider a choice of parameters:

$$\left|\frac{C}{\sqrt{A\left(4AB - C^2\right)}}\right| < \sigma_{xj} \le \frac{2\sqrt{B}}{\sqrt{4AB - C^2}}. \tag{3.42}$$

Using (3.26) and after some manipulations, the choice of (3.42) results in:

$$\sigma_{yj} \in \left(-d, d\right), \overline{\sigma}_{yj} \in \left(-d, d\right) \quad where\ d = 2\sqrt{A}/\sqrt{4AB - C^2}\,. \tag{3.43}$$

It can be seen from (3.25) that (3.42) ensures $c_j > 0, \overline{c}_j > 0$ and so we have $4n$ points of interpolation of the positive group velocity branch (3.40) (or equivalently (3.30)). Hence (3.42) is sufficient for well-posedness.

We next consider,

$$\sigma_{xj} > \frac{2\sqrt{B}}{\sqrt{4AB - C^2}}. \tag{3.44}$$

From Section 3.3.5, we have the usual four points of interpolation (including both positive and negative group velocity branches) $\sigma_y = \pm\sigma_{yj}, \pm\overline{\sigma}_{yj}$. Based on (3.26), none of these interpolation points are real and thus they belong to $\mathbb{C} - \mathbb{R}$. We further show that none of these points can interpolate the non-positive group velocity branch (3.41) thus asserting that all four points interpolate the positive group velocity branch (3.40) with $\sigma_y \in \mathbb{C} - \mathbb{R}$.

The (σ_y, σ_x) pairs of the four interpolation points were stated in Section 3.3.5 to be $(\sigma_{yj}, \sigma_{xj})$, $\left(-\sigma_{yj}, \sigma_{xj} + \left(C/A\right)\sigma_{yj}\right)$, $(\overline{\sigma}_{yj}, \sigma_{xj})$ and $\left(-\overline{\sigma}_{yj}, \sigma_{xj} + \left(C/A\right)\overline{\sigma}_{yj}\right)$. We will consider each of these separately.

Consider the point of interpolation $(\sigma_{yj}, \sigma_{xj})$: From (3.44) and (3.26) we have $\mathrm{Im}(\sigma_{yj}) \neq 0$. At the point of interpolation, $k_y = \omega\sigma_{yj}, k_x = \omega\sigma_{xj}$ and since $k_y \in \mathbb{R}$, we have $\mathrm{Im}(\omega) \neq 0$. If $\mathrm{Im}(\omega) > 0$, we get $\mathrm{Im}(k_x) > 0$ (because (3.44) implies $\sigma_{xj} > 0$). Hence k_x cannot lie on (3.41) because for $k_y \in \mathbb{R}$ the negative branch of the square root has $\mathrm{Im}(k_x) < 0$ (from the definition of square root). The same argument holds for the interpolation point $(\overline{\sigma}_{yj}, \sigma_{xj})$ with $k_y = \omega\overline{\sigma}_{yj}$.

Consider the point of interpolation $\left(-\sigma_{yj}, \sigma_{xj} + \left(C/A\right)\sigma_{yj}\right)$: From (3.44) and (3.26), we have $\mathrm{Im}(\sigma_{yj}) \neq 0$. At the point of interpolation, $k_y = \omega(-\sigma_{yj}), k_x = \omega\left(\sigma_{xj} + \left(C/A\right)\sigma_{yj}\right) = \omega\sigma_{xj} - \left(C/A\right)k_y$ and since $k_y \in \mathbb{R}$, we have

$\mathrm{Im}(\omega) \neq 0$. If $\mathrm{Im}(\omega) > 0$, we get $\mathrm{Im}(k_x) > 0$ (because (3.44) implies $\sigma_{xj} > 0$). The rest is identical to the above argument for $\left(\sigma_{yj}, \sigma_{xj}\right)$ and the same holds for $\left(-\overline{\sigma}_{yj}, \sigma_{xj} + \left(C/A\right)\overline{\sigma}_{yj}\right)$.

The above arguments show that, for $\mathrm{Im}(\omega) > 0$, (3.44) ensures that the four points of interpolation lie in $\mathbb{C} - \mathbb{R}$ and interpolate (3.40). *To summarize*: The condition (3.42), and for $\mathrm{Im}(\omega) > 0$ the condition (3.44), ensure $4n$ points of interpolation of the positive branch (3.40) in $\left(-d, d\right)$ and $\mathbb{C} - \mathbb{R}$ respectively. Combining (3.42) and (3.44) we see that for,

$$\sigma_{xj} > \left| \frac{C}{\sqrt{A\left(4AB - C^2\right)}} \right|, \tag{3.45}$$

$\left(-C\sigma_y/2 + P_{2n,2n-2}\right)/A$ interpolates (3.40) at $4n$ points in $\mathbb{C} - \left(-\infty, -d\right] - \left[d, \infty\right)$ counted with multiplicity (again for $\mathrm{Im}\left(\omega\right) > 0$ where applicable) and we thus have a sufficient condition for well-posedness.

To show that (3.45) is also necessary, the above arguments (from (3.42) onwards) can easily be reversed to show that $\sigma_{xj} \leq \left| C/\sqrt{A\left(4AB - C^2\right)} \right|$ ensures at least one interpolation of the wrong branch (3.41) in $\mathbb{C} - \left(-\infty, -d\right] - \left[d, \infty\right)$. For example, for $-2\sqrt{B}/\sqrt{4AB - C^2} \leq \sigma_{xj} \leq \left| C/\sqrt{A\left(4AB - C^2\right)} \right|$, we get at least one of the reference group velocities to be non-positive i.e. $c_j \leq 0$ and/or $\overline{c}_j \leq 0$ from (3.25). This implies at least one corresponding point of interpolation of the wrong branch. For $\sigma_{xj} < -2\sqrt{B}/\sqrt{4AB - C^2}$, we can reverse the arguments immediately following (3.44) using the fact that $\sigma_{xj} < 0$.

The above arguments show that (3.45) is *both* a *necessary* and a *sufficient* condition for satisfying the well-posedness criterion presented at the beginning of this sub-section.

We assumed $P_{2n,2n-2}\left(\sigma_y\right) \neq 0,\infty$ for $\sigma_y = 0$, in deriving the well-posedness criterion (3.45) (see the ending of the last sub-section); this assumption can now be verified as follows. At $\sigma_y = 0$, $c_{gx} = \sqrt{A}$ from (3.6) and (3.7). Since (3.45) is the same as the sufficient condition for accuracy (3.28) , based on the definition of accuracy in (3.27) and given that $c_{gx} = \sqrt{A} > 0$, we have $\left|R_n\right| < 1$. Since $\left|R_n\right| < 1$, based on (3.23) , $P_{2n,2n-2}\left(\sigma_y\right) \neq 0,\infty$ for $\sigma_y = 0$.

Hence, (3.45) is a necessary and sufficient condition for well-posedness of a n-layer PMDL with parameters $\sigma_{xj} \in \mathbb{R} \quad \left(j = 1 \ldots n\right)$. Since this is the same as (3.28), well-posedness *guarantees* accuracy. The geometric representation of (3.45) is shown in Figure 3.4.

It was shown in [40] that (3.28) is a sufficient condition for accuracy. It might be possible to show that it is also necessary for accuracy in some sense. We do not bother to do this because any change in (3.28) will only lead to ill-posedness as (3.28) is already a necessary condition for well-posedness.

3.5.5 Relation between Tilted and Untilted Anisotropy

We were able to arrive at the well-posedness condition (3.45) for tilted anisotropic media by using the results already available for isotropic acoustics. We have already noted in Section 3.4 and in [40], that the distinguishing characteristic of PMDL is that it approximates stiffness instead of the horizontal wave number. This characteristic is precisely the one that allows us to borrow the results from isotropic acoustics and apply them to tilted anisotropy. The two properties that distinguish tilted anisotropy from isotropy are obviously the anisotropy $\left(A \neq B\right)$ and the tilt $\left(C \neq 0\right)$ as shown inFigure 3.2. Untilted anisotropy can be easily converted to isotropy by a simple scaling of variable as in (3.37). Hence, if we wish to

somehow connect tilted anisotropy to isotropy, the difficulty mainly lies in converting tilted anisotropy to untilted anisotropy.

The exact horizontal slowness (3.9) represents a tilted ellipse in $\left(\sigma_y, \sigma_x\right)$ space for $A \neq B$ and $C \neq 0$. However, the exact stiffness given by (3.11) represents an *untilted* ellipse in $\left(\sigma_y, iK/\omega\right)$ space. Since the current PMDL approximates stiffness (or iK/ω to be more precise) by a rational function $P_{2n,2n-2}$ (3.20), we are in essence approximating an *untilted* ellipse by a rational function even though we are dealing with tilted anisotropic media. But approximating untilted ellipses by rational functions is precisely what occurs in rational approximations of untilted anisotropy [35]. Hence, approximating stiffness in general, and the form of our PMDL (3.19) in particular, provides a natural connection between tilted and untilted anisotropy. This explains our ability to use the well-posedness results of isotropic acoustics.

Well-posedness (or stability) of PML for convective acoustics with uniform parallel and oblique mean flow (dispersion relation of shifted and/or tilted ellipse) has been possible due to linear variable transformations (see [23-30,32]). Among other things, such variable transformations result in removing the tilt; or, in other words, they convert the dispersion relation from a tilted ellipse to an untilted ellipse. Though we approach the well-posedness of PMDL from the viewpoint of rational ABCs, the ideas of variable transformations used for PML ([23-30,32]) and other rational ABCs ([33]) are similar to the one discussed previously of converting a tilted ellipse in $\left(\sigma_y, \sigma_x\right)$ space to an untilted ellipse in $\left(\sigma_y, iK/\omega\right)$ space. However, the reference to untilted cases is made in this work purely to gain a better understanding of the inner workings of PMDL and for comparison purposes only. Note that the PMDL formulation (of approximating stiffness instead of wavenumbers) is such that *no explicit coordinate transformation is required*. This, we hope, will facilitate a relatively straightforward extension to the well-posedness studies of models involving corners and heterogeneous (layered) media; work on this is currently ongoing.

We also mention that the proof of well-posedness presented here *does not* contradict the result of [26] which, in essence, states that a necessary condition for stability of PML with complex coordinate stretching in the direction of unboundedness (x) is $c_{gx}c_{px} \geq 0$. The result in [26] is derived for a full-space PML medium with *constant complex* coordinate stretching; it considers the continuous, un-truncated PML. The n-layer PMDL considered here has purely imaginary layer lengths; it is discrete and truncated to begin with. Moreover, the PMDL formulation is such that there is *no* discretization error (*only* truncation error). Hence, it seems that even in the limit of fine discretization, the n-layer PMDL tends to the *truncated* continuous PML and not the full-space PML (both PML and PMDL considered with similar stretching i.e. both with complex or purely imaginary stretching). While it may seem counterintuitive, ongoing work suggests that it is this truncation that contributes to the well-posedness of PMDL. A detailed analysis is outside the scope of this paper.

3.6 Numerical Stability

It is known that well-posedness by itself does not guarantee numerical stability. Typically well-posedness is associated with boundedness of continuous models while stability deals with their discretized counterparts. It is important to recognize that well-posedness by itself may not exclude exponential growth, but stability requirements impose no growth, or at most polynomial growth [26]. Moreover, numerical stability deals with issues arising out of numerical implementation and finite precision arithmetic. PMDL as presented till now is continuous in time but discrete in space to begin with. Hence numerical stability here refers to time discretization and finite precision arithmetic.

We are interested in asymptotic stability i.e. boundedness of the solution as $t \to \infty$. It is well known from eigenvalue analysis that if λ denotes an eigenvalue of a matrix $\mathbf{M}$, a first order system of the form $\partial \mathbf{u} \big/ \partial t = \mathbf{M}\mathbf{u}$ is asymptotically stable if and only if, (a) $\mathrm{Re}(\lambda) \leq 0$ and (b) $\mathrm{Re}(\lambda) = 0 \Rightarrow \lambda$ is semi-simple. Stability proof of the time discretized equations can be simplified using the results of continuous time stability presented in the following sub-section.

3.6.1 Continuous Time Stability

Inverse Fourier transforming (3.17) through the duality $\partial/\partial t \leftrightarrow -i\omega$, and defining $\mathbf{v} = \partial\mathbf{u}/\partial t$, $\mathbf{w} = \int \mathbf{u}\,dt$, we get,

$$\mathbf{F} = \mathbf{C}\mathbf{v} + \mathbf{K}\mathbf{u} + \mathbf{R}\mathbf{w}. \tag{3.46}$$

The matrix $\mathbf{C}$ can easily be seen to be invertible from (3.16). For $\mathbf{F} = \mathbf{0}$, (3.46) can be reformulated as,

$$\frac{\partial}{\partial t}\begin{Bmatrix}\mathbf{u}\\ \mathbf{w}\end{Bmatrix} = \begin{bmatrix}\text{-}\mathbf{C}^{-1}\mathbf{K} & \text{-}\mathbf{C}^{-1}\mathbf{R}\\ \mathbf{I} & \mathbf{0}\end{bmatrix}\begin{Bmatrix}\mathbf{u}\\ \mathbf{w}\end{Bmatrix}. \tag{3.47}$$

Equation (3.47) is of the form $\partial\mathbf{u}/\partial t = \mathbf{M}\mathbf{u}$, and if λ are the eigenvalues, then,

$$\begin{aligned} 0 = \left|\mathbf{M} - \lambda\mathbf{I}\right| &= \begin{vmatrix}\text{-}\mathbf{C}^{-1}\mathbf{K} - \lambda\mathbf{I} & \text{-}\mathbf{C}^{-1}\mathbf{R}\\ \mathbf{I} & -\lambda\mathbf{I}\end{vmatrix}\\ &= \left|\lambda^2\mathbf{I} + \lambda\mathbf{C}^{-1}\mathbf{K} + \mathbf{C}^{-1}\mathbf{R}\right| = \left|\mathbf{C}^{-1}\right|\left|\lambda^2\mathbf{C} + \lambda\mathbf{K} + \mathbf{R}\right| \end{aligned}, \tag{3.48}$$

where the third equality follows from the standard block determinant of matrices simplified by the presence of the identity matrices in the lower two blocks with the assumption of $\lambda \neq 0$. Comparing (3.48) with (3.17), and noting that $\left|\mathbf{C}^{-1}\right| \neq 0$, we get $\lambda = -i\omega_R$, where ω_R are the resonant frequencies (i.e. ω_R satisfy $\left|-i\omega_R\mathbf{C} + \mathbf{K} + \left(i/\omega_R\right)\mathbf{R}\right| = 0$). Note that the assumption $\lambda \neq 0$ is now validated because $\omega_R \neq 0$.

In the previous section we proved that (3.45) ensured well-posedness. Trefethen and Halpern [35] have proved that a necessary condition for well-posedness is that the zeroes of $\tilde{P}_{2n,2n-2}(\tilde{\sigma}_y)/\tilde{\sigma}_y$ (defined in (3.37)) are real and simple (Theorem 2 in [35]). Using (3.37),

(3.19) and (3.22), the theorem regarding the zeroes of $\tilde{P}_{2n,2n-2}(\tilde{\sigma}_y)\big/\tilde{\sigma}_y$ translates to the resonant frequencies ω_R being real and simple. This ensures asymptotic stability.

3.6.2 Discretized Time Stability

A Crank-Nicolson discretization of (3.47) gives,

$$\frac{1}{\Delta t}\begin{Bmatrix}\mathbf{u}_{t+\Delta t}-\mathbf{u}_t\\ \mathbf{w}_{t+\Delta t}-\mathbf{w}_t\end{Bmatrix}=\frac{1}{2}\begin{bmatrix}\text{-}\mathbf{C}^{-1}\mathbf{K} & \text{-}\mathbf{C}^{-1}\mathbf{R}\\ \mathbf{I} & \mathbf{0}\end{bmatrix}\begin{Bmatrix}\mathbf{u}_{t+\Delta t}+\mathbf{u}_t\\ \mathbf{w}_{t+\Delta t}+\mathbf{w}_t\end{Bmatrix}. \tag{3.49}$$

From the previous subsection we know that the eigenvalues $\lambda=-i\omega_R$ of $\mathbf{M}$ are simple. Hence $\mathbf{M}$ is diagonalizable and we have $\mathbf{MV}=\mathbf{VD}$ where $D=diag\{\lambda_1\ldots\lambda_{2n}\}$. Using this, (3.49) can be manipulated as follows:

$$\begin{aligned}
&\frac{1}{\Delta t}\mathbf{V}\mathbf{V}^{-1}\begin{Bmatrix}\mathbf{u}_{t+\Delta t}-\mathbf{u}_t\\ \mathbf{w}_{t+\Delta t}-\mathbf{w}_t\end{Bmatrix}=\frac{1}{2}\begin{bmatrix}\text{-}\mathbf{C}^{-1}\mathbf{K} & \text{-}\mathbf{C}^{-1}\mathbf{R}\\ \mathbf{I} & \mathbf{0}\end{bmatrix}\mathbf{V}\mathbf{V}^{-1}\begin{Bmatrix}\mathbf{u}_{t+\Delta t}+\mathbf{u}_t\\ \mathbf{w}_{t+\Delta t}+\mathbf{w}_t\end{Bmatrix}\\
&\frac{1}{\Delta t}\mathbf{V}^{-1}\begin{Bmatrix}\mathbf{u}_{t+\Delta t}-\mathbf{u}_t\\ \mathbf{w}_{t+\Delta t}-\mathbf{w}_t\end{Bmatrix}=\frac{1}{2}\mathbf{D}\mathbf{V}^{-1}\begin{Bmatrix}\mathbf{u}_{t+\Delta t}+\mathbf{u}_t\\ \mathbf{w}_{t+\Delta t}+\mathbf{w}_t\end{Bmatrix}\\
&-\left[\frac{1}{2}\mathbf{D}+\frac{1}{\Delta t}\mathbf{I}\right]\mathbf{V}^{-1}\begin{Bmatrix}\mathbf{u}_t\\ \mathbf{w}_t\end{Bmatrix}=\left[\frac{1}{2}\mathbf{D}-\frac{1}{\Delta t}\mathbf{I}\right]\mathbf{V}^{-1}\begin{Bmatrix}\mathbf{u}_{t+\Delta t}\\ \mathbf{w}_{t+\Delta t}\end{Bmatrix}
\end{aligned}. \tag{3.50}$$

Since $\mathbf{D}$ is diagonal, the last system in (3.50) is a set of decoupled equations of the general form,

$$\phi_{t+\Delta t}=\left(\frac{1/\Delta t+\lambda/2}{1/\Delta t-\lambda/2}\right)\phi_t=\left(\frac{2+\lambda\Delta t}{2-\lambda\Delta t}\right)\phi_t, \tag{3.51}$$

with ϕ denoting *any* component of the vector $\mathbf{V}^{-1}\{\mathbf{u}\ \mathbf{w}\}^T$ and λ the corresponding eigenvalue. Since $\lambda=-i\omega_R$, we have $\left|\phi_{t+\Delta t}\right|=\left|\phi_t\right|$. This implies asymptotic stability of the time discretized form (3.49). Note that (3.46) models only the exterior and hence the numerical stability assured by (3.51) does not consider the effect of the interior on the

stability of the coupled (interior+exterior) model. As mentioned before, we do not consider issues related to interior discretization in this work. We mention however, that in the presence of an interior, time discretization is performed using the implicit extended constant average acceleration (instead of Crank-Nicolson) and details of its implementation can be found in [38,45,49].

3.6.3 Finite Precision Issues

While (3.51) ensures asymptotic stability, it still neglects issues related to finite precision arithmetic. While the theorem of Trefethen and Halpern (Theorem 2 in [35]) ensures that the resonant frequencies are simple (and hence distinct), they can be arbitrarily close to each other, especially for large number of layers. If round off errors due to finite precision make these frequencies indistinguishable, there will be polynomial growth associated with repeated eigenvalues. In the case of multiple absorbing boundaries, this can also manifest as exponential growth [48]. The variable in (3.51) is also not the original field variable $\{\mathbf{u}\ \mathbf{w}\}^T$, but $\mathbf{V}^{-1}\{\mathbf{u}\ \mathbf{w}\}^T$. In the presence of $\mathbf{V}^{-1}$, the magnitude of the field variables will depend on the condition number of $\mathbf{V}$ which may be large. Moreover, $\lambda = -i\omega_R$ only ensures $\mathrm{Re}(\lambda) = 0$ and not the stronger form $\mathrm{Re}(\lambda) < 0$. Numerical perturbations due to finite precision arithmetic may result in $\mathrm{Re}(\lambda) > 0$ and this implies growth in time. Finite precision issues are beyond the scope of this work.

3.7 Numerical Examples

We consider a 2D model problem with a square interior consisting of a scalar tilted anisotropic medium that is modeled by a mesh of 200×200 regular square bilinear finite elements of size $h = 2\times10^{-4}$. The exterior is represented by ABCs on all four edges/corners. Using the material parameters $a = 1, b = 2, \beta = 30^o$ in (3.3), the well-posedness and accuracy condition for PMDL in the *x* direction is $\sigma_{xj} > 0.72$ (3.45). For PMDL in the *y* direction we have $a = 1, b = 2, \beta = 60^o$ and hence (3.45) results in $\sigma_{yj} > 0.98$. For

simplicity, we assume $\sigma_{yj} = 1.5\sigma_{xj}$ and $\sigma_{x1} = \sigma_{x2} = \ldots = \sigma_{xn}$, thus reducing the number the PMDL parameters to just one. The excitation is assumed to be $\sin^2\left(\pi x/5h\right) \times \sin^2\left(\pi y/5h\right) \times \sin^2\left(\pi t/10\Delta t\right)$ for $|x| \le 5h, |y| \le 5h$ and $t \le 10\Delta t$ where $\Delta t = 2 \times 10^{-4}$ is the time step size. The excitation is taken to occur at the origin of the coordinate system with the four corners of the interior domain being positioned at (-0.01, 0.01), (0.03, 0.01), (0.03, -0.03) and (-0.01, -0.03). This ensures that the excitation is at the center of the upper left quarter of the interior i.e. it is placed closer to some interior boundaries and corners than others. For comparison, the reference solution is obtained using a 500×500 interior with the same element and time step size as before. The relative error in norm is calculated as $\left\|u_{PMDL} - u_{reference}\right\|_2 / \left\|u_{reference}\right\|_2$ and expressed as a percentage. The interior chosen and the reference solution at various times is shown in Figure 3.5.

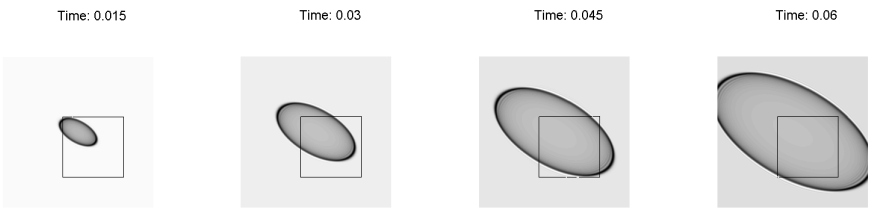

Figure 3.5. Reference solution in a large (500x500) domain at various times. For numerical experiments, the interior chosen is denoted by the square and PMDL is applied at the edges of this square.

The accuracy obtained for different values of the PMDL parameters σ_{xj} for a 2 layer PMDL can be visually inferred from Figure 3.6 and is numerically quantified in Figure 3.7. The inaccuracies of violating (3.45) are obvious in Figure 3.6 and Figure 3.7 shows that the least accurate results are obtained when σ_{xj} is below the cusp i.e. when the parameters violate the accuracy and well-posedness criterion (3.45). In the present case (3.45) implies

$\sigma_{xj} > 0.72$ and since we use $\sigma_{yj} = 1.5\sigma_{xj}$, (3.45) is also violated in the y direction when $\sigma_{xj} = 0.2, 0.4, 0.6$. The relative error is also seen to increase when the parameters are chosen above the peak of the ellipse. This is because of the fact that for such parameters there will be no interpolation points on the ellipse (see [40]) and since we wish to capture a part of the ellipse (the positive group velocity part) we should expect some loss in accuracy in this case. The slowness diagram from [40] is presented again in Figure 3.8 to clarify this point.

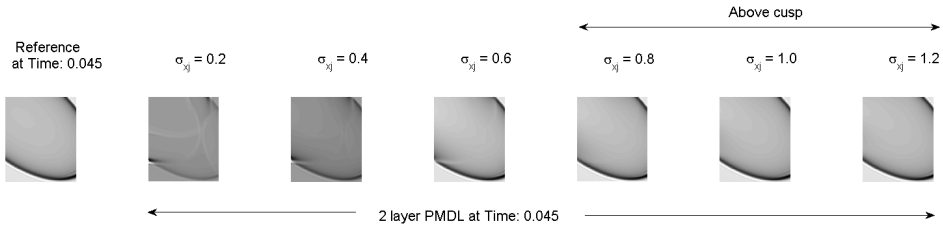

Figure 3.6. Interior solution for a 2 – layer PMDL exterior with various PMDL parameters. Only the last three simulations have parameters above the cusp and thus satisfy the well-posedness and accuracy criterion.

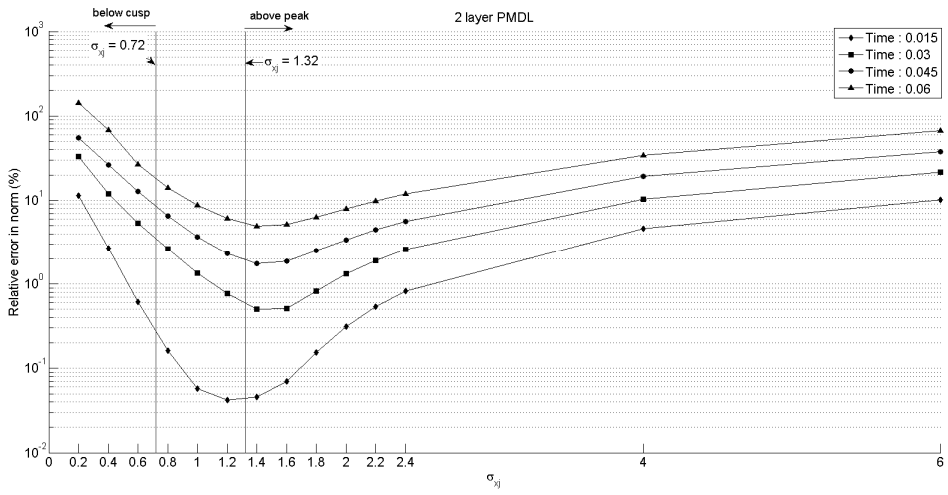

Figure 3.7. Relative error in norm for a 2 layer PMDL with various parameters at different times. The lines demarcating the cusp of the slowness ellipse and its peak are shown.

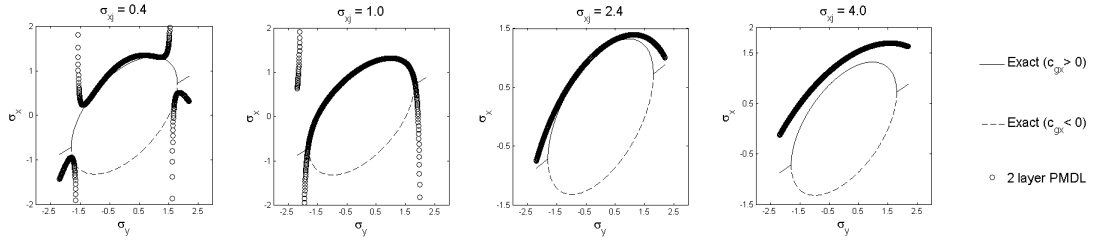

Figure 3.8. Slowness diagrams for 2 layer PMDL approximation with parameters chosen below the cusp, between the cusp and peak and above the peak. The first figure has interpolation points with negative group velocity while the second one has interpolation points with positive group velocity. The last two do not have any interpolation points on the ellipse though they do approximate only the positive group velocity branch.

Increasing the number of PMDL layers will improve the accuracy *only if* the parameters satisfy (3.45). This is clearly demonstrated in Figure 3.9. By comparing Figure 3.7 and Figure 3.9, we see that for parameters chosen below the cusp, there is an improvement in accuracy only at earlier times. With increasing time, and hence with increasing number of reflections from the PMDL boundaries, the solution deteriorates. The gain in accuracy when parameters satisfying (3.45) are chosen is also evident from these two figures.

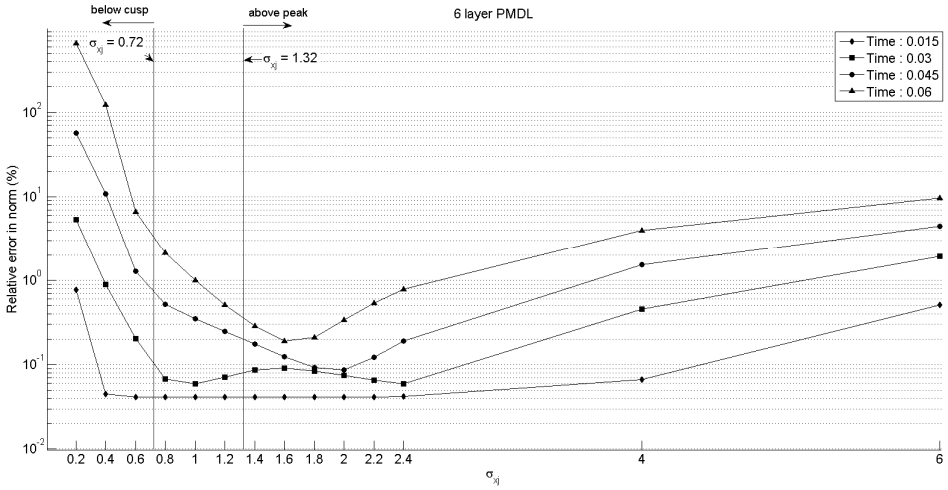

Figure 3.9. Relative error in norm for a 6 layer PMDL with various parameters. The lines demarcating the cusp of the slowness ellipse and its peak are shown.

The importance of (3.45) on the well-posedness and stability of the problem at hand is demonstrated by examining the long time behavior of the numerical solution. Figure 3.10 shows that except for the case of $\sigma_{xj} = 0.8$, instability occurs *only* when the parameters violate (3.45) i.e. when $\sigma_{xj} \leq 0.72$ and the solution is stable when (3.45) is satisfied.

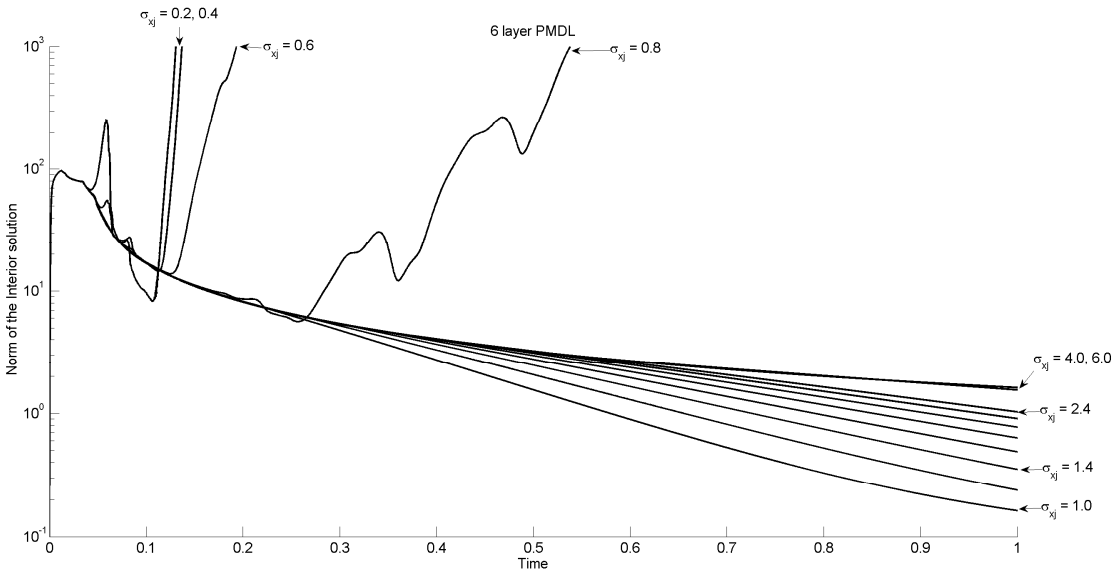

Figure 3.10. Long time behavior of the interior solution with a 6 layer PMDL approximating the exterior with various parameters.

The case of $\sigma_{xj} = 0.8$ becoming unstable even while satisfying (3.45) can be explained by observing the interior solution shown in Figure 3.11. It was noted that when parameters are chosen above the cusp and very near to it, such instability occurs when the number of PMDL layers is large. For example it does not occur with a 2 layer PMDL. For a 6 layer PMDL, Figure 3.11 shows ripples along the boundary that are characteristic of this kind of instability. These ripples decay exponentially in a direction perpendicular to the boundary and propagate along the boundary with their amplitudes increasing with time. This suggests that they are due to a combination of the reflection of evanescent waves not handled by the PMDL used in this experiment and the highly oscillatory behavior of the PMDL approximation near the zero group velocity regions of the slowness diagram (see [40]). Such an instability can be handled as in [40] by either not using parameters very near the cusp or by using padding layers between the interior and PMDL. The effect of using parameters relatively far from the cusp is evident in Figure 3.10. Padding layers are a form of PMDL that can handle evanescent waves and consist of mid-point integrated linear finite elements

with real lengths [44,45] ; without delving into the behavior and design of padding layers, we present the effect of PMDL with padding in Figure 3.12 and Figure 3.13. When compared to Figure 3.10, Figure 3.12 clearly shows the stabilization of the $\sigma_{xj} = 0.8$ case. While the experiments with the correct parameters lead to stable solutions, their accuracy can be seen to reduce with time both in Figure 3.10 and in Figure 3.12. This loss in long term accuracy is consistent with the observation in [10] and can be attributed to the fact that we have either completely neglected the evanescent spectrum or only handled it in an ad hoc manner. We reemphasize that PMDL *can* handle evanescent modes effectively [44,45]; our restriction to propagating modes is intended only to make the well-posedness problem tractable. Unlike in the case of [45], the behavior of padding layers in the case of tilted anisotropic acoustics is not completely understood yet and the padding layers may only be delaying the onset of instability (instead of completely eliminating it). Their use here to handle instabilities is based on promising but preliminary studies.

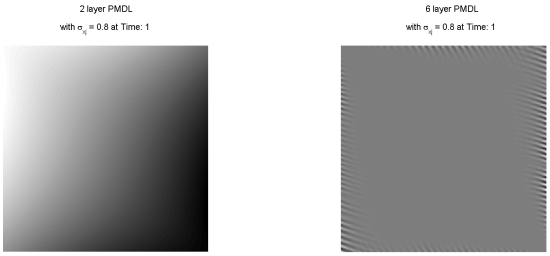

Figure 3.11. Interior solution for the case where the PMDL parameter is above the cusp but still close to it.

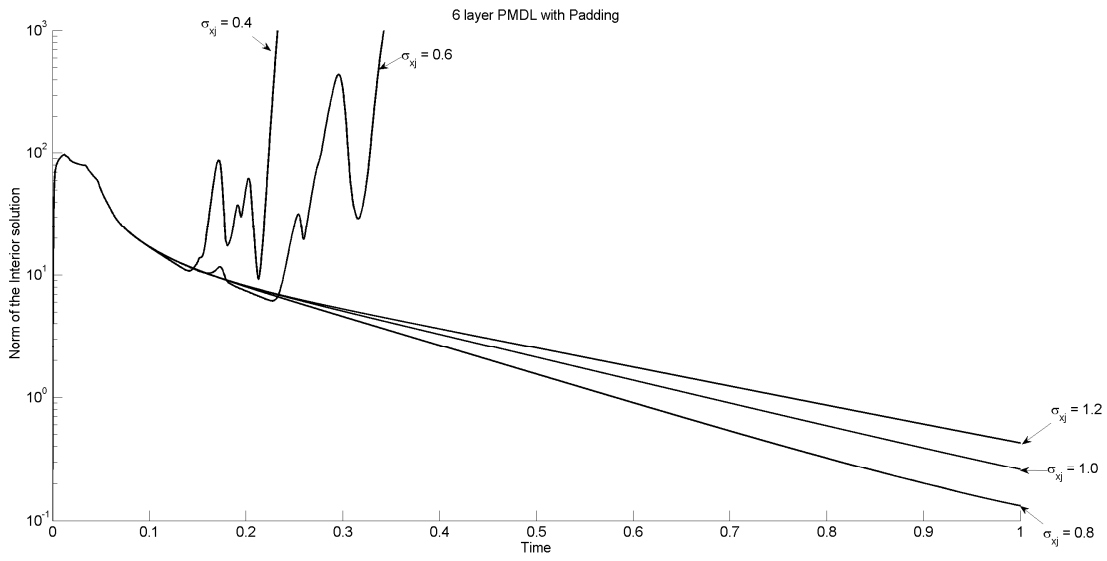

Figure 3.12. Long time behavior of the interior solution with a 6 layer PMDL approximating the exterior with parameters chosen near the cusp. The rogue behavior seen with $\sigma_{xj} = 0.8$ in Figure 3.10 is no longer present. Six padding layers with ad hoc parameters were used.

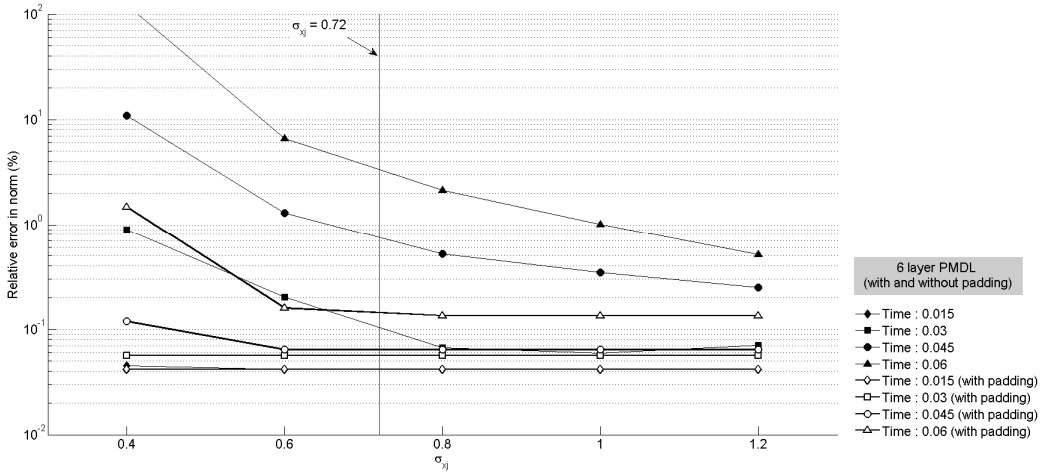

Figure 3.13. Comparison of accuracy achieved with and without padding layers. The gain in accuracy can be attributed to the handling of the evanescent spectrum and the smoothening of the PMDL approximation near zero group velocity modes.

3.8 Summary and Conclusions

A necessary and sufficient condition for well-posedness of PMDL is presented for the scalar anisotropic wave equation. This condition also turns out to be sufficient for accuracy. The algebraic criterion derived here provides a simple bound for PMDL layer lengths and ensures well-posedness in Kreiss's sense. This bound depends on the anisotropy of the medium, in particular the tilt, and guarantees strong well-posedness of any PMDL satisfying the bound.

The final form of the well-posed PMDL derived here is similar to the well-posed PML [23-30,32] and rational ABC [33] obtained through coordinate rotations, but has two important differences: (a) Well-posedness analyses of PML typically consider full-space IVPs, while we consider the IBVPs obtained from coupling the interior with truncated PMDL. (b) Existing analyses consider continuous PMLs, while we consider PMDL, which is already a discretized version of PML, with the important property of perfect matching even after discretization. Thus, the problem considered in this paper is closer to the computational problem which involves both discretization and truncation (although we do not consider the issue of *interior* discretization).

To make the well-posedness problem tractable, the PMDL formulation is not considered in all its generality. The present study is confined to propagating wave modes, single straight computational boundary and homogeneous though anisotropic exteriors. None of the these restrictions, however, are due to actual limitations of PMDL and the PMDL formulation shows promise of being extendible to more complex media. For instance, in deriving the well-posedness criterion, the PMDL formulation is shown to naturally overcome challenges posed by the existence of wave modes with differing phase and group velocity signs *without the need of an explicit coordinate transformation.* This is unlike the techniques used to handle opposing phase and group velocity signs for the design of both PMLs [23-30,32] and rational ABCs [33]. Since techniques involving coordinate rotations cannot be directly extended to heterogeneous (layered) media, the PMDL ABC holds greater promise for such media. Moreover, the distinctive property of PMDL, namely approximation of half-space stiffness instead of the wavenumber, is central to the ability of PMDL to capture the correct

group velocities even when the group and phase velocities are not aligned in the same direction. This is because the group velocity and stiffness are related (at least in this case) and PMDL approximates the stiffness. We hypothesize that the link between group velocity and stiffness extends to general vector systems and that this link can be used to ensure well-posedness of PMDL even in more complicated media (like elastodynamics) that are governed by vector equations. Further investigation in this direction is underway.

3.9 References

[1] D. Givoli, Nonreflecting Boundary-Conditions, J. Comput. Phys. 1 (1991), 1-29.

[2] S.V. Tsynkov, Numerical solution of problems on unbounded domains. A review, Appl. Numer. Math. 4 (1998), 465-532.

[3] T. Hagstrom, New results on absorbing layers and radiation boundary conditions, Topics in Computational Wave Propagation - Direct and Inverse Problems (2003), 1-42.

[4] E.L. Lindman, Free-Space Boundary-Conditions for Time-Dependent Wave-Equation, J. Comput. Phys. 1 (1975), 66-78.

[5] B. Engquist and A. Majda, Absorbing Boundary-Conditions for Numerical-Simulation of Waves, Math. Comput. 139 (1977), 629-651.

[6] B. Engquist and A. Majda, Radiation Boundary-Conditions for Acoustic and Elastic Wave Calculations, Commun. Pure Appl. Math. 3 (1979), 313-357.

[7] A. Bayliss and E. Turkel, Radiation Boundary-Conditions for Wave-Like Equations, Commun. Pure Appl. Math. 6 (1980), 707-725.

[8] R.L. Higdon, Numerical Absorbing Boundary-Conditions for the Wave-Equation, Math. Comput. 179 (1987), 65-90.

[9] D. Givoli, High-order local non-reflecting boundary conditions: a review, Wave Motion 4 (2004), 319-326.

[10] T. Hagstrom, A. Mar-Or and D. Givoli, High-order local absorbing conditions for the wave equation: Extensions and improvements, J. Comput. Phys. 6 (2008), 3322-3357.

[11] J.P. Bérenger, A Perfectly Matched Layer for the Absorption of Electromagnetic-Waves, J. Comput. Phys. 2 (1994), 185-200.

[12] W.C. Chew, J.M. Jin and E. Michielssen, Complex coordinate stretching as a generalized absorbing boundary condition, Microwave Opt Technol Lett 6 (1997), 363-369.

[13] W.C. Chew and W.H. Weedon, A 3d Perfectly Matched Medium from Modified Maxwells Equations with Stretched Coordinates, Microwave Opt Technol Lett 13 (1994), 599-604.

[14] Z.S. Sacks, D.M. Kingsland, R. Lee and J.F. Lee, A perfectly matched anisotropic absorber for use as an absorbing boundary condition, IEEE Trans. Antennas Propag. 12 (1995), 1460-1463.

[15] F. L. Teixeira, W. C. Chew, Analytical Derivation of a Conformal Perfectly Matched Absorber for Electromagnetic Waves, Microwave Opt Technol Lett 17 (1998), 231-236.

[16] Kuzuoglu and Mittra, Frequency dependence of the constitutive parameters of causal perfectly matched anisotropic absorbers, IEEE Microwave Guided Wave Lett. 12 (1996), 447.

[17] Roden and Gedney, Convolution PML (CPML): An efficient FDTD implementation of the CFS-PML for arbitrary media, Microwave Opt Technol Lett 5 (2000), 334.

[18] Meza-Fajardo, Papageorgiou, A nonconvolutional, split-field, perfectly matched layer for wave propagation in isotropic and anisotropic elastic media: Stability analysis. Bulletin of the Seismological Society of America 4 (2008), 1811-1836.

[19] S. Abarbanel and D. Gottlieb, A mathematical analysis of the PML method, J. Comput. Phys. 2 (1997), 357-363.

[20] J.S. Hesthaven, On the analysis and construction of perfectly matched layers for the linearized Euler equations, J. Comput. Phys. 1 (1998), 129-147.

[21] P.G. Petropoulos, L. Zhao and A.C. Cangellaris, A reflectionless sponge layer absorbing boundary condition for the solution of Maxwell's equations with high-order staggered finite difference schemes, J. Comput. Phys. 1 (1998), 184-208.

[22] Feng, Absorbing boundary conditions for electromagnetic wave propagation, Math. Comput. 225 (1999), 145.

[23] S. Abarbanel, D. Gottlieb and J.S. Hesthaven, Well-posed perfectly matched layers for advective acoustics, J. Comput. Phys. 2 (1999), 266-283.

[24] F.Q. Hu, A stable, perfectly matched layer for linearized Euler equations in unsplit physical variables, J. Comput. Phys. 2 (2001), 455-480.

[25] Hagstrom T. A new construction of perfectly matched layers for hyperbolic systems with applications to the linearized Euler equations, in: Mathematical and numerical aspects of wave propagation, Proceedings Waves 2003, Cohen et al, ed., Springer-Verlag, 2003, pp. 125-129.

[26] E. Bécache, S. Fauqueux and P. Joly, Stability of perfectly matched layers, group velocities and anisotropic waves, J. Comput. Phys. 2 (2003), 399-433.

[27] E. Bécache, A.S. Bonnet-Ben Dhia and G. Legendre, Perfectly matched layers for the convected Helmholtz equation, SIAM J. Numer. Anal. 1 (2004), 409-433.

[28] F.Q. Hu, A Perfectly Matched Layer absorbing boundary condition for linearized Euler equations with a non-uniform mean flow, Journal of Computational Physics. 208(2005), 469-492.

[29] E. Bécache, A.S.B.B. Dhia and G. Legendre, Perfectly matched layers for time-harmonic acoustics in the presence of a uniform flow, SIAM J. Numer. Anal. 3 (2006), 1191-1217.

[30] J. Diaz and P. Joly, A time domain analysis of PML models in acoustics, Comput. Methods Appl. Mech. Eng. 29-32 (2006), 3820-3853.

[31] D. Appelö and G. Kreiss, A new absorbing layer for elastic waves, J. Comput. Phys. 2 (2006), 642-660.

[32] Parrish S, Hu F. PML absorbing boundary conditions for the linearized and nonlinear Euler equations in the case of oblique mean flow. Int.J.Numer.Methods Fluids, 60(2009), 565-589.

[33] Becache E, Givoli D, Hagstrom T. High-order Absorbing Boundary Conditions for anisotropic and convective wave equations. Journal of Computational Physics, 229(2010), 1099-1129.

[34] R.L. Higdon, Initial-Boundary Value-Problems for Linear Hyperbolic Systems, SIAM Rev 2 (1986), 177-217.

[35] L.N. Trefethen and L. Halpern, Well-Posedness of One-Way Wave-Equations and Absorbing Boundary-Conditions, Math. Comput. 176 (1986), 421-435.

[36] D. Appelö, T. Hagstrom and G. Kreiss, Perfectly matched layers for hyperbolic systems: General formulation, well-posedness, and stability, SIAM J Appl Math 1 (2006), 1-23.

[37] K.W. Lim, Absorbing Boundary Conditions For Corner Regions, Master's Thesis, North Carolina State University, 2003.

[38] M.N. Guddati and K.W. Lim, Continued fraction absorbing boundary conditions for convex polygonal domains, Int J Numer Methods Eng 6 (2006), 949-977.

[39] M.N. Guddati, K.W. Lim and M.A. Zahid, Perfectly Matched Discrete layers for Unbounded Domain Modeling, in: Computational Methods for Acoustics Problem, F. Magoulès, ed., Saxe-Coburg Publications, Scotland, 2008, pp. 69-98.

[40] S. Savadatti, M.N. Guddati, Absorbing Boundary Conditions for Scalar Waves in Anisotropic Media. Part 1: Time harmonic modeling, J. Comput. Phys. 229-19 (2010), pp. 6696-6714.

[41] H.O. Kreiss, Initial Boundary Value Problems for Hyperbolic Systems, Commun. Pure Appl. Math. 3 (1970), 277-&.

[42] H. Kreiss and J. Lorenz, Initial-boundary value problems and the Navier-Stokes equations, Academic Press, Boston, 1989, pp. 402.

[43] S. Asvadurov, V. Druskin, M.N. Guddati and L. Knizhnerman, On optimal finite-difference approximation of PML, SIAM J. Numer. Anal. 1 (2003), 287-305.

[44] M.N. Guddati, Arbitrarily wide-angle wave equations for complex media, Comput. Methods Appl. Mech. Eng. 1-3 (2006), 65-93.

[45] M.A. Zahid, M.N. Guddati, Padded continued fraction absorbing boundary conditions for dispersive waves, Comput. Methods Appl. Mech. Eng. 29-32 (2006), 3797-3819.

[46] T. Hagstrom and T. Warburton, Complete radiation boundary conditions: minimizing the long time error growth of local methods, http://faculty.smu.edu/thagstrom/HWcomplete.pdf (2008).

[47] R.L. Higdon, Absorbing Boundary-Conditions for Difference Approximations to the Multidimensional Wave-Equation, Math. Comput. 176 (1986), 437-459.

[48] L.N. Trefethen, Group-Velocity Interpretation of the Stability Theory of Gustafsson, Kreiss, and Sundstrom, J. Comput. Phys. 2 (1983), 199-217.

[49] M.N. Guddati and J.L. Tassoulas, Continued-fraction absorbing boundary conditions for the wave equation, J. Comput. Acoust. 1 (2000), 139-156.

Chapter 4 Accurate Absorbing Boundary Condition for Tilted Elliptic Anisotropic Elasticity

This chapter is intended to be submitted for publication as a self-sufficient manuscript.

4.1 Abstract

With the ultimate goal of devising effective absorbing boundary conditions (ABCs) for general elastic media, we investigate the accuracy aspects of local ABCs designed for tilted elliptic anisotropic media in the frequency domain (time-harmonic case). Such media support both anti-plane and in-plane wavemodes with opposing signs of phase and group velocities $(c_{px}c_{gx} < 0)$ that have long posed a significant challenge to the design of accurate (and stable) local ABCs. By first considering the simpler case of scalar anti-plane waves, we show that it is possible to overcome the challenges posed by $c_{px}c_{gx} < 0$ by simply utilizing the inevitable reflections occurring at the truncation boundaries. This understanding helps us explain the ability of a recently developed local ABC – the perfectly matched *discrete* layer (PMDL) – to handle the challenges posed by $c_{px}c_{gx} < 0$ *without* the need of intervening space-time transformations. PMDL is a simple variant of perfectly matched layers (PML) that is also equivalent to rational approximation-based local ABCs (rational ABCs); it inherits the straightforward approximation properties of rational ABCs along with the versatility of PML. The approximation properties of PMDL quantified through its reflection matrix is used to derive simple bounds on the PMDL parameters necessary for the accurate absorption of all outgoing anti-plane and in-plane wavemodes present in tilted elliptic anisotropic elasticity – even those with $c_{px}c_{gx} < 0$. Beyond the previously derived bound on the real parameters of PMDL sufficient for the absorption of outgoing propagating anti-plane wavemodes, we present bounds on the *complex* parameters of PMDL necessary for the absorption of outgoing propagating *and* evanescent wavemodes for both anti-plane and

coupled in-plane pressure and shear waves of tilted elliptic anisotropic elasticity. The validity of this work is demonstrated through a series of slowness diagrams.

4.2 Introduction

Absorbing boundary conditions (ABCs) have long been used to include the effect of 'exterior' unbounded domains on computational models of finite 'interiors' at the 'computational boundary' (boundary between exterior and interior). Time-harmonic modeling of such domains requires the ABCs to *accurately* represent the unbounded exterior i.e. the ABC should absorb *all* outgoing waves while allowing *none* of the incoming waves at the computational boundary.

The availability of exact ABCs is typically limited to simple (homogeneous and isotropic) exteriors with regular computational boundaries and their implementations tend to be prohibitively expensive for large scale simulations. Approximate ABCs that contain nonlocal spatial and temporal operators (global ABCs) are similarly unsuitable for large scale problems (in-spite of their accuracy) and hence local ABCs are preferred [1,2]. The most popular local ABCs currently available are rational approximation based ABCs (rational ABCs) and perfectly matched layers (PMLs) [3]. Rational ABCs approximate the exact stiffness (or associated dispersion relation) of an exterior with rational functions and were independently introduced by Lindman [4] and Engquist and Majda [5]. Notable ABCs developed later, like those of Higdon's [6,7] also fall under the category of rational ABCs. Originally limited to low order implementations, rational ABCs are now implementable to an arbitrarily high order through auxiliary variable formulations [8-12]. The PML, is a 'special' absorbing medium that uses complex coordinate stretching to dampen (or decay) propagating waves without creating artificial reflections at the computational boundary. PML was introduced by Bérenger [13], with the more elegant complex coordinate stretching viewpoint provided by Chew *et al.* [14-16]. Originally presented in a split variable formulation, PMLs are now available in unsplit forms along with variations like the conformal PML [17], complex frequency shifted PML (CFS-PML) [18], convolutional PML (CPML) [19] and multiaxial PML (M-PML) [20].

As stated before, the accuracy of ABCs is dependent on their treatment of outgoing and incoming wavemodes. While the categorization of wavemodes into outgoing and incoming is based on their group velocities (c_{gx}), both rational ABCs and PML are known to treat wavemodes based on their phase velocities (c_{px}). Hence, in media supporting wavemodes with opposing signs of phase and group velocities rational ABCs and PML correctly treat *only* those wavemodes which have the same sign of phase and group velocity. This implies that *not all* outgoing modes get absorbed while at the same time, *some* incoming modes get allowed into the interior. These 'wrongly' treated modes lead to inaccuracies in time-harmonic simulations and both inaccuracies and ill-posedness (or instabilities) in time-dependent simulations.

Inaccuracies and instabilities tied to the existence of modes with $c_{px}c_{gx} < 0$ have been observed and studied extensively over the last decade [20-35]. While most of these studies concentrate on issues of stability in time domain simulations, the understanding gained from them is also applicable to time-harmonic simulations. While *not capturing* an outgoing mode $(c_{gx} > 0)$ leads to inaccuracies, *capturing* an incoming mode $(c_{gx} \leq 0)$ leads to ill-posedness (or instability). The study of issues related to $c_{px}c_{gx} < 0$ has led to proofs that establish, in one way or another, the impossibility of designing accurate and stable local ABCs in the presence of $c_{px}c_{gx} < 0$. The existence of such proofs, mainly for PML, has led to the belief that prior to the application of PML, the medium should be 'treated' in a way that eliminates the discrepancy between the phase and group velocity signs; many such treatments use space-time transformations for ensuring $c_{px}c_{gx} \geq 0$ before the application of PML [23,24,30,36].

While various space-time transformations have been proposed over the last decade, they all suffer from two main limitations: (a) their extension to heterogeneous (layered) media is unclear because e.g. each layer requires its own unique transformation and (b) to date, such transformations have only been applicable to media with elliptic anisotropy (see Figure 4.1).

No space-time transformation is known to exist for the much more complicated case of *non-elliptic* anisotropy [26,35]. Other ways of dealing with instabilities especially for non-elliptic anisotropy can be found in [20,35,37-40] but these studies do not directly seem to tackle the issue of $c_{px}c_{gx} < 0$ and their precise effect on the inaccuracies and instabilities created by wavemodes with $c_{px}c_{gx} < 0$ is not clear.

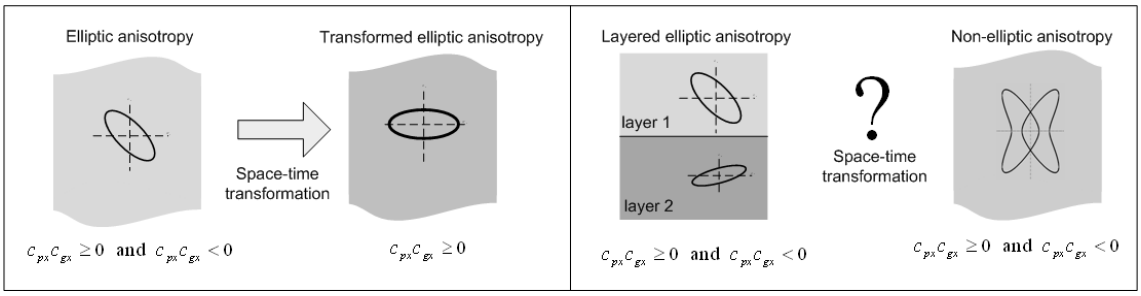

Figure 4.1. *Left:* Space-time transformations are only available for elliptic anisotropies in homogeneous media. *Right:* No such transformations exist for heterogeneous (layered) and non-elliptic anisotropic media

The purpose of this paper is twofold. Firstly, we show that it is possible to circumvent the difficulty of designing ABCs for media with $c_{px}c_{gx} < 0$ by utilizing the reflections that are already present in truncated local ABCs. This helps us explain the ability of a recently developed local ABC to handle wavemodes with $c_{px}c_{gx} < 0$ *without* the use of space-time transformations. The utility of reflections is explicitly demonstrated in the case of propagating anti-plane shear waves present in tilted elliptic anisotropic elasticity followed by an extension that includes the accurate absorption of evanescent wavemodes. Secondly we extend these results to the more complicated, yet somewhat similar, case of in-plane waves of tilted elliptic anisotropic elasticity – this extension is non-trivial because of the coupling that exists between the pressure and shear modes of in-plane waves. Through this extension we will show that it is necessary for this elastic local ABC to have *complex-valued* parameters and derive sufficient conditions for its accuracy. These conditions happen to be bounds on the real and imaginary parts of the complex parameters.

Since we show that it is possible to design a local ABC *without* space-time transformations, we will have paved the way for tackling the issues with $c_{px}c_{gx} < 0$ for heterogeneous (layered) media, thus addressing one of the two limitations listed before. It should be noted that since we only deal with elliptic anisotropy, *only one* of the two limitations are addressed here. The other limitation of space-time transformations being limited to elliptic anisotropic media remains. In a sequel to this paper (Chapter 5) we present an unconventional mesh stretching idea that handles the opposing signs of phase/group velocity in elastic *non-elliptic* anisotropy (see Figure 4.1).

The local ABC studied in this paper is the perfectly matched *discrete* layer (PMDL), formerly known as continued fraction ABC (CFABC) [11,41,42]. PMDL uses mid-point integrated linear finite elements to approximate the stiffness of an unbounded domain *without* discretization error. The parameters of this approximation are the element lengths, which can in general be complex [12]. PMDL is a local ABC that exploits the underlying links between rational ABCs and PML [43]. These links can be used to view certain rational ABCs as particular versions of PML e.g. a rational ABC designed purely for propagating waves can be viewed as an efficient form of PML with purely imaginary coordinate stretching. PMDL inherits the straightforward approximation properties of rational ABCs along with the versatility of PML and is thus used for the present study. Approximation properties here refer to the relation between the ABC parameters (typically layer lengths) and the closeness of the ABC approximation to the exact solution with an unbounded exterior, while versatility refers to the applicability of an ABC to material and geometrical complications (like heterogeneities, anisotropy, corners and conformal boundaries). Moreover, the underlying links make the results of this paper applicable to other rational ABCs and PML in general.

This paper is concerned with the accuracy issues of the frequency domain analysis of the continuous problem with a straight computational boundary. These accuracy considerations are *not* just limited to propagating waves; they include *all* outgoing waves, both propagating and evanescent. Interior discretization errors, corners and curved computational boundaries are outside the scope of this paper. It should be noted that the above restrictions are imposed

to make the problem more tractable; they are, with the exception of curved boundaries, not due to any limitations of the PMDL formulation. PMDLs have already been implemented on domains with convex polygonal corners in [41]. As such, this paper can be considered as the necessary first step towards a complete PMDL implementation for anisotropic elastic media. Analogous studies for time-harmonic *and* transient modeling of anti-plane waves can be found in [44,45].

The outline of the rest of the paper is as follows. Section 4.3 contains preliminaries related to elliptic anisotropic elasticity, a characterization of wavemodes as outgoing and incoming, and the general form of the reflection matrix for anisotropic elasticity. In Section 4.4 we discuss the steps involved in the construction of PML, draw parallels to PMDL and list the properties of PMDL that allow the establishment of a suitable reflection matrix to be used in deriving the sufficient conditions for accuracy. The analogies we establish in this section and the proof of concept presented here clearly explain the ability of truncated ABCs to handle opposing signs of phase and group velocity *without* the need for space-time transformations. The criterion for accuracy along with some equivalent conditions are presented in Section 4.5. Section 4.6 contains the derivation of bounds on the *complex-valued* PMDL parameters that ensure the accurate absorption of all outgoing modes irrespective of the signs of their phase and group velocities. Both propagating and evanescent outgoing modes are considered for both anti-plane and in-plane deformations in elliptic anisotropic media. Various slowness diagrams are presented in Section 4.7 and finally, Section 4.8 contains a summary and conclusions. References are presented in Section 4.9.

4.3 Preliminaries

4.3.1 Model Problem

The ultimate aim of this paper is to provide a practical ABC for the time-harmonic vector anisotropic wave equation. To this end, we choose the simplest possible boundary in two dimensions: a straight edge without corners. Figure 4.2 (*left*) shows such a boundary ($x = 0$) and the model problem shown therein consists of replacing the exact full-space by a left half-

space (interior) along with an ABC that simulates the effect of the right half-space (exterior). The interior and exterior in Figure 4.2 (*left*) are given by $x < 0$ and $x > 0$ respectively.

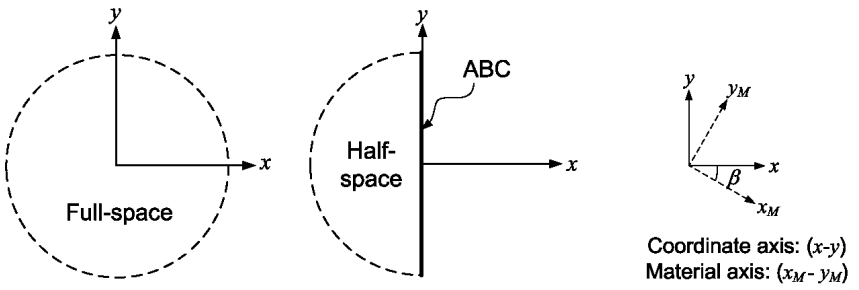

Figure 4.2. *Left:* The model problem consists of replacing a full space by a left half-space and an efficient ABC that is accurate for a scalar anisotropic medium. *Right:* Global coordinate and material axes.

4.3.2 Anisotropic Elastic Media

We consider the time-harmonic scalar and vector wave equations representing, respectively, anti-plane and in-plane waves in homogeneous anisotropic elastic media in two dimensions:

$$\left(A_{xx} \frac{\partial^2}{\partial x^2} + \left(A_{xy} + A_{xy}^T \right) \frac{\partial^2}{\partial x \partial y} + A_{yy} \frac{\partial^2}{\partial y^2} + \omega^2 \right) u_z = 0 , \tag{4.1}$$

$$\left(\mathbf{G}_{xx} \frac{\partial^2}{\partial x^2} + \left(\mathbf{G}_{xy} + \mathbf{G}_{xy}^T \right) \frac{\partial^2}{\partial x \partial y} + \mathbf{G}_{yy} \frac{\partial^2}{\partial y^2} + \omega^2 \mathbf{I} \right) \mathbf{u} = \mathbf{0} , \tag{4.2}$$

where $\omega \in \mathbb{R}$ is the temporal frequency, $\mathbf{u} = \left\{ u_x \;\; u_y \right\}^T$ is the infinitesimal in-plane displacement vector, u_z is the infinitesimal anti-plane displacement, A_{xx}, A_{yy}, A_{xy} are the anti-plane scalar coefficients with

$$
\begin{aligned}
A_{xx} &= \left(c_{xM}^2 \cos^2\beta + c_{yM}^2 \sin^2\beta\right), \\
A_{yy} &= \left(c_{xM}^2 \sin^2\beta + c_{yM}^2 \cos^2\beta\right), \\
A_{xy} &= -\left(c_{xM}^2 - c_{yM}^2\right)\sin\beta\cos\beta,
\end{aligned} \tag{4.3}
$$

and $\mathbf{G}_{xx}, \mathbf{G}_{yy}, \mathbf{G}_{xy}$ are the in-plane matrix coefficients with

$$E_{22} = c_p^2,\ E_{33} = c_s^2,\ E_{11} = \left(1+2\varepsilon\right)E_{22},$$

$$E_{12} = \sqrt{\left(\left(1+2\delta\right)E_{22} - E_{33}\right)\left(E_{22} - E_{33}\right)} - E_{33},$$

$$\tilde{\mathbf{G}}_{xx} = \begin{bmatrix} E_{11} & 0 \\ 0 & E_{33} \end{bmatrix}, \tilde{\mathbf{G}}_{yy} = \begin{bmatrix} E_{33} & 0 \\ 0 & E_{22} \end{bmatrix}, \tilde{\mathbf{G}}_{xy} = \begin{bmatrix} 0 & E_{12} \\ E_{33} & 0 \end{bmatrix}, \tag{4.4}$$

$$
\begin{aligned}
\mathbf{G}_{xx} &= \tilde{\mathbf{G}}_{xx}\cos^2\beta + \tilde{\mathbf{G}}_{yy}\sin^2\beta + \left(\tilde{\mathbf{G}}_{xy} + \tilde{\mathbf{G}}_{xy}^T\right)\sin\beta\cos\beta, \\
\mathbf{G}_{yy} &= \tilde{\mathbf{G}}_{xx}\sin^2\beta + \tilde{\mathbf{G}}_{yy}\cos^2\beta - \left(\tilde{\mathbf{G}}_{xy} + \tilde{\mathbf{G}}_{xy}^T\right)\sin\beta\cos\beta, \\
\mathbf{G}_{xy} &= -\left(\tilde{\mathbf{G}}_{xx} - \tilde{\mathbf{G}}_{yy}\right)\sin\beta\cos\beta + \tilde{\mathbf{G}}_{xy}\cos^2\beta - \tilde{\mathbf{G}}_{xy}^T\sin^2\beta.
\end{aligned}
$$

The variables c_{xM}, c_{yM} in (4.3) represent the anti-plane wave velocities along the principal material axis $\left(x_M - y_M\right)$ while in (4.4) c_p is the in-plane pressure wave velocity, c_s is the in-plane shear wave velocity, ε and δ are the parameters of anisotropy given by Thomsen's representation of transversely isotropic homogeneous elastic media [46], and E_{ij} denote the elements of the 3×3 elasticity matrix used in the in-plane stress-strain relationship of 2D elasticity along the principal material axis $\left(x_M - y_M\right)$. The angle β in both (4.3) and (4.4) represents the tilt of the principal material axis $\left(x_M - y_M\right)$ with respect to the coordinate axis $\left(x - y\right)$, see Figure 4.2. Also $c_P \geq c_s$ and a unit material density is assumed.

For the sake of presentation, we Fourier transform (4.1) and (4.2) in y to obtain the following reduced equations:

$$\left(A_{xx}\frac{\partial^2}{\partial x^2}+ik_y\left(A_{xy}+A_{xy}^T\right)\frac{\partial}{\partial x}-\left(k_y^2A_{yy}-\omega^2\right)\right)u_z=0\,, \tag{4.5}$$

$$\left(\mathbf{G}_{xx}\frac{\partial^2}{\partial x^2}+ik_y\left(\mathbf{G}_{xy}+\mathbf{G}_{xy}^T\right)\frac{\partial}{\partial x}-\left(k_y^2\mathbf{G}_{yy}-\omega^2\mathbf{I}\right)\right)\mathbf{u}=\mathbf{0}\,, \tag{4.6}$$

where the duality $\partial\big/\partial y\leftrightarrow ik_y$ applies and the same notations $u_z,\mathbf{u}$ are used for both the field variable and its Fourier transform. Equations (4.5) and (4.6) admit individual *normalized* ($\|\cdot\|=1$) modes of the kind e^{ik_xx}, $\mathbf{a}e^{ik_xx}$ which, in the general case are defined by their wavenumber-wavemode pair $(k_x,\mathbf{a})$ *for a given* $\left(k_y,\omega\right)\in\mathbb{R}^2$ pair. Defining

$$\Lambda^{anti}\equiv\left(k_x^2A_{xx}+k_xk_y\left(A_{xy}+A_{xy}^T\right)+k_y^2A_{yy}-\omega^2\right), \tag{4.7}$$

$$\mathbf{\Lambda}^{in}\equiv\left(k_x^2\mathbf{G}_{xx}+k_xk_y\left(\mathbf{G}_{xy}+\mathbf{G}_{xy}^T\right)+k_y^2\mathbf{G}_{yy}-\omega^2\mathbf{I}\right), \tag{4.8}$$

it can be seen that the horizontal wavenumber k_x is a solution of the dispersion relation $\Lambda^{anti}=0$ or $\det\left(\mathbf{\Lambda}^{in}\right)=0$ and the wavemode $\mathbf{a}$ satisfies $\mathbf{\Lambda}^{in}\mathbf{a}=\mathbf{0}$.

For later reference we will need the traction at the computational boundary $(x=0)$. For the wavemodes governed by (4.5) and (4.6), the tractions at $x=0$ are given by,

$$\begin{aligned}T_x^{anti}\Big|_{x=0}&=-\left(A_{xx}\frac{\partial}{\partial x}+ik_yA_{xy}\right)u_z\Big|_{x=0}\,,\\ \mathbf{T}_x^{in}\Big|_{x=0}&=-\left(\mathbf{G}_{xx}\frac{\partial}{\partial x}+ik_y\mathbf{G}_{xy}\right)\mathbf{u}\Big|_{x=0}\,.\end{aligned} \tag{4.9}$$

For the rest of the paper $\Re e(\cdot),\Im m(\cdot)$ are used to represent respectively, the real and imaginary parts.

4.3.3 Outgoing and Incoming Wavemodes

Propagating wavemodes $\left(k_x \in \mathbb{R}\right)$ can be characterized based on the direction in which they propagate energy. The energy propagating velocity or group velocity is given by $c_{gx} = \partial\omega \big/ \partial k_x$ where $\omega = f(k_x, k_y)$ is obtained from the dispersion relation $\Lambda^{anti} = 0$ or $\det\left(\mathbf{\Lambda}^{in}\right) = 0$. Taking evanescent modes $\left(k_x \notin \mathbb{R}\right)$ into consideration we can characterize every wavemode as either outgoing or incoming. Outgoing modes are either forward propagating or forward decaying modes and incoming wavemodes are either backward propagating or backward decaying as shown below:

$$\left.\begin{array}{lll} \text{forward propagating} & : & \Im\mathfrak{m}(k_x) = 0 \ \text{ and } \ c_{gx} = \dfrac{\partial\omega}{\partial k_x} > 0, \\ \text{forward decaying} & : & \Im\mathfrak{m}(k_x) > 0, \end{array}\right\} \begin{array}{l} outgoing \\ modes \end{array}, \tag{4.10}$$

$$\left.\begin{array}{lll} \text{backward propagating} & : & \Im\mathfrak{m}(k_x) = 0 \ \text{ and } \ c_{gx} = \dfrac{\partial\omega}{\partial k_x} \le 0, \\ \text{backward decaying} & : & \Im\mathfrak{m}(k_x) < 0. \end{array}\right\} \begin{array}{l} incoming \\ modes \end{array}. \tag{4.11}$$

The characterization of propagating wavemodes with zero group velocity $\left(c_{gx} = 0\right)$ as incoming modes in (4.11) is arbitrary; it will not affect our analysis.

Outgoing and incoming wavemodes can be conveniently viewed through slowness diagrams that are plots of horizontal slowness $\sigma_x = k_x \big/ \omega$ against vertical slowness $\sigma_y = k_y \big/ \omega$. Variations of the three parameters c_{xM}, c_{yM}, β for anti-plane waves and the five parameters $c_p, c_s, \beta, \varepsilon, \delta$ for in-plane waves result in various slowness diagrams as shown in Figure 4.3 and Figure 4.4. Since modes with positive phase velocities have $\sigma_x > 0$, media with slowness diagrams having $c_{gx} > 0$ (bold lines) in the lower half plane or those with $c_{gx} \le 0$ (thin lines) in the upper half plane in Figure 4.3 and Figure 4.4 support wavemodes

with opposing signs of phase/group velocity . This paper deals with tilted $\left(\beta \neq 0\right)$ elliptic $\left(c_{xM} \neq c_{yM}, \epsilon = \delta \neq 0\right)$ anisotropy. Untilted $\left(\beta = 0\right)$ non-elliptic $\left(\varepsilon \neq \delta\right)$ anisotropy is studied in a sequel to this paper (Chapter 5) and tilted $\left(\beta \neq 0\right)$ non-elliptic $\left(\varepsilon \neq \delta\right)$ anisotropy is currently under investigation.

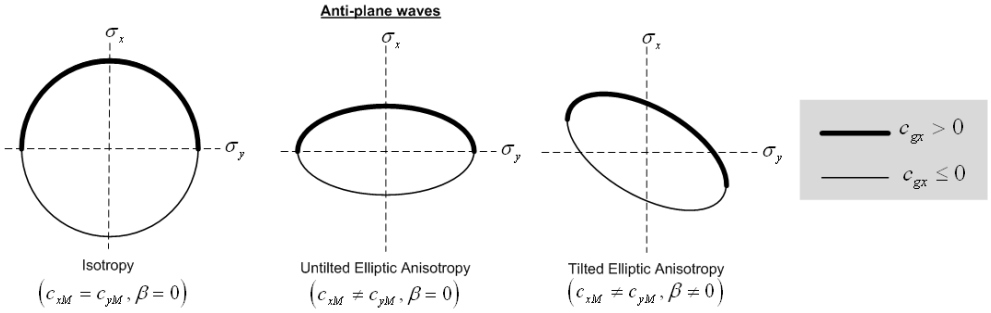

Figure 4.3. Slowness diagrams for scalar anti-plane waves in elasticity. Only slownesses pertaining to propagating modes are shown $\left(\sigma_x \in \mathbb{R}\right)$

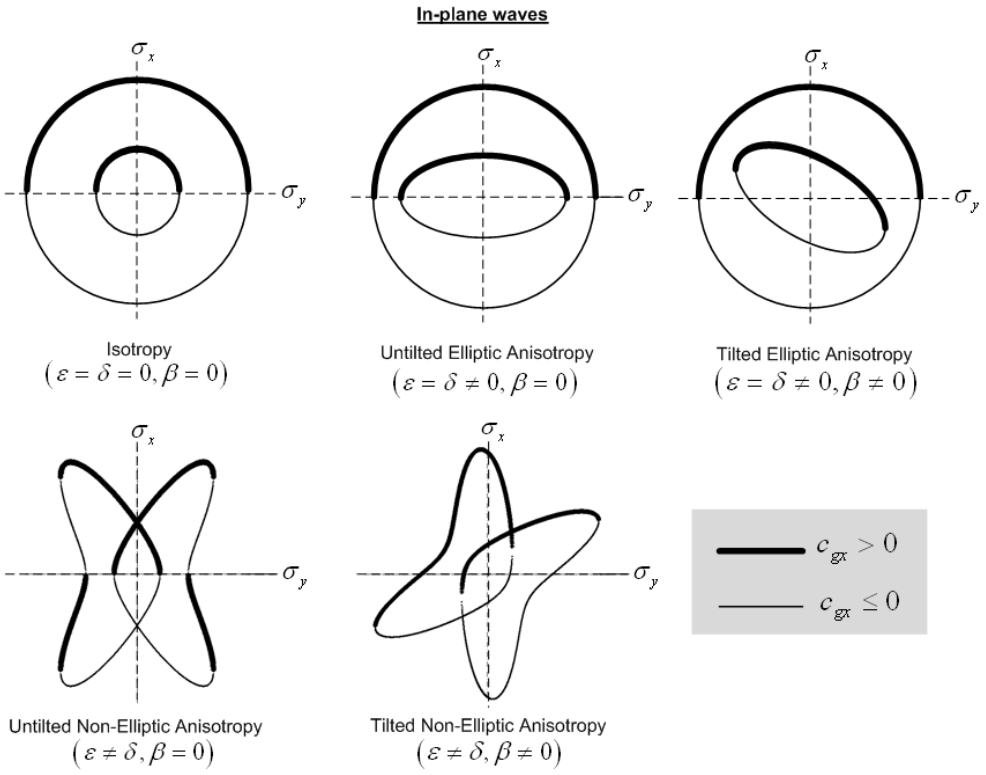

Figure 4.4. Slowness diagrams for coupled in-plane pressure and shear waves in elasticity. Only slownesses pertaining to propagating modes are shown $\left(\sigma_x \in \mathbb{R}\right)$. This paper deals with tilted elliptic anisotropy.

To summarize, wavemodes are solutions of (4.5) or (4.6) for a given (k_y, ω) pair. They are of the form $u_z = e^{ik_x x}$ or $u = \mathbf{a}e^{ik_x x}$ with k_x satisfying the dispersion relations $\Lambda^{anti} = 0$ or $\det\left(\Lambda^{in}\right) = 0$ respectively. For a given (k_y, ω) pair i.e. for a given σ_y, the dispersion relations are quadratic or quartic in σ_x and hence there are two or four wavemodes for every (k_y, ω) pair . One half of these are outgoing and the other half consists of incoming modes. Outgoing propagating wavemodes are represented by the bold lines in Figure 4.3 and Figure 4.4.

4.3.4 Half-space and Finite Layer Wavemodes

The model problem of Section 4.3.1 contains an exterior right half-space ($x > 0$) that, in the absence of exterior sources admits only outgoing wavemodes (4.10). An exact ABC thus needs to support *all* outgoing modes and *none* of the incoming modes (4.11). We will later need to consider the effect of truncation boundaries on propagating wavemodes; truncation boundaries convert an unbounded exterior to a finite layer. Since truncation generates reflections, a finite layer supports both outgoing and incoming (reflected) modes.

The scalar anti-plane equation (4.5) supports two wavemodes for a given (k_y, ω) pair; one outgoing and one incoming wavemode. Defining the scalar *truncation reflection coefficient* R_T as the ratio of the reflected mode amplitude to the incident mode amplitude at the truncation boundary $x = L$, the total wavefield can be conveniently expressed as

$$u_z = e^{ik_x x} + e^{i\widetilde{k}_x (x-L)} R_T e^{ik_x L}. \tag{4.12}$$

In (4.12), k_x and $\widetilde{k}_x$ are roots of the quadratic dispersion relation $\Lambda^{anti} = 0$ satisfying (4.10) and (4.11) respectively. Hence $e^{ik_x x}$ represents the outgoing mode variation, $e^{i\widetilde{k}_x (x-L)}$ represents the incoming mode variation, $e^{ik_x L}$ is the amplitude of the outgoing mode at the truncation boundary and $R_T e^{ik_x L}$ represents the amplitude of the incoming (reflected) mode at $x = L$. The truncation reflection coefficient depends on the truncation boundary condition e.g. $R_T = -1$ for a homogeneous Dirichlet condition. Since we are interested only in the interior solution, the effect of a finite layer can be measured at the computational boundary by defining the *computational reflection coefficient* R_C as the ratio of the incoming mode amplitude to the outgoing mode amplitude at the computational boundary $\left(x = 0\right)$. Substituting $x = 0$ in (4.12) we get

$$R_C = e^{-i\widetilde{k}_x L} R_T e^{ik_x L}. \tag{4.13}$$

The vector in-plane equation (4.6) supports four wavemodes (two pressure and two shear modes) for a given (k_y, ω) pair; two outgoing and two incoming. Because of the multiplicity of modes it is helpful to view the in-plane wavemodes through matrix notation. It is obvious that the wavenumber, wavemode pair $(k_x, \mathbf{a})$ is an eigenpair of the quadratic eigenvalue problem $\mathbf{\Lambda}^{anti}\mathbf{a} = \mathbf{0}$. Denoting by $\mathbf{X}$ the matrix of all *outgoing* normalized eigenvectors and by $\tilde{\mathbf{X}}$ the matrix of all *incoming* normalized eigenvectors, *outgoing* and *incoming* wavemodes can be represented as $\mathbf{X}(\cdot, q)e^{ik_{xq}x}$ and $\tilde{\mathbf{X}}(\cdot, q)e^{i\widetilde{k_{xq}}x}$ respectively. Normalization here refers to unit wavemode amplitude $\left(\left\|\mathbf{a}\right\| = 1\right)$. Any outgoing wave can thus be expressed as $\mathbf{XP}(x)\Gamma$ while any incoming wave can be expressed as $\tilde{\mathbf{X}}\tilde{\mathbf{P}}(x)\tilde{\Gamma}$, where $\Gamma, \tilde{\Gamma}$ are vectors of participation factors and $\mathbf{P}(x) = diag\left(e^{ik_{x1}x}, e^{ik_{x2}x}\right)$, $\tilde{\mathbf{P}}(x) = diag\left(e^{i\widetilde{k_{x1}}x}, e^{i\widetilde{k_{x2}}x}\right)$.

Analysis similar to the anti-plane case can be performed for the in-plane case to obtain equations corresponding to (4.12) and (4.13). The only difference is that the multiplicity of modes for a given (k_y, ω) pair implies that the truncation and computational reflection coefficients are *matrices* $\mathbf{R}_T$ and $\mathbf{R}_C$. This is due to the fact that an incident wavemode in general gives rise to multiple reflected wavemodes because of mode coupling at the truncation boundary. Hence a single outgoing wavemode $\mathbf{X}(\cdot, q)e^{ik_{xq}x}$ generates a reflected waveform that is a linear combination of incoming modes $\tilde{\mathbf{X}}(\cdot, q)e^{i\widetilde{k_{xq}}x}$s and the coefficients of this combination are the truncation reflection coefficients. Hence there exists a *vector* of reflection coefficients $\mathbf{R}_T(\cdot, q)$ for a given outgoing (incident) wavemode and the corresponding incoming (reflected) wave is given by $\tilde{\mathbf{X}}\tilde{\mathbf{P}}(x - L)\mathbf{R}_T(\cdot, q)e^{ik_{xq}L}$. For a general outgoing wave $\mathbf{XP}(x)\Gamma$, the total wavefield can be expressed as

$$\mathbf{u} = \left(\mathbf{XP}(x) + \tilde{\mathbf{X}}\tilde{\mathbf{P}}(x - L)\mathbf{R}_T\mathbf{P}(L)\right)\Gamma. \tag{4.14}$$

Since $\mathbf{P}(x=0) = diag(1,1)$, equation (4.14) becomes $\mathbf{u}\Big|_{x=0} = \left(\mathbf{X} + \tilde{\mathbf{X}}\tilde{\mathbf{P}}(-L)\mathbf{R}_{_T}\mathbf{P}(L)\right)\Gamma$ at the computational boundary $x=0$ and thus we can define the computational reflection matrix as,

$$\mathbf{R}_{_C} = \tilde{\mathbf{P}}(-L)\mathbf{R}_{_T}\mathbf{P}(L)\,. \tag{4.15}$$

Comparing (4.14) and (4.15) with (4.12) and (4.13) respectively shows the similarity and differences between in-plane and anti-plane wavefields. Equation (4.15) provides a measure of the reflections due to truncation. When the outgoing and incoming wavemodes are ordered appropriately, the simplest truncation reflection matrix is $\mathbf{R}_{_T} = -\mathbf{I}$ (where $\mathbf{I}$ is the identity matrix) and this occurs e.g. in the case of symmetric/antisymmetric truncation boundaries with isotropic media where an outgoing mode generates a *single* incoming mode. No symmetric/antisymmetric truncation boundary conditions are available for tilted anisotropy and a homogeneous Dirichlet boundary, in general, will result in a *full* $\mathbf{R}_{_T}$ i.e. an outgoing wavemode results in a reflection that is made up of *all* incoming modes.

A finite layer can approximate the absorption of an unbounded exterior if every element of the computational reflection matrix is *small enough* i.e. the norm of the elements of the computational reflection matrix in some sense should be $<<1$. Of course, a finite layer of the same material as the interior is expected to have no effect on the amplitude of propagating waves with the computational reflection coefficient essentially being unity.

4.4 Local ABCs: PML and PMDL

As mentioned in the introduction, PML and rational ABCs are the most popular local ABCs; though seemingly disparate, recent works have demonstrated underlying links between the two. It was shown in [43] that an optimal PML for propagating wave modes can be obtained by purely imaginary stretching and as such PML discretization is algebraically equivalent to rational ABCs obtained by approximating the square root operator. Hence, in the case of purely imaginary stretching, rational ABCs can also be viewed as PML. The advantage of this is that we can choose the viewpoint that best suits the problem at hand. For example, in

the case of perfectly matched *discrete* layer (PMDL), both accuracy of time-harmonic simulations and well-posedness of transient ones were proved solely relying on the rational ABC point of view in [44,45]. In this paper we will look at PMDL mainly through the PML viewpoint. This is done partly because the PML viewpoint leads to a more physically intuitive explanation and partly because most of the current work in dealing with the issue of opposing phase/group velocity signs has been performed for the PML.

4.4.1 Construction and Analogies

Devising a PML that mimics the wave absorption characteristics of an unbounded exterior involves three main steps: **(i)** *complex coordinate stretching*, **(ii)** *truncation* and **(iii)** *discretization*. **Step (i)** involves stretching the unbounded exterior coordinates into the complex plane – this is equivalent to replacing the *real* unbounded exterior by a *complex* infinite medium sometimes known as the perfectly matched medium (PMM). In order for this replacement to work, there should be *perfect matching* at the computational boundary – by perfect matching we mean the transmission of outgoing waves from the interior into the PMM without reflection. In the absence of perfect matching reflections occur due to material discontinuity at the computational boundary and the reflections become spurious incoming waves that pollute the solution in the interior. **Step (ii)** involves truncating the PMM by specifying a truncation boundary that converts the infinite PMM into a finite PML. Truncation is necessitated for practicality and in order for it to work, there should be decay of the transmitted wave amplitude in the PML. In the absence of amplitude decay, an outgoing mode progresses through the PML region, gets reflected from the truncation boundary, travels in the opposite direction in the PML and enters back into the interior as spurious incoming waves that again pollute the interior solution. This constitutes the truncation error. If the amplitude is conserved in the PML and if the truncation boundary is the typical homogeneous Dirichlet boundary, the spurious incoming waves will have the same amplitude as the outgoing waves that were supposed to have been absorbed by the PML. In case there is amplitude *growth* in the PML it is expected that the amplitudes of the spurious incoming waves are greater than the amplitudes of the outgoing waves. On the other hand, in the

presence of amplitude decay, the spurious incoming mode will have an amplitude smaller than the outgoing wave with the amount of decay being a function of the length of PML and its decay function. Incoming wave amplitudes that are smaller than outgoing ones make the PML mimic an absorber. Note that since this PML is *continuous* (as against discretized), decaying functions with arbitrarily steep decay rates can be used to reduce the spurious incoming wave amplitudes to negligible values. **Step (iii)** involves discretization of the *continuous* PML for numerical implementation. For traditional discretizations, the *discretized* PML is no longer perfectly matched at the computational boundary and this results in more reflections that constitute the discretization error [47]. In spite of the presence of both truncation and discretization errors, the resulting spurious incoming wave amplitudes can be made sufficiently small for the discretized PML to behave as an effective absorber. The absorption properties of a discretized PML depend on the parameters of the finite number of layers in it (say *'n'* layers) and we thus term it the *n*-layer discretized PML. These three steps are illustrated in Figure 4.5**.**

It should be noted that not all discretizations lead to loss of perfect matching. The local ABC obtained by approximating the half-space stiffness using mid-point integrated linear finite elements is shown to have *no* disrcretization errors [12]. This ABC is the PMDL (perfectly matched *discrete* layer) and can be viewed as a *particular* discretization of PML that results in no discretization errors – hence not all discretized PMLs are termed PMDL. In fact, to avoid confusion we will reserve the term *discretized PML* to refer to PMLs obtained by arbitrary, non-PMDL like discretizations that have discretization errors. And just as for the *n*-layer discretized PML, the absorption properties of the *n*-layer PMDL depend on its *n* parameters which are the layer lengths.

The above three steps used in the design of local ABCs based on the PML idea are intended to create suitable notation and generate analogies between PML and PMDL. This is done by noting that:

- PMM is an exact ABC (no error) while continuous PML, *n*-layer discretized PML and *n*-layer PMDL are all approximate ABCs. Continuous PML has truncation error,

n-layer discretized PML has both truncation and discretization errors and an *n*-layer PMDL again has only truncation error.

- Since both the continuous PML and the *n*-layer PMDL have only truncation errors and since truncation errors are solely dependent on the reflection properties of the truncation boundary, we can gain insights into the behavior of a *n*-layer PMDL by studying the more physically intuitive continuous PML model for a given truncation boundary. This analogy is *key* to understanding the results of this paper. It should be noted that because of the presence of the discretization errors, no such analogy can be made between the continuous PML and the *n*-layer discretized PML (see Figure 4.5).
- One can view discretization to occur before truncation. So when the discretization is performed on the infinite PMM, we would get an infinite number of discretized layers that can be termed the ∞-layer discretized PML. Under traditional discretization schemes, there would be discretization errors making the ∞-layer discretized PML an approximate ABC. On the other hand, if we use the mid-point integrated linear finite element discretization, we obtain the corresponding ∞-layer PMDL. The *∞-layer PMDL is an exact ABC.* This is because there is no truncation error and the PMDL discretization results in no discretization errors. As such the ∞-layer PMDL is analogous to PMM just as the *n*-layer PMDL was shown to be analogous to continuous PML. Of course, after truncation, we obtain the *n*-layer PML or the *n*-layer PMDL as before (see Figure 4.5, Figure 4.6).

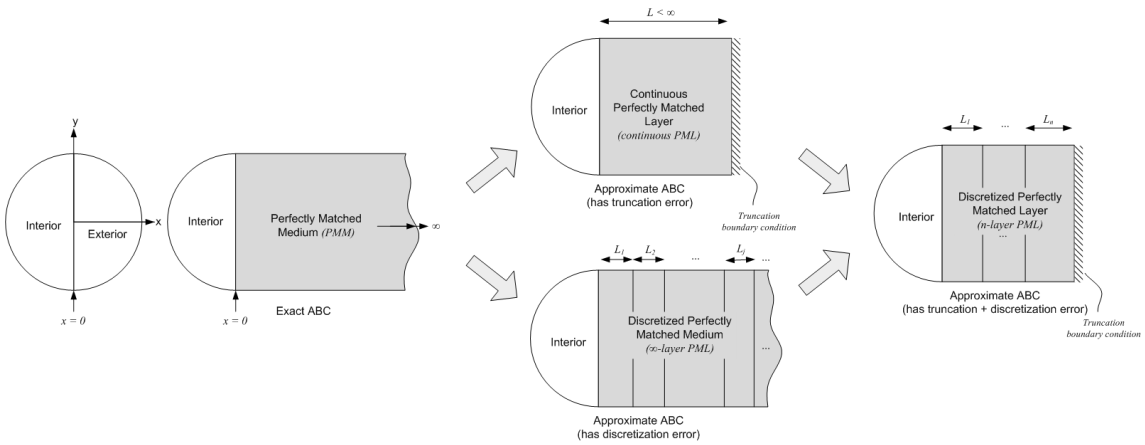

Figure 4.5. The three steps in the design of a PML based local ABC; complex coordinate stretching, truncation and discretization with truncation occurring before and after discretization.

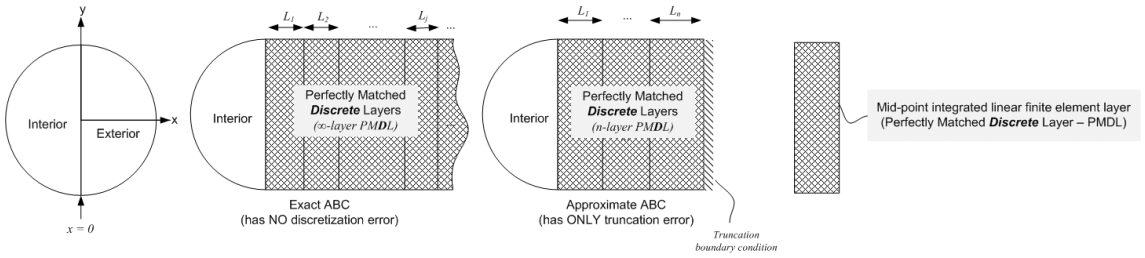

Figure 4.6. The two steps in the design of PMDL; replacing the exterior by an infinite number of mid-point integrated linear finite elements followed by truncation.

Moreover, the following *important* observations about amplitude decay need to be kept in mind:

- Amplitude decay is required only to reduce truncation errors. As such, amplitude decay is not essential for PMM to behave as an effective absorber. Even if there is amplitude growth inside the PMM region, this in no way affects the interior solution as long as perfect matching is preserved at the computational boundary (note that there is no truncation in PMM). So if it were physically possible to have a PMM it

would always behave as an exact ABC irrespective of amplitude modification in the PMM region. The same applies to the ∞-layer PMDL.

- Even in the presence of truncation, only *net* amplitude decay is necessary i.e. there is no necessity of a monotonic decay in amplitude. Amplitude may very well grow in certain parts and decay in others – absorption eventually occurs as long as there is *net* decay. For example an outgoing mode entering the ABC region may decay towards the truncation boundary and the reflected modes at the truncation boundary may grow as they travel towards the interior – but as long as the decay is greater than the growth, the spurious incoming modes will have amplitudes less than the outgoing mode amplitude thus mimicking absorption. The same is applicable for outgoing mode growth and reflected mode decay.

The above assertion about *net* decay may seem of little practical interest because if modes grow in the PML region in one direction, the reflected modes too typically grow in the opposite direction. However, this is only true of *isotropic* elasticity. It may be possible to obtain *net* decay even in the presence of growth at least for certain types of anisotropy. *Using the truncation reflections to ensure net decay is the main idea on which this work is based.*

4.4.2 Proof of concept using PML

In this sub-section we prove the utility of considering *net* decay by looking at the continuous PML. Since the *n*-layer PMDL is analogous to the continuous PML, we would have provided a proof of concept in the case of PMDL too.

Formally, we can illustrate the effect of PMM on a computational boundary at $x = 0$ for the scalar anti-plane equation (4.5) by using *purely imaginary* coordinate transformation like $x = i\alpha\tilde{x}$ with $\alpha \in \mathbb{R}$; purely imaginary stretching is sufficient to absorb propagating waves $\left(k_x \in \mathbb{R}\right)$ as we shall see shortly. Since $\partial\tilde{x}/\partial x = \left(1/i\alpha\right)$, (4.5) and (4.9) become respectively,

$$\left(A_{xx}\left(\frac{-1}{\alpha^2}\right)\frac{\partial^2}{\partial\tilde{x}^2}+ik_y\left(A_{xy}+A_{xy}^T\right)\left(\frac{1}{i\alpha}\right)\frac{\partial}{\partial\tilde{x}}-k_y^2A_{yy}+\rho\omega^2\right)\tilde{u}_z=0\,, \tag{4.16}$$

and

$$\tilde{T}_x^{anti}=-\left(A_{xx}\left(\frac{1}{i\alpha}\right)\frac{\partial}{\partial\tilde{x}}+ik_yA_{xy}\right)\tilde{u}_z\,. \tag{4.17}$$

One can easily see by direct substitution that (4.16) admits wavemodes of the form $\tilde{u}_z=e^{-\alpha k_x\tilde{x}}$. Since the corresponding modes for a right half space $[0,+\infty)$ governed by (4.5) are of the form $u_z=e^{ik_xx}$ (with k_x satisfying (4.10)), we obtain $u_z\big|_{x=0}=\tilde{u}_z\big|_{x=0}$ and using (4.9) and (4.17) we get $T_x^{anti}\big|_{x=0}=\tilde{T}_x^{anti}\big|_{x=0}$ at the computational boundary. This implies that both displacement and traction continuity are satisfied at $x=0$ guaranteeing no reflections at the computational boundary (the 'perfect matching' property). Moreover, for propagating waves $\left(k_x\in\mathbb{R}\right)$, if $\alpha k_x>0$, the wavemode $\tilde{u}_z=e^{-\alpha k_x\tilde{x}}$ decays as $\tilde{x}\to+\infty$; if $\alpha k_x<0$, there is amplitude growth with $\tilde{x}\to+\infty$. Hence the decay or growth of amplitude depends on the sign of the product αk_x where k_x represents the wavenumber of an outgoing wavemode. The difficulty of absorbing wavemodes with opposite signs of phase/group velocity is now apparent by checking Figure 4.3 for tilted elliptic anisotropic media. If we chose $\alpha>0$, then there are those outgoing propagating modes with $k_x<0$ that experience growth and if we choose $\alpha<0$ there are the other outgoing propagating modes with $k_x>0$ that experience growth. This of course is thought to create problems on truncation.

In the case of truncations, i.e. in the case of continuous PML of finite width L with a homogeneous Dirichlet boundary at $x=L$ $\left(R_T=-1\right)$, we can use (4.13) to get

$$\left|R_C\right|=e^{\alpha\widetilde{k}_xL}e^{-\alpha k_xL}=e^{-\alpha\left(k_x-\widetilde{k}_x\right)L}, \tag{4.18}$$

where $\widetilde{k}_x$ is the incoming (reflected) wavenumber. Note that now, because of truncations, the *net* amplitude decay or growth in (4.18) depends on the sign of $\alpha\left(k_x - \widetilde{k}_x\right)$ and not just on αk_x. A quick look at the slowness diagram for tilted elliptic anisotropy in Figure 4.3 shows that for propagating modes, we always have $\left(k_x - \widetilde{k}_x\right) \geq 0$ even when $k_x < 0$ i.e. $e^{-\alpha\left(k_x - \widetilde{k}_x\right)L} < 1$ even when $e^{-\alpha k_x L} > 1$. So there is *net* decay at the computational boundary even though there is growth of the outgoing mode in the PML. Hence PML with $\alpha > 0$ will result in $\left|R_C\right| \leq 1$(with equality attained only in the case of zero group velocity modes). This implies that it is possible to have a continuous PML that acts as an effective absorber *even in the presence of wavemodes with opposite signs of phase/group velocities.*

The above example is given for illustrative purposes only; to generate confidence in our idea that reflections from truncations can be used to ensure net decay. In Sections 4.5 and 4.6, we will show mathematically that this is indeed so for the *n*-layer PMDL for both scalar anti-plane and vector in-plane waves of elliptic anisotropic elasticity.

4.4.3 PMDL Properties

Before we tackle the issue of designing an accurate *n*-layer PMDL for anisotropic elasticity, we will list the main properties of PMDL that will aid us in later sections. We present here the properties of PMDL for the vector in-plane case (4.6); the properties for the simpler scalar anti-plane case (4.5) are similar.

The PMDL formulation approximates the exterior right half-space stiffness with $n\ (<\infty)$ mid-point integrated linear finite element layers of lengths $L_1, \ldots, L_n$ followed by a homogeneous Dirichlet truncation boundary condition (see Figure 4.6) [12]. For the model problem in Figure 4.2, the traction at the boundary of the exterior right half space is given by (4.9) for in-plane displacements and hence the stiffness of the right half space becomes

$$\mathbf{K}_{exact} = -\left(ik_x \mathbf{G}_{xx} + ik_y \mathbf{G}_{xy}\right). \tag{4.19}$$

The stiffness above is termed exact because an ABC that provides this stiffness will exactly mimic the right half-space at the computational boundary. Also k_x in (4.19) satisfies (4.10) because a right half-space can only support outgoing modes. The *n*-layer PMDL provides an approximation of (4.19) and the rationale behind this approximation is summarized in four steps below. These steps are also graphically depicted in Figure 4.7 and Figure 4.8.

STEP 1, involves splitting the exterior right half-space $[0,\infty)$ into a finite element $[0,L_1]$ and another half-space $[L_1,\infty)$, with the finite element using linear shape functions to represent the displacement in $[0,L_1]$. As expected, the stiffness of the finite element $[0,L_1]$ plus half space $[L_1,\infty)$ model can only approximate $\mathbf{K}_{exact}$ because of the error in the finite element discretization (see Figure 4.7).

STEP 2, *which is the key to PMDL development*, involves the elimination of the finite-element discretization error with respect to the half-space stiffness at $x=0$. This is achieved by simply using mid-point integration to evaluate the finite element stiffness matrix (see [12]). The stiffness of this mid-point integrated linear finite element is denoted by $\mathbf{S}_j$ (with $j=1$) and given by:

$$\mathbf{S}_j=\begin{bmatrix}\mathbf{S}_j^{11} & \mathbf{S}_j^{12}\\ \mathbf{S}_j^{21} & \mathbf{S}_j^{22}\end{bmatrix}=\frac{1}{L_j}\begin{bmatrix}\mathbf{G}_{xx} & -\mathbf{G}_{xx}\\ -\mathbf{G}_{xx} & \mathbf{G}_{xx}\end{bmatrix}+\frac{ik_y}{2}\begin{bmatrix}-\mathbf{G}_{xy} & -\mathbf{G}_{xy}\\ \mathbf{G}_{xy} & \mathbf{G}_{xy}\end{bmatrix}$$
$$-\frac{ik_y}{2}\begin{bmatrix}-\mathbf{G}_{xy}^T & \mathbf{G}_{xy}^T\\ -\mathbf{G}_{xy}^T & \mathbf{G}_{xy}^T\end{bmatrix}-\frac{L_j}{4}\begin{bmatrix}\omega^2\mathbf{I}-k_y^2\mathbf{G}_{yy} & \omega^2\mathbf{I}-k_y^2\mathbf{G}_{yy}\\ \omega^2\mathbf{I}-k_y^2\mathbf{G}_{yy} & \omega^2\mathbf{I}-k_y^2\mathbf{G}_{yy}\end{bmatrix}, \tag{4.20}$$

The mid-point integrated linear finite element $[0,L_1]$ plus the right half space $[L_1,\infty)$ model recovers the *exact* stiffness of the original half-space $[0,\infty)$ at $x=0$. This can be quickly illustrated by writing the assembled stiffness matrix (see Figure 4.7)

$$\begin{Bmatrix}\mathbf{T}_{x=0}^{1-pmdl+HS}\\ \mathbf{0}\end{Bmatrix}=\begin{bmatrix}\mathbf{S}_1^{11} & \mathbf{S}_1^{12}\\ \mathbf{S}_1^{21} & \mathbf{S}_1^{22}+\mathbf{K}_{exact}\end{bmatrix}\begin{Bmatrix}\tilde{\mathbf{u}}_{x=0}\\ \tilde{\mathbf{u}}_{x=L_1}\end{Bmatrix}, \tag{4.21}$$

where the $\mathbf{K}_{exact}$ term represents the 'smaller' half space $[L_1, \infty)$, $\tilde{\mathbf{u}}_{x=0}$ and $\tilde{\mathbf{u}}_{x=L_1}$ are the field variables at the left at right edges of the PMDL layer and $\mathbf{T}_{x=0}^{1-pmdl+HS}$ is the traction at the computational boundary. Since $\tilde{\mathbf{u}}_{x=L_1}$ is the displacement at the boundary of the 'smaller' half space $[L_1, \infty)$, we can take $\tilde{\mathbf{u}}_{x=L_1} = \mathbf{a}_1 e^{ik_x L_1}$ and check by direct substitution that $\tilde{\mathbf{u}}_{x=0} = \left(\left(1 - ik_x L_1 / 2\right) \Big/ \left(1 + ik_x L_1 / 2\right)\right) \tilde{\mathbf{u}}_{x=L_1}$ satisfies (4.21) with (4.19) and results in $\mathbf{T}_{x=0}^{1-pmdl+HS} = -\left(ik_x \mathbf{G}_{xx} + ik_y \mathbf{G}_{xy}\right) \tilde{\mathbf{u}}_{x=0}$ i.e. $\mathbf{T}_{x=0}^{1-pmdl+HS} = \mathbf{K}_{exact} \tilde{\mathbf{u}}_{x=0}$. This implies recovery of the exact half-space stiffness even after the addition of a discrete mid-point integrated linear finite element to a half-space. Of course, recovery of $\mathbf{K}_{exact}$ implies 'perfect matching' and the relation between $\tilde{\mathbf{u}}_{x=0}$ and $\tilde{\mathbf{u}}_{x=L_1}$ shows that $\tilde{\mathbf{u}}_{x=0}$ decays (or grows) by a factor of $\left(1 + ik_x L_1 / 2\right) \Big/ \left(1 - ik_x L_1 / 2\right)$ when it passes through the mid-point integrated layer of length L_1. Note that the mid-point integrated linear finite element $[0, L_1]$ plus the right half space $[L_1, \infty)$ model represents the *exact* stiffness of the original half-space $[0, \infty)$ at $x = 0$ *irrespective* of the element length L_j; it can be arbitrarily large and is not even restricted to real numbers [12].

STEP 3 involves applying the above splitting recursively to discretize the original half-space into an infinite number of finite element layers, $[0, L_1]$, $[L_1, L_1 + L_2]$, … as shown in Figure 4.8. Such splitting does not introduce any further discretization error because the mid-point integration in step 2 has no discretization errors in the half-space stiffness. Hence, this discretized half-space containing an infinite number of PMDL layers is *exact* as far as the stiffness at $x = 0$ $\left(\mathbf{K}_{exact}\right)$ is concerned. This is the ∞-layer PMDL which is an *exact ABC* analogous to PMM as discussed before. Due to perfect matching, the decay (or growth) factors multiply as the mode progresses through subsequent layers with

$$\tilde{\mathbf{u}}_{x=\left(L_1+\ldots+L_n\right)} = \prod_{j=1}^{n}\left(\frac{1+ik_xL_j\,/\,2}{1-ik_xL_j\,/\,2}\right)\tilde{\mathbf{u}}_{x=0}\,. \tag{4.22}$$

STEP 4 involves limiting the number of layers for computational tractability. The number of layers is limited to n with a homogeneous Dirichlet boundary condition applied at $x=\sum L_j$ as shown in Figure 4.8. This results in an *n*-layer PMDL whose stiffness $\mathbf{K}_n$ is an approximation of $\mathbf{K}_{exact}$ due to truncation errors. Since truncation error is the only kind of error present in an *n*-layer PMDL model, it is analogous to a continuous PML.

If we use $\tilde{\mathbf{u}}_1,\ldots\tilde{\mathbf{u}}_{n-1},\tilde{\mathbf{u}}_n$ to denote the values of the field variable at the right edge of each layer, the Dirichlet condition becomes $\tilde{\mathbf{u}}_n=\mathbf{0}$ and along the lines of (4.21), the assembled *n*-layer PMDL model takes the form,

$$\begin{Bmatrix}\mathbf{T}_{x=0}^{n-pmdl}\\ \mathbf{0}\\ \mathbf{0}\\ \vdots\\ \mathbf{0}\\ \mathbf{0}\end{Bmatrix} = \begin{bmatrix}\mathbf{S}_1^{11} & \mathbf{S}_1^{12} & & & & \\ \mathbf{S}_1^{21} & \mathbf{S}_1^{22}+\mathbf{S}_2^{11} & \mathbf{S}_2^{12} & & & \\ & \mathbf{S}_2^{21} & \mathbf{S}_2^{22}+\mathbf{S}_3^{11} & \mathbf{S}_3^{12} & & \\ & & \ddots & \ddots & \ddots & \\ & & & \mathbf{S}_{n-2}^{21} & \mathbf{S}_{n-2}^{22}+\mathbf{S}_{n-1}^{11} & \mathbf{S}_{n-1}^{12} \\ & & & & \mathbf{S}_{n-1}^{21} & \mathbf{S}_{n-1}^{22}+\mathbf{S}_n^{11}\end{bmatrix}\begin{Bmatrix}\tilde{\mathbf{u}}_{x=0}\\ \tilde{\mathbf{u}}_1\\ \tilde{\mathbf{u}}_2\\ \vdots\\ \tilde{\mathbf{u}}_{n-2}\\ \tilde{\mathbf{u}}_{n-1}\end{Bmatrix}, \tag{4.23}$$

where the element stiffness matrices $\mathbf{S}_j\ \left(j=1\ldots n\right)$ are given by (4.20) and $\tilde{\mathbf{u}}_{x=0}$, $\mathbf{T}_{x=0}^{n-pmdl}$ are respectively the displacement vector and traction at the computational boundary (i.e. at the leftmost edge of the n-layer PMDL model). It should be noted that $\tilde{\mathbf{u}}_1,\ldots\tilde{\mathbf{u}}_{n-1},\tilde{\mathbf{u}}_n$ are auxiliary variables that do *not* approximate in any way the actual displacements in the exterior. However, since we are only interested in the field variable in the interior and at the computational boundary, this is of no particular importance [12].

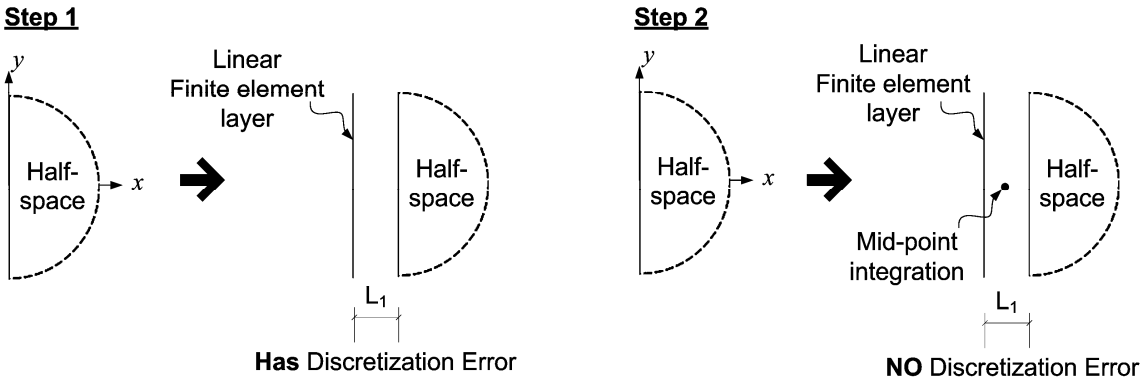

Figure 4.7. Steps 1 and 2 of PMDL derivation: Replacing a half-space by a linear finite element and another half-space. The use of mid-point integration in the *x* direction eliminates the discretization error.

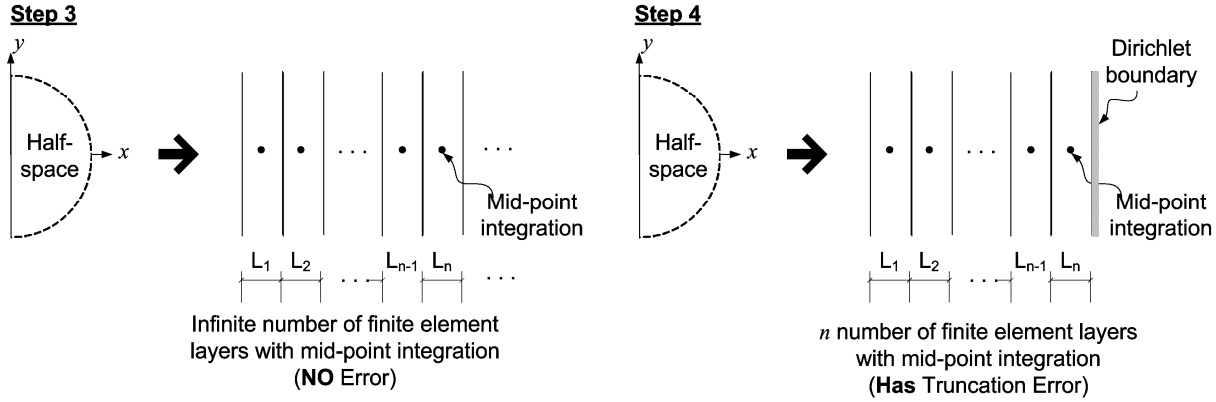

Figure 4.8. Steps 3 and 4 of PMDL derivation: Replacing the half-space by an infinite number of mid-point integrated linear finite elements produces the exact stiffness at *x=0*. Truncating the number of layers to *n* with a Dirichlet boundary at the end results in an implementable but approximate ABC; this is the *n* – layer PMDL

We can determine the computational reflection matrix (4.15) by noting that the decay (or growth) achieved when going in the opposite direction i.e. from right to left in the layer is $\left(1-i\widetilde{k}_x L_1/2\right)\Big/\left(1+i\widetilde{k}_x L_1/2\right)$ where $\widetilde{k}_x$ is the incoming (reflected) wavenumber satisfying (4.11). This leads us to an expression similar to (4.22) and using the notation of (4.15) we can write

$$\mathbf{P} = \begin{bmatrix} \prod_{j=1}^{n}\left(\dfrac{2i/L_j - k_{x1}}{2i/L_j + k_{x1}}\right) & 0 \\ 0 & \prod_{j=1}^{n}\left(\dfrac{2i/L_j - k_{x2}}{2i/L_j + k_{x2}}\right) \end{bmatrix},$$

$$\tilde{\mathbf{P}} = \begin{bmatrix} \prod_{j=1}^{n}\left(\dfrac{2i/L_j + \widetilde{k_{x1}}}{2i/L_j - \widetilde{k_{x1}}}\right) & 0 \\ 0 & \prod_{j=1}^{n}\left(\dfrac{2i/L_j + \widetilde{k_{x2}}}{2i/L_j - \widetilde{k_{x2}}}\right) \end{bmatrix}. \qquad (4.24)$$

In (4.24), $k_{x1}\left(\widetilde{k_{x1}}\right)$ and $k_{x2}\left(\widetilde{k_{x2}}\right)$ are the outgoing (incoming) horizontal wavenumbers for the epressure and shear waves respectively. The expressions in (4.24) along with (4.15) give us the computational reflection matrix $\mathbf{R}_C$. Of the three matrices $\mathbf{P}, \tilde{\mathbf{P}}, \mathbf{R}_T$, the matrices $\mathbf{P}, \tilde{\mathbf{P}}$ depend on the PMDL parameters (the layer lengths) while $\mathbf{R}_T$ depends on the truncation boundary at the end of PMDL. Each element $\mathbf{R}_C\left(\xi,\eta\right)$ takes the form, from equations (4.24) and (4.15):

$$\begin{aligned} \mathbf{R}_C(\xi,\eta) &= \tilde{\mathbf{P}}(\xi,\xi)\mathbf{R}_T(\xi,\eta)\mathbf{P}(\eta,\eta) \\ &= \underbrace{\mathbf{R}_T(\xi,\eta)}_{\substack{truncation \\ BC}} \underbrace{\left(\prod_{j=1}^{n}\left(\frac{2i/L_j + \widetilde{k_{x\xi}}}{2i/L_j - \widetilde{k_{x\xi}}}\right)\left(\frac{2i/L_j - k_{x\eta}}{2i/L_j + k_{x\eta}}\right)\right)}_{PMDL \quad contribution} \qquad \forall\ \xi,\eta \in \{1,2\}. \end{aligned} \qquad (4.25)$$

In order to facilitate later derivations we use the following notation to denote the PMDL contribution in (4.25) (see Figure 4.9),

$$R_j\left(\xi,\eta\right)=\left(\frac{\widetilde{\sigma_{x\xi}}+\sigma_{xj}^{ref}}{\widetilde{\sigma_{x\xi}}-\sigma_{xj}^{ref}}\right)\left(\frac{\sigma_{x\eta}-\sigma_{xj}^{ref}}{\sigma_{x\eta}+\sigma_{xj}^{ref}}\right),$$

where:

$$\sigma_{xj}^{ref}=2i\big/\omega L_j\,, \tag{4.26}$$

$$\left(\xi,\eta\right)\in\left\{1,2\right\}\quad\Rightarrow\quad\begin{cases}\widetilde{\sigma_{x1(2)}} & :\text{outgoing } \sigma_x \text{ for pressure (shear) wavemode}\\ \sigma_{x1(2)} & :\text{incoming } \sigma_x \text{ for pressure (shear) wavemode}\end{cases}$$

Using (4.26), (4.25) can be re-written as,

$$\mathbf{R}_C(\xi,\eta)=\underbrace{\mathbf{R}_T(\xi,\eta)}_{\substack{truncation\\ BC}}\underbrace{\left(\prod_{j=1}^{n}R_j(\xi,\eta)\right)}_{PMDL\quad contribution}. \tag{4.27}$$

It can be clearly seen from (4.26) and (4.27) that a choice of layer lengths $L_j=2i\big/\omega\,\sigma_{xj}^{ref}$ will make the n-layer PMDL exact for a choice of slownesses $\sigma_x=\sigma_{xj}^{ref}$ and these σ_{xj}^{ref} are termed the n parameters of PMDL.

For the simpler case of anti-plane displacements the matrices/vectors in (4.19), (4.21) and (4.23) can be replaced by their corresponding scalars. The scalar decay (or growth) factor $\left(1+ik_xL_1\,/\,2\right)\big/\left(1-ik_xL_1\,/\,2\right)$ remains the same.

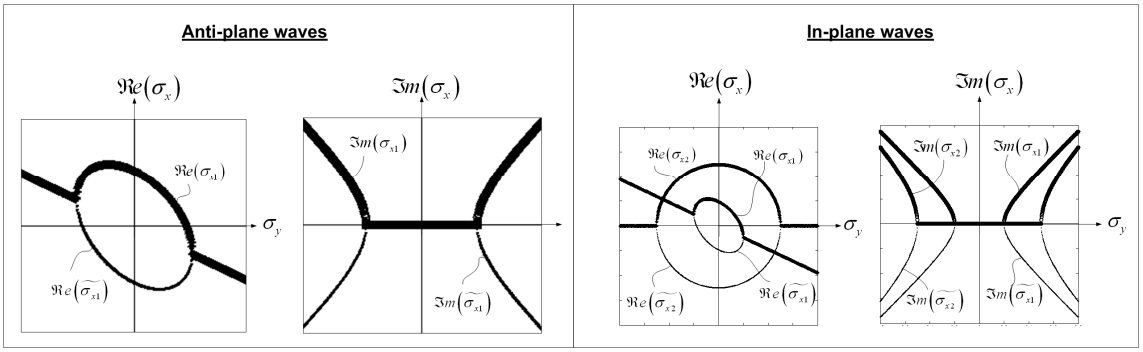

Figure 4.9. Notation for representing outgoing and incoming horizontal slownesses. For anti-plane waves σ_{x1} and $\widetilde{\sigma_{x1}}$ represent respectively the horizontal slownesses of outgoing and incoming wavemodes. For in-plane waves $\sigma_{x1}\left(\sigma_{x2}\right)$ and $\widetilde{\sigma_{x1}}\left(\widetilde{\sigma_{x2}}\right)$ represent respectively the horizontal slownesses for outgoing and incoming pressure (shear) wavemodes.

4.5 Accuracy Requirements

4.5.1 Accuracy Criterion

An ABC is considered exact if $\mathbf{R}_C(\xi,\eta)=0$ for all ξ,η in (4.27). Accuracy of an approximate ABC hence translates to making $\mathbf{R}_C(\xi,\eta)$ as small as possible. Typically the accuracy of ABCs is a function of the ABC parameters and the computational effort that can be reasonably expended. For an ABC to be considered accurate in any sense it should yield the exact solution in the limit of infinite computational effort. In other words, an ABC is termed accurate if its parameters can be chosen to yield $\mathbf{R}_C(\xi,\eta)\to 0$ with increasing computational effort.

Accuracy criterion: An n-layer PMDL is considered accurate if, by increasing the number of layers n, the magnitude of every element of its computational reflection matrix can be made arbitrarily small for every wavemode, i.e.,

$$\lim_{n\to\infty}\left|\mathbf{R}_C(\xi,\eta)\right|=0 \qquad \forall\ \xi,\eta : Accuracy\ criterion\,. \tag{4.28}$$

To be precise (4.28) is a *convergence* criterion that is necessary for a PMDL to act as a meaningful ABC for any wavemode. If the rate of convergence is slow, the number of PMDL layers required for sufficient accuracy might render the ABC inefficient. The usage of the term *accuracy* instead of the term *convergence* is mainly for the sake of compatibility with existing ABC literature e.g. [48].

4.5.2 Sufficient Conditions for Accuracy

For a homogeneous Dirichlet truncation boundary condition, the elements of $\mathbf{R}_T$ are bounded and hence a simple sufficient condition for (4.28) using (4.27) is

$$\left|R_j\left(\xi,\eta\right)\right| = \left|\left(\frac{\widetilde{\sigma_{x\xi}} + \sigma_{xj}^{ref}}{\widetilde{\sigma_{x\xi}} - \sigma_{xj}^{ref}}\right)\left(\frac{\sigma_{x\eta} - \sigma_{xj}^{ref}}{\sigma_{x\eta} + \sigma_{xj}^{ref}}\right)\right| < 1 \qquad \forall \xi,\eta \in \left\{1,2\right\},\ j = \left(1...n\right). \tag{4.29}$$

The first factor in (4.29) is related, as specified in (4.26), to the incoming (reflected) wavemodes that exist because of the truncation boundary while the second factor is related to the outgoing wavemodes (4.26). Hence even if there is growth in the outgoing modes because of the opposing phase and group velocity signs (second factor is greater than 1), it is possible that the first factor produces enough decay to ensure *net* decay in the j^{th} PMDL layer. It should be noted that the availability of an expression like (4.29) that relates explicitly the parameters of the ABC to its approximation properties is essential in understanding and exploiting the concept of *net* decay. General discretizations of PML do not lend themselves to such expressions. While the form of (4.29) is common in rational ABCs, their behavior cannot be studied in analogy to the more intuitive PML as we did in Section 4.4.1 with PMDL.

Expanding the expression for $R_j(\xi,\eta)$ in (4.29) and introducing variables χ,γ we get

$$\begin{aligned}
&\left|R_j\left(\xi,\eta\right)\right| = \frac{\left|\chi+\gamma\right|}{\left|\chi-\gamma\right|},\\
&\chi = \widetilde{\sigma_{x\xi}}\sigma_{x\eta} - \left(\sigma_{xj}^{ref}\right)^2,\\
&\gamma = \sigma_{xj}^{ref}(\sigma_{x\eta} - \widetilde{\sigma_{x\xi}}).
\end{aligned} \tag{4.30}$$

By using the parallelogram law of addition of vectors, the condition (4.29) with (4.30) can be expressed in the following equivalent conditions:

$$\left|R_j\left(\xi,\eta\right)\right| < 1 \quad \Leftrightarrow \quad \left|\chi+\gamma\right| < \left|\chi-\gamma\right|,$$

$$\begin{aligned}
\left|\chi+\gamma\right| < \left|\chi-\gamma\right| \quad &\Leftrightarrow \quad \Re e\left(\chi\right)\Re e\left(\gamma\right) + \Im m\left(\chi\right)\Im m\left(\gamma\right) < 0\\
&\Leftrightarrow \quad \left(\ 90^o < \psi < 270^o\right),
\end{aligned} \tag{4.31}$$

where ψ is the angle between the vectors $\vec{\chi}$ and $\vec{\gamma}$ in the complex plane. Of course, for $\chi,\gamma \in \mathbb{R}$, (4.31) reduces to $\chi\gamma < 0$.

Since the decay (or growth) factors are the same for the simpler anti-plane shear case, the sufficient condition for accuracy (4.29) is applicable to (4.5) too (see [44]). Moreover, since (4.5) has only one kind of outgoing/incoming mode which is similar in slowness to the in-plane pressure wave, we will just use $R_j\left(1,1\right)$ for the anti-plane case (see Figure 4.9).

4.6 Accurate PMDL

In this section, we will derive conditions on the PMDL parameters σ_{xj}^{ref} that ensure (4.29) for anti-plane shear waves and in-plane pressure and shear waves of tilted elliptic anisotropic elasticity.

4.6.1 Anti-plane shear waves

The sufficient condition for accuracy (4.29) can be applied to Figure 4.10 to derive a condition on the parameters of the PMDL - the layer lengths. This was done for the case of

propagating waves in [44]. We provide here a simpler alternative proof and establish conditions on σ_{xj}^{ref} that ensure (4.29) for *all* – propagating and evanescent – wavemodes.

Using (4.7) in the dispersion relation $\Lambda^{anti} = 0$ for anti-plane shear, we get,

$$\sigma_{x1} = \frac{-A_{xy}\sigma_y + \sqrt{A_{xx} - \left(A_{xx}A_{yy} - A_{xy}^2\right)\sigma_y^2}}{A_{xx}},$$
$$\widetilde{\sigma}_{x1} = \frac{-A_{xy}\sigma_y - \sqrt{A_{xx} - \left(A_{xx}A_{yy} - A_{xy}^2\right)\sigma_y^2}}{A_{xx}}. \tag{4.32}$$

We first see whether we can satisfy (4.31) with $\sigma_{xj}^{ref} > 0$. We try $\sigma_{xj}^{ref} \in \mathbb{R}$ first because we are mainly interested in absorbing propagating waves $\left(\sigma_{x1} \in \mathbb{R}\right)$. The reason for assuming $\sigma_{xj}^{ref} > 0$ is that for the isotropic case, this is true and we expect the anisotropic condition to simplify to this case in the case of isotropy. We also define $\sigma_{y1} = +\sqrt{A_{xx}\Big/\left(A_{xx}A_{yy} - A_{xy}^2\right)}$ for the sake of partitioning as shown in Figure 4.10.

For $\sigma_y \in \left(-\sigma_{y1}, \sigma_{y1}\right)$ we have $\left(\sigma_{x1}, \widetilde{\sigma_{x1}}\right) \in \mathbb{R}$ and this implies $\chi, \gamma \in \mathbb{R}$ since we assume $\sigma_{xj}^{ref} \in \mathbb{R}$. Hence (4.31) reduces to $\chi\gamma < 0$. Using $\left(\sigma_{x1} - \widetilde{\sigma_{x1}}\right) > 0$ from (4.32) and $\sigma_{xj}^{ref} > 0$, we have $\gamma > 0$. Hence $\chi < 0$ or simply $\left(\sigma_{xj}^{ref}\right)^2 > \widetilde{\sigma}_{x1}\sigma_{x1}$. From (4.32), $\sigma_{x1}\widetilde{\sigma_{x1}} = \left(A_{yy}\sigma_y^2 - 1\right)\Big/A_{xx}$ and hence $max\left(\sigma_{x1}\widetilde{\sigma_{x1}}\right) = \left(A_{yy}\sigma_{y1}^2 - 1\right)\Big/A_{xx}$. Since $\sigma_y = \pm\sigma_{y1}$ denotes the position where the *cusp* of the tilted ellipse occurs (see Figure 4.10), we define $\sigma_{cusp} = \left|\sqrt{\left(A_{yy}\sigma_{y1}^2 - 1\right)\Big/A_{xx}}\right|$ and the sufficient condition for accuracy becomes $\sigma_{xj}^{ref} > \sigma_{cusp}$ or in expanded form,

$$\sigma_{xj}^{ref} > \underbrace{\left| \frac{A_{xy}}{\sqrt{A_{xx}\left(A_{xx}A_{yy} - A_{xy}^2\right)}} \right|}_{\sigma_{cusp}}. \tag{4.33}$$

This is the same condition that was obtained in [44]. Note that (4.3) ensures $\left(A_{xx}A_{yy} - A_{xy}^2\right) > 0$, $A_{xx} > 0$ and $A_{xy} > 0$.

For $\sigma_y = \pm\sigma_{y1}$, we have $\sigma_{x1} = \widetilde{\sigma_{x1}} = \pm\sigma_{cusp}$ from (4.32) and hence (4.29) results in $\left|R_j\left(1,1\right)\right| = 1$ unless $\sigma_j = \sigma_{cusp}$. This implies that accuracy can be ensured at $\sigma_y = \pm\sigma_{y1}$ only if, for at least one $j \in \left(1,\ldots,n\right)$, $\sigma_{xj}^{ref} = \sigma_{cusp}$. While we can ensure this for time-harmonic simulations without any trouble, corresponding transient simulations lead to ill-posedness due to the admittance of modes with zero group velocities (like those that occur at $\sigma_y = \pm\sigma_{y1}$). Hence we violate (4.29) at $\sigma_y = \pm\sigma_{y1}$ and accept $\left|R_j\left(1,1\right)\right| = 1$ at those points as accurate enough. See [44] for a more detailed discussion.

For $\sigma_y \notin \left[-\sigma_{y1}, \sigma_{y1}\right]$, we can see from (4.32) that σ_{x1} and $\widetilde{\sigma_{x1}}$ are complex conjugates and hence for $\sigma_{xj}^{ref} \in \mathbb{R}$, we have $\left|R_j(1,1)\right| = 1$. This implies complete reflection of all evanescent modes. This is true in general whenever the PMDL parameters σ_{xj}^{ref} are chosen to be real. Hence if we are only interested in absorbing outgoing propagating modes (and neither evanescent nor zero group velocity modes), (4.33) is a sufficient condition for accuracy. If we wish to absorb both outgoing propagating and zero group velocity modes, a sufficient condition for accuracy is $\sigma_{x1}^{ref} = \sigma_{cusp}$ with (4.33) satisfied for $j = 2,\ldots,n$.

Reflection of evanescent modes is less harmful than reflection of propagating modes because evanescent modes eventually decay into the interior after reflection. However, evanescent modes typically pollute the interior solution at least near the boundary and, in

time domain simulations, they are known to affect the long term accuracy of the solution [48]. Evanescent modes can be absorbed by considering $\sigma_{xj}^{ref} \notin \mathbb{R}$.

For $\sigma_{xj}^{ref} \notin \mathbb{R}$, it can be easily seen that (4.29) is violated e.g. (a) in $\sigma_y \in \left[-\sigma_{y1}, \sigma_{y1}\right]$ if $\Re e\left(\sigma_{xj}^{ref}\right) \leq 0$, and (b) in $\sigma_y \notin \left[-\sigma_{y1}, \sigma_{y1}\right]$ if $\Im m\left(\sigma_{xj}^{ref}\right) < 0$. Hence we use $\Re e\left(\sigma_{xj}^{ref}\right) > 0$ and $\Im m\left(\sigma_{xj}^{ref}\right) > 0$ for $\sigma_{xj}^{ref} \notin \mathbb{R}$.

Let $\sigma_{xj}^{ref} = e + if$ with $e > 0, f > 0$. For $\sigma_y \in \left(-\sigma_{y1}, 0\right]$ the slownesses take the form $\sigma_{x1} = \left(a + b\right), \widetilde{\sigma_{x1}} = \left(a - b\right)$ with $a \geq 0, b > 0$ as evident from (4.32). Using (4.31) with $\chi = a^2 - b^2 - \left(e + if\right)^2$ and $\gamma = 2b\left(e + if\right)$ we get, after some manipulation, the condition for $\left|R_j\left(1,1\right)\right| < 1$ to be $e^2 + f^2 > a^2 - b^2$ which can be written as $\left|\sigma_{xj}^{ref}\right|^2 > \sigma_{x1}\widetilde{\sigma_{x1}}$. We already know from the analysis for $\sigma_{xj}^{ref} \in \mathbb{R}$ that $max\left(\sigma_{x1}\widetilde{\sigma_{x1}}\right) = \left(\sigma_{cusp}\right)^2$ and hence the condition for accuracy reduces to

$$\left|\sigma_{xj}^{ref}\right| > \left|\frac{A_{xy}}{\sqrt{A_{xx}\left(A_{xx}A_{yy} - A_{xy}^2\right)}}\right| \text{ with } \Re e\left(\sigma_{xj}^{ref}\right) > 0, \Im m\left(\sigma_{xj}^{ref}\right) > 0. \tag{4.34}$$

Similar arguments hold for $\sigma_y \in \left(0, \sigma_{y1}\right)$. Here, $\sigma_{x1} = \left(-a + b\right), \widetilde{\sigma_{x1}} = \left(-a - b\right)$ with $a > 0, b > 0$ and we again get (4.34). For $\sigma_y \notin \left[-\sigma_{y1}, \sigma_{y1}\right]$, we can use the forms $\sigma_{x1} = \left(\pm a + ib\right), \widetilde{\sigma_{x1}} = \left(\pm a - ib\right)$ with $a > 0, b > 0$ and by substitution into (4.29) directly, we see that each factor therein is less than unity. Hence for $\sigma_y \notin \left[-\sigma_{y1}, \sigma_{y1}\right]$, any $\sigma_{xj}^{ref} \in \mathbb{C}$ with $\Re e\left(\sigma_{xj}^{ref}\right) > 0, \Im m\left(\sigma_{xj}^{ref}\right) > 0$ will satisfy (4.31).

To summarize, (4.34) is sufficient to ensure $\left|R_j\left(1,1\right)\right|<1$ for all $\sigma_y \neq \pm\sigma_{y1}$. At the isolated points $\sigma_y = \pm\sigma_{y1}$, we have $\left|R_j\left(1,1\right)\right|=1$ and these are the zero group velocity modes whose exclusion was discussed before and considered acceptable. In-fact, unlike in the case of $\sigma_{xj}^{ref} \in \mathbb{R}$ it is not at all possible to absorb modes at $\sigma_y \neq \pm\sigma_{y1}$ when $\Im m\left(\sigma_{xj}^{ref}\right) > 0$.

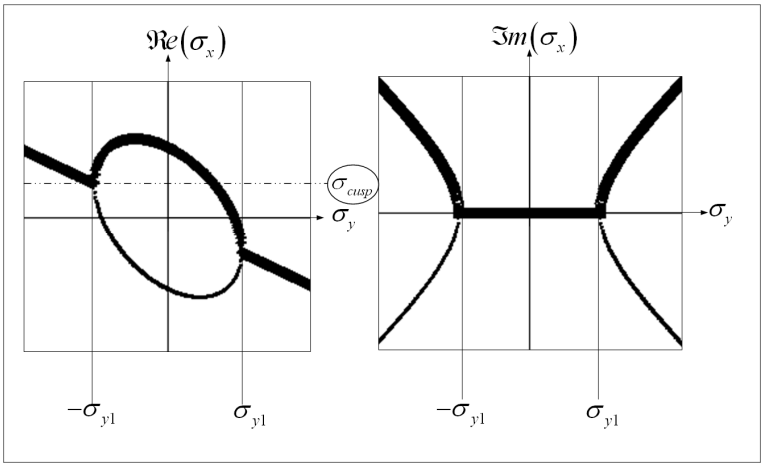

Figure 4.10. Partitioning of the vertical slowness to facilitate the derivation of accuracy bounds for anti-plane waves.

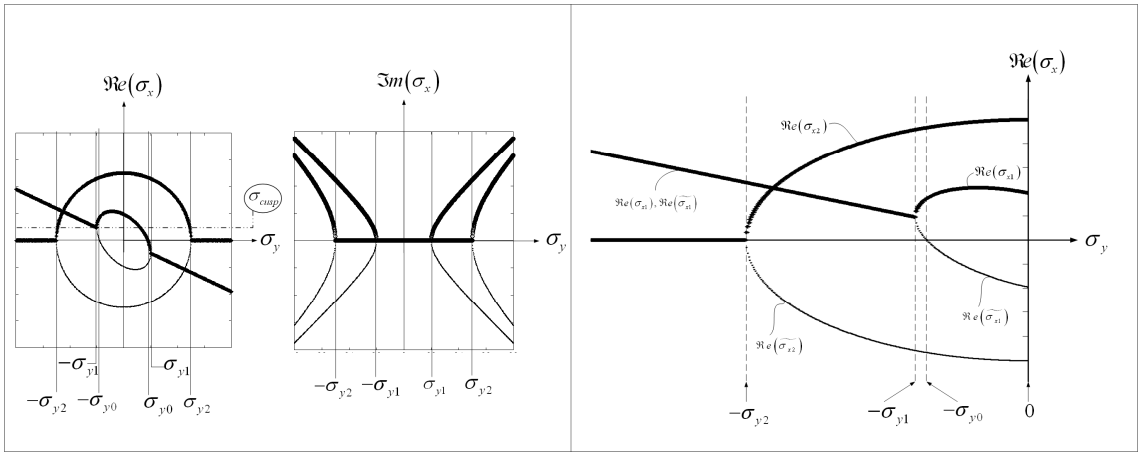

Figure 4.11. *Left:* Partitioning of the vertical slowness to facilitate the derivation of accuracy bounds for in-plane waves. *Right:* Expanded view of the left half plane of the real part of the slowness diagram for in-plane waves.

4.6.2 In-plane waves

Using the in-plane dispersion relation $\det\left(\mathbf{\Lambda}^{anti}\right)=0$ (see (4.8)), for tilted elliptic anisotropic elasticity $\left(\varepsilon=\delta\right)$, we get the slowness relations,

$$\begin{aligned}\sigma_{x1} &= \frac{\varepsilon\sin\left(2\beta\right)\sigma_y+\sqrt{\left(1+2\varepsilon\cos^2\beta\right)/c_p^2-\left(1+2\varepsilon\right)\sigma_y^2}}{1+2\varepsilon\cos^2\beta},\\ \widetilde{\sigma}_{x1} &= \frac{\varepsilon\sin\left(2\beta\right)\sigma_y-\sqrt{\left(1+2\varepsilon\cos^2\beta\right)/c_p^2-\left(1+2\varepsilon\right)\sigma_y^2}}{1+2\varepsilon\cos^2\beta},\end{aligned} \tag{4.35}$$

$$\sigma_{x2}=+\sqrt{1/c_s^2-\sigma_y^2},\qquad \widetilde{\sigma_{x2}}=-\sqrt{1/c_s^2-\sigma_y^2}. \tag{4.36}$$

We divide the vertical slowness into eight regions using partitions at $\sigma_y=0,\pm\sigma_{y0},\pm\sigma_{y1},\pm\sigma_{y2}$ as shown in Figure 4.11, and derive conditions for ensuring $\left|R_j(\xi,\eta)\right|<1$ for each of these domains separately. Here $\pm\sigma_{y0}$ denotes the point where $\Re e\left(\sigma_{x1}\right)$ changes sign, $\pm\sigma_{y1}$ denotes the point where σ_{x1} changes from purely real to

complex (or imaginary) and $\pm\sigma_{y2}$ denotes the point where σ_{x2} changes from purely real to imaginary. Hence, using (4.35) and (4.36) we get $\sigma_{y0} = c_p^{-1}\sqrt{\left(1+2\varepsilon\sin^2\beta\right)^{-1}}$, $\sigma_{y1} = c_p^{-1}\sqrt{\left(1+2\varepsilon\cos^2\beta\right)\left(1+2\varepsilon\right)^{-1}}$ and $\sigma_{y2} = c_s^{-1}$.

We first show that it is *not* possible to satisfy (4.29) with $\sigma_{xj}^{ref} \in \mathbb{R}$. Since the analysis of conditions for ensuring $\left|R_j(1,1)\right| < 1$ involves no mode coupling and since (4.35) is similar to (4.32), the accuracy condition $\sigma_{xj}^{ref} > \sigma_{cusp}$ expressed in (4.33) still holds with σ_{cusp} calculated for (4.35) instead of for (4.32). Hence, from (4.33) we know that the condition for $\left|R_j\left(1,1\right)\right| < 1$ is $\sigma_{xj}^{ref} > \sigma_{cusp}$ where σ_{cusp} is a finite positive number (we will use this fact shortly). Now consider $\left|R_j\left(1,2\right)\right|$ in the domain $\sigma_y \in \left(-\infty, -\sigma_{y2}\right)$. Here we have $\widetilde{\sigma_{x1}} = a - ib$, $\sigma_{x2} = ic$ with $a > 0, b > 0, c > 0$. Also from (4.31), $\chi = bc - \left(\sigma_{xj}^{ref}\right)^2 + i\left(ac\right)$ and $\gamma = -a\sigma_{xj}^{ref} + i\left(b+c\right)\sigma_{xj}^{ref}$. From this we can see that χ is in the 1st or 2nd quadrant depending on whether $\left(bc - \left(\sigma_{xj}^{ref}\right)^2\right) > 0$ or $\left(bc - \left(\sigma_{xj}^{ref}\right)^2\right) < 0$ respectively. γ of course is always in the 2nd quadrant. Hence for $\left(bc - \left(\sigma_{xj}^{ref}\right)^2\right) < 0$ both χ, γ are in the 2nd quadrant and the angle ψ between them cannot satisfy (4.31). Since $\sigma_{xj}^{ref} > \sigma_{cusp}$ for $\left|R_j\left(1,1\right)\right| < 1$ and $bc \to 0$ as $\sigma_y \to -\sigma_{y1}$ from the left, we will always have a region in the vicinity of $\sigma_y = -\sigma_{y1}$ where $\left(bc - \left(\sigma_{xj}^{ref}\right)^2\right) < 0$ and hence it is impossible to satisfy (4.29) with $\sigma_{xj}^{ref} \in \mathbb{R}$. We are thus left with $\sigma_{xj}^{ref} \notin \mathbb{R}$.

For $\sigma_{xj}^{ref} \notin \mathbb{R}$, we again require $\Re e\left(\sigma_{xj}^{ref}\right) > 0$ and $\Im m\left(\sigma_{xj}^{ref}\right) > 0$ because the conditions for ensuring $\left|R_j(1,1)\right| < 1$ for in-plane waves will be the same as those for anti-plane waves. Hence we can assume $\sigma_{xj}^{ref} = e + if$ with $e > 0, f > 0$.

Since there are two modes, pressure and shear, we have four $R_j s$ $\left(R_j\left(1,1\right), R_j\left(2,2\right), R_j\left(1,2\right), R_j\left(2,1\right)\right)$ for each domain leading to a total count of thirty two. Since the calculations for $\sigma_y \leq 0$ are similar to those for $\sigma_y \geq 0$ and the conditions end up being the same, we restrict ourselves to sixteen cases. Of these, the conditions for ensuring $\left|R_j(1,1)\right| < 1$ and $\left|R_j(2,2)\right| < 1$ are the same as that for anti-plane waves and hence we already know the condition to be $\left|\sigma_{xj}^{ref}\right| > \sigma_{cusp}$ from (4.34). Note that for $R_j(1,1)$, $\sigma_{cusp} = \left|\varepsilon \sin\left(2\beta\right)\left(c_p\sqrt{\left(1+2\varepsilon\cos^2\beta\right)\left(1+2\varepsilon\right)}\right)^{-1}\right|$ and it occurs at $\sigma_y = \pm\sigma_{y1}$ as evidenced from (4.35). The *cusp* for $R_j(2,2)$ is $\sigma_{cusp} = 0$ and it occurs at $\sigma_y = \pm\sigma_{y2}$. These two conditions are listed below for later use. Note that as in the case of anti-plane waves, it is not possible to satisfy (4.29) for the zero group velocity modes occurring at $\sigma_y = \pm\sigma_{y1}$ for pressure modes, and at $\sigma_y = \pm\sigma_{y2}$ for shear modes when $\Im m\left(\sigma_{xj}^{ref}\right) > 0$ and this is considered acceptable.

Given $\sigma_{xj}^{ref} = e + if$ $\left(e > 0, f > 0\right)$:

For the entire region $\sigma_y \in \left(-\infty, \infty\right)$:

- For $\left|R_j\left(1,1\right)\right| < 1$ we require:

$$\left|\sigma_{xj}^{ref}\right| > \underbrace{\left|\frac{\varepsilon \sin\left(2\beta\right)}{c_p\sqrt{\left(1+2\varepsilon\cos^2\beta\right)\left(1+2\varepsilon\right)}}\right|}_{\sigma_{cusp}}. \tag{4.37}$$

- For $\left|R_j\left(2,2\right)\right| < 1$ we require $\left|\sigma_{xj}^{ref}\right| > 0$ which is trivially satisfied.

We thus have eight remaining conditions to derive, namely the conditions for ensuring $\left|R_j(2,1)\right| < 1$ and $\left|R_j(1,2)\right| < 1$ for σ_y in the regions $\left(-\infty, -\sigma_{y2}\right)$, $\left[-\sigma_{y2}, -\sigma_{y1}\right]$, $\left(-\sigma_{y1}, -\sigma_{y0}\right)$ and $\left[-\sigma_{y0}, 0\right]$.

For $\sigma_y \in \left(-\infty, -\sigma_{y2}\right)$:

From (4.35), (4.36) and Figure 4.11 we can write

$\sigma_{x1} = a + ib$, $\sigma_{x2} = ic$, $\widetilde{\sigma_{x1}} = a - ib$, $\widetilde{\sigma_{x2}} = -ic$ where $a > 0, b > 0, c > 0$.

- For $\left|R_j\left(1,2\right)\right| < 1$ we have:

$$\begin{aligned} \chi &= \widetilde{\sigma_{x1}}\sigma_{x2} - \left(\sigma_{xj}^{ref}\right)^2 = (a-ib)(ic) - (e+if)^2, \\ \gamma &= \sigma_{xj}^{ref}(\sigma_{x2} - \widetilde{\sigma_{x1}}) = (e+if)(ic-a+ib). \end{aligned} \tag{4.38}$$

Substituting (4.38) into $\Re e\left(\chi\right)\Re e\left(\gamma\right) + \Im m\left(\chi\right)\Im m\left(\gamma\right) < 0$ from (4.31) and after some manipulations we arrive at

$$\left(\frac{e}{f}\right) < \left(\frac{b}{a}\right) + \left(\frac{c}{a}\right)\left(\frac{a^2 + b^2 + e^2 + f^2}{c^2 + e^2 + f^2}\right). \tag{4.39}$$

We can replace (4.39) by the simple sufficient condition

$e/f < \inf\left(b/a\right) = \left(b/a\right)_{\sigma_y = -\sigma_{y2}}$, where the equality is obtained using (4.35).

This simple condition, when expanded using (4.35), results in

$$\left|\frac{\Re e\left(\sigma_{xj}^{ref}\right)}{\Im m\left(\sigma_{xj}^{ref}\right)}\right| < \left|\frac{\sqrt{\left(c_p^2 - c_s^2\right)\left(1+2\varepsilon\right) + c_s^2\left(2\varepsilon \sin^2\beta\right)}}{c_p \varepsilon \sin 2\beta}\right|. \qquad (4.40)$$

- For $\left|R_j\left(2,1\right)\right| < 1$ we have $\chi = (-ic)(a+ib) - (e+if)^2$ and $\gamma = (e+if)(a+ib+ic)$ which when substituted into $\Re e\left(\chi\right)\Re e\left(\gamma\right) + \Im m\left(\chi\right)\Im m\left(\gamma\right) < 0$ from (4.31) leads to the expression $-\left(e/f\right) < a^{-1}b + \left(a^{-1}c\right)\left(a^2 + b^2 + e^2 + f^2\right)\left(c^2 + e^2 + f^2\right)^{-1}$ which is trivially satisfied.

For $\sigma_y \in \left[-\sigma_{y2}, -\sigma_{y1}\right]$:

From (4.35), (4.36) and Figure 4.11 we can write $\sigma_{x1} = a + ib$, $\sigma_{x2} = c$, $\widetilde{\sigma_{x1}} = a - ib$, $\widetilde{\sigma_{x2}} = -c$ where $a > 0, b \geq 0, c \geq 0$.

- For $\left|R_j\left(1,2\right)\right| < 1$ we get:

$$\left(\frac{e}{f}\right)\left(1 - \left(\frac{c}{a}\right)\left(\frac{a^2 + b^2 + e^2 + f^2}{c^2 + e^2 + f^2}\right)\right) < \left(\frac{b}{a}\right). \qquad (4.41)$$

As $\sigma_y \to -\sigma_{y2}$ from the right, $c \to 0$ while a, b and b/a tend to finite non-zero values. As $\sigma_y \to -\sigma_{y1}$ from the left, $b/a \to 0$ and to prevent (4.41) from becoming impossible to satisfy with finite e/f, the factor multiplying e/f in (4.41) should either become negative or, be positive and tend to zero faster than b/a. Simple manipulation shows $\left(a-c\right)\left(ac - e^2 - f^2\right) + cb^2 > 0$ to be the condition for $1 - ca^{-1}\left(a^2 + b^2 + e^2 + f^2\right)\left(c^2 + e^2 + f^2\right)^{-1} < 0$. Since, as $\sigma_y \to -\sigma_{y1}$ we have $c > a$ and $b \to 0$, $\left(a-c\right)\left(ac - e^2 - f^2\right) + cb^2 > 0$

boils down to $e^2 + f^2 > ac$. As ac is bounded from above in $\sigma_y \in \left[-\sigma_{y2}, -\sigma_{y1}\right]$, this condition is not hard to satisfy. Note that near $\sigma_y = -\sigma_{y2}$, we have $c \le a$; but in this case b/a is a finite number and the above issue no longer exists. However, even though $e^2 + f^2 > ac$ is required to be satisfied only as $\sigma_y \to -\sigma_{y1}$, to simplify matters, we will ensure $e^2 + f^2 > ac$ over the entire domain $\sigma_y \in \left[-\sigma_{y2}, -\sigma_{y1}\right]$ as this does not contradict (4.41). Recasting (4.41) and $e^2 + f^2 > ac$ in terms of $\sigma_{x1}, \sigma_{x2}, \widetilde{\sigma_{x1}}, \widetilde{\sigma_{x2}}$ we get:

$$\left(\frac{\Re e\left(\sigma_{xj}^{ref}\right)}{\Im m\left(\sigma_{xj}^{ref}\right)}\right)\left(1 - \left(\frac{\left|\Re e\left(\sigma_{x2}\right)\right|}{\left|\Re e\left(\sigma_{x1}\right)\right|}\right)\left(\frac{\left|\sigma_{x1}\right|^2 + \left|\sigma_{xj}^{ref}\right|^2}{\left|\sigma_{x2}\right|^2 + \left|\sigma_{xj}^{ref}\right|^2}\right)\right) < \left(\frac{\left|\Im m\left(\sigma_{x1}\right)\right|}{\left|\Re e\left(\sigma_{x1}\right)\right|}\right), \qquad (4.42)$$

$$\left|\sigma_{xj}^{ref}\right|^2 > \left|\Re e\left(\sigma_{x1}\right)\sigma_{x2}\right|. \qquad (4.43)$$

- For $\left|R_j\left(2,1\right)\right| < 1$ we get $-\left(e/f\right)\left(1 + \left(a^{-1}c\right)\left(a^2 + b^2 + e^2 + f^2\right)\left(c^2 + e^2 + f^2\right)^{-1}\right) < a^{-1}b$ which is trivially satisfied.

For $\sigma_y \in \left(-\sigma_{y1}, -\sigma_{y0}\right)$:

From (4.35), (4.36) and Figure 4.11 we can write $\sigma_{x1} = a + b$, $\sigma_{x2} = c$, $\widetilde{\sigma_{x1}} = a - b$, $\widetilde{\sigma_{x2}} = -c$ where $a > 0, b > 0, c > 0$ and moreover $a > b, c > a + b$.

- For $\left|R_j\left(1,2\right)\right| < 1$ we get:

$$\left|\sigma_{xj}^{ref}\right|^2 > \left|\widetilde{\sigma_{x1}}\sigma_{x2}\right|. \tag{4.44}$$

Since $\left|\widetilde{\sigma_{x1}}\sigma_{x2}\right|$ is bounded from above in $\sigma_y \in \left(-\sigma_{y1}, -\sigma_{y0}\right)$, it is possible to satisfy (4.44).

- For $\left|R_j\left(2,1\right)\right| < 1$ we get $\left|\sigma_{xj}^{ref}\right|^2 > -\left|\sigma_{x2}\sigma_{x1}\right|$ which is trivially satisfied.

For $\sigma_y \in \left[-\sigma_{y0}, 0\right]$:

From (4.35), (4.36) and Figure 4.11 we can write $\sigma_{x1} = a + b$, $\sigma_{x2} = c$, $\widetilde{\sigma_{x1}} = a - b$, $\widetilde{\sigma_{x2}} = -c$, where $a \geq 0, b > 0, c > 0$ and moreover $a \leq b, c > a + b$. For both $\left|R_j\left(1,2\right)\right|$ and $\left|R_j\left(2,1\right)\right|$, (4.29) will have both factors less than unity. Hence $\left|R_j\left(1,2\right)\right| < 1$ and $\left|R_j\left(2,1\right)\right| < 1$ is always ensured in this region.

No additional bounds are required for $\sigma_y \in \left[0, +\infty\right)$. To get the governing conditions from amongst the above, we use (4.35) and (4.36) to realize that (4.44) overshadows (4.37) because $\sigma_{x2} \geq \sigma_{cusp} = \max\left(\left|\widetilde{\sigma_{x1}}\right|\right)$ in $\sigma_y \in \left(-\sigma_{y1}, -\sigma_{y0}\right)$. Moreover, since $\sigma_{x2} \leq c_s^{-1}$ in $\sigma_y \in \left[-\sigma_{y2}, 0\right]$ and we can see from Figure 4.11 that $\max\left\{\left|\Re e\left(\sigma_{x1}\right)\right|_{\left(-\sigma_{y2} \leq \sigma_y \leq -\sigma_{y1}\right)}, \left|\widetilde{\sigma_{x1}}\right|_{\left(-\sigma_{y1} \leq \sigma_y \leq 0\right)}\right\} \leq \left|\Re e\left(\sigma_{x1}\right)\right|_{\left(\sigma_y = -\sigma_{y2}\right)}$ with $\left|\Re e\left(\sigma_{x1}\right)\right|_{\left(\sigma_y = -\sigma_{y2}\right)} = \left|\left(\varepsilon \sin 2\beta\right)\sigma_{y2} \Big/ \left(1 + 2\varepsilon \cos^2 \beta\right)\right|$, both (4.43) and (4.44) can be satisfied by using $\left|\sigma_{xj}^{ref}\right|^2 > \left|c_s^{-2}\left(\varepsilon \sin 2\beta\right) \Big/ \left(1 + 2\varepsilon \cos^2 \beta\right)\right|$; this along with (4.40) and (4.42) are the governing equations for ensuring $\left|R_j\left(\cdot,\cdot\right)\right| < 1$.

To summarize, the accuracy conditions for σ_{xj}^{ref} with $\Re e\left(\sigma_{xj}^{ref}\right) > 0, \Im m\left(\sigma_{xj}^{ref}\right) > 0$ are:

$$\left|\sigma_{xj}^{ref}\right|^2 > \frac{\varepsilon \sin 2\beta}{c_s^2\left(1 + 2\varepsilon \cos^2 \beta\right)}, \tag{4.45}$$

$$\left(\frac{\Re e\left(\sigma_{xj}^{ref}\right)}{\Im m\left(\sigma_{xj}^{ref}\right)}\right) < \left|\frac{\sqrt{\left(c_p^2 - c_s^2\right)\left(1 + 2\varepsilon\right) + c_s^2\left(2\varepsilon \sin^2 \beta\right)}}{c_p \varepsilon \sin 2\beta}\right|, \tag{4.46}$$

$$\left(\frac{\Re e\left(\sigma_{xj}^{ref}\right)}{\Im m\left(\sigma_{xj}^{ref}\right)}\right)\left(1 - \left(\frac{\left|\Re e\left(\sigma_{x2}\right)\right|}{\left|\Re e\left(\sigma_{x1}\right)\right|}\right)\left(\frac{\left|\sigma_{x1}\right|^2 + \left|\sigma_{xj}^{ref}\right|^2}{\left|\sigma_{x2}\right|^2 + \left|\sigma_{xj}^{ref}\right|^2}\right)\right) < \left(\frac{\left|\Im m\left(\sigma_{x1}\right)\right|}{\left|\Re e\left(\sigma_{x1}\right)\right|}\right), \tag{4.47}$$

$$for\ \sigma_y \in \left[-\sigma_{y2}, -\sigma_{y1}\right].$$

It is important to note that the governing conditions, namely (4.45), (4.46) and (4.47) are not contradictory i.e. there exists some σ_{xj}^{ref} which satisfies these three conditions simultaneously. It is fairly simple to observe that all the above conditions can be easily satisfied if $\Im m\left(\sigma_{xj}^{ref}\right)$ is '*large enough*'. Presented below is a simple algorithm for satisfying (4.45), (4.46) and (4.47).

Algorithm for Accuracy: Use equality limits of (4.45) and (4.46) to get $\Re e\left(\sigma_{xj}^{ref}\right)$ and $\Im m\left(\sigma_{xj}^{ref}\right)$. Check whether (4.47) is satisfied. If not, keep increasing $\Im m\left(\sigma_{xj}^{ref}\right)$ until (4.47) is satisfied.

Note that if σ_{xj}^{ref} satisfies the accuracy conditions, so will any $\lambda\sigma_{xj}^{ref}$ with $\lambda > 1$. Having different σ_{xj}^{ref} might result in better approximations as this is equivalent to choosing distinct interpolation points as opposed to choosing the same interpolation point with greater multiplicity.

4.7 Numerical Experiments

In this section we present slowness diagrams to illustrate the accuracy condition developed in the paper. Using arbitrarily chosen values of $c_p = 2, c_s = 1, \varepsilon = \delta = 0.6 \text{ and } \beta = 50^o$ we obtain $\left|\sigma_{xj}^{ref}\right|^2 > 0.3950$ from (4.45) and $\Re e\left(\sigma_{xj}^{ref}\right) \Big/ \Im m\left(\sigma_{xj}^{ref}\right) < 2.287$ from (4.46). Satisfying these two conditions, we choose $\sigma_{xj}^{ref} = 0.576 + 0.252i$, which also satisfies (4.47), thus guaranteeing accuracy in the sense of (4.28) i.e. the PMDL with these parameters will converge to the exact ABC as the number of layers are increased. We consider various σ_{xj}^{ref} that violate at least one of the accuracy criteria e.g. $\sigma_{xj}^{ref} = 0.650 + 0.250i$, $\sigma_{xj}^{ref} = 0.650 + 0.150i$, $\sigma_{xj}^{ref} = 0.250 + 0.250i$, and $\sigma_{xj}^{ref} = 0.250 + 0.150i$. Since we are looking for attaining better accuracy as number of layers increases, we plot the horizontal slownesses for a 200-layer PMDL.

Figure 4.12 contains the exact slowness diagrams with the outgoing branches marked in think lines. An exact ABC should capture all of the outgoing and none of the incoming branches. The details of the slowness diagrams in the vicinity of $\sigma_y = \sigma_{y1}$ $\left(0.405 \le \sigma_y \le 0.425\right)$ and $\sigma_y = \sigma_{y2}$ $\left(0.999 \le \sigma_y \le 1.001\right)$ are also shown. Figure 4.13 contains the PMDL approximation with $\sigma_{xj}^{ref} = 0.576 + 0.252i$ and it can be clearly seen by comparison with Figure 4.12 that the correct branch of both the real and imaginary parts of the slowness diagram are captured. Figure 4.14 and Figure 4.15 contain PMDL approximations with parameters violating at least one of the accuracy criteria specified in the previous section. The resulting inaccuracies are evident on comparison with Figure 4.12.

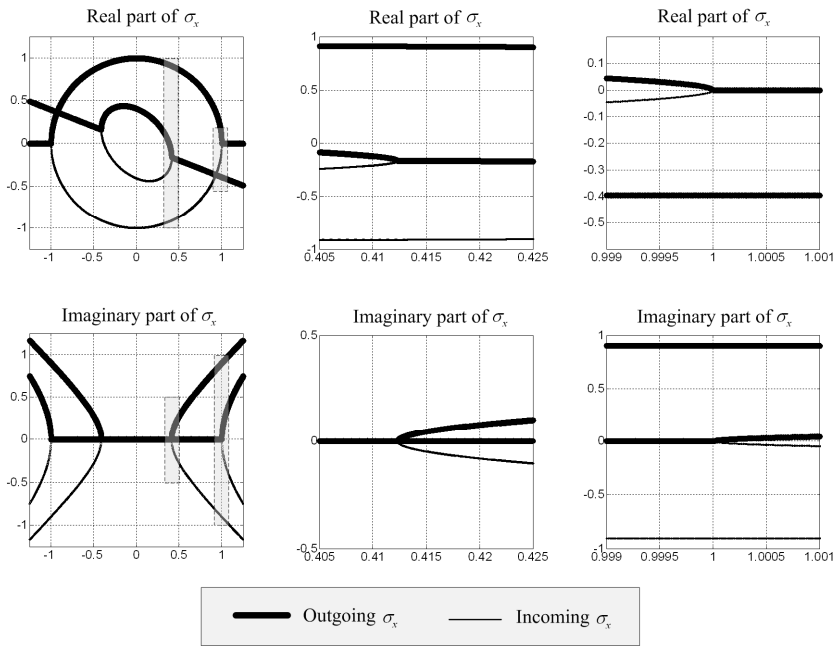

Figure 4.12. Real and Imaginary parts of the horizontal slowness with the outgoing branch in thick lines. An accurate ABC should capture all of the outgoing branch and none of the incoming branch. The first column contains complete slowness diagrams with dotted rectangles being blown up and shown in the second and third columns.

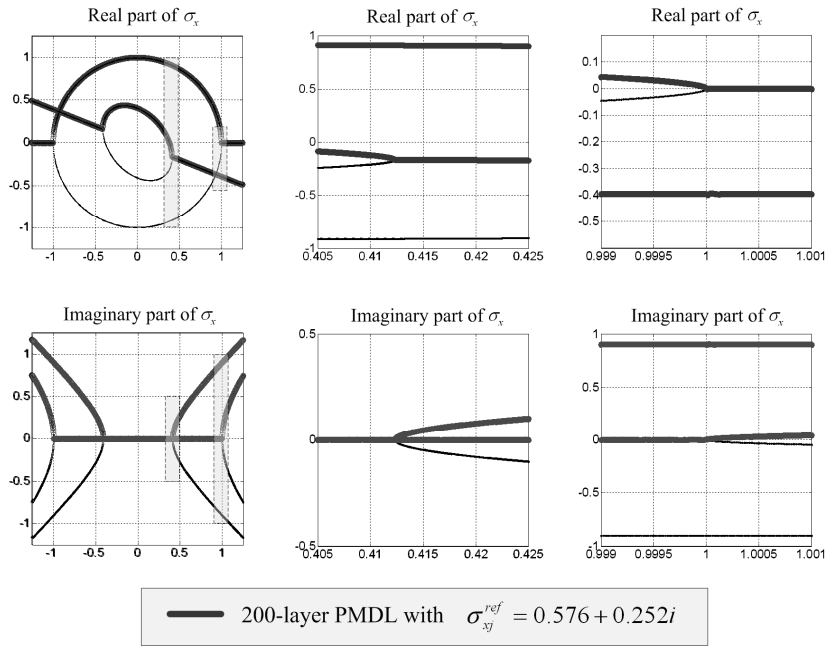

Figure 4.13. Real and Imaginary parts of the horizontal slowness obtained by a 200-layer PMDL (thick lines) with reference wavenumbers $\sigma_{xj}^{ref} = 0.576 + 0.252i$. As in Figure 4.12, the first column contains complete slowness diagrams with dotted rectangles being blown up and shown in the second and third columns.

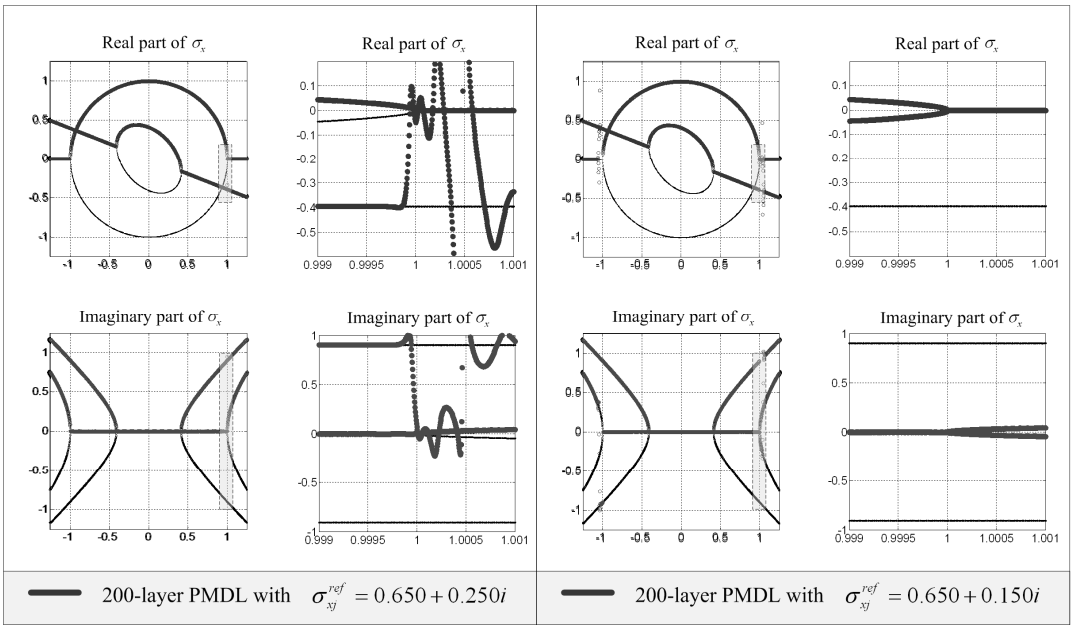

Figure 4.14. Real and Imaginary parts of the horizontal slowness obtained by a 200-layer PMDL (thick lines) with reference wavenumbers $\sigma_{xj}^{ref} = 0.650 + 0.250i$ (left) and $\sigma_{xj}^{ref} = 0.650 + 0.150i$ (right). As in Figure 4.12, the dotted rectangles are blown up and shown in the figures that follow.

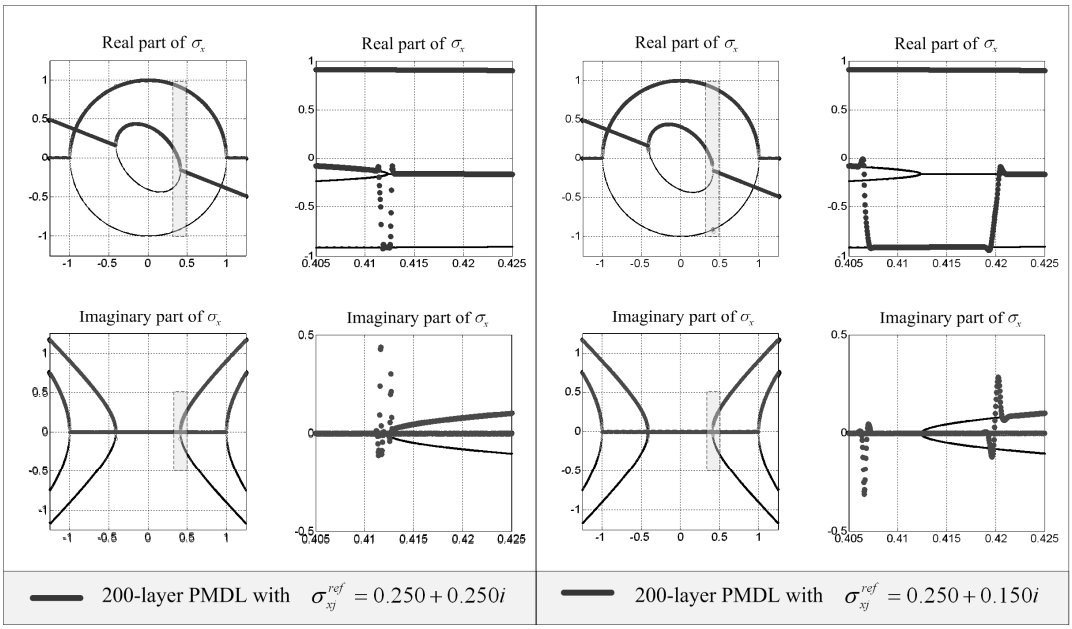

Figure 4.15. Real and Imaginary parts of the horizontal slowness obtained by a 200-layer PMDL (thick lines) with reference wavenumbers $\sigma_{xj}^{ref} = 0.250 + 0.250i$ (left) and $\sigma_{xj}^{ref} = 0.50 + 0.150i$ (right). As in Figure 4.12, the dotted rectangles are blown up and shown in the figures that follow.

4.8 Summary and Conclusions

Sufficient conditions for the accuracy of the PMDL ABC for the time-harmonic modeling of anti-plane and in-plane propagating and evanescent waves in homogeneous elliptic anisotropic elastic media are presented. These conditions turn out to be bounds on the *complex-valued* PMDL parameters (its layer lengths).

By constructing analogies with PML and using the concept of *net* decay, we are able to overcome the challenges posed by the existence of wave modes with differing phase and group velocity signs *without the need of space-time transformations;* the absence of such transformations make the current study more amenable to extensions involving layered media. The ability of PMDL to be viewed as both rational ABC and PML is central to this work; its similarity to the more intuitive PML along with the transparency in its

approximation properties reminiscent of rational ABCs are both essential in facilitating the current understanding.

Since many results on PML instabilities are based on the fact that wavemodes with opposite signs of phase and group velocities lead to amplitude growth (not decay) in the untruncated PML region, and since this work shows that it is possible to ensure *net* decay even in the presence of growth, the main idea presented here, *namely that of utilizing reflections that are inevitable in truncated local ABCs to enforce net decay*, might aid the stability studies of truncated local ABCs in general.

4.9 References

[1] Givoli D. Nonreflecting Boundary-Conditions. J.Comput.Phys. 1991 MAY;94(1):1-29.

[2] Tsynkov SV. Numerical solution of problems on unbounded domains. A review. Appl.Numer.Math. 1998 AUG;27(4):465-532.

[3] Hagstrom T. New results on absorbing layers and radiation boundary conditions. Topics in Computational Wave Propagation - Direct and Inverse Problems 2003;31:1-42.

[4] Lindman EL. Free-Space Boundary-Conditions for Time-Dependent Wave-Equation. J.Comput.Phys. 1975;18(1):66-78.

[5] Engquist B, Majda A. Absorbing Boundary-Conditions for Numerical-Simulation of Waves. Math.Comput. 1977;31(139):629-51.

[6] Higdon RL. Absorbing Boundary-Conditions for Difference Approximations to the Multidimensional Wave-Equation. Math.Comput. 1986 OCT;47(176):437-59.

[7] Higdon RL. Numerical Absorbing Boundary-Conditions for the Wave-Equation. Math.Comput. 1987 JUL;49(179):65-90.

[8] Givoli D. High-order local non-reflecting boundary conditions: a review. Wave Motion 2004;39(4):319-26.

[9] Givoli D, Neta B. High-order non-reflecting boundary scheme for time-dependent waves. J.Comput.Phys. 2003 MAR 20;186(1):24-46.

[10] Hagstrom T, Warburton T. A new auxiliary variable formulation of high-order local radiation boundary conditions: corner compatibility conditions and extensions to first-order systems. Wave Motion 2004 APR;39(4):327-38.

[11] Keng Wit Lim. Absorbing Boundary Conditions For Corner Regions. Raleigh: North Carolina State University; 2003.

[12] Guddati MN. Arbitrarily wide-angle wave equations for complex media. Comput.Methods Appl.Mech.Eng. 2006;195(1-3):65-93.

[13] Berenger JP. A Perfectly Matched Layer for the Absorption of Electromagnetic-Waves. J.Comput.Phys. 1994 OCT;114(2):185-200.

[14] Chew WC, Weedon WH. A 3d Perfectly Matched Medium from Modified Maxwells Equations with Stretched Coordinates. Microwave Opt Technol Lett 1994 SEP;7(13):599-604.

[15] Chew WC, Jin JM, Michielssen E. Complex coordinate stretching as a generalized absorbing boundary condition. Microwave Opt Technol Lett 1997 AUG 20;15(6):363-9.

[16] Sacks ZS, Kingsland DM, Lee R, Lee JF. A perfectly matched anisotropic absorber for use as an absorbing boundary condition. IEEE Trans.Antennas Propag. 1995 DEC;43(12):1460-3.

[17] Teixeira FL, Chew WC. Analytical derivation of a conformal perfectly matched absorber for electromagnetic waves. Microwave Opt Technol Lett 1998;17(4):231-6.

[18] Kuzuoglu , Mittra . Frequency dependence of the constitutive parameters of causal perfectly matched anisotropic absorbers. IEEE Microwave Guided Wave Lett. 1996;6(12):447.

[19] Roden , Gedney . Convolution PML (CPML): An efficient FDTD implementation of the CFS-PML for arbitrary media. Microwave Opt Technol Lett 2000;27(5):334.

[20] Meza-Fajardo , Papageorgiou . A nonconvolutional, split-field, perfectly matched layer for wave propagation in isotropic and anisotropic elastic media: Stability analysis. Bulletin of the Seismological Society of America 2008;98(4):1811.

[21] Tam CKW, Auriault L, Cambuli F. Perfectly matched layer as an absorbing boundary condition for the linearized Euler equations in open and ducted domains. Journal of Computational Physics 1998;144(1):213-34.

[22] Turkel E, Yefet A. Absorbing PML boundary layers for wave-like equations. Applied Numerical Mathematics 1998;27(4):533-57.

[23] Abarbanel S, Gottlieb D, Hesthaven JS. Well-posed perfectly matched layers for advective acoustics. J.Comput.Phys. 1999 SEP 20;154(2):266-83.

[24] Hu FQ. A stable, perfectly matched layer for linearized Euler equations in unsplit physical variables. J.Comput.Phys. 2001 NOV 1;173(2):455-80.

[25] Hagstrom T. A new construction of perfectly matched layers for hyperbolic systems with applications to the linearized Euler equations. 2003;:125.

[26] Becache E, Fauqueux S, Joly P. Stability of perfectly matched layers, group velocities and anisotropic waves. J.Comput.Phys. 2003 JUL 1;188(2):399-433.

[27] Becache E, Bonnet-Ben Dhia AS, Legendre G. Perfectly matched layers for the convected Helmholtz equation. SIAM J.Numer.Anal. 2004;42(1):409-33.

[28] Hu FQ. A Perfectly Matched Layer absorbing boundary condition for linearized Euler equations with a non-uniform mean flow. J.Comput.Phys. 2005 SEP 20;208(2):469-92.

[29] Becache E, Dhia ASBB, Legendre G. Perfectly matched layers for time-harmonic acoustics in the presence of a uniform flow. Siam Journal on Numerical Analysis 2006;44(3):1191-217.

[30] Diaz J, Joly P. A time domain analysis of PML models in acoustics. Comput.Methods Appl.Mech.Eng. 2006;195(29-32):3820-53.

[31] Parrish S, Hu F. PML absorbing boundary conditions for the linearized and nonlinear Euler equations in the case of oblique mean flow. Int.J.Numer.Methods Fluids 2009;60(5):565.

[32] Becache E, Givoli D, Hagstrom T. High-order Absorbing Boundary Conditions for anisotropic and convective wave equations. Journal of Computational Physics 2010;229(4):1099.

[33] Operto S, Virieux J, Ribodetti A, Anderson J. Finite-difference frequency-domain modeling of viscoacoustic wave propagation in 2D tilted transversely isotropic (TTI) media. Geophysics 2009;74(5):T75-T95.

[34] Skelton EA, Adams SDM, Craster RV. Guided elastic waves and perfectly matched layers. Wave Motion 2007 AUG;44(7-8):573-92.

[35] Appelo D, Kreiss G. A new absorbing layer for elastic waves. Journal of Computational Physics 2006;215(2):642-60.

[36] Hu FQ. Development of PML absorbing boundary conditions for computational aeroacoustics: A progress review. Comput.Fluids 2008 MAY;37(4):336-48.

[37] Appelo D, Hagstrom T, Kreiss G. Perfectly matched layers for hyperbolic systems: General formulation, well-posedness, and stability. SIAM J Appl Math 2006;67(1):1-23.

[38] Appeloe D, Colonius T. A high-order super-grid-scale absorbing layer and its application to linear hyperbolic systems. J.Comput.Phys. 2009 JUN 20;228(11):4200-17.

[39] Lisitsa V, Lys E. Reflection less truncation of target area for axially symmetric anisotropic elasticity. J.Comput.Appl.Math. 2010;234(6):1803-9.

[40] Sofronov IL, Zaitsev NA. Transparent boundary conditions for the elastic waves in anisotropic media. Hyperbolic Problems: Theory, Numerics, Applications 2008:997-1004.

[41] Guddati MN, Lim KW. Continued fraction absorbing boundary conditions for convex polygonal domains. Int J Numer Methods Eng 2006;66(6):949-77.

[42] Guddati MN, Lim KW, Zahid MA. Perfectly Matched Discrete layers for Unbounded Domain Modeling. In: Magoulès F, editor. Computational Methods for Acoustics ProblemU.K.: Saxe-Coburg Publications; 2008, p. 69-98.

[43] Asvadurov S, Druskin V, Guddati MN, Knizhnerman L. On optimal finite-difference approximation of PML. Siam Journal on Numerical Analysis 2003;41(1):287-305.

[44] Savadatti S, Guddati MN. Absorbing boundary conditions for scalar waves in anisotropic media. Part 1: Time harmonic modeling. Journal of Computational Physics 2010;229(19):6696-714.

[45] Savadatti S, Guddati MN. Absorbing boundary conditions for scalar waves in anisotropic media. Part 2: Time-dependent modeling. Journal of Computational Physics 2010;229(18):6644-62.

[46] Thomsen L. Weak Elastic-Anisotropy. Geophysics 1986;51(10):1954-66.

[47] Collino F, Monk PB. Optimizing the perfectly matched layer. Comput.Methods Appl.Mech.Eng. 1998;164(1-2):157-71.

[48] Hagstrom T, Warburton T. Complete radiation boundary conditions: minimizing the long time error growth of local methods. 2008;.

Chapter 5 Accurate Absorbing Boundary Condition for Untilted Non-Elliptic Anisotropic Elasticity

This chapter is intended to be submitted for publication as a self-sufficient manuscript.

5.1 Abstract

With the ultimate goal of devising effective absorbing boundary conditions (ABCs) for general elastic media, we investigate the accuracy aspects of local ABCs designed for untilted non-elliptic anisotropy in the frequency domain (time-harmonic case). While simple space-time transformations are available to treat the wavemodes with opposing phase and group velocities present in elliptic anisotropic media, no such transformations are known to exist for the case of non-elliptic anisotropy. In this paper, we use the concept of layer groupings along with an unconventional stretching of the finite element mesh to guarantee the accuracy of a local ABC designed to treat all propagating wavemodes, even those with opposing phase and group velocities. The local ABC used here is the perfectly matched discrete layer (PMDL) which is a simple variant of perfectly matched layers (PML) that is also equivalent to rational approximation-based local ABCs (rational ABCs); it inherits the straightforward approximation properties of rational ABCs along with the versatility of PML. The approximation properties of PMDL quantified through its reflection matrix allow us to (a) show that it is impossible to design an accurate PMDL with wavenumber-independent parameters, (b) demonstrate theoretically, the ability of wavenumber-dependent parameters to ensure accuracy, and finally (c) design a practical though unconventional stretching of the finite element PMDL mesh that facilitates the implementation of wavenumber-dependent parameters. The validity of this work is demonstrated through a series of numerical experiments.

5.2 Introduction

Absorbing boundary conditions (ABCs) have long been used to include the effect of ‘exterior’ unbounded domains on computational models of finite ‘interiors’ at the

‘computational boundary’ (boundary between exterior and interior). Time-harmonic modeling of such domains requires the ABCs to *accurately* represent the unbounded exterior i.e. the ABC should absorb *all* outgoing waves while allowing *none* of the incoming waves at the computational boundary.

ABCs can be categorized into exact and approximate ABCs; unlike exact ABCs, approximate ABCs are more readily available for complex anisotropic and/or heterogeneous media. Approximate ABCs can be divided into global and local ABCs; global ABCs are prohibitively expensive for large scale simulations and hence the more efficient though less accurate local ABCs are preferred. The most popular local ABCs currently available are rational approximation based ABCs (rational ABCs) and perfectly matched layers (PMLs). Earlier formulations of rational ABCs and PML can be found in [1-10] with later extensions and advancements being presented in [11-21].

Though based on disparate ideas, rational ABCs and PML are now known to share underlying links that have made it possible to view certain rational ABCs as modified versions of PML [22]. One such local ABC is the perfectly matched *discrete* layer (PMDL) that inherits the versatility of PML along with the more transparent approximation characteristics of rational ABCs [23]. Since PMDL can be viewed as either rational ABCs or as PML, we have the luxury of choosing the viewpoint that best facilitates the study at hand. While some studies on the accuracy and well-posedness of PMDL for anisotropic acoustics are based primarily on the rational ABC viewpoint [24,25], other studies like those in Chapter 4 on the accuracy of PMDL for elliptic anisotropic elasticity have been based primarily on the PML viewpoint. In this work we look at PMDL through both viewpoints with due reference to its characteristics borrowed from each kind.

The PML works primarily on the concept of mimicking the exterior wave absorption characteristics by enforcing wave amplitude decay. Its superiority over other absorbing media can be attributed to its ‘perfect matching’ property that allows (in theory) a reflectionless transmission of waves across the computational boundary. The rate and sign of decay depends on the phase velocity of the outgoing wavemodes (those leaving the interior)

with certain phase velocities (say positive) leading to decay and consequently other phase velocities (like negative) leading to growth. Hence PML acts as an absorber as long as the outgoing wavemodes have positive phase velocities. Since wavemodes are categorized into outgoing and incoming wavemodes based on the sign of their group velocity (say positive and negative respectively), PML acts as an absorber as long as the phase $\left(c_{px}\right)$ and group $\left(c_{gx}\right)$ velocity signs match i.e. as long as $c_{px}c_{gx} \geq 0$. However, there exist many anisotropic and/or heterogeneous media that support wavemodes with $c_{px}c_{gx} < 0$. For such media, PML results in amplitude growth (not decay) and such growth ends up mimicking energy input instead of energy absorption. Rational ABCs are also known to demonstrate such behavior in the epresence of $c_{px}c_{gx} < 0$.

Space-time transformations that result in a transformed space with $c_{px}c_{gx} \geq 0$ are the most frequently used method for tackling issues related to $c_{px}c_{gx} < 0$ [26-29]. While easy to understand, space –time transformations have two major drawbacks: their extension to heterogeneous (layered) media is unclear and their applicability is restricted to *elliptic* anisotropy (Figure 5.1). Part 1 of this paper (Chapter 4) dealt with the first drawback by providing a solution for *elliptic* anisotropic elasticity *without* the use of space-time transformations thus making the solution more amenable to extensions involving heterogeneous (layered) media. In this part, we address the second drawback of limited applicability (to only *elliptic* anisotropy) by presenting an unconventional mesh stretching idea that ensures the accurate absorption of propagating wavemodes in *non-elliptic* anisotropic media.

The purpose of this paper is limited to providing a local ABC that accurately treats the propagating wavemodes of untilted non-elliptic anisotropic elasticity in the frequency domain. However, accuracy in the frequency domain is intricately linked to accuracy, wellposedness and stability in the time domain e.g. local ABCs that allow incoming propagating modes are known to be ill-posed or unstable in the time domain and the same

ABCs end up being inaccurate in the frequency domain because incoming modes are equivalent to spurious reflections at the computational boundary. Though inaccuracies and instabilities tied to the existence of modes with $c_{px}c_{gx} < 0$ have been studied extensively [14,19,27-40], we wish to assert that there exists no solution – to the best of our knowledge– that rigorously ensures accurate absorption of wavemodes with $c_{px}c_{gx} < 0$ present in *non-elliptic* anisotropic elasticity, both untilted and tilted. This paper provides an accurate ABC for the untilted case (see Figure 5.3). It should be pointed out that there do exist ways of ensuring stability for non-elliptic anisotropy e.g. [14,15,40-43]. However, these studies do not seem to tackle directly, the issue of $c_{px}c_{gx} < 0$ and their precise effect on the inaccuracies and instabilities created by wavemodes with $c_{px}c_{gx} < 0$ is not clear.

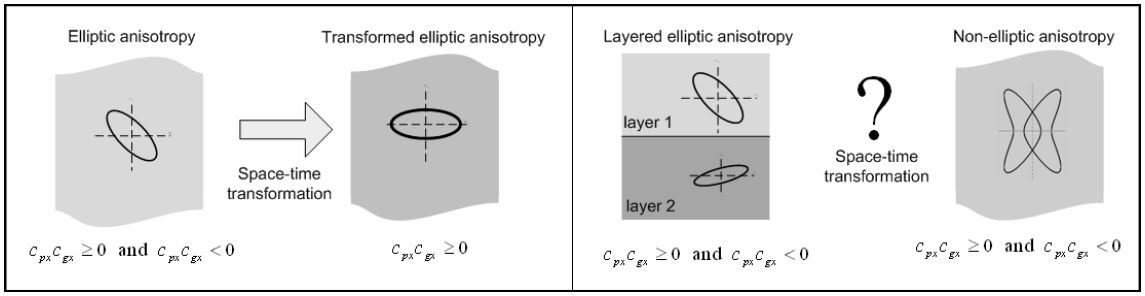

Figure 5.1. *Left:* Space-time transformations are only available for elliptic anisotropies in homogeneous media. *Right*: No such transformations exist for heterogeneous (layered) and non-elliptic anisotropic media

We design an accurate local ABC for untilted non-elliptic anisotropic elasticity based on PMDL. Using the reflection matrix, we first specify a sequence of successively weak sufficient conditions by utilizing the concept of layer groupings. We next show the impossibility of traditional PMDL with wavenumber-independent parameters to meet any of these sufficient conditions. This is followed by a proof that reveals the accuracy of a PMDL with wavenumber-dependent parameters. We finally present an unconventional stretching of

the finite element PMDL mesh that facilitates the implementation of these wavenumber-dependent parameters.

This paper borrows heavily from Part 1 (Chapter 4) and familiarity with the basic notation is assumed (even though some of the equations are repeated for clarity). Also, this paper is only concerned with the accuracy issues of propagating wavemodes in the frequency domain analysis of the continuous problem with a straight computational boundary. As such, interior discretization errors, corners, curved computational boundaries, and inaccuracies due to the neglect of evanescent wavemodes are outside the scope of this paper. It should be noted that the above restrictions are imposed to make the problem more tractable; they are, with the exception of curved boundaries, not due to any limitations of the PMDL formulation. PMDLs capable of absorbing both propagating and evanescent waves have already been implemented on domains with convex polygonal corners in [44]. As such, this paper can be considered as a necessary step towards a complete PMDL implementation for anisotropic elastic media. Analogous studies for time-harmonic *and* transient modeling of anti-plane shear waves can be found in [24,25].

The outline of the rest of the paper is as follows. Section 5.3 contains preliminaries mostly summarized from Chapter 4. In Section 5.4 we present the criterion for accuracy along with a sequence of sufficient conditions followed by two necessary conditions based on the concept of layer groupings. Section 5.5 proves that it is impossible to design an accurate PMDL for propagating wavemodes with wavenumber-independent parameters. It also contains the derivation of wavenumber-dependent PMDL parameters that ensure the accurate treatment of propagating modes, followed by an unconventional stretching of the PMDL mesh that facilitates implementation. Various numerical experiments are presented in Section 5.6 and finally, Section 5.7 contains a summary and conclusions. References are presented in Section 5.9.

5.3 Preliminaries

This section borrows heavily from the corresponding section of Part 1 (Chapter 4).

5.3.1 Model Problem and Anisotropic Elasticity

The model problem consists of replacing an exact full-space by a left half-space (interior) along with an ABC that simulates the effect of the right half-space (exterior) at the computational boundary $\left(x=0\right)$ as shown in Figure 5.2. The time-harmonic vector wave equation representing in-plane wave motions in homogeneous anisotropic elastic media is,

$$\left(\mathbf{G}_{xx}\frac{\partial^2}{\partial x^2}+\left(\mathbf{G}_{xy}+\mathbf{G}_{xy}^T\right)\frac{\partial^2}{\partial x\partial y}+\mathbf{G}_{yy}\frac{\partial^2}{\partial y^2}+\omega^2\mathbf{I}\right)\mathbf{u}=\mathbf{0}\,, \tag{5.1}$$

where $\omega\in\mathbb{R}$ is the temporal frequency, $\mathbf{u}=\left\{u_x\ \ u_y\right\}^T$ is the infinitesimal in-plane displacement vector and $\mathbf{G}_{xx},\mathbf{G}_{yy},\mathbf{G}_{xy}$ are the in-plane matrix coefficients given by,

$$E_{22}=c_p^2,\ E_{33}=c_s^2,\ E_{11}=\left(1+2\varepsilon\right)E_{22},$$

$$E_{12}=\sqrt{\left(\left(1+2\delta\right)E_{22}-E_{33}\right)\left(E_{22}-E_{33}\right)}-E_{33},$$

$$\tilde{\mathbf{G}}_{xx}=\begin{bmatrix}E_{11}&0\\0&E_{33}\end{bmatrix},\ \tilde{\mathbf{G}}_{yy}=\begin{bmatrix}E_{33}&0\\0&E_{22}\end{bmatrix},\ \tilde{\mathbf{G}}_{xy}=\begin{bmatrix}0&E_{12}\\E_{33}&0\end{bmatrix}, \tag{5.2}$$

$$\begin{aligned}\mathbf{G}_{xx}&=\tilde{\mathbf{G}}_{xx}\cos^2\beta+\tilde{\mathbf{G}}_{yy}\sin^2\beta+\left(\tilde{\mathbf{G}}_{xy}+\tilde{\mathbf{G}}_{xy}^T\right)\sin\beta\cos\beta,\\ \mathbf{G}_{yy}&=\tilde{\mathbf{G}}_{xx}\sin^2\beta+\tilde{\mathbf{G}}_{yy}\cos^2\beta-\left(\tilde{\mathbf{G}}_{xy}+\tilde{\mathbf{G}}_{xy}^T\right)\sin\beta\cos\beta,\\ \mathbf{G}_{xy}&=-\left(\tilde{\mathbf{G}}_{xx}-\tilde{\mathbf{G}}_{yy}\right)\sin\beta\cos\beta+\tilde{\mathbf{G}}_{xy}\cos^2\beta-\tilde{\mathbf{G}}_{xy}^T\sin^2\beta.\end{aligned}$$

In (5.2), c_p is the pressure wave velocity, c_s is the shear wave velocity, and ε, δ are the parameters of anisotropy [17,45]. As shown in Figure 5.2, the angle β represents the tilt of the principal material axis $\left(x_M-y_M\right)$ with respect to the coordinate axis $\left(x-y\right)$. Also, it is assumed that $c_P\geq c_s$ and the material density is unity. For the sake of presentation, we Fourier transform (5.1) in y to obtain the reduced equation with the duality $\partial/\partial y\leftrightarrow ik_y$,

$$\left(\mathbf{G}_{xx}\frac{\partial^2}{\partial x^2}+ik_y\left(\mathbf{G}_{xy}+\mathbf{G}_{xy}^T\right)\frac{\partial}{\partial x}-\left(k_y^2\mathbf{G}_{yy}-\omega^2\mathbf{I}\right)\right)\mathbf{u}=\mathbf{0}\,. \tag{5.3}$$

Equation (5.3) admits individual *normalized* ($\|\cdot\|=1$) modes of the kind $\mathbf{a}e^{ik_x x}$ which, in the general case are defined by their wavenumber-wavemode pair $(k_x,\mathbf{a})$ *for a given* $\left(k_y,\omega\right)\in\mathbb{R}^2$. The dispersion relation is given by $\det\left(\mathbf{\Lambda}^{in}\right)=0$ where,

$$\mathbf{\Lambda}^{in}\equiv\left(k_x^2\mathbf{G}_{xx}+k_xk_y\left(\mathbf{G}_{xy}+\mathbf{G}_{xy}^T\right)+k_y^2\mathbf{G}_{yy}-\omega^2\mathbf{I}\right). \tag{5.4}$$

Plots of $\det\left(\mathbf{\Lambda}^{in}\right)=0$ are viewed through slowness diagrams (plots of $\sigma_x=k_x\big/\omega$ vs. $\sigma_y=k_y\big/\omega$) with the cases of tilted elliptic anisotropy $\left(\beta\neq0,\varepsilon=\delta\right)$, untilted non-elliptic anisotropy $\left(\beta=0,\varepsilon\neq\delta\right)$ and tilted non-elliptic anisotropy $\left(\beta\neq0,\varepsilon\neq\delta\right)$ all exhibiting modes with $c_{px}c_{gx}<0$ as shown in Figure 5.3. Note that in Figure 5.3, the part of the slowness diagram in the upper half plane $\left(\sigma_x>0\right)$ represents wavemodes with positive phase velocities and the part of the slowness diagrams marked with a thick line have positive group velocities. We concentrate in this paper on untilted non-elliptic anisotropy $\left(\beta=0,\varepsilon\neq\delta\right)$.

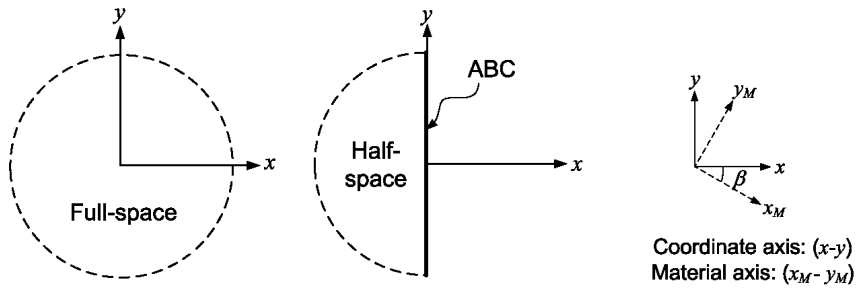

Figure 5.2. *Left:* The model problem consists of replacing a full space of untilted non-elliptic anisotropic elastic media by a left half-space and an efficient ABC that accurately mimics the behavior of the right half-space. *Right:* Global coordinate and material axes.

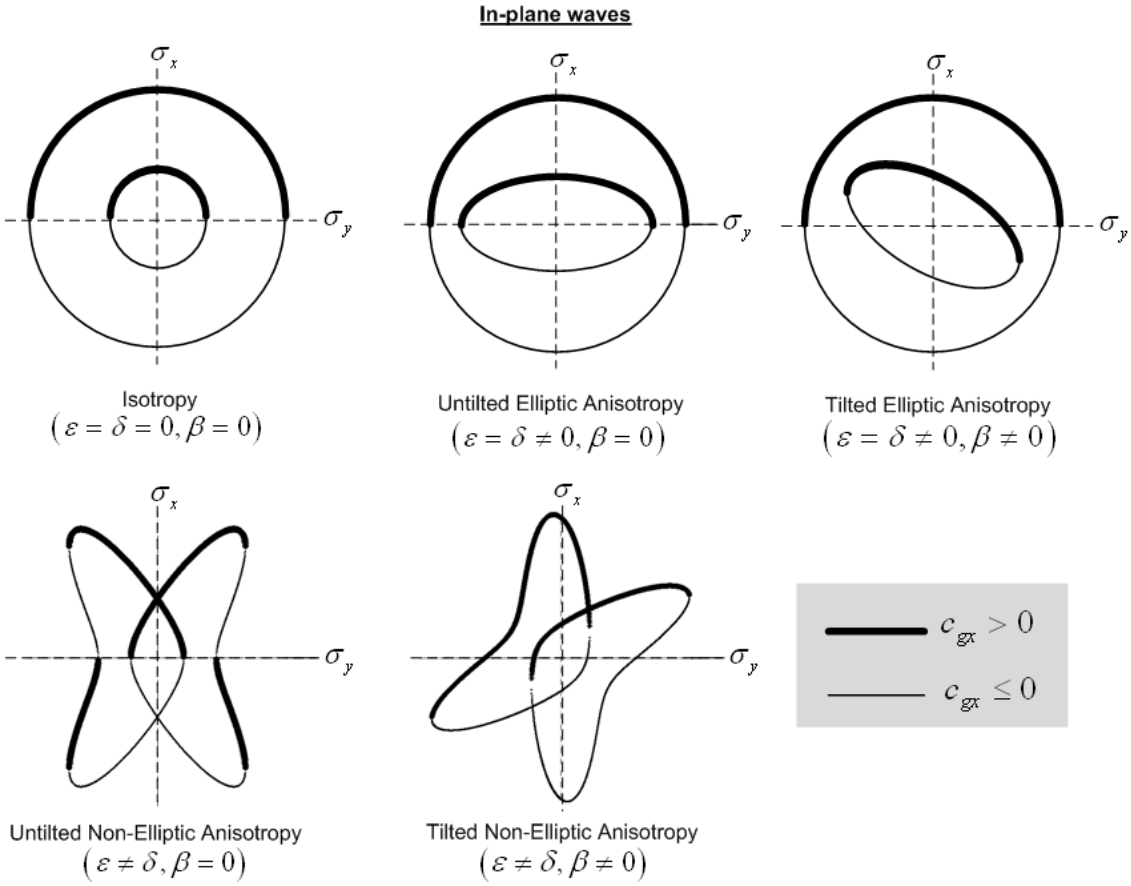

Figure 5.3. Slowness diagrams for in-plane propagating $\left(\sigma_x \in \mathbb{R}\right)$ wavemodes in elasticity. This paper concentrates on accuracy aspects of untilted non-elliptic anisotropy.

Propagating $\left(k_x \in \mathbb{R}\right)$ and evanescent wavemodes $\left(k_x \notin \mathbb{R}\right)$ can be characterized into outgoing or incoming wavemodes as follows:

$$\left.\begin{array}{lll} \text{forward propagating} & : & \mathfrak{Im}(k_x) = 0 \ \text{ and } \ c_{gx} = \dfrac{\partial \omega}{\partial k_x} > 0, \\ \text{forward decaying} & : & \mathfrak{Im}(k_x) > 0, \end{array}\right\} \begin{array}{l} \text{outgoing} \\ \text{modes} \end{array}, \tag{5.5}$$

$$\left.\begin{array}{lll} \text{backward propagating} : & \mathfrak{Im}(k_x) = 0 \ \text{ and } \ c_{gx} = \dfrac{\partial \omega}{\partial k_x} \leq 0, \\ \text{backward decaying} & : & \mathfrak{Im}(k_x) < 0. \end{array}\right\} \begin{array}{l} \text{incoming} \\ \text{modes} \end{array}, \tag{5.6}$$

where $\Im m(\cdot)$ denotes the imaginary part (for later reference, $\Re e(\cdot)$ denotes the real part).

The traction at the computational boundary $(x = 0)$ is given by,

$$\mathbf{T}_x^{in}\Big|_{x=0} = -\left(\mathbf{G}_{xx}\frac{\partial}{\partial x} + ik_y\mathbf{G}_{xy}\right)\mathbf{u}\Big|_{x=0}. \tag{5.7}$$

5.3.2 Reflection Matrix

In the absence of sources in $x > 0$, an unbounded domain defined by $x \geq 0$ admits wavesmodes of the form $\mathbf{u} = \mathbf{a}e^{ik_x x}$ where the wavenumber, wavemode pair $(k_x, \mathbf{a})$ is an eigenpair of the quadratic eigenvalue problem $\mathbf{\Lambda}^{in}\mathbf{a} = \mathbf{0}$ with k_x satisfying (5.5) i.e. it admits only outgoing modes. A finite layer obtained by truncating the unbounded domain at $x = L > 0$ admits both outgoing and incoming wavemodes. In the absence of sources in $0 < x \leq L$, the incoming modes can be seen as reflections of the outgoing modes generated at the truncation boundary condition. The total wavefield in this case can be written as (see Chapter 4),

$$\mathbf{u} = \left(\mathbf{X}\mathbf{P}(x) + \tilde{\mathbf{X}}\tilde{\mathbf{P}}(x-L)\mathbf{R}_T\mathbf{P}(L)\right)\Gamma, \tag{5.8}$$

where $\mathbf{X}$ denotes the matrix of all *outgoing* normalized eigenvectors, $\tilde{\mathbf{X}}$ denotes the matrix of all *incoming* normalized eigenvectors and normalization implies

$\left\|\mathbf{X}(\cdot,j)\right\|=1,\left\|\tilde{\mathbf{X}}(\cdot,j)\right\|=1,\ \forall j\in\left(1,2\right)$. $\mathbf{P}(x)=diag\left(e^{ik_{x1}x},e^{ik_{x2}x}\right)$ and $\tilde{\mathbf{P}}(x)=diag\left(e^{i\widetilde{k_{x1}}x},e^{i\widetilde{k_{x2}}x}\right)$ are the propagator matrices with k_{x1},k_{x2} satisfying (5.5) and $\widetilde{k_{x1}},\widetilde{k_{x2}}$ satisfying (5.6). $\mathbf{R}_T$ here represents the truncation reflection matrix. Any purely outgoing wave can be expressed as $\mathbf{XP}(x)\Gamma$ while any purely incoming wave can be expressed as $\tilde{\mathbf{X}}\tilde{\mathbf{P}}(x)\tilde{\Gamma}$, with $\Gamma,\tilde{\Gamma}$ being the vectors of participation factors. Defining the computational reflection matrix as,

$$\mathbf{R}_C=\tilde{\mathbf{P}}(-L)\mathbf{R}_T\mathbf{P}(L), \tag{5.9}$$

we can write $\mathbf{u}\Big|_{x=0}=\left(\mathbf{X}+\tilde{\mathbf{X}}\mathbf{R}_C\right)\Gamma$ with (5.9) being a measure of the reflections due to truncation.

5.3.3 PMDL Properties

The PMDL formulation approximates the exterior right half-space stiffness with $n\ (<\infty)$ mid-point integrated linear finite element layers of lengths $L_1,\ldots,L_n$ followed by a homogeneous Dirichlet truncation boundary condition (see [17]). For the model problem in Figure 5.2, the traction at the computational boundary of the exterior right half space is given by (5.7) and hence the (exact) stiffness of the right half space becomes

$$\mathbf{K}_{exact}=-\left(ik_x\mathbf{G}_{xx}+ik_y\mathbf{G}_{xy}\right). \tag{5.10}$$

k_x in (5.10) satisfies (5.5) because a right half-space can only support outgoing modes. The *n*-layer PMDL approximates (5.10) by $\mathbf{K}_n$, the stiffness of a n-layer mid-point integrated linear finite element mesh with a homogeneous Dirichlet truncation boundary. The rationale behind this approximation can be found in Part 1 of this paper (Chapter 4). The stiffness of a mid-point integrated linear finite element with length L_j is denoted by $\mathbf{S}_\mathbf{j}$ and given by (see [17]**)**,

$$\mathbf{S}_j = \begin{bmatrix} \mathbf{S}_j^{11} & \mathbf{S}_j^{12} \\ \mathbf{S}_j^{21} & \mathbf{S}_j^{22} \end{bmatrix} = \frac{1}{L_j}\begin{bmatrix} \mathbf{G}_{xx} & -\mathbf{G}_{xx} \\ -\mathbf{G}_{xx} & \mathbf{G}_{xx} \end{bmatrix} + \frac{ik_y}{2}\begin{bmatrix} -\mathbf{G}_{xy} & -\mathbf{G}_{xy} \\ \mathbf{G}_{xy} & \mathbf{G}_{xy} \end{bmatrix} - \frac{ik_y}{2}\begin{bmatrix} -\mathbf{G}_{xy}^T & \mathbf{G}_{xy}^T \\ -\mathbf{G}_{xy}^T & \mathbf{G}_{xy}^T \end{bmatrix} - \frac{L_j}{4}\begin{bmatrix} \omega^2\mathbf{I} - k_y^2\mathbf{G}_{yy} & \omega^2\mathbf{I} - k_y^2\mathbf{G}_{yy} \\ \omega^2\mathbf{I} - k_y^2\mathbf{G}_{yy} & \omega^2\mathbf{I} - k_y^2\mathbf{G}_{yy} \end{bmatrix}. \tag{5.11}$$

If we use $\tilde{\mathbf{u}}_1, \ldots \tilde{\mathbf{u}}_{n-1}, \tilde{\mathbf{u}}_n$ to denote the values of the field variable at the right edge of each layer, the Dirichlet condition becomes $\tilde{\mathbf{u}}_n = \mathbf{0}$ and the assembled *n*-layer PMDL model takes the form,

$$\begin{Bmatrix} \mathbf{T}_{x=0}^{n-pmdl} \\ \mathbf{0} \\ \mathbf{0} \\ \vdots \\ \mathbf{0} \\ \mathbf{0} \end{Bmatrix} = \begin{bmatrix} \mathbf{S}_1^{11} & \mathbf{S}_1^{12} & & & & & \\ \mathbf{S}_1^{21} & \mathbf{S}_1^{22} + \mathbf{S}_2^{11} & \mathbf{S}_2^{12} & & & & \\ & \mathbf{S}_2^{21} & \mathbf{S}_2^{22} + \mathbf{S}_3^{11} & \mathbf{S}_3^{12} & & & \\ & & \ddots & \ddots & \ddots & & \\ & & & \mathbf{S}_{n-2}^{21} & \mathbf{S}_{n-2}^{22} + \mathbf{S}_{n-1}^{11} & \mathbf{S}_{n-1}^{12} & \\ & & & & \mathbf{S}_{n-1}^{21} & \mathbf{S}_{n-1}^{22} + \mathbf{S}_n^{11} & \end{bmatrix} \begin{Bmatrix} \tilde{\mathbf{u}}_{x=0} \\ \tilde{\mathbf{u}}_1 \\ \tilde{\mathbf{u}}_2 \\ \vdots \\ \tilde{\mathbf{u}}_{n-2} \\ \tilde{\mathbf{u}}_{n-1} \end{Bmatrix}, \tag{5.12}$$

where $\tilde{\mathbf{u}}_{x=0}, \mathbf{T}_{x=0}^{n-pmdl}$ are respectively the displacement vector and traction at the computational boundary (i.e. at the leftmost edge of the n-layer PMDL model). We can determine the computational reflection matrix (5.9) by noting that the decay (or growth) in amplitude achieved as the wavemode progresses from left to the right of each layer is $\left(1 + ik_x L_j / 2\right) \Big/ \left(1 - ik_x L_j / 2\right)$ and that achieved as the mode progresses from right to the left of each layer is $\left(1 - i\widetilde{k}_x L_j / 2\right) \Big/ \left(1 + i\widetilde{k}_x L_j / 2\right)$ where k_x is the outgoing wavenumber (5.5) and $\widetilde{k}_x$ is the incoming (reflected) wavenumber (5.6) (see [44]**)**. This leads us to the expressions,

$$\mathbf{P} = \begin{bmatrix} \prod_{j=1}^{n}\left(\dfrac{2i/L_j - k_{x1}}{2i/L_j + k_{x1}}\right) & 0 \\ 0 & \prod_{j=1}^{n}\left(\dfrac{2i/L_j - k_{x2}}{2i/L_j + k_{x2}}\right) \end{bmatrix},$$

$$\tilde{\mathbf{P}} = \begin{bmatrix} \prod_{j=1}^{n}\left(\dfrac{2i/L_j + \widetilde{k_{x1}}}{2i/L_j - \widetilde{k_{x1}}}\right) & 0 \\ 0 & \prod_{j=1}^{n}\left(\dfrac{2i/L_j + \widetilde{k_{x2}}}{2i/L_j - \widetilde{k_{x2}}}\right) \end{bmatrix}. \qquad (5.13)$$

In (5.13), $k_{x1}\left(\widetilde{k_{x1}}\right)$ and $k_{x2}\left(\widetilde{k_{x2}}\right)$ are the outgoing (incoming) horizontal wavenumbers (see Figure 5.4b). In cases where the distinction of pressure and shear waves can be clearly made, like in elliptic anisotropy, we can assume $k_{x1}\left(\widetilde{k_{x1}}\right)$ and $k_{x2}\left(\widetilde{k_{x2}}\right)$ to refer to pressure and shear wavemodes respectively. The expressions in (5.13) along with (5.9) give us the computational reflection matrix $\mathbf{R}_C$. Of the three matrices $\mathbf{P}, \tilde{\mathbf{P}}, \mathbf{R}_T$, the matrices $\mathbf{P}, \tilde{\mathbf{P}}$ depend on the PMDL parameters (the layer lengths) while $\mathbf{R}_T$ depends on the truncation boundary at the end of PMDL. Each element $\mathbf{R}_C\left(\xi,\eta\right)$ takes the form, from (5.13) and (5.9):

$$\begin{aligned} \mathbf{R}_C\left(\xi,\eta\right) &= \tilde{\mathbf{P}}\left(\xi,\xi\right)\mathbf{R}_T\left(\xi,\eta\right)\mathbf{P}\left(\eta,\eta\right) \\ &= \underbrace{\mathbf{R}_T\left(\xi,\eta\right)}_{\substack{truncation \\ BC}} \underbrace{\left(\prod_{j=1}^{n}\left(\frac{2i/L_j + \widetilde{k_{x\xi}}}{2i/L_j - \widetilde{k_{x\xi}}}\right)\left(\frac{2i/L_j - k_{x\eta}}{2i/L_j + k_{x\eta}}\right)\right)}_{PMDL \quad contribution} \qquad \forall\ \xi,\eta \in \{1,2\}. \end{aligned} \qquad (5.14)$$

We assume that $\mathbf{R}_T \neq \mathbf{0}$ and the elements of $\mathbf{R}_T$ are bounded independent of $\left(k_x, k_y\right)$; this is typical e.g. the homogeneous Dirichlet boundary condition considered here satisfies these assumptions.

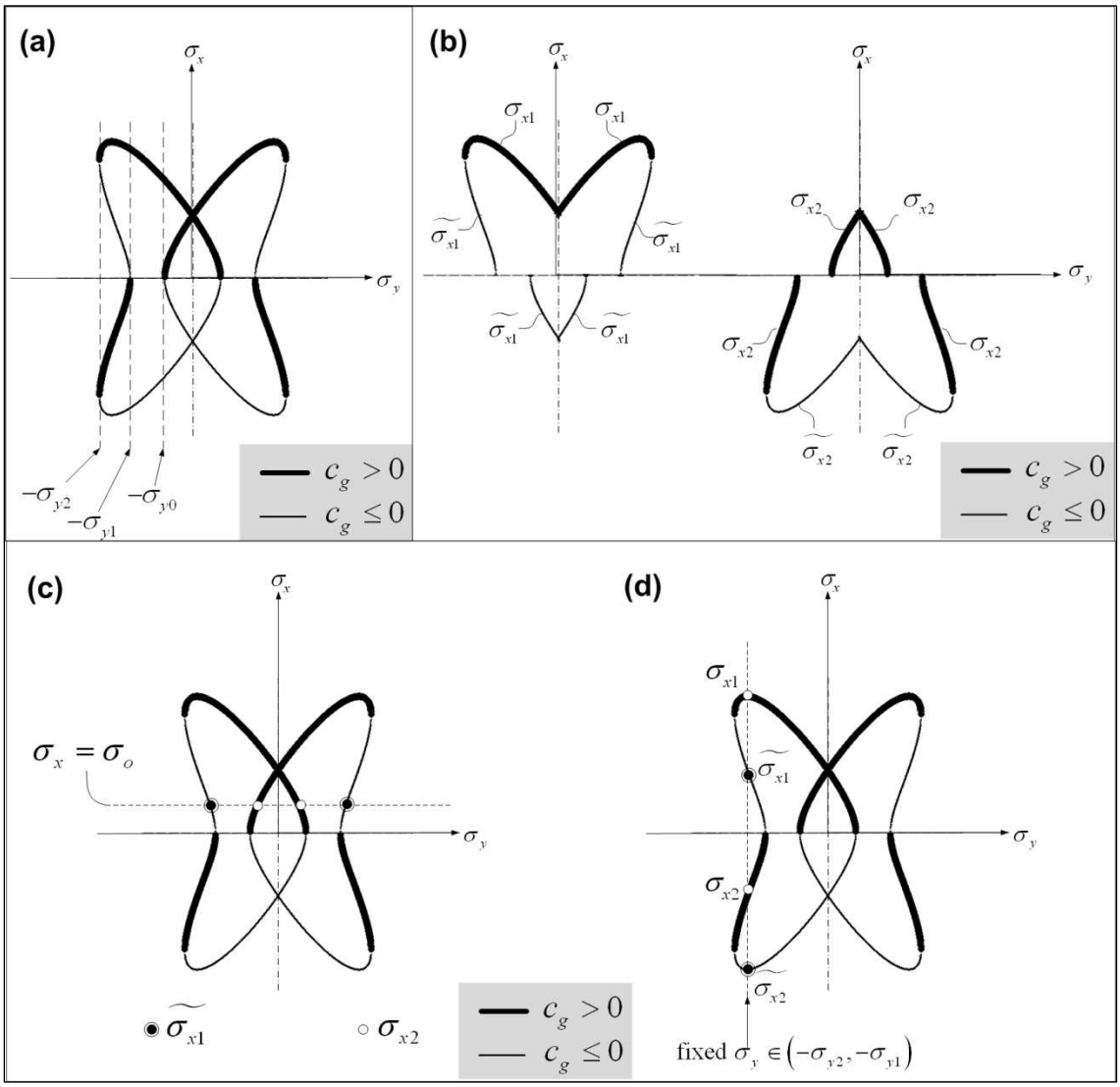

Figure 5.4. (a) Demarcation of outgoing and incoming propagating slownesses with various intervals of vertical slowness σ_y. (b) Notation for representing outgoing and incoming propagating horizontal slownesses $\left(\sigma_x \in \mathbb{R}\right)$. σ_{x1}, σ_{x2} represent the horizontal slownesses for outgoing wavemodes and $\widetilde{\sigma}_{x1}, \widetilde{\sigma}_{x2}$ represent the horizontal slownesses for incoming wavemodes. (c) Both outgoing and incoming wavemodes with the same horizontal slowness σ_o. (d) Various horizontal slownesses for a fixed vertical slowness $\sigma_y \in \left(-\sigma_{y2}, -\sigma_{y1}\right)$.

5.4 Accuracy

In order to facilitate later derivations we use the following notation to denote the PMDL contribution in (5.14) (see Figure 5.4b),

$$R_j\left(\xi,\eta\right)=\left(\frac{\widetilde{\sigma_{x\xi}}+\sigma_{xj}^{ref}}{\widetilde{\sigma_{x\xi}}-\sigma_{xj}^{ref}}\right)\left(\frac{\sigma_{x\eta}-\sigma_{xj}^{ref}}{\sigma_{x\eta}+\sigma_{xj}^{ref}}\right)\qquad\forall\ \xi,\eta\in\left\{1,2\right\},\tag{5.15}$$

where, $\sigma_{xj}^{ref}=2i/\omega L_j$ is the j^{th} PMDL parameter with L_j being the PMDL layer length, $\sigma_{x1,2}$ and $\widetilde{\sigma_{x1,2}}$ being respectively the outgoing and incoming horizontal slownesses for the two in-plane wavemodes. Writing (5.14) using slownesses instead of wavenumbers and then using (5.15) results in,

$$\mathbf{R}_C(\xi,\eta)=\underbrace{\mathbf{R}_T(\xi,\eta)}_{\substack{truncation\\BC}}\ \underbrace{\mathbf{R}_{PMDL}(\xi,\eta)}_{PMDL\quad contribution}\qquad\forall\ \xi,\eta\in\left\{1,2\right\},\tag{5.16}$$

where,

$$\mathbf{R}_{PMDL}(\xi,\eta)=\left(\prod_{j=1}^{n}R_j(\xi,\eta)\right)\qquad\text{for } n\text{-layer PMDL}\,.\tag{5.17}$$

It can be clearly seen from (5.15), (5.16) and (5.17) that a choice of PMDL layer lengths of $L_j=2i/\omega\,\sigma_{xj}^{ref}$ will make the n-layer PMDL exact for a choice of slownesses $\sigma_x=\sigma_{xj}^{ref}$. Hence σ_{xj}^{ref} are the interpolation points for the approximation of (5.10) by the *n*-layer PMDL stiffness $\left(\mathbf{K}_n\right)$. $\sigma_{x1}^{ref},\sigma_{x2}^{ref},\ldots,\sigma_{xn}^{ref}$ are thus the n parameters of PMDL, also known as its reference slownesses.

5.4.1 Accuracy Criterion

An ABC is considered exact if $\mathbf{R}_C(\xi,\eta)=0$ for all $\xi,\eta\in\left\{1,2\right\}$. Accuracy of an approximate ABC hence translates to making $\mathbf{R}_C(\xi,\eta)$ as small as possible. Typically the

accuracy of ABCs is a function of the ABC parameters and the computational effort that can be reasonably expended. For an ABC to be considered accurate in any sense, it has to be convergent i.e., it should yield the exact solution in the limit of infinite computational effort. In other words, an ABC is termed accurate if its parameters can be chosen to yield $\mathbf{R}_C(\xi,\eta) \to 0$ with increasing computational effort.

Accuracy criterion: A n-layer PMDL is considered accurate if, by increasing the number of layers n, the magnitude of every element of its computational reflection matrix can be made arbitrarily small for every wavemode, i.e.,

$$\lim_{n\to\infty}\left|\mathbf{R}_C(\xi,\eta)\right| = 0 \qquad \forall\ \xi,\eta \in \{1,2\}: \begin{matrix}\text{Accuracy criterion for} \\ n\text{-layer PMDL}\end{matrix}. \tag{5.18}$$

To be precise (5.18) is a *convergence* criterion that is necessary for a PMDL to act as a meaningful ABC for any wavemode. If the rate of convergence is slow, the number of PMDL layers required for sufficient accuracy might render the ABC inefficient. The usage of the term *accuracy* instead of the term *convergence* is mainly for the sake of compatibility with existing ABC literature [46].

For a homogeneous Dirichlet truncation boundary condition, the elements of $\mathbf{R}_T$ are independent of the slownesses, finite and non-zero, and hence using (5.16), (5.18) reduces to,

$$\lim_{n\to\infty}\left|\mathbf{R}_{PMDL}(\xi,\eta)\right| = 0 \qquad \forall\ \xi,\eta \in \{1,2\}: \begin{matrix}\text{Accuracy criterion for} \\ n\text{-layer PMDL}\end{matrix}. \tag{5.19}$$

5.4.2 Accuracy Criterion for Layer Groups

For later use we specify a more general accuracy criterion that is a modification of the criterion given in the previous section. To facilitate this, we define a $m \times n$-layer PMDL $\left(m \geq 1, n \geq 1\right)$ as a PMDL with mn layers that is viewed as made up of n groups of m layers each. Note that a $m \times n$-layer PMDL is just a regular PMDL viewed differently. We now define the following modified accuracy criterion.

Accuracy criterion: A $m \times n$ -layer PMDL is considered accurate if, by increasing the number of *groups (n)*, the magnitude of every element of its computational reflection matrix can be made arbitrarily small for every wavemode, i.e.,

$$\lim_{n\to\infty}\left|\mathbf{R}_{C}(\xi,\eta)\right| = 0 \qquad \forall\ \xi,\eta \in \{1,2\}: \begin{matrix}\text{Accuracy criterion for} \\ m\times n\text{-layer PMDL}\end{matrix}. \tag{5.20}$$

As before, (5.20) reduces to,

$$\lim_{n\to\infty}\left|\mathbf{R}_{PMDL}(\xi,\eta)\right| = 0 \qquad \forall\ \xi,\eta \in \{1,2\}: \begin{matrix}\text{Accuracy criterion for} \\ m\times n\text{-layer PMDL}\end{matrix}. \tag{5.21}$$

The only difference between (5.21) and (5.19) is the *way* in which we increase the total number of layers. For (5.21), we increase the number of *groups* with a fixed number of layers per group. To complete this distinction, we rewrite (5.17) in a grouped form as

$$\mathbf{R}_{PMDL}(\xi,\eta) = \prod_{p=1}^{n}\left(\prod_{s=1}^{m} R_{m\cdot p-(s-1)}(\xi,\eta)\right) \qquad \text{for } m\times n\text{-layer PMDL}. \tag{5.22}$$

Of course, (5.19) is just a special case of (5.21) with groups of 1 layer each, or in other words (5.19) is the accuracy criterion for a $1\times n$ layer PMDL. We will hence use (5.22) for all later calculations. The utility of grouping will become evident in the next section.

5.4.3 Sufficient Conditions for Accuracy

A simple sufficient condition for accuracy of a $m \times n$ -layer PMDL obtained by using (5.22) in (5.21) is

$$\left|\prod_{s=1}^{m} R_{m\cdot p-(s-1)}\left(\xi,\eta\right)\right| = \left|\prod_{s=1}^{m}\left(\frac{\widetilde{\sigma}_{x\xi} + \sigma^{ref}_{x\left(m\cdot p-(s-1)\right)}}{\widetilde{\sigma}_{x\xi} - \sigma^{ref}_{x\left(m\cdot p-(s-1)\right)}}\right)\left(\frac{\sigma_{x\eta} - \sigma^{ref}_{x\left(m\cdot p-(s-1)\right)}}{\sigma_{x\eta} + \sigma^{ref}_{x\left(m\cdot p-(s-1)\right)}}\right)\right| < 1, \tag{5.23}$$
$$\forall \xi,\eta \in \{1,2\},\ p = (1\ldots n).$$

Note that the advantage of the grouping in (5.23) is that we now have m parameters to choose, $\sigma^{ref}_{x(m\cdot p)}, \sigma^{ref}_{x(m\cdot p-1)}, \ldots, \sigma^{ref}_{x(m\cdot p-(m-1))}$, to ensure accuracy. Each layer need not satisfy

$\left|R_j\left(\xi,\eta\right)\right|<1$ by itself; only a group of every m layers together need to satisfy (5.23). Of course this is at the cost of efficiency and for a given total number of layers, satisfying $\left|R_j\left(\xi,\eta\right)\right|<1$ for every layer will lead to faster convergence as compared to satisfying the inequality in (5.23).

It should be noted that there are multiple ways of grouping layers e.g. a PMDL with a total of 6 layers can be viewed as a 1×6, 2×3, 3×2 or 6×1 layer PMDL with 1, 2, 3 and 6 parameters respectively to choose from to ensure (5.23). Therefore (5.23) defines a *sequence* of successively less conservative sufficient conditions with increasing m. We can simplify (5.23) by dropping the index p and deriving conditions on the m arbitrary parameters $\sigma_{x1}^{ref},\sigma_{x2}^{ref},\ldots,\sigma_{xm}^{ref}$ to satisfy (5.23). Hence a sufficient condition for accuracy of a $m\times n$-layer PMDL is

$$\left|\prod_{s=1}^{m}R_s\left(\xi,\eta\right)\right|=\left|\prod_{s=1}^{m}\left(\frac{\widetilde{\sigma_{x\xi}}+\sigma_{xs}^{ref}}{\widetilde{\sigma_{x\xi}}-\sigma_{xs}^{ref}}\right)\left(\frac{\sigma_{x\eta}-\sigma_{xs}^{ref}}{\sigma_{x\eta}+\sigma_{xs}^{ref}}\right)\right|<1\quad\forall\xi,\eta\in\left\{1,2\right\}. \tag{5.24}$$

To simplify later notation we define:

$$r_m\left(\sigma_x,\sigma_{x1}^{ref},\ldots,\sigma_{xm}^{ref}\right)=\prod_{s=1}^{m}\left(\frac{\sigma_x-\sigma_{xs}^{ref}}{\sigma_x+\sigma_{xs}^{ref}}\right). \tag{5.25}$$

Using (5.25) in (5.24) we get

$$\left|\prod_{s=1}^{m}R_s\left(\xi,\eta\right)\right|=\left|r_m\left(\sigma_{x\eta},\sigma_{x1}^{ref},\ldots,\sigma_{xm}^{ref}\right)\right|\left|r_m\left(\widetilde{\sigma_{x\xi}},\sigma_{x1}^{ref},\ldots,\sigma_{xm}^{ref}\right)\right|^{-1}<1\quad\forall\xi,\eta\in\left\{1,2\right\}. \tag{5.26}$$

The form in (5.26) uses the notation $r_m\left(\sigma_x,\sigma_{x1}^{ref},\ldots,\sigma_{xm}^{ref}\right)$ to underscore the dependence of r_m on the horizontal wavenumber and the m parameters of PMDL; r_m in this case is σ_y-*independent*.

5.4.4 Necessary Conditions for Accuracy

The expression in (5.26) provides, as mentioned before, a sequence of progressively *less* conservative sufficient conditions. A simple necessary condition then can be stated as:

There exists an $m < \infty$ *for which* (5.26) *is satisfied*

for all propagating wavemodes. (5.27)

If (5.26) is not satisfied for *any* m, that implies that there exists no layer grouping that provides accuracy. As $m \to \infty$ if every $\left|\prod_{s=1}^{m} R_{m\cdot j-(s-1)}\left(\xi,\eta\right)\right| \geq 1$, then we can see from (5.22) that (5.21) can no longer be satisfied , indicating that it is not possible for the ABC to be accurate..

Another necessary condition is,

$$\sigma_{xj}^{ref} \neq \widetilde{\sigma_{x\xi}} \quad \forall \xi = \left\{1,2\right\}. \tag{5.28}$$

The necessity of (5.28) is fairly obvious. For if $\sigma_{xj}^{ref} = \widetilde{\sigma_{x\xi}}$ for a pair $\left(\xi, j\right)$, $\left|R_{j}\left(\xi,\eta\right)\right| = \infty$ since $\sigma_{x\eta} \neq \widetilde{\sigma_{x\xi}} \quad \forall \xi,\eta = \left\{1,2\right\}$ and (5.19) cannot be achieved. Since σ_{xj}^{ref} represent the points of interpolation, (5.28) simply implies that we cannot interpolate the wrong branch (5.6) of the slowness diagram. In a sense an infinite element of the reflection matrix implies that the ABC allows purely incoming wavemodes in the absence of outgoing modes. This mimics spurious input of energy from the exterior leading to inaccuracies and instabilities.

5.5 Design and Implementation of an Accurate PMDL

In this section, we first show that irrespective of how large m is, it is impossible to satisfy (5.26) for all the propagating wavemodes of untilted non-elliptic anisotropic elasticity with a traditional PMDL having σ_{y}-*independent* parameters $\sigma_{xj}^{ref} \in \mathbb{C}$. We then determine the conditions on the real-valued, σ_{y}-*dependent* parameters $\sigma_{xj}^{ref}\left(\sigma_{y}\right) \in \mathbb{R}$ required to satisfy

(5.26) with the smallest m. These conditions are sufficient to absorb all outgoing propagating wavemodes but are not implementable. Their implementation is eventually facilitated by noting that the choice of σ_y *-dependent* parameters $\sigma_{xj}^{ref}\left(\sigma_y\right)$ can be viewed as an unconventional stretching of the finite element PMDL mesh.

5.5.1 Inadequacy of Wavenumber-Independent Parameters

In standard PMDL, the parameters σ_{xj}^{ref} are independent of the vertical wavenumber σ_y. In this sub-section, we simply show that for *any* given set of σ_y *-independent* parameters, there exists a propagating wavemode $\left(\sigma_x \in \mathbb{R}\right)$ such that (5.26) cannot be satisfied for any m. According to (5.27), this proves that it is impossible to design an accurate PMDL with σ_y *-independent* σ_{xj}^{ref}.

Using (5.26), and the fact that the slowness diagram is symmetric about the σ_y axis (see Figure 5.4a,b), we make the following simple observations:

$$\begin{aligned}
&\sigma_{x1} = -\widetilde{\sigma_{x2}},\\
&\sigma_{x2} = -\widetilde{\sigma_{x1}},\\
&\left|r_m\left(\sigma_x, \sigma_{x1}^{ref}, ..., \sigma_{xm}^{ref}\right)\right| = \left|r_m\left(-\sigma_x, , \sigma_{x1}^{ref}, ..., \sigma_{xm}^{ref}\right)\right|^{-1}.
\end{aligned} \tag{5.29}$$

Consider an arbitrary fixed $\sigma_x = \sigma_o > 0$ such that there exist both outgoing and incoming wavemodes with the horizontal wavenumber σ_o i.e, using our standard notation we choose a $\sigma_o > 0$ such that there exists $\widetilde{\sigma_{x1}} = \sigma_o, \sigma_{x2} = \sigma_o$ as shown in Figure 5.4c. Also choose m arbitrary complex-valued PMDL parameters $\sigma_{x1}^{ref}, \sigma_{x2}^{ref}, \ldots, \sigma_{xm}^{ref}$. For the given σ_o, the choice of parameters could be such that $\left|r_m\left(\sigma_o, \sigma_{x1}^{ref}, ..., \sigma_{xm}^{ref}\right)\right| < 1$, $\left|r_m\left(\sigma_o, \sigma_{x1}^{ref}, ..., \sigma_{xm}^{ref}\right)\right| > 1$ or $\left|r_m\left(\sigma_o, \sigma_{x1}^{ref}, ..., \sigma_{xm}^{ref}\right)\right| = 1$. Consider the three separate cases:

Case 1: $\left|r_m\left(\sigma_o,\cdot\right)\right|<1$. Since there exists an incoming wavemode $\widetilde{\sigma_{x1}}=\sigma_o$ (see Figure 5.4c), we have $\left|r_m\left(\widetilde{\sigma_{x1}},\cdot\right)\right|<1$. Using (5.29) and $\sigma_{x2}=-\widetilde{\sigma_{x1}}$, we get $\left|r_m\left(\widetilde{\sigma_{x1}},\cdot\right)\right|=\left|r_m\left(-\widetilde{\sigma_{x1}},\cdot\right)\right|^{-1}=\left|r_m\left(\sigma_{x2},\cdot\right)\right|^{-1}$. Hence $\left|r_m\left(\sigma_{x2},\cdot\right)\right|^{-1}<1$ or equivalently $\left|r_m\left(\sigma_{x2},\cdot\right)\right|\left|r_m\left(\widetilde{\sigma_{x1}},\cdot\right)\right|^{-1}>1$. This implies $\left|\prod_{s=1}^{m}R_s\left(1,2\right)\right|>1$, thus violating (5.26).

Case2: $\left|r_m\left(\sigma_o,\cdot\right)\right|>1$. Since there exists an outgoing wavemode $\sigma_{x2}=\sigma_o$ (see Figure 5.4c), we have $\left|r_m\left(\sigma_{x2},\cdot\right)\right|>1$. Similar to the previous paragraph, we get $\left|r_m\left(\widetilde{\sigma_{x1}},\cdot\right)\right|=\left|r_m\left(\sigma_{x2},\cdot\right)\right|^{-1}$ and hence $\left|r_m\left(\sigma_{x2},\cdot\right)\right|\left|r_m\left(\widetilde{\sigma_{x1}},\cdot\right)\right|^{-1}>1$. This implies $\left|\prod_{s=1}^{m}R_s\left(1,2\right)\right|>1$, which violates (5.26).

Case 3: $\left|r_m\left(\sigma_o,\cdot\right)\right|=1$. By the same arguments as above, there exists $\left|\prod_{s=1}^{m}R_s\left(1,2\right)\right|=1$ that violates (5.26).

Since both m and the parameters of PMDL were completely arbitrary, the above analysis shows that (5.26) cannot be satisfied with any number of σ_y*-independent* parameters.

5.5.2 Wavenumber-Dependent Parameters: Requirements

A careful study of the proof in the previous sub-section reveals the fact that it is the presence of both outgoing and incoming wavemodes with identical horizontal wavenumbers σ_o that makes it impossible to satisfy (5.26). In fact, the deeper reason behind it is that the PMDL parameters are independent of σ_y. For, even though both σ_{x2} and $\widetilde{\sigma_{x1}}$ are equal to σ_o, they

occur at different σ_y as evident from Figure 5.4c and this may be used to our advantage to satisfy (5.26).

For propagating wavemodes $\left(\sigma_x \in \mathbb{R}\right)$, it can be easily shown that we cannot satisfy (5.26) with a $1 \times n$ layer PMDL even with σ_y-*dependent* parameters. Consider for example σ_{x1}^{ref} (note that $m = 1$ for a $1 \times n$ layer PMDL) to be an arbitrary complex function of σ_y i.e. $\sigma_{x1}^{ref}\left(\sigma_y\right) \in \mathbb{C}$. Consider now a fixed $\sigma_y \in \left(-\sigma_{y2}, -\sigma_{y1}\right)$ as shown in Figure 5.4d. At this fixed σ_y we have two outward propagating wavemodes $\sigma_{x1} > 0, \sigma_{x2} < 0$ and two inward propagating modes $\widetilde{\sigma_{x1}} > 0, \widetilde{\sigma_{x2}} < 0$ as shown in Figure 5.4d. Also at this fixed σ_y, $\sigma_{x1}^{ref}\left(\sigma_y\right)$ is a constant complex number with either $\Re e\left(\sigma_{x1}^{ref}\left(\sigma_y\right)\right) > 0$, or $\Re e\left(\sigma_{x1}^{ref}\left(\sigma_y\right)\right) < 0$, or $\Re e\left(\sigma_{x1}^{ref}\left(\sigma_y\right)\right) = 0$. Consider the three separate cases:

Case 1: $\Re e\left(\sigma_{x1}^{ref}\left(\sigma_y\right)\right) > 0$. Checking (5.15) with $\widetilde{\sigma_{x1}} > 0$ and $\sigma_{x2} < 0$, we can easily conclude that $\left|R_j\left(1,2\right)\right| > 1$ i.e. (5.26) is not satisfied.

Case 2: $\Re e\left(\sigma_{x1}^{ref}\left(\sigma_y\right)\right) < 0$. Checking (5.15) with $\widetilde{\sigma_{x2}} < 0$ and $\sigma_{x1} > 0$, we can conclude that $\left|R_j\left(2,1\right)\right| > 1$, i.e., (5.26) is again not satisfied.

Case 3: $\Re e\left(\sigma_{xj}^{ref}\left(\sigma_y\right)\right) = 0$. Checking (5.15) we see that the numerator and denominator will be complex conjugates with $\left|R_j\left(\cdot,\cdot\right)\right| = 1$, i.e., (5.26) is not satisfied.

Given that the above analysis proves that a $1 \times n$ layer PMDL will not work, we now examine whether a two layer grouping, i.e., a $2 \times n$ layer PMDL, can satisfy (5.26) and guarantee accuracy, first with $\sigma_{xj}^{ref}\left(\sigma_y\right) \in \mathbb{R}$. We resort to the earlier notation of $\sigma_{x1}^{ref}, \sigma_{x2}^{ref}$

with the understanding that henceforth, σ_{xj}^{ref} will be a function of σ_y. Moreover, now $r_2\left(\cdot\right)$ is also a function of σ_y, but we will again drop the σ_y. For a $2\times n$ layer PMDL, (5.26) can simply be satisfied by ensuring

$$\left|r_2\left(\sigma_{x\eta},\sigma_{x1}^{ref},\sigma_{x2}^{ref}\right)\right|<1,\quad \left|r_2\left(\widetilde{\sigma_{x\xi}},\sigma_{x1}^{ref},\sigma_{x2}^{ref}\right)\right|\geq 1 \qquad \forall\xi,\eta\in\left\{1,2\right\}. \tag{5.30}$$

The inequalities in (5.30) essentially imply that the choice of the PMDL parameters $\sigma_{x1}^{ref},\sigma_{x2}^{ref}$ should be such that the rational function $r_2\left(\sigma_x,\cdot\right)$ should have a magnitude less than 1 for outgoing σ_x and a magnitude greater than or equal to 1 for incoming σ_x. If, for a given set of PMDL parameters $\sigma_{x1}^{ref},\sigma_{x2}^{ref}$, we can determine the regions in $\sigma_x\in\left(-\infty,\infty\right)$ for which $\left|r_2\left(\sigma_x,\sigma_{x1}^{ref},\sigma_{x2}^{ref}\right)\right|<1$, we might be able to ensure all outgoing σ_x to fall within these regions and all incoming σ_x to fall outside these regions thus satisfying (5.30).

We reassert that we are considering real-valued PMDL parameters and propagating waves, i.e., $\sigma_x,\sigma_{x1}^{ref},\sigma_{x2}^{ref}\in\mathbb{R}$. Without loss of generality we assume $\left|\sigma_{x1}^{ref}\right|>\left|\sigma_{x2}^{ref}\right|$. Expanding $r_2\left(\sigma_x,\cdot\right)$ using (5.25) and noting that all variables are real-valued, we get the following:

$$\begin{aligned}\left|r_2\left(\sigma_x,\cdot\right)\right|<1 \;\Leftrightarrow\; & \left|\left(\sigma_x^2+\sigma_{x1}^{ref}\sigma_{x2}^{ref}\right)-\sigma_x\left(\sigma_{x1}^{ref}+\sigma_{x2}^{ref}\right)\right| \\ & <\left|\left(\sigma_x^2+\sigma_{x1}^{ref}\sigma_{x2}^{ref}\right)+\sigma_x\left(\sigma_{x1}^{ref}+\sigma_{x2}^{ref}\right)\right| \\ \Leftrightarrow\; & \left(\sigma_x^2+\sigma_{x1}^{ref}\sigma_{x2}^{ref}\right)\sigma_x\left(\sigma_{x1}^{ref}+\sigma_{x2}^{ref}\right)>0.\end{aligned} \tag{5.31}$$

Depending on the values of the parameters σ_{x1}^{ref} and σ_{x2}^{ref}, equation (5.31) is satisfied on different regions of σ_x. These regions are enumerated below for later convenience.

$$\begin{array}{ll}
\sigma_{x1}^{ref} > 0,\, \sigma_{x2}^{ref} > 0: & \left|r_2\left(\sigma_x,\cdot\right)\right| < 1 \quad \forall \sigma_x \in \left(0,\infty\right) - - - - - - - - - - - - \textbf{I} \\
\sigma_{x1}^{ref} < 0,\, \sigma_{x2}^{ref} < 0: & \left|r_2\left(\sigma_x,\cdot\right)\right| < 1 \quad \forall \sigma_x \in \left(-\infty,0\right) - - - - - - - - - - - - \textbf{II} \\
\sigma_{x1}^{ref} > 0,\, \sigma_{x2}^{ref} < 0: & \left|r_2\left(\sigma_x,\cdot\right)\right| < 1 \quad \forall \sigma_x \in \left(-\alpha\left(\sigma_y\right),0\right) \cup \left(\alpha\left(\sigma_y\right),+\infty\right) - \textbf{III} \\
\sigma_{x1}^{ref} < 0,\, \sigma_{x2}^{ref} > 0: & \left|r_2\left(\sigma_x,\cdot\right)\right| < 1 \quad \forall \sigma_x \in \left(-\infty,-\alpha\left(\sigma_y\right)\right) \cup \left(0,\alpha\left(\sigma_y\right)\right) - \textbf{IV}
\end{array} . \qquad (5.32)$$

In the above $\alpha\left(\sigma_y\right) = \left|\sigma_{x1}^{ref}\sigma_{x2}^{ref}\right|^{1/2}$. Implications of (5.32) are shown in Figure 5.5 for a fixed $\sigma_y = \sigma_y^*$. Comparing Figure 5.5 with the slowness diagram that we wish to capture (thick line in Figure 5.4a), we can easily see that (5.30) can be satisfied if $\sigma_{x\eta}$ falls *within* the four regions $\left(\mathbf{I},\ldots,\mathbf{IV}\right)$ specified by (5.32) and $\widetilde{\sigma_{x\xi}}$ falls *outside* these regions. Hence for example, one valid choice of σ_{x1}^{ref}, σ_{x2}^{ref} could be such that for $\sigma_y \in \left(-\sigma_{y2},-\sigma_{y1}\right) \bigcup \left(\sigma_{y1},\sigma_{y2}\right)$, σ_x falls in region **III** and for $\sigma_y \in \left(-\sigma_{y1},\sigma_{y1}\right)$, σ_x falls in region **I** (see Figure 5.6a) i.e. $\sigma_{x1}^{ref} > 0, \sigma_{x2}^{ref} < 0$ for $\sigma_y \in \left(-\sigma_{y2},-\sigma_{y1}\right) \bigcup \left(\sigma_{y1},\sigma_{y2}\right)$ and $\sigma_{x1}^{ref} > 0, \sigma_{x2}^{ref} > 0$ for $\sigma_y \in \left(-\sigma_{y1},\sigma_{y1}\right)$.

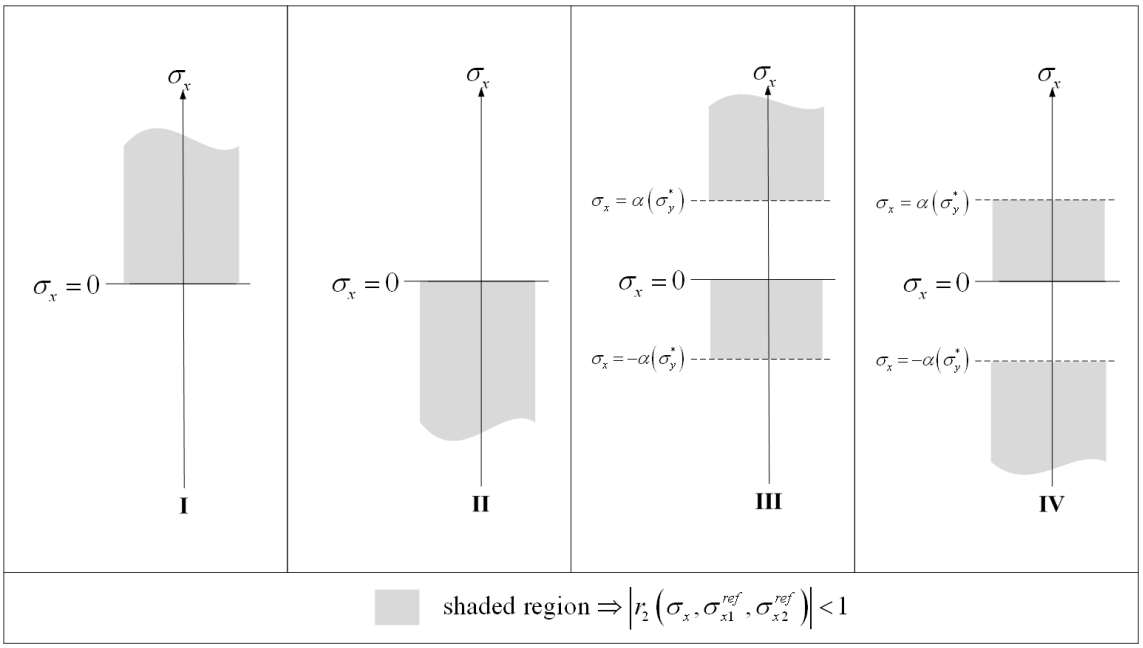

Figure 5.5. Regions with $\left| r_2\left(\sigma_x, \sigma_{x1}^{ref}, \sigma_{x2}^{ref}\right)\right| < 1$ for a 2-layer grouping of PMDL for a fixed $\sigma_y = \sigma_y^*$.

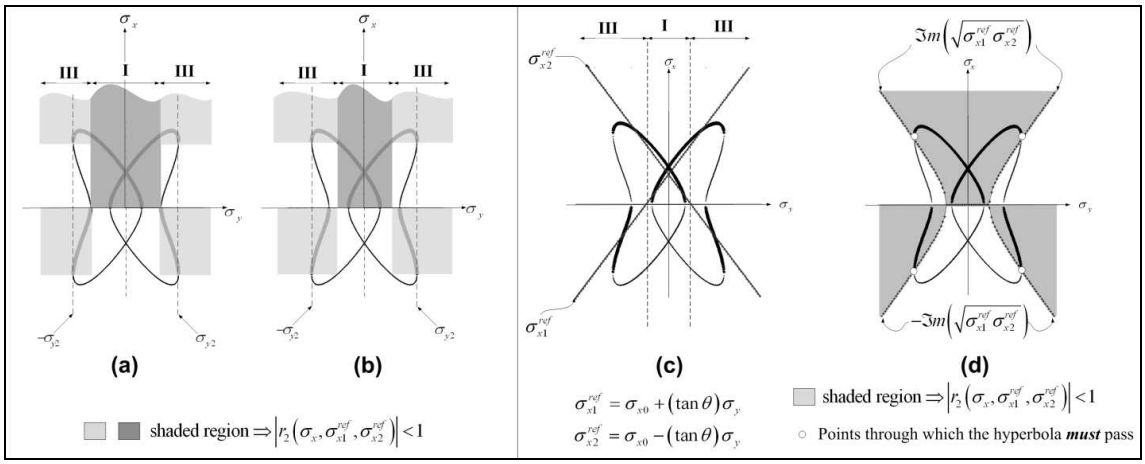

Figure 5.6. (a), (b) Valid choices that ensure *only* the outgoing wavemodes (thick lines) fall in the shaded region and consequently the incoming wavemodes (thin lines) fall outside the shaded region. (c) The two PMDL parameters that are linearly dependent on vertical slownesses σ_y for a 2-layer grouping. (d) Shaded regions with $\left|r_2\left(\sigma_x, \cdot\right)\right| < 1$ for the parameters that are linearly dependent on σ_y. Note that all the outgoing wavemodes (thick lines) fall in the shaded region while all the incoming wavemodes (thin lines) fall outside the shaded region.

The above analysis shows that the σ_y-dependent parameters $\sigma_{x1}^{ref}, \sigma_{x2}^{ref}$ should at least change signs over different intervals of σ_y. Linear dependence on σ_y will provide a simple choice of such parameters and we can assume $\sigma_{x1}^{ref} = \sigma_{x0} - \left(\tan\theta\right)\sigma_y$, $\sigma_{x2}^{ref} = \sigma_{x0} + \left(\tan\theta\right)\sigma_y$ (Figure 5.6c). The usage of $\pm\tan\theta$ is suggested by the symmetry of the slowness diagram with respect to σ_y. Such a choice leads to the bounds $\pm\alpha\left(\sigma_y\right)$ in (5.32) being defined by a hyperbola shown in Figure 5.6d where the shaded regions have $\left|r_2\left(\sigma_x, \cdot\right)\right| < 1$. Note that $\pm\alpha\left(\sigma_y\right)$ forms the bound only in region **III**; region **I** has a lower bound of zero according to (5.32).

Knowing that **(a)** the positioning of the hyperbola should be such that the outgoing wavemodes $\sigma_{x\eta}$ fall within the regions specified by (5.32) and the incoming wavemodes $\widetilde{\sigma_{x\xi}}$

fall outside these regions and **(b)** the outgoing and incoming slownesses are identical at $\sigma_y = \pm\sigma_{y2}, \pm\sigma_{y1}$ and $\pm\sigma_{y0}$, we can conclude that *the hyperbola has to pass through the slowness at points* $\pm\sigma_{y2}$ *and should cross the* σ_y *axis in the intervals* $\left[-\sigma_{y1}, -\sigma_{y0}\right]$ *and* $\left[\sigma_{y0}, \sigma_{y1}\right]$. The reason why the hyperbola need not cross the σ_y axis at precisely $\pm\sigma_{y1}$ or $\pm\sigma_{y0}$ is because the slownesses are zero there and zero forms a natural bound of the intervals in (5.32).

Since the hyperbola forms a bound only for region **III** and as $\sigma_{x1}^{ref}\sigma_{x2}^{ref} < 0$ there (see (5.32) and Figure 5.6(c)), the hyperbola can be defined by $\pm\alpha\left(\sigma_y\right) = \pm\left(-\sigma_{x1}^{ref}\sigma_{x2}^{ref}\right)^{1/2} = \pm\left(\left(\tan^2\theta\right)\sigma_y^2 - \sigma_{xo}^2\right)^{1/2}$ and is shown in Figure 5.6d. A simple procedure can now be stated to obtain σ_{xo} and θ for the 2-layer grouping. Denoting the horizontal slowness at $\sigma_y = \pm\sigma_{y2}$ by $\sigma_x\big|_{\sigma_y=\pm\sigma_{y2}}$, we have the following methodology for choosing σ_{xo} and θ:

(i) Choose $\sigma_y^* \in \left[\sigma_{y0}, \sigma_{y1}\right]$,

(ii) Determine $\sigma_{xo} = \dfrac{\sigma_{x1}\Big|_{\sigma_y=\pm\sigma_{y2}}}{\left(\left(\dfrac{\sigma_{y2}}{\sigma_y^*}\right)^2 - 1\right)^{1/2}}$, (5.33)

(iii) Get $\theta = \tan^{-1}\left(\dfrac{\sigma_{x0}}{\sigma_y^*}\right)$.

Step **(i)** in (5.33) chooses an arbitrary σ_y^* which is assumed to be such that $\alpha\left(\sigma_y^*\right) = 0$; this gives us $\tan\theta = \sigma_{xo} \,/\, \sigma_y^*$**.** Substituting this into the requirement $\alpha\left(\pm\sigma_{y2}\right) = \sigma_x\big|_{\sigma_y = \pm\sigma_{y2}}$ we get **(ii).** Of course, for our derivations to hold we should get $\sigma_{xo} \in \mathbb{R}$ and $\theta \in \mathbb{R}$.

A more intuitive reason for the need of σ_y-dependent σ_{xj}^{ref} can be obtained by noting the necessary condition for accuracy (5.28). According to (5.28), the parameters of PMDL σ_{xj}^{ref} should not interpolate the incoming branch of the slowness diagram i.e. it should not cut the *thin* lines in Figure 5.6d. We cannot achieve this by σ_y-independent σ_{xj}^{ref}; such σ_{xj}^{ref} are represented as horizontal lines on the slowness figure and they always cut one of the thin lines when they are within the bounds of the slowness diagram (not too far above or below). Only inclined lines as shown in Figure 5.6d will escape cutting the thin lines and σ_{xj}^{ref} represented by such inclined lines are σ_y-dependent . Of course, the above argument no longer holds when the σ_y-independent σ_{xj}^{ref} form horizontal lines far above the top or far below the bottom of the slowness diagram and to exclude those cases precisely we need the mathematical analysis provided above.

5.5.3 Wavenumber-Dependent Parameters: Implementation

The previous sub-section shows that it is theoretically possible to satisfy (5.21) with a $2 \times n$ layer PMDL, provided we have σ_y*-dependent* σ_{xj}^{ref} of the form $\sigma_{xj}^{ref} = \sigma_{x0} \pm \left(\tan\theta\right)\sigma_y$. We will now specify a way of implementing $\sigma_{xj}^{ref} = \sigma_{x0} \pm \left(\tan\theta\right)\sigma_y$. In this sub-section we show that an unconventional stretching of the finite element PMDL mesh will be equivalent to providing $\sigma_{xj}^{ref} = \sigma_{x0} \pm \left(\tan\theta\right)\sigma_y$.

We consider a simple coordinate stretching of the form $x' = x \,/\, \cos\theta$ and $y' = y - x\tan\theta$ on (5.1) and Fourier transform it in y' to get the reduced wave equation of a transformed exterior,

$$\left(\mathbf{G}'_{xx}\frac{\partial^2}{\partial x'^2}+ik_y\left(\mathbf{G}'_{xy}+\mathbf{G}'^{T}_{xy}\right)\frac{\partial}{\partial x'}-\left(k_y^2\mathbf{G}'_{yy}-\omega^2\mathbf{I}\right)\right)\mathbf{u}'=\mathbf{0}, \tag{5.34}$$

where the vertical wavenumber k_y remains the same as in (5.1) because $\partial/\partial y' = \partial/\partial y$ and the coefficient matrices are,

$$\begin{aligned}
\mathbf{G}'_{xx} &= \frac{\mathbf{G}_{xx}}{\cos^2\theta},\\
\mathbf{G}'_{yy} &= \mathbf{G}_{xx}\tan^2\theta+\mathbf{G}_{yy}-\left(\mathbf{G}_{xy}+\mathbf{G}_{xy}^{T}\right)\tan\theta,\\
\mathbf{G}'_{xy} &= \frac{-\mathbf{G}_{xx}\tan\theta+\mathbf{G}_{xy}}{\cos\theta}.
\end{aligned} \tag{5.35}$$

Such a transformed exterior is still 'perfectly matched' to the untransformed interior (see Appendix). The coordinate transformation is equivalent to stretching the exterior as shown in Figure 5.7 and the stretched exterior can be approximated by stretched PMDL layers as shown in the same figure. The properties of these layers remain the same as in Section 5.3.3 with the transformed variables $\mathbf{G}'_{xx},\mathbf{G}'_{yy},\mathbf{G}'_{xy},k_{x'},L'_j$ substituted for their original counterparts and L'_j being the PMDL layer length along x' (see Figure 5.7b). The elements of $\mathbf{P},\tilde{\mathbf{P}}$ in (5.13) and consequently the expression in (5.15) change accordingly to result in,

$$R'_j\left(\xi,\eta\right)=\left(\frac{\widetilde{\sigma'_{x\xi}}+\sigma'^{ref}_{xj}}{\widetilde{\sigma'_{x\xi}}-\sigma'^{ref}_{xj}}\right)\left(\frac{\sigma'_{x\eta}-\sigma'^{ref}_{xj}}{\sigma'_{x\eta}+\sigma'^{ref}_{xj}}\right). \tag{5.36}$$

Using $k_{x'}=k_x\cos\theta+k_y\sin\theta$ and $\sigma'^{ref}_{xj}=\sigma^{ref}_{xj}\cos\theta$ (because of $L'_j=L_j/\cos\theta$) in (5.36) we get,

$$R'_j\left(\xi,\eta\right)=\left(\frac{\widetilde{\sigma_{x\xi}}+\left(\sigma_y\tan\theta+\sigma^{ref}_{xj}\right)}{\widetilde{\sigma_{x\xi}}+\left(\sigma_y\tan\theta-\sigma^{ref}_{xj}\right)}\right)\left(\frac{\sigma_{x\eta}+\left(\sigma_y\tan\theta-\sigma^{ref}_{xj}\right)}{\sigma_{x\eta}+\left(\sigma_y\tan\theta+\sigma^{ref}_{xj}\right)}\right). \tag{5.37}$$

Note that (5.37) *cannot* be written in a form similar to (5.15) i.e. the above transformation of coordinates is *not* equivalent to (5.15) with σ_y ***dependent*** σ^{ref}_{xj}. Or in other words a

coordinate transformation $\sigma_x' = \sigma_x \cos\theta + \sigma_y \sin\theta$ is *not* equivalent to an identical transformation on the PMDL parameters, $\sigma'^{ref}_x \neq \sigma^{ref}_x \cos\theta + \sigma_y \sin\theta$.

However, we note that we wish to eventually get $\sigma^{ref}_{xj} = \sigma_{x0} \pm \left(\tan\theta\right)\sigma_y$ i.e. with both $+\theta$ and $-\theta$. Hence, we look into a *group* of two PMDL layers, one designed for a transformed exterior similar to the one above with $\left(x,y\right) \xrightarrow{+\theta} \left(x',y'\right)$ and the other designed for $\left(x,y\right) \xrightarrow{-\theta} \left(x'',y''\right)$. The previous arguments of perfect matching being unaffected by coordinate transformations still hold and the 2-layer condition of (5.24) transforms to,

$$R'_1\left(\xi,\eta\right)R''_2\left(\xi,\eta\right) = \left(\frac{\widetilde{\sigma'_{x\xi}} + \sigma'^{ref}_{x1}}{\widetilde{\sigma'_{x\xi}} - \sigma'^{ref}_{x1}}\right)\left(\frac{\sigma'_{x\eta} - \sigma'^{ref}_{x1}}{\sigma'_{x\eta} + \sigma'^{ref}_{x1}}\right)\left(\frac{\widetilde{\sigma''_{x\xi}} + \sigma''^{ref}_{x2}}{\widetilde{\sigma''_{x\xi}} - \sigma''^{ref}_{x2}}\right)\left(\frac{\sigma''_{x\eta} - \sigma''^{ref}_{x2}}{\sigma''_{x\eta} + \sigma''^{ref}_{x2}}\right). \quad (5.38)$$

Using $k_{x'} = k_x \cos\theta + k_y \sin\theta$, $k_{x''} = k_x \cos\theta - k_y \sin\theta$, $\sigma'^{ref}_{x1} = \sigma^{ref}_{x1} / \cos\theta$ and $\sigma''^{ref}_{x2} = \sigma^{ref}_{x2} / \cos\theta$ (because of $L''_2 = L_2 / \cos\theta$ and $L'_1 = L_1 / \cos\theta$) in (5.38) we get,

$$\begin{aligned} R'_1\left(\xi,\eta\right)R''_2\left(\xi,\eta\right) = &\left(\frac{\widetilde{\sigma_{x\xi}} + \left(\sigma_y \tan\theta + \sigma^{ref}_{x1}\right)}{\widetilde{\sigma_{x\xi}} + \left(\sigma_y \tan\theta - \sigma^{ref}_{x1}\right)}\right)\left(\frac{\sigma_{x\eta} + \left(\sigma_y \tan\theta - \sigma^{ref}_{x1}\right)}{\sigma_{x\eta} + \left(\sigma_y \tan\theta + \sigma^{ref}_{x1}\right)}\right) \times \\ &\left(\frac{\widetilde{\sigma_{x\xi}} + \left(-\sigma_y \tan\theta + \sigma^{ref}_{x2}\right)}{\widetilde{\sigma_{x\xi}} + \left(-\sigma_y \tan\theta - \sigma^{ref}_{x2}\right)}\right)\left(\frac{\sigma_{x\eta} + \left(-\sigma_y \tan\theta - \sigma^{ref}_{x2}\right)}{\sigma_{x\eta} + \left(-\sigma_y \tan\theta + \sigma^{ref}_{x2}\right)}\right). \end{aligned} \quad (5.39)$$

Rearranging (5.39) by shuffling the numerators and denominators, we can write,

$$\begin{aligned} R'_1\left(\xi,\eta\right)R''_2\left(\xi,\eta\right) = &\left(\frac{\widetilde{\sigma_{x\xi}} + \left(\sigma_y \tan\theta + \sigma^{ref}_{x1}\right)}{\widetilde{\sigma_{x\xi}} + \left(-\sigma_y \tan\theta - \sigma^{ref}_{x2}\right)}\right)\left(\frac{\sigma_{x\eta} + \left(-\sigma_y \tan\theta - \sigma^{ref}_{x2}\right)}{\sigma_{x\eta} + \left(\sigma_y \tan\theta + \sigma^{ref}_{x1}\right)}\right) \times \\ &\left(\frac{\widetilde{\sigma_{x\xi}} + \left(-\sigma_y \tan\theta + \sigma^{ref}_{x2}\right)}{\widetilde{\sigma_{x\xi}} + \left(\sigma_y \tan\theta - \sigma^{ref}_{x1}\right)}\right)\left(\frac{\sigma_{x\eta} + \left(\sigma_y \tan\theta - \sigma^{ref}_{x1}\right)}{\sigma_{x\eta} + \left(-\sigma_y \tan\theta + \sigma^{ref}_{x2}\right)}\right), \end{aligned} \quad (5.40)$$

which, with the assumption $L_1 = L_2$ (i.e. $\sigma_{x1}^{ref} = \sigma_{x2}^{ref}$), can be written as,

$$R'_1\left(\xi,\eta\right)R''_2\left(\xi,\eta\right) = \left(\frac{\widetilde{\sigma_{x\xi}} + {}_{+\theta}\sigma_{x1}^{ref}}{\widetilde{\sigma_{x\xi}} - {}_{+\theta}\sigma_{x1}^{ref}}\right)\left(\frac{\sigma_{x\eta} - {}_{+\theta}\sigma_{x1}^{ref}}{\sigma_{x\eta} + {}_{+\theta}\sigma_{x1}^{ref}}\right)\times \left(\frac{\widetilde{\sigma_{x\xi}} + {}_{-\theta}\sigma_{x1}^{ref}}{\widetilde{\sigma_{x\xi}} - {}_{-\theta}\sigma_{x1}^{ref}}\right)\left(\frac{\sigma_{x\eta} - {}_{-\theta}\sigma_{x1}^{ref}}{\sigma_{x\eta} + {}_{-\theta}\sigma_{x1}^{ref}}\right), \tag{5.41}$$

where,

$$\begin{aligned} {}_{+\theta}\sigma_{x1}^{ref} &= \sigma_{x1}^{ref} + \sigma_y \tan\theta, \\ {}_{-\theta}\sigma_{x1}^{ref} &= \sigma_{x1}^{ref} - \sigma_y \tan\theta, \\ \sigma_{x1}^{ref} &= 2i\big/\omega L_1 . \end{aligned} \tag{5.42}$$

Since (5.41) is identical to the corresponding expression in (5.24) for $\prod_{s=1}^{2} R_s\left(\xi,\eta\right)$, but with the σ_y-*dependent* parameters ${}_{+\theta}\sigma_{x1}^{ref}$, ${}_{-\theta}\sigma_{x1}^{ref}$ replacing the σ_y-*independent* $\sigma_{x1}^{ref}, \sigma_{x2}^{ref}$, we have achieved our objective of implementing σ_y-*dependent* parameters. In fact, comparing the form of ${}_{+\theta}\sigma_{x1}^{ref}$, ${}_{-\theta}\sigma_{x1}^{ref}$ to the linear form we started with, $\sigma_{xo} \pm \left(\tan\theta\right)\sigma_y$, we notice that $\sigma_{xo} = \sigma_{x1}^{ref}$. Hence the steps in (5.33) can directly be used to calculate the PMDL layer lengths $L_1 = 2i\big/\omega\sigma_{x1}^{ref} = 2i\big/\omega\sigma_{xo}$ and the angle of stretch θ.

The implication of (5.41) is shown in Figure 5.8. To summarize, an unusual mesh stretching involving groups of two layers each, with each group having $\pm\theta$ stretching and identical lengths, is equivalent to a PMDL whose parameters are linearly dependent on σ_y. It should be noted that the above does *not* hold if either the two lengths are different, or the stretches are not in $+\theta, -\theta$ pairs. A valid $2\times n$-layer PMDL mesh is shown in Figure 5.8.

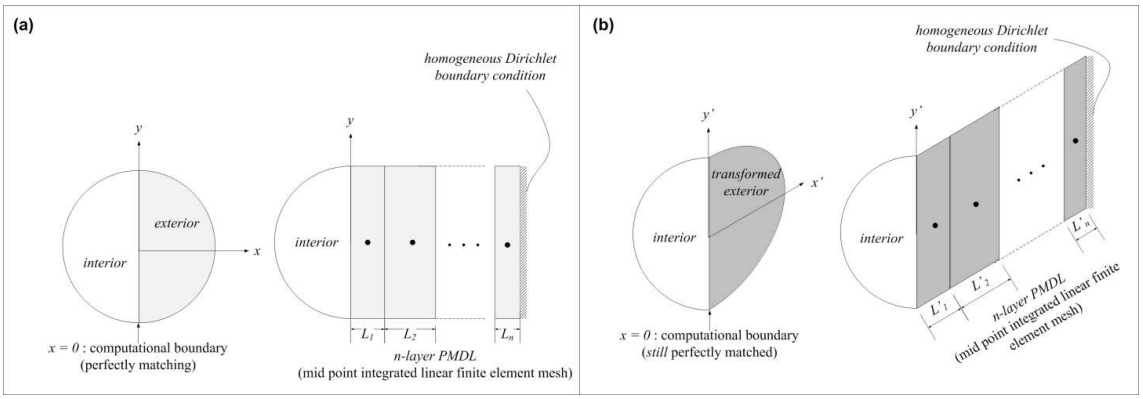

Figure 5.7. Untransformed (a) and transformed (b) exterior with corresponding *n*-layer PMDL mesh.

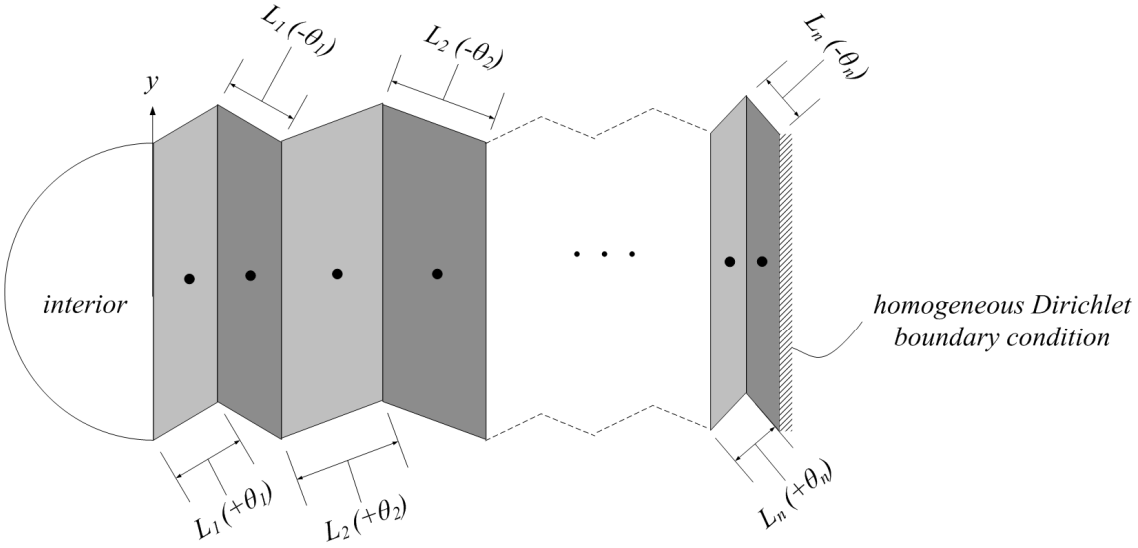

2n-layer PMDL
Unconventional stretching of the mid-point integrated linear finite element PMDL mesh

Figure 5.8. The unconventional stretching of the finite element PMDL mesh. The two layers in each 2-layer group have the same length with the stretch angles being equal in magnitude but opposite in sign.

The standard PMDL formulation (with wavenumber independent parameters) is known to be applicable to convex polygonal corners [44] with the corner PMDL mesh obtained as a

tensor product of the PMDLs from the two straight edges meeting at the corner. Analogously, we can obtain a corner mesh consistent with the above as a tensor product of two stretched PMDL meshes. Such a corner implementation for an orthogonal corner is shown in Figure 5.9 and it inherits its parameters $\left(L_j, \theta\right)$ from the corresponding edge PMDLs.

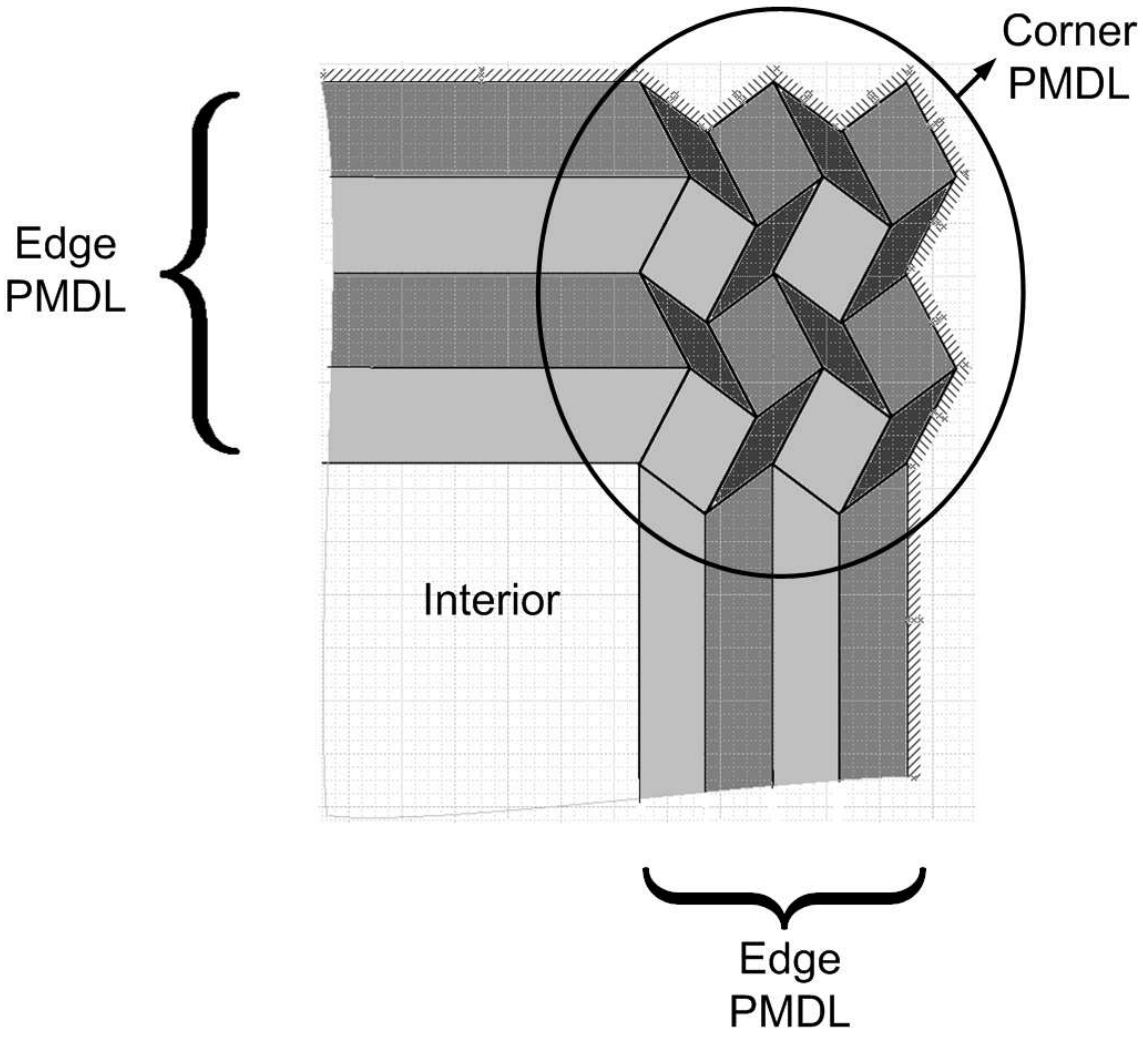

Figure 5.9. The unconventional stretching of the PMDL mesh for the two orthogonal edges leads to an unconventional corner implementation.

5.6 Numerical Experiments

We illustrate the performance of the proposed method for a representative case with $c_p = \sqrt{20}$, $c_s = 2$, $\varepsilon = -0.4$ and $\delta = -0.1934$. For these parameters, we get numerically, $\sigma_{y0} = 0.22361$, $\sigma_{y1} = 0.50000$, $\sigma_{y2} = 0.74538$ and $\sigma_x\Big|_{\sigma_y = \pm\sigma_{y2}} = 0.93752$. Using these values in (5.33) and by noting that $\sigma_x^{ref} = \sigma_{xo}.$, we have e.g. $\sigma_y^* = 0.3 \Rightarrow \left(\sigma_{x1}^{ref}, \theta\right) = \left(0.4122, 53.95^o\right)$, $\sigma_y^* = 0.4 \Rightarrow \left(\sigma_{x1}^{ref}, \theta\right) = \left(0.5962, 56.14^o\right)$ and $\sigma_y^* = 0.5 \Rightarrow \left(\sigma_{x1}^{ref}, \theta\right) = \left(0.8480, 59.48^o\right)$. Choosing arbitrary values of σ_{xo} and θ that violate (5.33) lead to inaccuracies e.g. we can choose $\left(\sigma_x^{ref}, \theta\right) = \left(0.5962, 0^o\right), \left(0.5962, 80^o\right)$. Or we could choose $\sigma_y^* \notin \left[\sigma_{y0}, \sigma_{y1}\right]$ in (5.33) e. g $\sigma_y^* = 0.15 \Rightarrow \left(\sigma_x^{ref}, \theta\right) = \left(0.1926, 52.09^o\right)$ and $\sigma_y^* = 0.65 \Rightarrow \left(\sigma_x^{ref}, \theta\right) = \left(1.6704, 68.74^o\right)$. Noting that the lengths are given by $L_1 = 2i/\omega\sigma_{x1}^{ref}$ we get the slowness curves in Figure 5.10-Figure 5.11.

All the parameter choices in Figure 5.10 are obtained by satisfying the sufficient conditions for accuracy of propagating wavemodes. While the real part of the correct slowness branch is captured rather closely, the non-real part of the slowness diagram is not approximated well. This is not surprising since we used only real PMDL parameters that are known in general to be effective against treating propagating wavemodes only. Figure 5.11 shows slowness curves for parameters that do not satisfy the criterion for accuracy specified in this paper. While the first two approximations are clearly inaccurate (they capture the incoming - negative group velocity branches), inaccuracies in the third and fourth slowness curves are not obvious. A close-up detail of these slownesses are shown in Figure 5.12 in the vicinity of the points σ_{y0} and σ_{y1}. Each wrongly chosen parameter set leads to inaccuracies in the vicinity of at least one of these two points σ_{y0}, σ_{y1}.

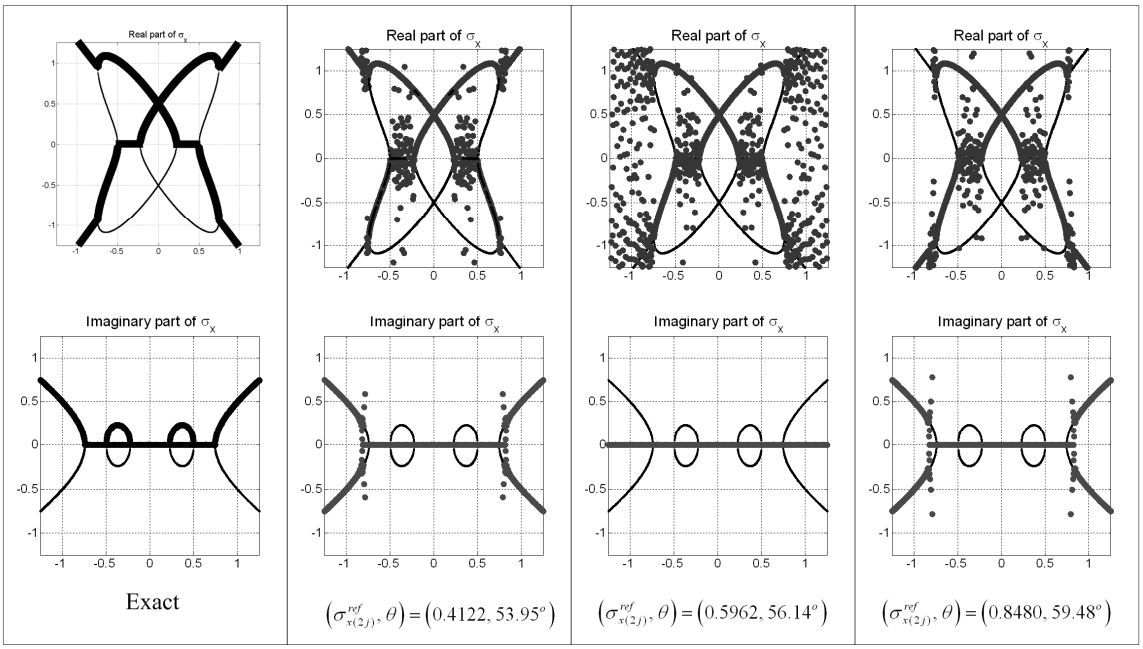

Figure 5.10. Exact slowness diagram followed by 200-layer PMDL slowness diagrams resulting from three different choices of parameters that all satisfy the accuracy criteria for treating propagating wavemodes $\left(\sigma_x \in \mathbb{R}\right)$ derived in this paper.

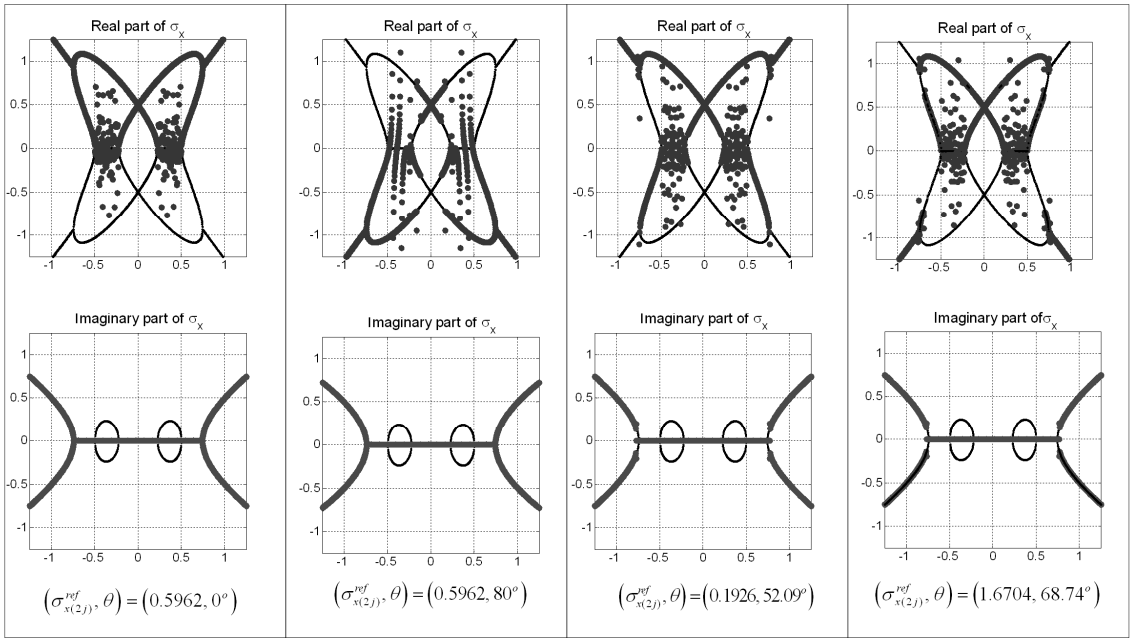

Figure 5.11. 200-layer PMDL slowness diagrams resulting from four different choices of parameters that all violate at least one of the accuracy criterion specified in this paper.

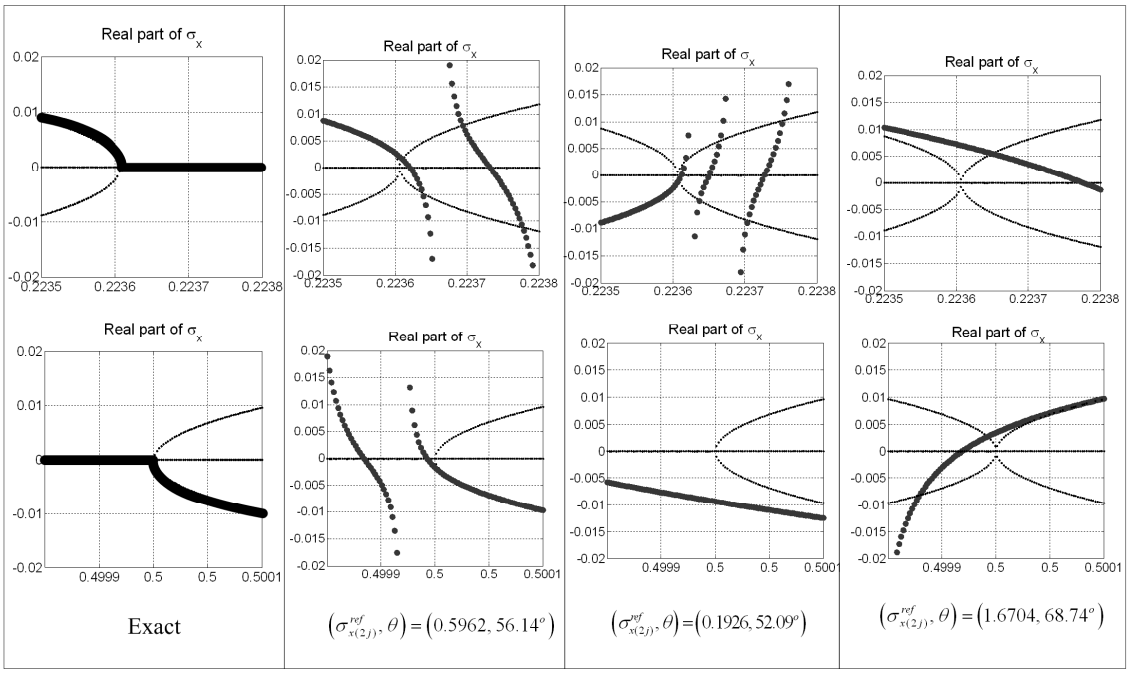

Figure 5.12. Detail of 200-layer PMDL slowness diagrams resulting from three different choices of parameters of which the third and fourth violate at least one of the accuracy criterion specified in this paper.

5.7 Summary and Conclusions

An accurate local ABC for the time-harmonic modeling of in-plane propagating waves in homogeneous untilted *non-elliptic* anisotropic elastic media is presented. This local ABC is based on PMDL and incorporates an unconventional stretching of the finite element PMDL mesh along with the concept of a two layer grouping to ensure the accurate treatment of propagating waves. The parameters of PMDL (related to its layer lengths) and the angles of stretch are required to satisfy certain conditions that are shown to be sufficient for accuracy.

By utilizing the form of the reflection matrix elements, we first showed that it is impossible for a traditional local ABC (PMDL with wavenumber-independent parameters) to accurately absorb all propagating modes. We then devised an accurate PMDL with parameters that depend linearly on the vertical wavenumbers; these parameters occur in pairs and need to satisfy a simple sufficient condition for accuracy. However, the wavenumber

dependence of PMDL parameters cannot be directly implemented and we thus presented an unconventional stretching of the finite element PMDL mesh that is equivalent to implementing wavenumber-dependent PMDL parameters.

This work presents, to the best of our knowledge, the *only* local ABC developed to date, whose accuracy is rigorously proven for all the propagating modes of untilted non-elliptic anisotropic elasticity. In doing so it has overcome one of the drawbacks of using simple space-time transformations to tackle the challenges associated with $c_{px}c_{gx}<0$, namely their inapplicability to non-elliptic anisotropic media. Further research is underway to extend the current methodology to *tilted* non-elliptic anisotropic media.

5.8 Appendix: Perfect matching of coordinate transformations

Perfect matching implies both displacement and traction continuity (no reflections) at the computational boundary. Perfect matching exists between the untransformed $\left(x,y\right)$ and transformed $\left(x',y'\right)$ space when $x'=x/\cos\theta$ and $y'=y-x\tan\theta$.

Similar to (5.3), (5.34) admits modes of the kind $\mathbf{u}'=\mathbf{a}'e^{ik_{x}x'}$ where the wavenumber $k_{x'}$ and mode $\mathbf{a}'$ satisfy the dispersion relation $\left|\mathbf{\Lambda}'\right|=0$ and the governing equation $\mathbf{\Lambda}'\mathbf{a}'=\mathbf{0}$ respectively with $\mathbf{\Lambda}'\equiv\left(k_{x'}^{2}\mathbf{G}'_{xx}+k_{x'}k_{y}\left(\mathbf{G}'_{xy}+\mathbf{G}'^{T}_{xy}\right)+k_{y}^{2}\mathbf{G}'_{yy}-\omega^{2}\mathbf{I}\right)$. It can be seen from direct substitution that $k_{x'}=k_{x}\cos\theta+k_{y}\sin\theta$ makes $\mathbf{\Lambda}'\equiv\mathbf{\Lambda}^{in}$ and $\mathbf{a}'\equiv\mathbf{a}$ where $\mathbf{\Lambda}^{in}\mathbf{a}=\mathbf{0}$ is the untransformed governing equation resulting in displacement being matched at the computational boundary $x=0$. The traction (5.7) under the transformation $k_{y}=k_{y'}$ and $\partial/\partial x=\left(\left(\partial/\partial x'\right)-ik_{y}\sin\theta\right)/\cos\theta$ becomes,

$$\mathbf{T}_{x}^{in}=-\left(\left(\frac{\mathbf{G}_{xx}}{\cos\theta}\right)\frac{\partial}{\partial x'}+ik_{y}\left(\mathbf{G}_{xy}-\mathbf{G}_{xx}\tan\theta\right)\right)\mathbf{u}, \tag{5.43}$$

which, with $\mathbf{u} = \mathbf{a}' e^{ik_x x'}$ gives back (5.7) at the computational boundary since $x = x' = 0$ and $\mathbf{a}' \equiv \mathbf{a}$.

5.9 References

[1] Lindman EL. Free-Space Boundary-Conditions for Time-Dependent Wave-Equation. J.Comput.Phys. 1975;18(1):66-78.

[2] Engquist B, Majda A. Absorbing Boundary-Conditions for Numerical-Simulation of Waves. Math.Comput. 1977;31(139):629-51.

[3] Engquist B, Majda A. Radiation Boundary-Conditions for Acoustic and Elastic Wave Calculations. Commun.Pure Appl.Math. 1979;32(3):313-57.

[4] Berenger JP. A Perfectly Matched Layer for the Absorption of Electromagnetic-Waves. J.Comput.Phys. 1994 OCT;114(2):185-200.

[5] Chew WC, Weedon WH. A 3d Perfectly Matched Medium from Modified Maxwells Equations with Stretched Coordinates. Microwave Opt Technol Lett 1994 SEP;7(13):599-604.

[6] Chew WC, Jin JM, Michielssen E. Complex coordinate stretching as a generalized absorbing boundary condition. Microwave Opt Technol Lett 1997 AUG 20;15(6):363-9.

[7] Sacks ZS, Kingsland DM, Lee R, Lee JF. A perfectly matched anisotropic absorber for use as an absorbing boundary condition. IEEE Trans.Antennas Propag. 1995 DEC;43(12):1460-3.

[8] Higdon RL. Numerical Absorbing Boundary-Conditions for the Wave-Equation. Math.Comput. 1987 JUL;49(179):65-90.

[9] Higdon RL. Radiation Boundary-Conditions for Elastic Wave-Propagation. Siam Journal on Numerical Analysis 1990;27(4):831-69.

[10] Bayliss A, Turkel E. Radiation Boundary-Conditions for Wave-Like Equations. Commun.Pure Appl.Math. 1980;33(6):707-25.

[11] Teixeira FL, Chew WC. Analytical derivation of a conformal perfectly matched absorber for electromagnetic waves. Microwave Opt Technol Lett 1998;17(4):231-6.

[12] Kuzuoglu , Mittra . Frequency dependence of the constitutive parameters of causal perfectly matched anisotropic absorbers. IEEE Microwave Guided Wave Lett. 1996;6(12):447.

[13] Roden , Gedney . Convolution PML (CPML): An efficient FDTD implementation of the CFS-PML for arbitrary media. Microwave Opt Technol Lett 2000;27(5):334.

[14] Meza-Fajardo , Papageorgiou . A nonconvolutional, split-field, perfectly matched layer for wave propagation in isotropic and anisotropic elastic media: Stability analysis. Bulletin of the Seismological Society of America 2008;98(4):1811.

[15] Appelo D, Hagstrom T, Kreiss G. Perfectly matched layers for hyperbolic systems: General formulation, well-posedness, and stability. SIAM J Appl Math 2006;67(1):1-23.

[16] Guddati MN, Tassoulas JL. Continued-fraction absorbing boundary conditions for the wave equation. J.Comput.Acoust. 2000;8(1):139-56.

[17] Guddati MN. Arbitrarily wide-angle wave equations for complex media. Comput.Methods Appl.Mech.Eng. 2006;195(1-3):65-93.

[18] Givoli D. High-order local non-reflecting boundary conditions: a review. Wave Motion 2004;39(4):319-26.

[19] Becache E, Givoli D, Hagstrom T. High-order Absorbing Boundary Conditions for anisotropic and convective wave equations. Journal of Computational Physics 2010;229(4):1099.

[20] Givoli D, Neta B. High-order non-reflecting boundary scheme for time-dependent waves. J.Comput.Phys. 2003 MAR 20;186(1):24-46.

[21] Hagstrom T, Warburton T. A new auxiliary variable formulation of high-order local radiation boundary conditions: corner compatibility conditions and extensions to first-order systems. Wave Motion 2004 APR;39(4):327-38.

[22] Asvadurov S, Druskin V, Guddati MN, Knizhnerman L. On optimal finite-difference approximation of PML. Siam Journal on Numerical Analysis 2003;41(1):287-305.

[23] Guddati MN, Lim KW, Zahid MA. Perfectly Matched Discrete layers for Unbounded Domain Modeling. In: Magoulès F, editor. Computational Methods for Acoustics ProblemU.K.: Saxe-Coburg Publications; 2008, p. 69-98.

[24] Savadatti S, Guddati MN. Absorbing boundary conditions for scalar waves in anisotropic media. Part 1: Time harmonic modeling. Journal of Computational Physics 2010;229(19):6696-714.

[25] Savadatti S, Guddati MN. Absorbing boundary conditions for scalar waves in anisotropic media. Part 2: Time-dependent modeling. Journal of Computational Physics 2010;229(18):6644-62.

[26] Hu FQ. Development of PML absorbing boundary conditions for computational aeroacoustics: A progress review. Comput.Fluids 2008 MAY;37(4):336-48.

[27] Diaz J, Joly P. A time domain analysis of PML models in acoustics. Comput.Methods Appl.Mech.Eng. 2006;195(29-32):3820-53.

[28] Abarbanel S, Gottlieb D, Hesthaven JS. Well-posed perfectly matched layers for advective acoustics. J.Comput.Phys. 1999 SEP 20;154(2):266-83.

[29] Hu FQ. A stable, perfectly matched layer for linearized Euler equations in unsplit physical variables. J.Comput.Phys. 2001 NOV 1;173(2):455-80.

[30] Tam CKW, Auriault L, Cambuli F. Perfectly matched layer as an absorbing boundary condition for the linearized Euler equations in open and ducted domains. Journal of Computational Physics 1998;144(1):213-34.

[31] Turkel E, Yefet A. Absorbing PML boundary layers for wave-like equations. Applied Numerical Mathematics 1998;27(4):533-57.

[32] Hagstrom T. A new construction of perfectly matched layers for hyperbolic systems with applications to the linearized Euler equations. 2003;:125.

[33] Becache E, Fauqueux S, Joly P. Stability of perfectly matched layers, group velocities and anisotropic waves. J.Comput.Phys. 2003 JUL 1;188(2):399-433.

[34] Becache E, Bonnet-Ben Dhia AS, Legendre G. Perfectly matched layers for the convected Helmholtz equation. SIAM J.Numer.Anal. 2004;42(1):409-33.

[35] Hu FQ. A Perfectly Matched Layer absorbing boundary condition for linearized Euler equations with a non-uniform mean flow. J.Comput.Phys. 2005 SEP 20;208(2):469-92.

[36] Becache E, Dhia ASBB, Legendre G. Perfectly matched layers for time-harmonic acoustics in the presence of a uniform flow. Siam Journal on Numerical Analysis 2006;44(3):1191-217.

[37] Parrish S, Hu F. PML absorbing boundary conditions for the linearized and nonlinear Euler equations in the case of oblique mean flow. Int.J.Numer.Methods Fluids 2009;60(5):565.

[38] Operto S, Virieux J, Ribodetti A, Anderson J. Finite-difference frequency-domain modeling of viscoacoustic wave propagation in 2D tilted transversely isotropic (TTI) media. Geophysics 2009;74(5):T75-T95.

[39] Skelton EA, Adams SDM, Craster RV. Guided elastic waves and perfectly matched layers. Wave Motion 2007 AUG;44(7-8):573-92.

[40] Appelo D, Kreiss G. A new absorbing layer for elastic waves. Journal of Computational Physics 2006;215(2):642-60.

[41] Appeloe D, Colonius T. A high-order super-grid-scale absorbing layer and its application to linear hyperbolic systems. J.Comput.Phys. 2009 JUN 20;228(11):4200-17.

[42] Lisitsa V, Lys E. Reflection less truncation of target area for axially symmetric anisotropic elasticity. J.Comput.Appl.Math. 2010;234(6):1803-9.

[43] Sofronov IL, Zaitsev NA. Transparent boundary conditions for the elastic waves in anisotropic media. Hyperbolic Problems: Theory, Numerics, Applications 2008:997-1004.

[44] Guddati MN, Lim KW. Continued fraction absorbing boundary conditions for convex polygonal domains. Int J Numer Methods Eng 2006;66(6):949-77.

[45] Thomsen L. Weak Elastic-Anisotropy. Geophysics 1986;51(10):1954-66.

[46] Hagstrom T, Warburton T. Complete radiation boundary conditions: minimizing the long time error growth of local methods. 2008;.

Chapter 6 Summary, Conclusions and Future Work

6.1 Summary

In this dissertation, we investigate the accuracy and well-posedness issues of local ABCs designed for anisotropic media and design local ABCs that are (a) accurate and well-posed for tilted anisotropic acoustic media, and (b) accurate for tilted elliptic and untilted non-elliptic anisotropic elastic media. This work focuses mainly on absorption of propagating waves with evanescent waves being considered only in the accuracy studies of tilted anisotropic acoustic and tilted elliptic anisotropic elastic media.

The anisotropic media considered here are those allowing wavemodes with opposing signs of phase and group velocities; such media pose a considerable challenge to the design of accurate, well-posed and stable local ABCs. Existing knowledge points to the fact that effective local ABCs can be designed for elliptic anisotropic media only through appropriate space-time transformations and no such transformations are available for non-elliptic anisotropic media. The overarching conclusions that can be derived from this dissertation are: (a) it is possible to design an effective local ABC for elliptic anisotropic media *without* the use of space-time transformations, and (b) there exists a space-time transformation for non-elliptic anisotropic media at least in the untilted case.

6.2 Conclusions

6.2.1 Accurate ABC for Tilted Anisotropic Acoustics

We provide a sufficient condition for accuracy of PMDL designed for propagating waves in anisotropic acoustic media. This condition is shown to be a simple bound on the real-valued PMDL parameters that are directly related to its layer lengths. By deriving the reflection coefficient and expressing it in terms of group (*not* phase) velocities, we understand the ability of PMDL to accurately absorb wavemodes with the correct group velocity without the use of space-time transformations. Various frequency domain simulations demonstrate the accuracy attained.

6.2.2 Accurate and Well-posed ABC for Tilted Anisotropic Acoustics

We prove that the sufficient condition for accuracy derived in chapter 2 is both necessary and sufficient for well-posedness of PMDL designed for propagating waves in anisotropic acoustic media. By utilizing the well-posedness theory developed by Kreiss and the well-posedness conditions derived by Trefthen and Halpern for isotropic acoustics, we derive conditions under which the use of PMDL leads to a strongly well-posed initial boundary value problem (IBVP). We hypothesize that the unexpected existence of a well-posed local ABC for media supporting opposing signs of phase and group velocities is due to the fact that we consider an IBVP instead of the commonly used though less appropriate initial value problem (IVP). Various time domain simulations demonstrate the accuracy, well-posedness and stability of PMDL that satisfy the required conditions.

6.2.3 Accurate ABC for Tilted Elliptic Anisotropic Elasticity

We provide a sufficient condition for accuracy of PMDL designed for both propagating and evanescent waves in tilted anisotropic elastic media. This condition is shown to be a simple bound on the *complex-valued* PMDL parameters that are directly related to its layer lengths. While the anti-plane shear waves of anisotropic elasticity are identical to the waves in anisotropic acoustics, the in-plane pressure and shear waves exhibit mode coupling that necessitates the use of complex-valued PMDL parameters. By constructing detailed analogies between PMDL and PML, and by studying the effect of truncation reflections on solution decay, we explain the ability of PMDL designed for anti-plane shear waves to accurately absorb wavemodes with the correct group velocity without the use of space-time transformations; this also provides an alternative, simpler derivation of the sufficient condition derived for accuracy of tilted anisotropic acoustics. Understanding the role of truncation reflections in stabilizing the solution also underscores the importance of studying the accuracy and well-posedness issues of ABCs from an IBVP point of view because IVPs do not support truncation reflections. Numerous slowness diagrams are used to demonstrate the accuracy attained.

6.2.4 Accurate ABC for Untilted Non-elliptic Anisotropic Elasticity

We provide a sufficient condition for accuracy of PMDL designed for propagating evanescent waves in utilted non-elliptic anisotropy. By grouping layers together, we define a sequence of sufficient conditions and two necessary conditions. Using one of the necessary conditions we prove the inadequacy of wavenumber-independent PMDL parameters to accurately model the propagating waves of non-elliptic anisotropy. We next present a PMDL with wavenumber-dependent parameters that satisfies the sufficient condition with a 2-layer grouping; the parameters of this PMDL are linearly dependent on the vertical wavenumber. The resulting choice of wave-number dependent parameters is shown to be equivalent to an unconventional stretching of the finite element PMDL mesh that is amenable for implementation. Note that this mesh stretching, though unconventional, nevertheless falls under the category of spatial transformations that were thought to be non-existent for non-elliptic anisotropy. Numerous slowness diagrams demonstrate the validity of the above results.

6.3 Future Work

6.3.1 Remaining Work on Absorbing Boundary Conditions for Anisotropic Media

6.3.1.1 Accuracy and Well-posedness

This dissertation provides a stepping stone for further studies on the accuracy and well-posedness of local ABCs in general and PMDL in particular. In the case of elasticity e.g. well-posedness needs to be ensured and work on accuracy still needs to be done on non-elliptic anisotropy (both untilted and tilted). All further work in this direction can start from closer examination of the parameters used in PMDL and the consequences to accuracy and/or wellposedness.

Real Parameters

Well-posedness of local ABCs with real-valued parameters needs to be ensured for untilted non-elliptic anisotropic elasticity. Since well-posedness is linked to accuracy in the sense that incoming wavemodes need to be excluded for both, and since this dissertation presents the

design of an ABC which does not allow incoming propagating modes, we can be optimistic about the ABC's well-posedness. However, unlike in the case of tilted anisotropic acoustics considered in Chapters 2 and 3 where an ABC with real parameters resulted in real-valued approximations, we have noticed complex-valued approximations for untilted non-elliptic anisotropic elasticity from an ABC with real-valued parameters. This issue should be kept in mind before tackling well-posedness in this case.

Complex Parameters

The focus of this dissertation has been propagating wavemodes and hence we have primarily dealt with local ABCs with *real-valued* parameters. Absorption of evanescent wavemodes requires the ABC parameters to be *complex-valued* and hence it is essential to study the accuracy and well-posedness issues of ABCs with complex-valued parameters.

Accuracy studies with complex-valued parameters are not expected to be much different from those of their real-valued counterparts (as seen in Chapter 4). The task of tackling the accuracy of non-elliptic anisotropic elasticity (both tilted and untilted) with complex-parameters remains.

Well-posedness studies involving complex-valued parameters may be significantly different in that it may necessitate going back to Kreiss's original algebraic criteria for well-posedness. We cannot use the simpler criteria of equivalent studies based on real-valued approximations as e.g. we were able to do in Chapter 2 when we used Trefethen and Halpern's work. Well-posedness of ABCs with complex-valued parameters still needs to be proved for all anisotropic media.

Real and Imaginary Parameters

It is known that both propagating and evanescent modes can be absorbed by using ABCs with some purely real and some purely imaginary (or complex) parameters (ex. padded ABCs). We do not currently know whether accuracy and well-posedness studies for such ABCs will turn out to be simpler or harder than ABCs with only purely real-valued or

complex-valued parameters. If these studies turn out to be easier and if the performance of such ABCs is on par with others, it might be worthwhile to investigate them first.

6.3.1.2 Stability

In this dissertation, we have adopted the terminology of well-posedness and stability being related to boundedness of the solution for continuous and time discretized versions respectively. In this sense we may need to use the stability theory developed by Kreiss, Gustafsson and Sundstörm for difference approximations. Since well-posedness is necessary, but not sufficient for stability, work still needs to be done in this regard. The first step in this direction is to investigate spatially continuous but temporally discretized models and then move on to completely discretized systems. Of course, ensuring stability through artificial numerical damping is always an option but even that needs to be investigated carefully to ensure long-term accuracy.

6.3.1.3 Heterogeneous Media

One of the major challenges to the design of effective ABCs for homogeneous anisotropic media is the existence of wavemodes with opposing phase and group velocities. Such wavemodes exist in heterogeneous media too (both isotropic and anisotropic) and hence extending all the above studies (of 6.3.1.1, 6.3.1.2) for heterogeneous media is the obvious next step. While some work done in this direction points to the possibility of traditional space-time transformations being capable of accurately capturing the correct group velocities in the frequency domain, the form of these transformations are not amenable to time domain simulations. New frequency domain transformations that are more amenable to time-domain extensions need to be designed or new techniques for dealing with time-domain simulations directly need to be investigated.

6.3.1.4 Far-field Response

In problems involving ABCs, we are only interested in the effect of the exterior at the computational boundary. Thus the exterior computational model developed in the case of ABCs need not represent the actual solution behavior in the exterior. However, it may be

possible to utilize the solution gathered in this ‘pseudo’ exterior to estimate the actual solution in the far-field and this needs to be investigated.

6.3.1.5 Comparative Studies

While this dissertation has revealed some qualitative links between PMDL and other local ABCs (rational ABCs and PML), work still needs be done with respect to quantitative comparisons. It also needs to be seen, as to how the results obtained for PMDL can be translated to PML and other rational ABCs. A further interesting question to consider here would be whether PMDL, which can be seen as *a* discretized version of PML, is actually *the* optimal discretized version of PML in general.

6.3.2 Absorbing Boundary Conditions for Other Complex Cases

6.3.2.1 Other Wave Equations

Issues of wavemodes with opposing signs of phase and group velocities also exist in the contexts of Maxwell’s and Navier-Stokes equations and, accuracy, well-posedness and stability of ABCs for such media need to be studied.

6.3.2.2 Geometrical Complexities

The above discussions are all focused on material complexities like heterogeneity and anisotropy with the assumption that the geometry of the ABC is simple (straight edge). Accuracy, well-posedness and stability studies of domains involving corners and curved boundaries need to be carried out for all the above cases (6.3.1.1-3, 6.3.2.1).

6.3.2.3 Discrete Systems

ABCs can be designed to match the impedance of a spatially discrete interior instead of the continuous interior that has been the focus of this dissertation. Accuracy, well-posedness and stability studies need to be conducted for such ABCs.

6.3.3 One-Way Wave Equations in the Context of Subsurface Imaging

ABCs can be viewed as one-way wave equations (OWWEs) that allow propagation of waves in a 180-degree cone. Given this special property, OWWEs have been central to marching

algorithms used in subsurface imaging. While accuracy issues are similar between ABCs and OWWEs, there exists an important difference between them: unlike the temporal well-posedness and stability issues of ABCs, marching techniques require well-posedness and stability primarily in the spatial domain. Hence, the results of ABCs are not trivially extendible to marching and require further study.